PHONOPHORESIS AND TOPICAL DRUG DELIVERY

VICTOR MOSHE MEIDAN

Doctor of Philosophy

THE UNIVERSITY OF ASTON IN BIRMINGHAM

September 1996

THESIS SUMMARY

Phonophoresis - the application of ultrasound to enhance percutaneous drug delivery - has been used by physiotherapists for over 30 years. However, since the treatment has been conducted on a highly subjective and non-quantitative basis, no clear consensus exists on the effectiveness of the technique nor on the nature of the phonophoretic mechanism(s). In this study, investigations into phonophoresis were conducted by employing 3 distinct *in vitro* models.

The aim of the first model was to evaluate the effect of ultrasound on the migration rate of different classes of molecules through agar gel. The derived data suggested that small, relatively hydrophobic molecules are more susceptible to ultrasound-enhanced diffusion through the water-filled channels of the agar gel. The application of heat alone increased drug migration by a similar magnitude as the ultrasound, indicating that ultrasonic heating directly increases the thermodynamic potential for diffusion.

In the second experimental system, whole rat skin was pre-sonicated and then examined for changes in its barrier properties. At high intensities (1 to 2W cm^{-2}), ultrasonic waves irreversibly compromised the barrier properties of the skin, following the general patterns described in the literature reports. At low intensities (< 1W cm^{-2}), ultrasound discharged sebum from the sebaceous glands so as to fill much of the hair follicle shafts. This entirely novel phenomenon is probably produced by the mechanical effects of the beam. The deposition of sebaceous lipids within the hair follicle shafts can mean that this absorption pathway is blocked for hydrophilic molecules that penetrate *via* this route. Consequently, this phenomenon can be utilised as a probe to measure the relative follicular contribution to total penetration for these molecules. In these studies, it was demonstrated that the shunt pathway was responsible for virtually all mannitol and sucrose penetration but negligible aminopyrine and 5-fluorouracil penetration.

In the final phonophoresis model, modified Franz cells were employed in order to assess the ultrasound effect on the concurrent transdermal permeation of various molecules through whole rat skin. The candidates were selected so as to encompass a wide range of octanol/water partition coefficient values. Sonication did not significantly increase the percutaneous absorption of any of the permeants. Although slightly hydrophilic molecules should be susceptible to phonophoresis through the stratum corneum, sonication actually reduced their skin surface concentration by promoting their diffusion into the overlying coupling gel. The more lipophilic molecules did not undergo phonophoresis as they permeate intrinsically rapidly through the stratum corneum. For the most lipophilic agent tested, the rate-limiting step of absorption was partitioning from the stratum corneum into the viable epidermis. Sonication did not accelerate this step. However, ultrasound, *via* its thermal effects, acted synergistically with azone in enhancing percutaneous hydrocortisone delivery.

In a separate series of *in vitro* stability studies, ultrasonic waves markedly degraded oligodeoxynucleotides at pH 1. Pilot studies indicated that the mechanical effects of the sound are probably mediating these sonochemical changes.

To my family

ACKNOWLEDGEMENTS

I would like to express my appreciation to Professor Bill Irwin for his continual supervision, advice and optimism and to Dr Damien Walmsley for his invaluable guidance and encouragement.

I must also extend my sincere thanks to Melvyn Docker at the Medical Physics Department of the Queen Elizabeth Hospital for his vital collaboration and helpful discussions on the physics of ultrasound propagation.

I am especially grateful to Dr Debbie Dunnion for her expertise and valued assistance on the relevant chapter. I would also like to thank Professor R. M. Browne and the staff of the Pathology Department at Birmingham University Dental School for their co-operation.

Finally, I must thank my parents and sister for their tremendous support and encouragement throughout this project.

CONTENTS

LIST OF FIGURES

LIST OF TABLES

ABBREVIATIONS

ac	alternating current
ATP	adenosine triphosphate
ATR-FTIR	attenuated total reflectance Fourier transform infra-red
Bq	Becquerel
BSI	British Standards Institute
cm	centimetres
c.w.	continuous wave
^{14}C	carbon-14 radiolabelled
Da	daltons
DMSO	dimethylsulphoxide
DNA	deoxyribonucleic acid
dpm	disintegrations per minute
f	frequency
g	grammes
g	gravity
h	hours
^{3}H	tritium radiolabelled
kg	kilogramme
K_p	permeability coefficient
L	litre
ln	natural logarithm (to base 2)
log	logarithm (to base 10)
m	metre
MBq	megabecquerels
mg	milligrammes
MHz	megahertz
mins	minutes
ml	millilitre
mm	millimetre
$m\ s^{-1}$	metres per second
N	Newton
nmol	nanomoles
n	number of replicate runs
ODN	oligodeoxynucleotide
P	statistical significance level
^{32}P	phosphorous-35 radiolabelled
$P_{(octanol/water)}$	octanol-water partition coefficient

pd	potential difference
pKa	$\log_{10}$ dissociation constant
pmol	picomoles
r	correlation coefficient
RNA	ribonucleic acid
rpm	revolutions per minute
^{35}S	sulphur 35 radiolabelled
SATA	spatial-average temporal-average (intensity)
s.d.	standard deviation
s.e.m.	standard error of the mean
SG	specific gravity
SOAB	sound-absorbing (rubber)
SPTA	spatial-peak temporal-average (intensity)
SPTP	spatial-peak temporal-peak (intensity)
TBq	terabecquerel
TLC	thin-layer chromatography
t-test	student's t-test for statistical significance
U/ml	units of insulin per millilitre of solution
UV	ultraviolet
V	volt
v/v	volume in volume
W	watt
W cm^{-2}	watts per centimetre square
w/v	weight in volume (w/v)
Z	acoustic impedance
α	ultrasound attenuation coefficient
λ	wavelength
µl	microlitres
µm	micrometres
µmol	micromoles
%	percentage
°C	degrees centigrade
'	inches
χ^2-test	chi-squared test for statistical significance

CHAPTER ONE

INTRODUCTION

1.1 THE STRUCTURE AND PERMEABILITY OF THE SKIN

The skin combines with the mucosal linings of the digestive and respiratory tracts to protect the internal body structure from a hostile external environment. The skin limits the ingress of toxic chemicals and micro-organisms as well as preventing injury arising from mechanical forces or electromagnetic radiation. Furthermore, it mediates thermoregulatory, sensory, endocrine and communicatory functions.

Human skin is essentially composed of three tissue layers, the hypodermis, the dermis and the outermost epidermis. See Figure 1.1. The hypodermis is an underlying layer of subcutaneous fat that mechanically cushions the skin from trauma as well as providing thermal insulation. The dermis, approximately 3-5mm thick, is an acellular matrix of connective tissue woven from fibrous proteins which are embedded in mucopolysaccharides. The dermis contains an extensive network of nerves, capillaries and lymphatics. The dense capillary network means the blood supply reaches to within 0.2mm of the skin surface. This feature allows any permeating compounds to be rapidly removed by the systemic circulation, hence maintaining sink conditions. The dermis also supports the skin appendages *i.e.* sweat glands (both eccrine and apocrine) and pilosebaceous units before they reach the skin surface. The multicellular epidermis, some 0.01 to 0.08mm thick, is considered to be architecturally unique as it is in a state of perpetual transition. At the basal layer, metabolically active and rapidly dividing columnar keratinocytes are constantly migrating upwards. As they ascend, these cells progressively degenerate into non-viable, anucleated, flattened corneocytes. These keratin-rich cells produced at the final phases of differentiation, combine with their intercellullar lipids to produce the horny layer or stratum corneum. Behaving as a lipoidal envelope, the stratum corneum acts as the major skin permeability barrier (Barry, 1983).

The main properties of the permeant which influence its percutaneous penetration are its concentration, partition coefficient and diffusivity. Once steady state has been achieved, the rate of drug penetration is proportional to its applied concentration. As only dissolved drug can diffuse from the vehicle phase into the skin, flux generally increases linearly with concentration until saturation is attained. The mathematics describing this behaviour is reviewed in section 4.1.5.

Figure 1.1: Cross-Sectional Diagrams of Skin Structure (from Barry, 1983)

(A) Section through Whole Skin

(B) Section through Epidermis

The affinity of the lipophilic horny layer for a specific drug largely depends upon the chemistry of the permeant. Absorption is facilitated for compounds exhibiting high lipid-water partition coefficients. Once the drug has partitioned into the stratum corneum, it diffuses through this layer as a result of the concentration gradient. There are two possible pathways through the stratum corneum. The transcellular route involves drug diffusion occuring directly through the corneocytes. The intercellular route involves the drug diffusing more tortuously *via* the intercellular channels. The relative contribution of each route has been considerably debated over the last decade. Both pathways may be important, depending upon the physicochemical properties of the permeating molecule (Wiechers, 1989). However, most authors now believe that the major route is probably through the intercellular lipid channels (Hadgraft *et al.*, 1995). Partitioning from the stratum corneum into the essentially aqueous viable epidermis is favoured by a hydrophilic drug character. This is the reverse of the requirement for partitioning into the stratum corneum. Therefore, optimal absorption is attained by compounds that exhibit intermediate partitioning behaviour. Refer to section 5.1.

It should be mentioned that while the sweat glands and pilosebaceous channels were traditionally regarded as constituting quantitatively unimportant routes for steady-state penetration, their importance is now being reconsidered (Lauer *et al.*, 1995), as discussed in section 5.2.

As a result of the low permeability of the stratum corneum (Scheuplein, 1978a; Scheuplein, 1978b; Wentz and Downing, 1989), the scope for percutaneous drug delivery is rather limited. The facilitation of transdermal drug delivery is an important area of pharmaceutical research and strategies include structural modification to optimise the physico-chemical properties of the drug (Chan and Li Wan Po, 1989; Sloan, 1992), diverse pharmaceutical formulations with a range of vehicles (Cooper, 1985; Barry, 1983), the use of permeability enhancers (Barry, 1991) and occlusion (Bucks *et al.*, 1989). Iontophoresis, in which drug flux is promoted by an electrical potential, also attracts considerable interest (Tyle and Kari, 1988). One further approach involves the application of ultrasound to increase the penetration of drugs into tissues - a phenomenon termed phonophoresis (Griffin *et al.*, 1967; Singh and Singh, 1990; Tyle and Agrawala, 1989) or sonophoresis (Bommannan *et al.*, 1992a,b).

For over 30 years, physiotherapists have used the combination of ultrasound plus steroid or analgesic in order to treat a variety of muscular and arthritic conditions. Unfortunately, most of this treatment has been conducted on a subjective and non-quantitative basis (Williams, 1983). Frequent limitations of the literature reports have included a lack of proper controls, incomplete accounts of the dosimetry and protocols employed, and the non-calibration of the ultrasound source. Consequently, much of the available data from these studies are inadequate and even contradictory (Famaey 1985; Pottenger and Karalfa 1989; Mohl *et al.*, 1990). In the last few years, some higher quality studies have been conducted by both pharmaceutical scientists and medical physicists. However, because individual research groups have used different methods and models, the nature of the ultrasound effect on percutaneous drug penetration is still not fully understood (Newman *et al.*, 1992; Sun and Liu, 1994; Ueda *et al.*, 1995).

This next part of this chapter describes the clinical use of phonophoresis within its established physiotherapeutic setting. Subsequently, there is a discussion of the biophysical interactions of ultrasound that may mediate enhanced drug delivery. The evidence for the occurrence of phonophoresis is then reviewed from the separate perspectives of *in vitro* research, animal studies, and human volunteer trials. The underlying ideas derived from this comprehensive literature review are then summarised. Finally, there is a statement as to the aims and objectives of the present study.

1.2 THE CLINICAL USE OF PHONOPHORESIS

Ultrasound is an acoustic vibration propagating in the form of longtitudinal compression waves at frequencies beyond the human auditory range *i.e.* frequencies exceeding 0.02MHz. The frequency is the number of complete compression-rarefaction cycles passing through a reference point per second. The intensity parameter (measured in W cm^{-2}) is used to establish ultrasound exposure. The physics of ultrasound propagation will be discussed in detail in Chapter 2.

Over the past 30 years, a general method for co-administering drug and ultrasound has gradually been established in physiotherapy clinics. The technique involves applying the therapeutic agent within a viscous ultrasonic coupling medium to the treatment site such that good contact is maintained between the skin surface and ultrasound transducer. The transducer emits the ultrasound beam through the drug layer into the tissue. Individual therapists prefer different frequencies and intensities. Generally, the ultrasonic frequency applied is between 0.020 MHz and 3MHz while intensity is rarely greater than 3W cm^{-2}. Frequently, physiotherapists will increase the intensity setting, stopping just short of the patient beginning to feel pain. Alternatively, the transducer can be set into circular or stroking motion over the skin surface, thus reducing the energy deposition per unit area. Sometimes, a beam of pulsed ultrasound is used to achieve the same purpose. The treatment time can be up to 10 minutes and can be made more complex by administering the drug and ultrasound in a non-simultaneous manner. It may be concluded that in the physiotherapeutic setting, the treatment parameters are highly dependent upon the subjective ideas of individual clinics and therapists.

Phonophoresis *in vivo* represents a complex system. Ultrasound energy can be partially reflected off bones and from the interfaces between two different tissue types, thus resulting in standing-wave production, as discussed in section 2.1.1. The extent to which this phenomenon occurs depends largely on the anatomy of the site which is being sonicated. However, to date, no research has been published on the effect of ultrasound standing waves on drug migration, either *in vivo* or *in vitro*. One other crucial aspect is the fact that in most phonophoresis work, researchers have neglected to map out the ultrasonic intensities at different points within the beam (refer to section 2.1.1). Consequently, it is quite possible that certain irradiated tissues have been subjected to ultrasound intensities that are either much lower or much higher than the intensity stated by the authors. This is

particularly true if the skin lies within the near zone of ultrasound which is frequently the case in much of the literature reports. Some workers have applied phonophoresis by having the transducer in continuous motion over a small specific area of the skin surface, a protocol which, to some extent overcomes this problem. Another important factor is the ultrasound effect on drug stability and on the relative partition coefficient of the drug between vehicle and skin. All these issues are commonly overlooked in much of the literature.

One further neglected variable relates to the use of a coupling gel or contact agent which is placed between the ultrasound transducer and the skin surface. This coupling medium is required so that an efficient transfer of ultrasonic energy between the transducer and the skin surface can take place. This is because air is a very poor medium for ultrasound propagation. An ideal coupling agent should exhibit an absorption coefficient similar to that of water and retain a gel or paste consistency at body temperature so that contact is maintained between the transducer and the skin. The presence of air bubbles in the contact medium obviously reduces ultrasound transmission and a good coupling agent will exhibit a low capacity for dissolved gases.

In some cases, topical pharmaceutical products containing the active drug have been used as the coupling material. However, the problem with this approach is that, unlike contact media designed specifically for that purpose, topical pharmaceutical products are generally not formulated to optimise their efficiency as ultrasound couplants. Consequently, much of the ultrasound energy may be lost before it reaches the skin. In this situation, the actual amount of energy that reaches the skin can be measured by placing calibrated hydrophones on the skin surface.

One group of investigators examined the transmission of ultrasound energy at frequencies of 0.75MHz, 1.5MHz and 3MHz through 41 different common topical pharmaceuticals (Benson and McElnay, 1988). Large variations in ultrasound transmissions were found between different products, as well as in some cases, between the same products at different frequencies. Specifically formulated ultrasound coupling agents generally exhibited better transmission than the other products. Another discernible trend was the fact that gel-type products on the whole, displayed better transmission than other formulations. Seven products were found not to transmit ultrasound at all at any of the tested

frequencies. Recently, one American group (Cameron and Monroe, 1992) compared the relative transmission of 25 popularly used coupling products with that of degassed water at a frequency of 1 MHz. The products tested could be grouped together into two classes; those where transmission was greater than 80% of water (6 products) and those where transmission was less than 40% of that of water (13 products). The media that transmitted ultrasound well included products specifically designed as ultrasound couplants, mineral oil, a corticosteroid gel and a methyl salicylate cream. Most of the creams and ointments tested exhibited poor transmission. Furthermore, it was found that adding an equal amount of medium that transmits well to a one that transmits poorly does not improve transmission.

The importance of vehicular effects has been recently demonstrated in experiments where hairless mice were partially immersed in either lignocaine gel or aqueous lignocaine solution and exposed to 0.048MHz ultrasound at 0.17W cm^{-2} (Tachibana and Tachibana, 1993). Anaesthetic absorption was evaluated by counting the number of animal reactions to electrical stimulation, both before and after drug application. Enhanced delivery was observed from the aqueous solution but not from the gel base. Unfortunately, the reasons for this difference were not explored.

1.3 POSSIBLE MECHANISMS OF PHONOPHORESIS

When ultrasound propagates through biological tissues, changes may be mediated by up to five different processes. These are the first-order forces, heating, radiation pressure, cavitation and acoustic microstreaming. Although these effects are to some extent interrelated, they can be conveniently treated as separate phenomena. Figure 1.2 presents a flow chart illustrating the processes involved.

Figure 1.2: The potential mechanisms through which phonophoretic enhancement of percutaneous absorption may be mediated

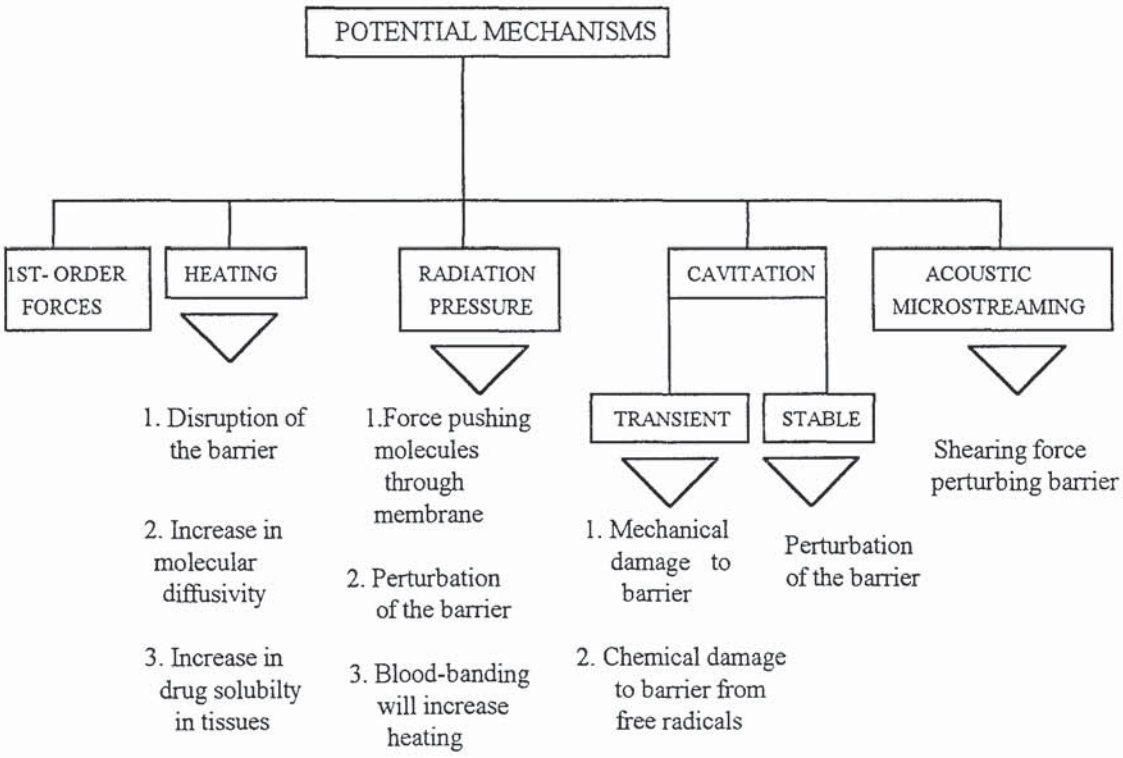

1.3.1 First-Order Forces

The first order forces are those directly associated with the alternating motion of the particles during wave propagation (these particles are strictly speaking not

atoms or molecules but theoretical points within the medium). At the intensities and frequencies commonly employed for phonophoresis, the first-order forces involve small particle displacements, moderate particle velocities but incredibly high values of instantaneous particle accelerations. For example, a 1MHz, 1W cm^{-2} ultrasonic field would induce particle displacements of 0.018μm, particle velocities of 12cm s^{-1} and a maximum acceleration of 71000*g*! However, in order for such forces to damage skin, different portions of the same skin structure must be subjected to different forces so that it is twisted or torn (Williams, 1983).

As an example, a 1MHz ultrasound wave exhibits a wavelength of about 1.5mm as it propagates through tissue. Therefore, the distance between the zones of maximum opposite motion is half a wavelength or approximately 750μm. Hence, structures of this order or larger, are subjected to cyclic strains equal to twice the maximum particle displacement. At an intensity of 1W cm^{-2}, a 1MHz beam stretches and compresses a structure 750μm long by about 0.04μm which is only 0.005% of its length. Whole human skin is approximately 3mm thick and will experience strains of this magnitude throughout its thickness. Although, these strains are being applied a million times a second, the overall fatigue induced is still considered rather small compared to the strains normally encountered in strenuous exercise (Williams, 1983). Skin structures much smaller than a wavelength, such as individual corneocytes or sebaceous gland cells are subjected to even smaller strains. This is because the whole cell and its immediate neighbours are displaced together in the same direction in a synchronised fashion. It is unlikely that the first-order effects of ultrasound mediate phonophoresis.

1.3.2 Heating

The energy of an ultrasonic beam is attenuated during its transit through tissue by the dual processes of scatter and absorption. Scatter develops as the beam propagates through regions exhibiting different acoustic impedance and this can develop at both the multicellular *i.e.* tissue as well as the cellular level. The absorption of ultrasound depends not only upon the molecular weight of the material but also its physical properties. For instance, the absorption of the individual amino acids of haemoglobin is much less than the larger combined

structure. Furthermore, absorption increases in a non-linear manner with increasing concentration. The absorption of ultrasound leads to heating.

Attenuation is commonly measured in terms of percentage energy loss per unit distance. For any given tissue, the intensity of the ultrasonic beam will decrease exponentially with tissue depth. In general, the attenuation coefficient increases with increasing structural protein content and with decreasing water content. Consequently, tissues of high collagen content, such as bone and joint capsular structures, undergo greater attenuation, and therefore greater heating, than skin and subcutaneous fat. This can be seen from Table 1.1, which lists the attenuation coefficients of various tissues. These measurements were made with a 1MHz ultrasound beam.

Table 1.1: Attenuation of a 1MHz ultrasound beam (From Ziskin and Michlovitch, 1986)

However, attenuation also depends upon frequency, with greater attenuation developing at higher frequencies. In the frequency range 0.5 to 10 MHz, the attenuation coefficients for tissues other than bone can be fairly well approximated by the relationship :

$$\alpha = \alpha_1 * f^{1.1} \qquad (1.1)$$

where α_1 is the attenuation coefficient at 1 MHz, f is the frequency (in MHz), and α is the attenuation coefficient at the specified frequency (Goss *et al.*, 1979).

As explained in section 2.1.1, the soft tissue/bone interface represents a large mismatch of acoustic impedance at which mode conversion can occur. When an ultrasonic wave meets a tissue/bone interface, part of the wave is reflected back into the tissue as a transverse (shear) ultrasonic wave. The transverse wave component is not propagated and will be deposited as heat at the bone/soft tissue interface. The region close to the bone is the periosteum and this tissue will be rapidly heated and this will be perceived as painful to the patient. Such periosteal pain limits the amount of ultrasonic exposure over bony anatomy. Heat will be dissipated over areas where there is a thick layer of absorbent tissue and this will enable the patient to tolerate the heating. A further area of acoustic impedance mismatch develops at the contact between transducer and skin. As discussed in section 1.2, coupling gel is usually used and heating will also develop at this interface.

It can be seen that it is extremely difficult to predict the amount of tissue heating that will develop during a specific ultrasound application. The situation is further complicated by the fact that the ultrasonic machines used by physiotherapists generally suffer from poor calibration and the amount of sound energy being emitted may not be truly reflected by the control dial on the machine (Walmsley and Squier, 1991). Furthermore, manufacturers have developed a sound-wave signal generation in which a square wave is electrically rounded to produce the required sine wave. Any non-sine sound waves will be of high frequency and will be rapidly absorbed by the soft tissues giving an artificially high skin temperature. Pulsed beams of ultrasound will also tend to contain a high component of non-sine sound waves. Such artificial effects will also contribute to ultrasonic heating.

During phonophoresis, ultrasound induces a rise in the average temperature of the exposed tissue. A temperature gradient results and heat diffuses away. This temperature rise initiates physiological reflexes resulting in vasodilatation which accelerates the rate of excess heat removal. Skin heating will increase the fluidity of stratum corneum lipids and directly increase the molecular diffusivity of the permeant molecule through this layer. Both these effects are known to enhance drug diffusion (Knutson *et al.*, 1985). Furthermore, ultrasound energy will pass into deeper tissues, thus increasing the solubility of drugs as well as leading to the

increased blood flow described above. *In vivo*, all of these processes can facilitate percutaneous drug delivery.

At the intensities used by physiotherapists, ultrasound typically heats tissues by several degrees centigrade and this is probably a major component of phonophoretic enhancement. In *in vivo* work with rats (Walmsley and Squier, 1991), it was established that continuous wave (c.w.) 0.7W cm^{-2} ultrasound induced a skin temperature which ranged from 28.5°C to 63°C. This heating could be reduced to a cutaneous increase of only 4°C by interposing a circulating water bag (28°C) between the skin and ultrasound transducer. In a sequential study (Walmsley *et al.*, 1992), these two protocols were compared in terms of their effect on triamcinolone acetonide transdermal delivery. It was found that steroid penetration was reduced when the beam had passed through the water path. This work was only conducted as a pilot study and further work is required, preferably including non-sonicated control treatments, in order to elucidate the magnitude of the thermal mechanism.

If phonophoresis is caused purely by ultrasonic heating then clearly the process is of no great therapeutic interest since the same penetration enhancement effect can be obtained by using any applied heat source. Ultrasonic heating can be minimised by applying the beam in the form of millisecond on-off pulses or alternatively by applying c.w. ultrasound from a transducer which is continually in motion over the skin surface.

1.3.3 Radiation Pressure

Any medium or object which absorbs some or part of a beam of energy is subjected to a force, termed the radiation pressure force, which tends to push that object in the direction of wave propagation. This will be greatest in a strongly absorbing medium.

A common view is that an induced radiation pressure, acting on the penetrant molecules, "pushes" the drug through the skin, thus accounting for the main non-thermal phonophoretic effect (Skauen and Zentner, 1984; Singh and Singh, 1990;

Saxena *et al.*, 1993). However, most of the evidence for this hypothesis is derived from studies involving artificial membranes. One group of investigators concluded that radiation pressure played a part in the observed ultrasound-accelerated transport of electrolytes through cellophane membranes (Lenart and Auslander, 1980). A model system of the diffusion of molecules through a water-cooled agar gel demonstrated differences in the phonophoretic effect of ultrasound. (Williams *et al.*, 1990). Sodium diethylene triamine penatacetic acid (DTPA) underwent ultrasound-accelerated diffusion whilst sodium pertechnetate did not; both were coordinated to ^{99m}Tc. It has been previously reported *in vitro* that the absorption of ultrasound by molecules can increase with increasing molecular weight (Kremkau and Cowgill, 1984). The authors suggested that the larger DTPA molecule may be consequently subjected to a greater radiation pressure force which increases its diffusion rate through gel although charge and other differences are also apparent.

Significantly, some physicists have rejected the pushed-penetrant hypothesis. It has been claimed that at the microscopic level of description, the particles merely oscillate about a fixed point according to the characteristics of the applied acoustic field. Consequently, the penetrant molecules would be subjected to zero radiation pressure (Simonin, 1995). Even if the hypothesis were valid, phonophoresis is often associated with partial standing wave effects and so the permeant molecules could be driven in different directions at different locations within the exposed skin.

Another proposed theory is that ultrasound exerts a radiation force on the skin, thus perturbing its barrier properties. However, at phonophoretic intensities, the radiation pressure force exerted by an ultrasound free-field is generally small and is unlikely to damage the skin membrane. One author considered a 1MHz free-field, at an intensity of 1W cm^{-2} and computed from theory, the radiation pressure such a beam would exert on the stratum corneum surface (Simonin *et al.*, 1995). It was calculated that the stratum corneum would experience a maximum pressure equivalent to that produced by 5mg of weight distributed over 1 cm^2 area of skin surface. Forces of this magnitude are too weak to damage the stratum corneum. However, it is conceivable that such radiation pressure may induce more subtle perturbations within sonicated skin.

Although the primary radiation pressure forces are too weak to damage well-anchored soft tissues, such forces are enhanced if a standing wave field is set up. For example, if a strong reflector such as bone is present, the ultrasonic beam is reflected back on itself. The reflected wave may interfere with the incident wave to produce a standing wave field. Any resultant radiation pressure forces act over a distance of 0.4 mm in soft tissue at 1 MHz so that unanchored particles which are denser than their suspending medium are pushed to the zones of maximum acoustic pressure. This process has been observed within small blood vessels where blood cells have accumulated together in discrete stationary bands separated by clear plasma (Dyson *et al.*, 1974). This impairment in microvascular blood perfusion can mean that heat is removed less efficiently from sonicated tissues, thus promoting the thermal phonophoretic mechanism.

1.3.4 Acoustic Microstreaming

When a structure within an acoustic field experiences an unequal distribution of radiation pressure forces across its length, it is subjected to a force known as the acoustic torque. In a liquid or semi-liquid medium, the acoustic torque can produce fluid currents and this is termed acoustic streaming. A simple type of acoustic streaming is known as quartz wind streaming. Quartz wind streaming occurs when liquid is pushed away from the front of a transducer so that a continuous circulation is produced.

The classic experiments of acoustic streaming involved immersing a stationary solid cylinder in a fluid through which an acoustic wave was propagating (Holtzmark *et al.*, 1954). Acoustic currents were observed as complex steady-state or time-independent streaming patterns. These patterns can be exactly duplicated if the ultrasound is switched off and the cylinder is driven to oscillate at exactly the same acoustic frequency. The dimensions of the streaming patterns are determined by the boundary layer thickness, the size of which is estimated to be about 3.6μm in water at an ultrasonic frequency of 0.025MHz. These small dimensions mean that the velocity gradients, the rate of change of velocity with distance, and hence the hydrodynamic shear stresses are large even though the actual streaming velocities which produce them are relatively low (of the order of a

few cm s^{-1}). Consequently, at ultrasonic frequencies, the streaming patterns are usually not visible and the process is termed acoustic microstreaming.

Microstreaming can also develop secondarily to cavitation (see section 1.3.5), when the rapid cyclical volume pulsation of a gas bubble results in an unequal distribution of time-independent forces around the bubble surface.

In research with artificial membranes, it has been shown that acoustic microstreaming can decrease the concentration gradient in the vicinity of the membrane. Such a mechanism was found to be responsible for the ultrasound-promoted transfer of sodium chloride across a commercial dialysis membrane (Howkins, 1969) as well as being the major factor responsible for the enhanced diffusion of sodium, potassium and calcium chlorides through synthetic cellophane membranes under the influence of 1 MHz ultrasound (Lenart and Auslander, 1980).

Quartz wind streaming has been implicated as a mechanism in ultrasound-enhanced oxygen diffusion through frog skin (Mortimer *et al.*, 1988) although this may not be an ideal model for poorly permeable human skin. The frog skin was maintained at a fixed temperature during sonication and the deduction that quartz wind streaming was responsible was made by comparing the effect of pulsed ultrasound with c.w. ultrasound.

Acoustic microstreaming has been generated experimentally in order to determine its biological effects. In practice, a small exponentially tapered metal probe with known tip geometry and diameter is driven to oscillate at the required frequency. Typically, the effect of this application on cellular and intracellular structures is analysed by light microscopy. Using such techniques, it has been demonstrated that the shearing forces associated with acoustic microstreaming can, under certain conditions, perturb intracellular contents, rupture cell membranes or dissagregate clumps of cells. For example, in *in vitro* experiments it was demonstrated that human platelets could be ruptured by induced acoustic microcurrents (Williams, 1974). Other workers have shown that acoustic microstreaming can disaggregate sheets of human cervical epithelial cells in suspension (Parry *et al.*, 1971). It has been postulated that such shear forces generated by acoustic microstreaming can perturb the skin barrier and thus may play a role in enhancing skin diffusion during phonophoresis (Ziskin and Michlovitch, 1986).

1.3.5 Cavitation

Encompassing a wide variety of bubble behaviour, cavitation has traditionally been classified as either stable or transient in nature. Stable cavitation is associated with the relatively gentle linear pulsations of gas-filled bodies while transient cavitation describes the violent and highly destructive formation and collapse of vapour-filled voids and cavities (Flynn, 1964; Nyborg, 1977; Williams, 1983). These bubbles are powered by the energy from the incident acoustic field, about 10% of which may be re-radiated from the bubble as an outgoing spherical wave (Nyborg, 1977). The remainder may be converted irreversibly into heat, or may reappear as shock waves or hydrodynamic shear fields to disrupt biological tissues (Nyborg, 1977; Williams, 1983).

The intensity threshold for the development of cavitation increases with increasing frequency in the MHz range (Esche, 1952). For example, at frequencies up to 0.1 MHz, the threshold intensity for transient cavitation in degassed aqueous media is ~1W cm^{-2} (0.1W cm^{-2} for an aerated sample) whereas at 1 MHz, the corresponding values are in the 10^2 - 10^3 region (Williams, 1983). One explanation for this relationship is that, at higher frequencies, there is not enough time for gas molecules to diffuse into cavities during the extremely short period of the rarefaction phase of the acoustic cycle. A tendency to inhibit cavitation development can also be obtained at lower frequencies if the same quantity of ultrasonic energy is beamed in the form of numerous short but intense pulses. This protocol allows time for any gaseous inclusions which may have begun to grow during the "on-time" to readily dissipate. In general, the threshold for stable cavitation is lower than for transient cavitation.

In studies involving synthetic membranes, cavitational processes have been claimed to play a part in ultrasound-promoted transport (Lenart and Auslander, 1980; Levy *et al.*, 1989). Also, in *in vitro* research with frog skin, cavitation was claimed to be primarily responsible for the observed ultrasound effects on ion transport (Dinno *et al.*, 1989). This was deduced from the fact that when cavitation was inhibited by employing degassed bathing fluid, the electrophysiological changes induced by sonication were also suppressed.

It has been suggested that transient cavitation may play a part in the mechanism of phonophoresis (Tyle and Agrawala, 1989). It has been proposed that the

application of higher frequency ultrasound results in proportionally greater energy deposition within the stratum corneum such that this layer is permeabilised to drug diffusion by cavitational damage (Bommannan *et al.*, 1992a, Bommannan *et al.*, 1992b). The authors used 2, 10 and 16MHz frequencies at 0.2W cm^{-2} although there is no detailed reference to calibration of the ultrasound source nor the mode used. Following sonication of guinea pig skin at both 10 and 16 MHz, electron microscopy revealed altered cellular morphology in the stratum corneum. Evidence for transient cavitation was shown as voids within cell tissues. The diameter of these voids was 4μm. It is unlikely, however, that the process is transient cavitation as its threshold increases dramatically at the high frequencies employed in the study. The changes in the stratum corneum are probably caused by some other mechanism such as acoustic microstreaming.

Although phonophoretic ultrasound is unlikely to generate transient cavitation within skin, the production of stable cavitation is a possibility. The occurrence of stable cavitation has been reported within several mammalian tissues *in vivo* (Williams, 1983). One team (ter Haar and Daniels, 1981; ter Haar *et al.*, 1982) demonstrated that a 0.75MHz c.w. beam induced stable gas bubbles to grow within the hind leg tissues of anaesthetised guinea pigs. Cavitation first developed at an intensity of 0.08W cm^{-2} and progressively greater numbers of bubbles were detected as the intensity was increased to 0.68W cm^{-2}. The bubbles mainly formed at the boundaries between the muscle bundles and within the fatty tissues. By analysing the frequency of the ultrasound reflected back by the cavities, the workers showed that the bubbles were undergoing volume-pulsations in the acoustic field. This indicates that the process was stable cavitation and not merely thermal out-gassing of the tissue. Another group found evidence of stable cavitation in various irradiated animal tissues at intensities as low as 0.1W cm^{-2} at 2.7MHz (Lele, 1978). It is probable that stable cavitation also develops within skin at these intensities and frequencies

The effects of pulsating gas bubbles on skin morphology remain unknown. Calculating from highly theoretical assumptions, one reviewer concluded that phonophoretic ultrasound is unlikely to generate sufficient stable cavitation within the stratum corneum so as to modify its structure (Simonin, 1995). However, without experimental evidence, this possibility cannot be excluded. There is a need for further work in this area where calibration of the source and better understanding of the potential biophysical interaction of the cavitational process is brought to bear on experimental design.

1.4 PHONOPHORESIS OF DIFFERENT COMPOUNDS

1.4.1 *In Vitro* Phonophoresis

In order to gain a greater understanding of the parameters which may influence phonophoresis, workers have conducted *in vitro* experiments using modified diffusion cells. The advantage of these systems is that a more controlled environment can be developed in which the key variables can be more precisely identified, measured, and controlled. Some researchers have attempted to minimise or control for ultrasonic heating (Al Suwayeh and Hikal, 1991; Brucks *et al.*, 1989; Pelucio-Lopes *et al.*, 1993) whilst others have not (Kost *et al.*, 1986; Nanavaty *et al.*, 1989; Pinton *et al.*, 1991; Machluf and Kost, 1993; Mitragotri *et al.*, 1995b; Ueda *et al.*,1995). Many different drug formulations have been used for *in vitro* work and a brief description of each type and the results obtained are outlined below.

1.4.1.1 Ibuprofen

One research group investigated ibuprofen phonophoresis using modified Franz-type equipment in which a stationary transducer was positioned inside each donor cell (Brucks *et al.*, 1989). A protocol was developed in which strips of human epidermis were sonicated for 30 minutes at both time zero and at 6 hours. 1MHz c.w. ultrasound was used at an intensity of 1W cm^{-2}. In order to control for ultrasonic heating, two controls were employed: one with no ultrasound and another where heat alone (simulating the ultrasonic heating profile) was applied. The penetration of [^{14}C]-ibuprofen was determined by scintillation counting of samples taken from the receptor solution.

It was found that ultrasound enhanced ibuprofen permeation through human epidermis to a greater extent than a control representing comparative heating effects with no ultrasound. Furthermore, the workers claimed that this real phonophoretic effect was associated with no permanent epidermal damage. This was deduced from two different observations. Firstly, the increase in ibuprofen transport developed at the beginning of the experiment only when ultrasound or heat was applied and remained for 10 minutes after the energy source was switched off. After this time period, drug transport in each of the three protocols was virtually the same. In addition, the measured skin temperature increases

induced by sonication did not visually damage the skin and were not of a magnitude that would be expected from theory to be destructive to tissue.

Interestingly, the lag time of drug delivery was not reduced in either the ultrasound or heat application controls. This contradicts the findings from *in vivo* research with rats and guinea pigs (Kost *et al.*, 1986; Levy *et al.*, 1989). Brucks and co-workers have proposed that ultrasound could enhance drug penetration through hair follicles to a greater extent than through the bulk stratum corneum. The greater number of hair follicles in animal skin as compared to the human breast samples could therefore explain this discrepancy.

An observation of this *in vitro* research was that the phonophoretic effect was less pronounced when the skin/vehicle partition coefficient was reduced following the evaporation of aqueous vehicle components. Unfortunately, the authors did not explore this issue further by actually making measurements of partition coefficient changes. This study may be criticised for having several technical shortcomings which perhaps cast doubt on some of the conclusions reached by the authors. For example, the distance between the transducer and epidermis sample was not stated while the skin temperature may have been not adequately monitored as the thermocouple was placed behind the epidermis. In addition, the calibration of the ultrasound source was not measured and the likely possibility of standing wave production was not explored.

The same group of investigators have also examined *in vitro* the effect of sonication on the structure of the epidermis (Nanavaty *et al.*, 1989). Human epidermis was irradiated with 2W cm^{-2}, 1MHz c.w. ultrasound for 30 minutes. The technique of Attenuated Total Reflectance Fourier Transform Infrared Spectroscopy (ATR-FTIR) was employed to compare sonicated epidermis with non-sonicated epidermis. No control of ultrasonic heating effects was reportedly carried out in this study. Ultrasound induced no major irreversible changes in the epidermis samples but it did cause minor conformational changes in either stratum corneum lipids and / or proteins.

Ibuprofen phonophoresis has been examined more recently by another group of workers who used abdominal sections of whole hairless rat skin as barrier membranes (Ueda *et al.*, 1995). High-Performance Liquid Chromatography was used as the analytical technique. 0.15MHz Ultrasound was applied as a c.w. beam

exhibiting an intensity of 2W cm^{-2}. In this model, no attempt was made to control for ultrasonic heating. It was demonstrated that during the 1 hour period of sonication, the mean ibuprofen flux more than doubled before returning to normal when the beam was switched off. Unfortunately, the statistical significance of this change is unclear from the literature report.

4.1.1.2 Indomethacin

Indomethacin was applied *in vitro* to hairless mouse skin cut from both the thoracic and abdominal areas (Al-Suwayeh and Hikal, 1991) although the authors did not report whether they used full thickness skin samples. The influence of 15 minutes of 0.48W cm^{-2} c.w. ultrasound at 1MHz on indomethacin penetration was investigated by UV. The donor compartment was maintained at pH=6 whilst the receptor compartment was at pH=7.4 thus simulating the *in vivo* pH gradient. Crucially, ultrasonic heating was minimised by circulating and maintaining both donor and receptor solutions at 37°C. It was reported that indomethacin permeation was increased by 113% during the phonophoresis as compared to the flux of drug before ultrasound exposure. The researchers also examined the system for synergism between phonophoresis and chemical enhancers. In the non-sonicated system, the addition of 5% ethanol or 50% DMSO did not affect indomethacin transport. However, these chemicals did promote drug penetration when combined with ultrasound but it is unclear if this was statistically significant.

1.4.1.3 Azidothymidine

One research team examined the effect of 1.1MHz c.w. ultrasound on the percutaneous absorption of the virustatic agent, azidothymidine (Pelucio-Lopes *et al.*, 1993). Both whole dorsal hairless mouse skin and whole abdominal human skin were employed as the barrier membranes. Notably, the thermal effects of ultrasound were suppressed by circulating cold water in specially jacketted donor cells. Quantitative analysis was performed by radioimmunoassay. For both types of skin, the application of 1.5W cm^{-2} ultrasound for 20 minutes did not significantly affect azidothymidine penetration.

1.4.1.4 Caffeine

One group of workers investigated caffeine permeation through full-thickness hairless mouse skin (Machluf and Kost, 1993). 1MHz pulsed ultrasound was

applied for 3 hours at an intensity of 3W cm^{-2}. There was no attempt made to minimise ultrasonic heating of the skin surface. Caffeine concentrations in the receptor compartment were determined by HPLC. It was found that sonication almost doubled mean drug permeation and that the effect was statistically significant. Varying the pH of the donor solution did not significantly affect the magnitude of ultrasonic enhancement. Interestingly, enhanced flux was observed even after the ultrasound had been switched off, thus indicating that the barrier had undergone irreversible structural changes. However, these could not be detected by either DSC or FTIR analysis.

One research team has recently examined the influence of ultrasound on caffeine permeation through human epidermis (Mitragotri *et al.*, 1995b). The ultrasonic energy was in the form of a 1MHz c.w. beam exhibiting an intensity of 2W cm^{-2}. Sonication lasted for 20 hours and it induced a 7°C increase in the equilibrium temperature of the cell solutions. The concentrations of radiolabelled caffeine within the receptor compartment were determined from liquid scintillation counting. It was determined that ultrasound exposure led to an insignificant increase in caffeine permeation.

1.4.1.5 Hydrocortisone

Hydrocortisone phonophoresis through whole sections of hairless mouse skin has been documented in recent *in vitro* studies (Machluf and Kost, 1993). These workers did not attempt to minimise ultrasonic heating at the skin surface. Liquid scintillation counting was employed as the analytical method. The authors reported a duration-responsive effect when a 1MHz pulsed beam was applied at an intensity of 3W cm^{-2}. Whilst 30 minutes of sonication did not affect hydrocortisone flux, sonication for 1.5 hours or more produced significant flux enhancement which persisted even after the energy had been switched off. Remarkably, DSC and FTIR analysis failed to reveal any perturbations of the stratum corneum structure.

1.4.1.6 Antipyrine

In diffusion experiments, it was shown that 0.15MHz ultrasound significantly enhanced antipyrine permeation through whole hairless rat skin by approximately 8 times (Ueda *et al.*, 1995). The ultrasound was irradiated for 1 hour in c.w. mode at an intensity of 2W cm^{-2}. Sonication increased the donor solution temperature

by 4°C. Interestingly, the high rate of penetration was maintained even after the ultrasound had been switched off. Unfortunately, the workers did not histologically analyse the rat skin in order to assess the integrity of the stratum corneum. HPLC was used to measure antipyrine concentrations.

1.4.1.7 Isosorbide dinitrate

In similar rat experiments with isosorbide dinitrate, 0.15MHz c.w. ultrasound was irradiated at whole skin at an intensity of 2W cm^{-2} for 1 hour (Ueda *et al.*, 1995). HPLC was employed as the analytical technique. Sonication significantly enhanced drug flux by over 4-fold. When the beam was switched off, the mean drug flux fell so that it was now double of its original control value. Again, there were no available data on the status of the horny layer.

1.4.1.8 Digoxin

An intensity-drug flux response has been demonstrated by another research team also employing a modified Franz diffusion cell system. (Pinton *et al.*, 1991). Liquid scintillation counting was used to monitor the diffusion of tritiated digoxin through hairless mouse skin under the influence of 10 minutes 3.3MHz c.w. ultrasound. However, these workers did not attempt any control of ultrasonic heating. Sonication at 3W cm^{-2} resulted in increased drug permeation but application of 1W cm^{-2} ultrasound did not. The authors speculated that this may be due to thermal and / or cavitational effects.

1.4.1.9 Mannitol

One group has demonstrated successful *in vitro* phonophoresis of tritiated mannitol through animal skin (Kost *et al.*, 1986). Dorsal skin samples obtained from rats and hairless mice were placed in a diffusion cell system with the stratum corneum facing a donor solution of tritiated mannitol. Ultrasound was irradiated for 2 hours at a frequency of 0.075MHz. It was determined that, compared to a non-sonicated control, ultrasound enhanced permeation in both rat and mouse skin. Again, no control of ultrasonic heating was attempted but more fundamentally the intensity and mode of the applied ultrasound was not reported.

1.4.2 *In Vivo* Phonophoresis: The Evidence from Animal Studies

In contrast to work with human volunteers, animal studies can involve the use of more invasive techniques such as tissue excision to derive more information about the nature and mechanisms involved in ultrasound-enhanced delivery. Numerous phonophoresis animal studies have been carried out over the last 30 years, especially in Eastern Europe (Mayev, 1985). However, in this section, emphasis has been placed on the original work of the 1960's as well as the most recent well-controlled studies. Several different agents have been used and these will be discussed in turn.

1.4.2.1 Hydrocortisone

In the 1960's, Griffin and co-workers conducted a series of studies investigating the effect of ultrasound on hydrocortisone delivery through mammalian skin. In their first trial, a hydrocortisone-containing ointment was applied to the shaved paravertebral skin areas of anaesthetised male pigs. Continuous wave 1MHz ultrasound was then applied for 5 minutes at intensities of both 1W cm^{-2} and 3W cm^{-2} (Griffin and Touchstone, 1963). The authors concluded that it was possible to drive hydrocortisone ultrasonically into the underlying muscle. In similar further work, the authors stated that hydrocortisone could be delivered to nerve structures by phonophoresis (Griffin *et al.*, 1965). In addition, it was claimed that more drug could be delivered to the underlying nerves and muscle by employing a low-intensity long-duration exposure rather than a high-intensity low-duration exposure (Griffin and Touchstone, 1968). A frequency of 0.25MHz was stated to be the most effective for hydrocortisone phonophoresis into muscle and nerve (Griffin and Touchstone, 1972). All these results have generated considerable publicity and interest in phonophoresis over the years (Quillen, 1980; Quillen, 1982; Antich, 1982). However, since 1963 many other researchers have criticised these findings (Williams, 1990). It has been suggested that the chemical assay system employed was inherently variable and consequently, the given results could have been obtained simply by statistical chance. Since the original study did not report information on errors, it is difficult to refute these criticisms.

Hydrocortisone phonophoresis has been examined more recently in a trial involving 15 mongrel dogs (Davick *et al.*, 1988). Samples of cream containing 5% and 10% tritiated hydrocortisone were applied separately to the surface of the medial aspect of the knee of the animals. 0.5W cm^{-2} c.w. ultrasound was applied

at 0.87MHz for 8 minutes. A non-sonicated drug application acted as a placebo. The treated skin site was then completely excised and processed so that autoradiography could be used to quantify the presence of hydrocortisone. The application of 10% hydrocortisone with ultrasound resulted in significantly more drug penetration into the viable epidermis than 10% hydrocortisone alone. For the five sonicated animals, hydrocortisone was detected on average in 3.44% of the cells in the viable epidermis as opposed to no steroid detected in three out of four control animals (in one of the control dogs, hydrocortisone was detected in 0.48% of the viable epidermal cells). Unfortunately, no control of induced heating was undertaken in this study. Consequently, the observed increase in drug permeation may have been a purely thermal effect and not necessarily ultrasound specific. Furthermore, as the work was conducted on mongrel dogs, it is likely that the knee dimensions differed between individual animals and this is a major limitation of this study.

The penetration of hydrocortisone into canine knee has also been assessed by Muir and co-workers in a refined study involving 24 pure bred greyhounds (Muir *et al.*, 1990). 2.75W cm^{-2} ultrasonic energy at 1 MHz frequency was beamed to the surface of canine joints through a layer of ultrasonic coupling gel containing 10% hydrocortisone. Fluorescence polarisation was used as the analytical technique. No statistically significant differences were found between phonophoretic applications and non-sonicated control treatments.

1.4.2.2 Mannitol

The effect of ultrasound on the transdermal transport of mannitol through shaved dorsal rat skin has been examined (Levy *et al.*, 1989) using a moving ultrasonic applicator (1 MHz) and operated at an intensity of 1.5W cm^{-2} c.w. for 3 minutes. The permeation of tritiated mannitol was determined by liquid scintillation counting of the urine. In an important step, ultrasonic heating was evaluated by placing a temperature probe on the treated surface sites immediately after sonication. Ultrasound was found to enhance mannitol absorption by about 11 times compared to a non-sonicated control, within 2 hours following treatment. Another effect due to ultrasound was a shortening of the lag time. Sonication increased skin surface temperatures by not more than 1-2°C and consequently cavitation and acoustic microcurrents in the skin were claimed to have caused the promoted drug flux.

1.4.2.3 Inulin

In similar rat experiments with inulin - a high molecular weight polysaccharide, 1MHz pulsed ultrasound was applied to the skin at an intensity of 3W cm^{-2} for 5 minutes (Levy *et al.*, 1989). During the first hour, the secretion rate of tritiated inulin was 5-fold higher in the ultrasound-treated group than in the controls. Phonophoretic treatment shortened the lag phase period and caused only small increases in skin surface temperature. Histological evaluation showed no visible differences between ultrasound-exposed and control skin. Again, the authors stated that microstreaming and / or cavitational changes in the skin caused the enhanced delivery.

1.4.2.4 Physostigmine

The use of pulsed 1MHz ultrasound at 3W cm^{-2} for 5 minutes has also been shown to significantly promote the dorsal topical absorption in both rats and guinea pigs of physostigmine - a lipophilic anticholinesterase (Levy *et al.*, 1989). Reduced lag times were observed in the guinea pigs but not in the rats where physostigmine absorption was very rapid. The reversible nature of the ultrasound enhancement was deduced from the observation that sonication of guinea pigs 1 hour before drug application did not alter the penetration rate of physostigmine through the skin. Also, the absorption rate of physostigmine in guinea pigs 5 hours after sonication was the same in both the treated animals and controls, as opposed to the large difference in absorption rate detected just after sonication.

1.4.2.5 Salicylic acid and Lanthanum hydroxide at High Frequencies

The hairless guinea pig model has been employed to investigate the *in vivo* phonophoresis of salicylic acid (Bommannan *et al.*, 1992b). A gel containing [^{14}C] salicylic acid acted as a coupling agent between the transducer and treatment site. 0.2W cm^{-2} c.w. ultrasound was then applied at frequencies of 2, 10, and 16MHz for 5 or 20 minutes. Drug absorption was quantified by the amount of radiolabelled salicylic acid present in stratum corneum tape strips and urine. Sonication for 20 minutes at 2MHz induced no significant increase in salicylic acid penetration over passive diffusion. However, ultrasound treatment at 10 and 16MHz did significantly promote drug permeation by 4-fold and 2.5-fold respectively. The lag time was also reduced with these frequencies. A shorter 5 minute period of sonication at the higher frequencies also resulted in enhanced drug delivery as compared to the control although the degree of enhancement was

lower than the 20 minute treatment. When the skin sites were pre-sonicated at 10 and 16 MHz and then subsequently exposed to the drug, enhanced delivery was also observed indicating that the phonophoretic effect was not immediately reversible.

In a homogeneous medium, high-frequency ultrasound will be attenuated over much shorter distances than lower frequency ultrasound (Williams, 1983). These researchers explained the effectiveness of high frequency ultrasound in terms of this protocol leading to proportionally greater energy deposition in the stratum corneum, thus permeabilising it. However, the authors did not fully substantiate this idea since the skin represents an acoustically heterogeneous medium. Furthermore, the groups' finding that surface skin temperature increased by not more than 1°C during sonication to some extent casts doubt on this assumption.

In a follow-up study (Bommannan *et al.*, 1992a), an identical ultrasound protocol was used to determine the nature of the phonophoretic mechanism. Transmission electron microscopy was used to track the skin permeation of the electron-dense tracer colloidal lanthanum hydroxide. Under non-sonicated conditions, the tracer was found not to penetrate the stratum corneum. However, at higher frequencies, the penetration of tracer by an intercellular route through the epidermis to the upper dermis was observed. This enhancement of drug delivery was not associated with any adverse cellular morphology except at the highest frequency (16MHz) for the longest time period (20 minutes). Since surface skin temperature increases of not more than 1°C were measured, the authors concluded that cavitational processes must be inducing the detrimental observations. However, as discussed in section 1.3.5, it is highly unlikely that the requisite transient cavitation will develop at such intensity and frequency in mammalian tissues. Therefore, other mechanical effects must be responsible.

One recent study has reported the effect of 5 minutes of 0.1W cm^{-2} ultrasound at 15MHz on hairless mouse skin (Menon *et al.*, 1994a). Skin biopsies were taken immediately after irradiation, as well as after 24, 48 and 96 hours, and examined by electron microscopy. Ruthenium tetroxide staining was used to investigate stratum corneum lamellar bilayer structure. Ultrasound was found to alter the usually compact structural organisation of lamellar body derived contents at the stratum granulosum-stratum corneum cell interface, producing distinct domain separation. These changes were present in the 24 h samples but not in the 48 and

96 h samples which were comparable to the non-sonicated controls. The authors noted the potential therapeutic significance of the reversible nature of the ultrasound effect. It was concluded that lamellar phase separation of stratum corneum lipids may be responsible for the phonophoretically enhanced penetration of colloidal lanthanum previously reported. These perturbations may be caused by radiation pressure forces or microstreaming.

In further work with this model (Menon *et al.*, 1994b), the investigators applied 15MHz ultrasound to the skin of anesthetised hairless mice. Two types of experiments were performed. In one version, the donor solution consisted of a physiological solution of calcium ions whilst in the other version the donor solution was ion-free. The workers used ion capture cytochemistry to examine the extracellular calcium ion gradient throughout the epidermis. Sonication in the absence of calcium ions resulted in a disrupted gradient caused by the downward displacement of calcium ions. This promoted lamellar body secretion from the upper stratum granulosum. In contrast, following phonophoresis of calcium-containing solutions, the gradient became obscured by excess calcium ions at all levels of the epidermis. This inhibited lamellar body secretion. Significantly, all these changes were not associated with a loss of barrier function as evaluated by transepidermal water loss measurements.

1.4.2.6 Insulin

In the *in vivo* studies discussed so far, ultrasonic heating may have been monitored but not controlled. One Japanese research team developed an ingenious method in order to minimise ultrasonic heating in their experiments with insulin (Tachibana and Tachibana, 1988; Tachibana and Tachibana, 1991). Fasted, hairless mice were partially immersed in a 100ml aqueous solution of 20U ml^{-1} insulin. The animals were then exposed for 5 minutes to 0.048MHz ultrasound at one of two intensity ranges (0.3 to 0.83W cm^{-2} and 0.83 to 2.13W cm^{-2}). The ultrasound mode was not stated but was presumably c.w. The exact intensity being irradiated on to each individual animal was measured by a hydrophone fixed beside each mouse. The controls consisted of insulin immersion with no ultrasound, saline immersion with no ultrasound, and saline immersion with ultrasound. Crucially, all the solutions were at a temperature of 37°C. Drug delivery was evaluated by glucose analysis of blood samples. Compared to the controls, ultrasound plus insulin immersion resulted in statistically significant reductions in blood glucose concentrations which persisted for 4 hours. The plasma glucose level decrease was more pronounced at

the higher intensity application indicating that the intensity parameter may control permeation.

One of the disadvantages of this study is that water itself acts as a potent transdermal enhancer. Consequently, another more conventional phonophoresis study with insulin was carried out (Tachibana, 1992). A metal cup that was attached to the ultrasonic transducer was filled with 3ml of 40U ml^{-1} insulin solution and placed on the skin sites of anaesthetised diabetic rabbits. Ultrasound (0.83W cm^{-2}, 0.105MHz) was then irradiated on to the skin site in pulsed 5s on, 5s off mode. The treatment period was 90 minutes. The transducer and drug reservoir employed were kept at 4°C representing only some control over ultrasound-induced heating. Drug absorption was evaluated by insulin and glucose analysis of blood samples taken in the 6 successive hours following sonication and the authors deduced that ultrasound enhanced the absorption of insulin and decreased blood glucose levels to a statistically significant extent. Furthermore, microscopic analysis of treated skin biopsy specimens indicated that no histological changes had been induced and that the stratum corneum was intact.

In recent experiments with hairless mice, Mitragotri and co-workers reported that the application of 0.02MHz ultrasound enhanced the percutaneous absorption of insulin (Mitragotri *et al.*, 1995a). A pulsed beam, exhibiting an intensity of 0.225W cm^{-2} was directed at the skin for periods of up to 1 hour. The workers assessed enhancement from measurements of blood glucose concentrations. The authors claimed that the process was not associated with any histological alterations to the skin structure.

Despite the above reports, insulin is unlikely to penetrate the skin barrier without substantial enhancement. The above findings can be explained by ultrasound totally damaging small, isolated regions of exposed stratum corneum. The eosin and haematoxylin staining techniques employed by these researchers are generally insensitive indicators for such localised alterations in structure. Alternatively, ultrasonic waves could be directly causing changes to the islets of Langerhans.

1.4.2.7 Indomethacin

Indomethacin phonophoresis has been investigated by Miyazaki and co-workers in a series of studies (Miyazaki *et al.*, 1991a; Miyazaki *et al.*, 1991b; Miyazaki *et al.*,

1992b). In these experiments, 1 g of 1% indomethacin ointment was applied to the shaved abdominal areas of anaesthetised Wistar rats. 1MHz c.w. ultrasound was then directed at the treated area for between 5 and 20 minutes with a range of intensities (0.25, 0.5, 0.75, and 1W cm^{-2}). Control animals underwent the same procedure except that the ultrasound transducer was not applied. Blood samples were taken by cardiac puncture in the hours following phonophoresis and indomethacin levels were quantified by HPLC. Both skin surface temperature and hypodermis temperature were monitored during the experiment. In addition, microscopic evaluation of excised skin samples were undertaken following their exposure to phonophoresis. It was found that 0.75W cm^{-2} was the intensity that induced the greatest absorption enhancement, whilst 10 minutes irradiation was the optimal duration for phonophoresis. However, the authors suggested that 0.5W cm^{-2} was the preferred intensity since its application for 10 minutes did not cause marked skin temperature increases or any significant skin tissue damage. With this protocol, indomethacin delivery was enhanced 2.7 times relative to the control.

Progressively worsening skin damage was observed as the intensity and duration of ultrasound administration were increased. Thus, sonication at 1W cm^{-2} for 10 minutes resulted in large scale degeneration and necrosis throughout all the strata of the skin. The authors proposed that this damage at 1W cm^{-2} reduces skin permeability and explains why this intensity is not as phonophoretically effective as 0.75W cm^{-2} This is despite the fact that damage generally reduces the effectiveness of the skin as a barrier.

In further work with the same model (Miyazaki *et al.*, 1992a), the effect of 1:3 pulsed output was examined, again at different intensities and durations. Pulsed ultrasound was found to be less effective as an enhancer than the same energy delivered in continuous mode. This is probably due to the pulsed mode causing less tissue heating. In a key step, the experimenters investigated the effect of heat alone on indomethacin penetration. The skin was heated in such a way as to simulate the ultrasonically induced time-temperature profile in the hypodermis. This heating did not influence indomethacin absorption. Consequently, the authors suggested that a non-thermal mechanism was causing the phonophoresis. However, one major limitation of this method is that ultrasonic heating may have developed in the stratum corneum.

The above results somewhat contradict the findings of another indomethacin study where phonophoresis was not observed (Pratzel *et al.*, 1986). These workers applied indomethacin gel to the shaven backs of anaesthetised pigs. Over a 5 hour period, ultrasound at 1W cm^{-2} was administered for 30 minutes at the start of the experiment and subsequently for 10 minutes at 30 minute intervals. The whole experiment lasted for 5 hours. Since the ultrasound mode and frequency were not stated, it is difficult to compare the results but such differences in these parameters may explain the discrepancies.

1.4.2.8 Amphotericin B

In order to assess the effectiveness of phonophoresis, one research team compared ultrasound with an established chemical enhancer (Romanenko and Aravisky, 1991). Amphotericin B ointment was applied to the sides of 24 shaved guinea pigs *in vivo*. The first group of animals were subjected to 1W cm^{-2} ultrasound at 2.64MHz for 15 minutes at both continuous and pulsed mode. A control group of animals were treated with amphotericin B without ultrasound. A third group of guinea pigs received applications of dimethylsulphoxide followed by amphotericin. Ultrasound-induced heating was not monitored or controlled. The skin and subcutaneous fatty tissues were sampled at regular time intervals up to 72 hours after treatments. Diffusion in agar with test cultivation of Candida utilis was employed as the analytic technique. It was found that, compared to the control treatment, both dimethylsulphoxide pre-treatment and phonophoresis resulted in enhanced amphotericin penetration. DMSO treatment was a better enhancer than phonophoresis during the first 48 hours but phonophoresis was more effective in maintaining amphotericin levels after this period. The results from this study lead to the idea of combining phonophoresis and DMSO in order to improve drug delivery further.

1.4.3. *In Vivo* Phonophoresis: The Evidence from Human Volunteer Studies

Most human volunteer trials have been conducted on an extremely subjective and non-quantitative basis. For example, in some reports, at least some of the parameters of the applied ultrasound beam have not been stated (Cameroy, 1966; Chaterjee, 1977; Antich *et al.*, 1986; Halle *et al.*, 1986; Moldover and Danish,

1986; Stratford *et al.*, 1989; Roques *et al.*, 1992). Other authors have omitted to conduct controls (Coodley, 1960; Kahn, 1980; Wing, 1982; Smith *et al.*, 1986).

In one trial involving 102 arthritic patients (Griffin *et al.*, 1967), hydrocortisone with 1MHz ultrasound was compared to 1MHz ultrasound alone. Treatment efficacy was evaluated by pain and range of motion criteria that assessed limb movement. It was determined that the combination of ultrasound plus steroid was more effective than ultrasound alone ($P=0.001$, χ^2 test). In a retrospective study of 285 patients treated for several different types of inflammatory conditions (Kleinkort and Wood, 1975), the authors compared 1MHz ultrasound plus 10% hydrocortisone versus 1 MHz ultrasound plus 1% hydrocortisone. Statistical analysis indicated that phonophoresis of 10% steroid was superior to phonophoresis of 1% steroid. However, in both studies, there were no non-sonicated control groups and the beam intensity was varied according to individual patient tolerance. Moll divided 52 patients, each suffering from various painful conditions, into 3 groups (Moll, 1977). One group received 0.87MHz ultrasound together with a gel containing 32 mg of dexamethasone and 60 ml of 2% lignocaine jelly. Another group was treated with ultrasound plus a placebo whilst yet a third group received sham ultrasound with placebo gel. It was found that the use of lignocaine and dexamethasone with ultrasound was the most beneficial protocol but much larger scale trials would be required in order to establish conclusive statistical significance.

In recent years, a range of superior studies has been conducted by McElnay and co-workers. In one trial (McElnay *et al.*, 1985a; McElnay *et al.*, 1987), 3 g of 0.025% fluocinolone acetonide gel was applied to the flexor surface of the forearms of 12 human volunteers. 2W cm^{-2} pulsed output ultrasound at 0.87MHz was administered for 5 minutes. The study was of a double blind, sham ultrasound controlled, cross-over nature. The skin blanching test was used to evaluate drug absorption. It was found that ultrasound treatment resulted in significantly enhanced steroid penetration. Unfortunately, the magnitude of the effect was small and as such it is not likely to result in greater therapeutic efficacy in the clinical setting.

Similarly controlled studies on lignocaine phonophoresis in human forearm skin have been conducted using a 2W cm^{-2} pulsed output at 0.87MHz for 5 minutes (McElnay *et al.*, 1985b). Compared to non-sonicated applications of drug, a

statistically insignificant increase in anaesthesia onset rate was reported when ultrasound energy was applied. In sequential work with a cream containing both lignocaine and prilocaine (Benson *et al.*, 1988), these workers identified a significant increase in anaesthesia duration.

This group (Benson *et al.*, 1991) also investigated the influence of 5 minutes of 1W cm^{-2}, 3MHz c.w. ultrasound on the percutaneous absorption of ethyl nicotinate, methyl nicotinate, and hexyl nicotinate across human forearm skin. The workers employed laser Doppler velocimetry in order to measure nicotinate absorption. All three nicotinate esters were found to undergo ultrasound-enhanced delivery, though for hexyl nicotinate the difference was not statistically significant. In further trials with methyl and hexyl nicotinates (Murphy and Hadgraft, 1990), a method of sonication followed by drug application was compared to drug application followed by sonication. For hexyl nicotinate, which is more lipophilic, the rate-limiting step was assumed to be partitioning from the lipid-rich stratum corneum. This process was not affected by ultrasound pre-treatment but was enhanced by ultrasound postreatment. The authors suggested that ultrasound may be able to enhance the rate of partitioning of drug out of the intercellular lipids once a reservoir has been formed. For methyl nicotinate, the major barrier to penetration are the structured stratum corneum lipids and thus both ultrasonic treatments similarly enhanced methyl nicotinate absorption. The authors postulated that this may be due to the fluidisation of the stratum corneum lipids by ultrasound.

One research team has demonstrated successful phonophoresis of benzyl nicotinate through human skin (Hofmann and Moll, 1993). The workers employed a reflection photometry method to measure the skin reddening effect caused by benzyl nicotinate. The lag time of drug delivery was significantly reduced by the application of a 0.5W cm^{-2} c.w. beam. Unfortunately, the authors did not state the ultrasonic frequency of their equipment.

In other double-blind, placebo-controlled trials (Benson *et al.*, 1986; Benson *et al.*, 1989), these workers evaluated the effect of ultrasound at different modes, intensities and frequencies on benzydamine absorption. It was found that sonication did not influence benzydamine absorption across human flexor surface skin. Negative findings have also been reported in attempts to phonophoretically deliver trolamine salicylate (Oziomek *et al.*, 1991).

In all of the above trials, ultrasonic heating was not monitored or controlled thus yielding no information on the mechanisms involved in any observed phonophoresis. One research team developed a sensory perception method in which anaesthetic absorption could be reproducibly quantified by measuring the pain threshold associated with an applied small electric shock (Williams, 1987). In a follow up study (Williams, 1990), this system was used to determine the effect of 50 min of 0.25W cm^{-2}, 1.1MHz ultrasound on the penetration of Americaine, containing 20% benzocaine and 0.1% benzethonium; Emla cream, containing 2.5% lignocaine and 2.5% prilocaine; and Nupercainal containing 1% dibucaine. A water path maintained at 37°C was placed between the transducer and skin in order to minimise the thermal effects of sonication. It was found that ultrasound induced no detectable effects upon the penetration rates of any of the agents tested.

1.4.4 Summary

A summarised compilation of important studies is presented in Table 1.2 Only those which have incorporated adequate controls and a comprehensive account of the applied ultrasonic protocols have been included. The enhancement values represent the percentage increase over the control value so that 100% enhancement indicates a doubling in drug absorption as measured by the appropriate end-point. Where a research group has conducted more than one method or experimental type, the enhancement figure listed is the maximal value obtained using the most optimal conditions. It can be seen that due to the multiplicity of drugs, methods, models and end-point evaluation techniques used, it is difficult to discern any trends between ultrasonic frequency, intensity, molecular structure and the degree of enhancement. In preliminary work, I have attempted to fit various mathematical models to these data but no meaningful relationship could be found between the ultrasonic / molecular parameters and the magnitude of the enhancement effect.

Table 1.2: A summary of the findings from the phonophoretic literature

Compound	Molecular mass (Da)	f (MHz)	Intensity (W cm^{-2})	% maximal enhancement	End-point evaluation	Reference
Amphotericin B	945	2.64	1 (P)	36	skin concentrations 1h after application	Romanenko and Aravisky, 1991
Antipyrene	188	0.15	2	742	mean flux	Ueda *et al.*, 1995
Azidothymidine	267.2	1.14	1.5[a]	0	mean flux	Pelucio-Lopes *et al.*, 1993
Benzocaine / benzethonium chloride	165.2/ 448.1	1.1	0.25[a]	0	electrical sensory perception	Williams, 1990
Benzydamine HCl	345.9	0.75	1.5	0	residual amounts in vehicle	Benson *et al.*, 1989
		1.5	1.5	0		
		3	1.5	0		
Caffeine	194	1	3 (P)	92	mean flux	Machluf and Kost, 1993
		1	2	0	mean flux	Mitragotri *et al.*, 1995b
Dibucaine	379.9	1.1	0.25a	0	electrical sensory perception	Williams, 1990
Ethyl nicotinate	151.2	3	1	79	AUC vasodilation from LDV	Benson *et al.*, 1991
Fluocinolone acetonide	425.5	0.87	2 (P)	32	AUC from skin blanching	McElnay *et al.*, 1987
Hexyl nicotinate	207.3	3	1	0	AUC vasodilation from LDV	Benson *et al.*, 1991
Hydrocortisone	362.5	0.87	1	272	liver concentrations 30 min after application	Gatev, 1970
		0.87	0.5	617	epidermal cell radiograph	Davick *et al.*, 1988
		1	2.75	0	blood concentrations 10min after application	Muir *et al.*, 1990
		1	3 (P)	17	mean flux	Machluf and Kost, 1993
Ibuprofen	206.3	1	1	82	flux rate over 30min	Brucks *et al.*, 1989
Indomethacin	357.8	1	0.75	240	AUC blood concentrations	Miyazaki *et al.*, 1992
		1	0.48[a]	113	mean flux over 90min	Al-Suwayeh and Hikal, 1991

Compound	Molecular mass (Da)	f (MHz)	Intensity (W cm^{-2})	% maximal enhancement	End-point evaluation	Reference
Insulin	≈6000	0.105	0.83[a]	684	maximum blood concentration during experiment	Tachibana, 1992
Inulin	≈5200	1	3 (P)	400	urinary secretion	Levy *et al.*, 1989
Isosorbide dinitrate	236.1	0.15	2	319	mean flux	Ueda *et al.*, 1995
Lignocaine	288.8	0.87	2 (P)	0	time to onset of anaesthesia	McElnay *et al.*, 1985b
Lignocaine / prilocaine	288.8 / 257	1.1	0.25[a]	0	electrical sensory perception	Williams, 1990
		1.5	1 (P)	56	time to total sensation recovery	Benson *et al.*, 1988
		3	1 (P)	101	time to partial sensation recovery	Benson *et al.*, 1988
Mannitol	182.2	1	1.5	10200	urinary secretion	Levy *et al.*, 1989
Methyl nicotinate	137.1	3	1	59	AUC vasodilation from LDV	Benson *et al.*, 1991
		3	1	104	AUC vasodilation from LDV	McElnay *et al.*, 1993
Salicylic acid	138.1	2	0.2	0	stratum corneum concentration from tape strips	Bommannan *et al.*, 1992b
		10	0.2	315		
		16	0.2	153		

[a] denotes that controlling for thermal effects was conducted by minimising ultrasonic heating. P denotes pulsed ultrasound otherwise c.w. mode ultrasound

It can be seen that the most dramatic enhancement effects have been documented with molecules that are either too large (inulin, insulin) or too hydrophilic (mannitol) to normally permeate through the stratum corneum - perhaps suggesting that transfollicular pathways are more susceptible to ultrasonic enhancement than are transcellular processes. However, these observations have not been confirmed elsewhere and they may be due to poor experimental design such as animal ingestion of the applied substance, or direct ultrasonic effects on pancreatic activity in the case of insulin.

Nevertheless, there are a large number of studies which report modest but significant enhancement for drugs that can normally penetrate the skin. This indicates that phonophoresis is indeed a reality for certain molecules under specific conditions. The main component of phonophoresis is ultrasonic heating. It has been established that a skin surface temperature increase of 10°C will double water permeability and enhance the absorption of a range of substances by between 1.4 and 3 times *in vivo* (Scheuplein, 1978a). Ultrasonic heating on a smaller magnitude is largely responsible for the modest improvements in drug delivery reported in the literature. As well as intensity, frequency and mode, the degree of heating is greatly influenced by subtle factors such as transducer motion, anatomical site as well as the quantity and type of vehicle/coupling medium. Variations in all these explain the conflicting results obtained by different workers. It is interesting to note that when heating was removed as an artifact of phonophoresis, the penetration of 5 different anaesthetic molecules (Williams, 1990) and a protein (Pelucio-Lopes *et al.*, 1993) were not affected by ultrasound.

However, ultrasound-enhanced delivery has also been documented in experiments where negligible ultrasonic heating developed (Al-Suwayeh and Hikal, 1991; Bommannan *et al.*, 1992b). This indicates the existence of other phonophoretic mechanisms. It has been shown that the enhanced absorption of methyl nicotinate, hexyl nicotinate and salicylic acid could be obtained by sonicating tissues prior to drug application (Murphy and Hadgraft, 1990; Bommannan *et al.*, 1992b; McElnay *et al.*, 1993). This means that drug molecules are not being pushed through by radiation pressure since accelerated delivery occurred after the ultrasound had been switched off. In these situations, effects such as radiation pressure, acoustic microstreaming or stable cavitation are perturbing the stratum corneum structure, thus permeabilising it to drug delivery. There is good evidence

that these changes are reversible and hence the process is potentially useful within the clinical setting.

From the literature reports, it can be concluded that phonophoresis does exist and that it operates by several different mechanisms. However, at present its therapeutic value is still under question. Clearly, more research needs to be conducted in order to identify the role of the various parameters which influence phonophoresis so that the process may be optimised.

1.5 THE AIMS AND OBJECTIVES OF THE PRESENT STUDY

The overall aim of this project is to develop a more comprehensive understanding of phonophoresis and in particular of the ultrasonic and / or physico-chemical parameters that may control the process. The first objective (Chapter 3) was to examine how ultrasonic intensity, molecular weight and lipophilicity influence phonophoretic enhancement in an *in vitro* hydrogel model. Secondly (Chapter 4), to investigate the effect of ultrasound, at different intensities, frequencies and modes, on the barrier properties of animal skin *in vitro*. A third objective was to assess the role of lipophilicity in the control of phonophoretic enhancement by a study of *in vitro* percutaneous absorption through animal skin (Chapter 5). In all these models, the ultrasound was frequently substituted by an equivalent heat-alone application. This facilitated the removal of ultrasonic heating as an artefact of any enhancement effect.

Prior to discussing these phonophoresis studies, Chapter 2 deals with the ultrasonic dosimetry for each of the three subsequent model-systems as well as describing the ultrasound source used in all the experiments. This chapter also reviews the basic physics of ultrasound generation and propagation. The final objective (Chapter 6) was to determine the effect of ultrasound on the *in vitro* stability of oligodeoxynucleotides in aqueous solution. These compounds are of particular interest as they are currently at the forefront of research as inhibitors of gene expression.

CHAPTER TWO

ULTRASOUND CALIBRATION AND DOSIMETRY

2.1 INTRODUCTION

This chapter starts by establishing the basic physics of ultrasound propagation and the main dosimetry techniques that can be employed to measure acoustic energy. Secondly, the chapter considers the ultrasound source used for the phonophoresis studies reported in this thesis. After a basic description of the generator, this section describes the measurement experiments that were used to validate the outputs of this device. The final part of the chapter deals with the ultrasonic dosimetry within each of the three phonophoresis models examined in the subsequent chapters. Finally, a summary lists the underlying ideas developed in this chapter.

2.1.1 The Physics of Ultrasound Propagation

Therapeutic ultrasound is normally generated by a transducer that converts electrical energy to ultrasound by utilising the piezoelectric principle. This effect describes the behaviour of certain ceramics, most commonly formulated of lead zirconate, titanate and crystalline quartz, which expand or contract when a voltage is applied across them. For continuous wave (c.w.) ultrasound production, an alternating voltage of the appropriate frequency is applied to the transducer resulting in the continuous emission of ultrasound of the same frequency. To produce pulsed ultrasound, short bursts of alternating voltage are repeatedly applied to the transducer. The ultrasound emitted by the transducer propagates away from the front face in the direction in which the transducer is pointing. Once generated, ultrasound retains a specific waveform and constant frequency irrespective of the medium that the beam is passing through (this is strictly speaking not always true but non-linear effects are negligible at phonophoretic intensities). It should be noted that ultrasonic waves travel at the same velocity in the bulk phase of any one medium. Table 2.1 presents some data relating to the sound velocity in different media.

The velocity, frequency and wavelength are interrelated according to the equation:

$$v = f\lambda \qquad (2.1)$$

Where v is the velocity (in m s^{-1}), f is the frequency (in Hz) and λ is the wavelength (in m). Since the frequency remains constant but the velocity changes as the wave travels from one medium to another, it follows that the wavelength must also change.

Table 2.1: Ultrasound Velocity in Different Media (from Williams, 1983)

In these studies, ultrasound was generated at frequencies of both 1.1MHz and 3.3MHz. By applying eqn (2.1), it can be calculated that the wavelengths of these beams, as they propagated through skin or water were 1.36mm and 0.45mm respectively.

The quantity of energy contained in an ultrasonic wave as it passes through any given point is usually expressed in terms of the intensity at that site. Intensity is defined as the power developed through an imaginary plane orientated at right angles to the direction of wave propagation. *i.e.*

$$I = \frac{P}{A} \qquad (2.2)$$

Where I is the intensity (in W cm^{-2}), P is the beam power (in W) and A is the area of the imaginary plane (in cm^2).

The pressure exerted by an ultrasound beam can be determined from its intensity according to the relationship:

$$p = \sqrt{I\rho c} \qquad (2.3)$$

Where p is the acoustic pressure (in Pa), I is the intensity (in W m^{-2}), ρ is the density of the medium (in kg m^{-3}) and c is the velocity of sound (in m s^{-1}). For example, in these studies, the most intense beam applied exhibited an intensity of 2.5W cm^{-2}. It can be calculated that this beam exerted a pressure of 18.37Pa (or 2.56 atmospheres) as it propagated through water. *i.e.*:

$$p = \sqrt{2.25 \times 10^{-4} \times 1000 \times 1500}$$

$$p = \sqrt{337.5} = 18.37Pa$$

Another unit of sound measurement is the bel (B) and this unit is used to compare the intensity of a given ultrasonic wave with another standard, reference source. An arbitary 0B value has been fixed at 10^{-8}W cm^{-2} and from there on each 10-fold intensity increase represents a unit increase. In this project, ultrasound was irradiated in the intensity range 0.1 to 2.25W cm^{-2} representing the range 7 to 8.35B.

As an ultrasound beam propagates away from the transducer, it can be described as consisting of two regions (Figure 2.1). These are the near-field or Fresnel zone and the far-field or Fraunhofer zone. The near field is a cylindrical beam of spatially fluctuating acoustic intensity caused by the constructive and destructive interference of ultrasonic waves. The far field is a diverging beam exhibiting a central acoustic intensity peak in the centre of the beam which smoothly falls off at either side. The boundary between these two zones occurs at a distance d from the transducer which may be determined from the equation:

$$d = \frac{r^2}{\lambda} \qquad (2.4)$$

where r is the radius of the radiating surface of the transducer and λ is the wavelength. As long as $r > 5\lambda$, which usually holds true, the beam diverges in the far zone, with divergence angle θ (in degrees):

$$\theta = \frac{35\lambda}{r} \qquad (2.5)$$

Figure 2.1: Ultrasonic Profile showing diagrammatic representation of beam shapes and intensities produced from a large transducer typically used in phonophoresis (adapted from Williams, 1983)

A, the transducer; B, cylindrical beam in Fresnel zone or near field; C, diverging beam in Frauenhofer zone or far field; D, E, F, acoustic energy contours such that D>E >F. Angle subtended by the divergent beam at the generator surface is 2θ.

For the purposes of this thesis, 1.1MHz ultrasonic beams (λ = 0.136cm) were generated from radiating areas of both 4.4cm^2 (r = 1.183cm, r^2 = 1.400cm^2) and 0.7cm^2 (r = 0.472cm, r^2 = 0.223cm^2). In addition, 3.3MHz beams (λ = 0.045cm) were generated from radiating areas of 3.9cm^2 (r = 1.113, r^2 = 1.241cm^2) and 0.6cm^2 (r = 0.437, r^2 = 0.191cm^2). For each of these beams, the distance to the far field and the divergence angle can be calculated by substituting the appropriate values into eqn (2.4) and eqn (2.5):

1.1MHz beam, large transducer: $$d = \frac{1.4}{0.136} = 10.29cm$$

$$\theta = \frac{35 \times 0.136}{1.183} = 4.02°$$

1.1MHz beam, small transducer: $d = \frac{0.223}{0.136} = 1.65cm$

$r < 5\lambda$ [eqn (2.5) is not applicable]

3.3MHz beam, large transducer: $d = \frac{1.241}{0.045} = 27.58cm$

$$\theta = \frac{35 \times 0.045}{1.113} = 1.42°$$

3.3MHz beam, small transducer: $d = \frac{0.191}{0.045} = 4.24cm$

$$\theta = \frac{35 \times 0.045}{0.437} = 3.60°$$

As can be seen from Figure 2.1, the acoustic intensity distribution in the near field is complex and consists of many maxima and minima. Along the central axis of the beam, the positions of the ultrasonic 'hot' and 'cold' spots can be mathematically determined from:

$$d_{max} = \frac{4r^2 - \lambda(2m+1)^2}{4\lambda(2m+1)} \quad (2.6)$$

$$d_{min} = \frac{r^2 - \lambda^2 m^2}{2m\lambda} \quad (2.7)$$

Where d_{max} represents the distance to the axial acoustic maxima, d_{min} represents the distance to the axial acoustic minima, r is the radius of the radiating surface of the transducer and m is an integer that increases towards the source.

Since acoustic intensity is not homogeneously distributed throughout the beam space or in time (in the case of pulsed ultrasound), several intensity parameters have therefore been defined. The spatial-average temporal-average (SATA) intensity is the most commonly employed parameter. It is calculated by dividing the total power in an ultrasonic beam by the beam area and, in the case of pulsed

ultrasound, averaged over the pulse repetition cycle. However, it has to be remembered that at certain sites, much greater ultrasound intensities will develop. Consequently, a spatial-peak temporal-average (SPTA) intensity parameter has been defined as the maximum value of the time-averaged intensity within the acoustic field. The greatest SPTA intensity within an ultrasonic beam occurs in the centre of the beginning of the far zone. Furthermore, since the acoustic output of a transducer commonly undergoes temporal fluctuations in intensity, a spatial-peak temporal-peak (SPTP) intensity parameter is also sometimes quoted. This is defined as the maximum value of the temporal-peak intensity within the acoustic field.

When ultrasound propagates from one medium into another medium, part of the acoustic energy is transmitted into the second medium whilst part of the energy undergoes reflection at the interface. For a plane wave propagating in a direction that is perpendicular to the interface, the proportion of ultrasound which undergoes reflection is given by:

$$\frac{I_r}{I_i} = \frac{(Z_2 - Z_1)^2}{(Z_2 + Z_1)^2} \qquad (2.8)$$

Where I_r and I_i are the intensities of the reflected and incident ultrasound respectively (in W m^{-2}) and Z_1 and Z_2 are the characteristic acoustic impedances (measured in kg s m^{-2}) on each side of the interface, with the wave being incident in medium 1. The acoustic impedance of a medium is given by:

$$Z = \rho c \qquad (2.9)$$

Where ρ is the medium density (in kg m^{-3}) and c is the velocity of the ultrasound in that medium (in m s^{-1}).

Table 2.2 presents some data relating to the reflectivity of different materials in water.

Table 2.2: Intensity Reflectivity of Different Materials in Water adapted from (Chivers, 1991)

For waves incident to the interface at an angle, the angle of incidence (i) and the angle of refraction (r) are related to each other according to Snell's laws:

$$\frac{\sin i}{\sin r} = \frac{v_1}{v_2} \qquad (2.10)$$

Where v_1 is the velocity of the incident beam in medium 1 and v_2 is the velocity of the refracted beam in medium 2.

Normally, an ultrasound beam is made up of longtitudinal waves in which the particles of the medium oscillate in the same direction as the direction of wave propagation. However, at the interface between a fluid (or soft tissue) and a solid, ultrasonic waves can be partially converted into transverse (shear) waves in which the particles of the medium oscillate at right angles to the direction of wave propagation. This process is termed mode conversion.

When an ultrasonic beam is reflected back along its own path, it interferes with that portion of itself which has not yet been reflected to form a standing wave. A standing wave field consists of a regular repeating pattern of nodes (where the displacement is zero) and antinodes (where the displacement varies from positive to negative at the same frequency as the incoming wave, but at twice its

amplitude). It is possible to have a partial standing wave if the reflector is less than 100% effective.

2.1.2 Ultrasound Dosimetry Techniques

Ultrasonic dosimetry is necessary in order to quantify the ultrasonic energy emitted by a specific transducer at a set driving voltage and, perhaps to determine the size and location of acoustic hot spots. Amongst the numerous dosimetry methods available, radiation-force techniques, piezoelectric techniques, calorimetric techniques and laser interferometry are the most important and these are discussed below.

2.1.2.1. Radiation-Force Techniques

One of the most convenient ways of determining ultrasonic power is to measure the radiation pressure force. The radiation force develops as a consequence of the transfer of momentum from the ultrasound to an intercepting target. A large target in a non-compensating system will intercept the entire beam and thus experience a radiation force which will result in its displacement to an extent proportional to the beam power. *i.e.*

$$F = \frac{h\,P}{v} \qquad (2.11)$$

Where F is the force experienced by the target (in N), P is the acoustic power (in W) and v is the speed of the ultrasonic wave through the propagating medium in metres per second. The quantity h depends upon the the geometry of the target. For a target which is totally absorbing or one which reflects at 45°, h=1. Various types of large-target balances are commercially available and these can be used to measure the total acoustic power of an ultrasonic beam. These instruments have the advantage that consistent measurements can be made independent of the precise position of the target relative to the beam (Davidson, 1991).

In order to determine the radiation pressure force at a specific point within an ultrasonic field, a small-target balance, also known as a ball radiometer, can be

employed. A stainless steel ball, usually 2-4 mm in diameter, is suspended from two thin nylon threads which are designed so that the sphere may be displaced away from the transducer but cannot be displaced from side to side. The deflection of the ball bearing is measured with a travelling microscope and consequently an absolute value of the radiation pressure force over the area of the sphere is obtained (Zeqiri, 1991).

2.1.2.2. Piezoelectric Techniques

Perhaps the most direct measurement method involves the use of hydrophones. These consist of thin plates of piezoelectric material fabricated in the form of small sensing elements which convert the incident ultrasonic pressure into an electrical signal which is visually displayed. Modern hydrophones are available in two general types - needle-point hydrophones and membrane hydrophones. Membrane hydrophones generally exhibit superior sensitivity but they are bulky and cannot be used within small, enclosed spaces. One advantage which hydrophones have other devices is that they can provide data relating to the acoustic frequency and waveshape. Hydrophones are small, adaptable instruments that exhibit a high temporal and spatial resolution. They are therefore powerful tools for measuring most types of ultrasonic fields (Zeqiri, 1991).

Some piezoelectric transducers are designed to work reversibly so as to act simultaneously as both the ultrasound source and the detecting hydrophone. Such transducers can be employed to measure the intensity of acoustic echoes of brief pulses of emitted ultrasound. The electrical signal of the echo can be visually displayed in one of a number of scanning modes. The simplest scan is termed the A-mode in which reflected amplitude is displayed as a function of time (Williams, 1983).

Whereas a single-element hydrophone can only measure the intensity at a point, it is also possible to use a multi-element hydrophone to sample the acoustic intensity distribution throughout the entire ultrasonic field. This is the principle behind the Ultrasound Beam Calibrator (BECA2) which has been developed by the NPL as a reference class instrument (Preston, 1988). The BECA2 consists of 4 integrated components - the sensor, high speed digitising unit, computer and test rig and Figure 2.2 displays a schematic diagram of the system.

Figure 2.2: A Schematic Illustration of the BECA2 System

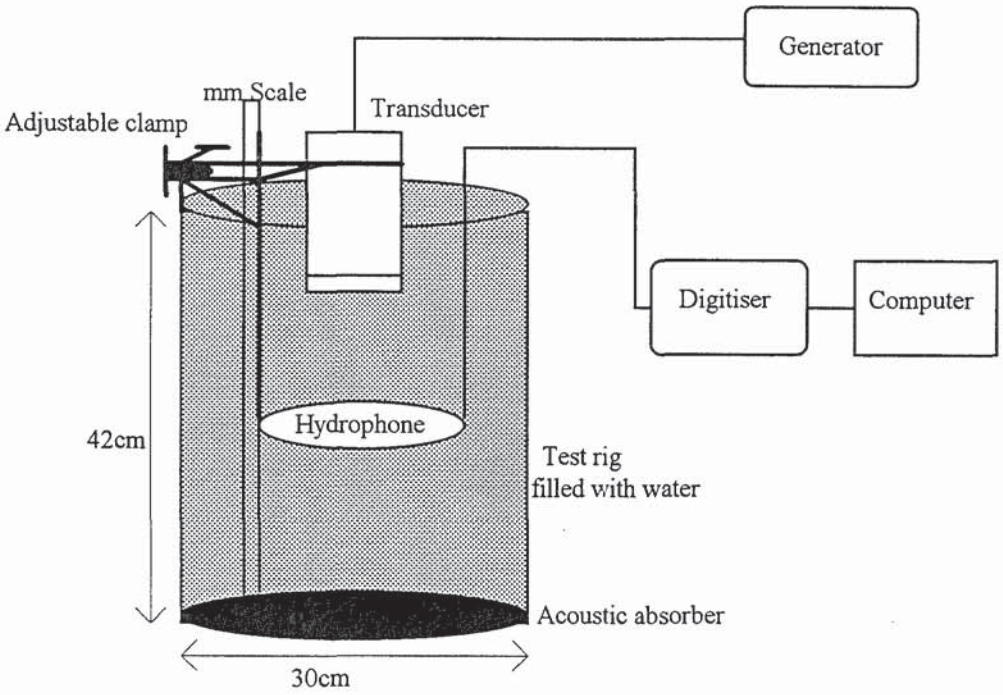

The sensor in this device is a bilaminar shielded membrane hydrophone consisting of a linear array of 21 active elements. These active elements are 0.5mm wide and 1mm apart. The sensor is attached to the Beam Calibrator Rack (Nuclear Enterprises Ltd) such that each hydrophone element has its own amplification channel which is connected to a fast digitiser, sampling at up to 60MHz. An IBM-compatible computer with a purpose-designed interface card connects to the digitising unit, thus achieving control of the system. The software is menu-driven, with relevant parameters being entered prior to display of the data from the transducer under test. The BECA2 system includes a cylindrical test tank which is covered at its base with a corrugated, circular mat of sound-absorbing rubber. An incorporated clamp holds both the transducer and multi-hydrophone in position within the test tank. The clamp can be adjusted so as to translate the transducer along the 3 orthogonal axes. The hydrophone can also be tilted and this ensures that the energy component which is reflected by the hydrophone is directed away from the incident beam. The test rig is labelled with both angular and orthogonal

scales so that the precise position and orientation of the hydrophone and transducer can be described.

2.1.2.3 Calorimetric Techniques

As ultrasound propagates in a medium, its amplitude decays due to attenuation or absorption in the medium. This transfer of energy results in a temperature rise whose measurement forms the basis of yet another dosimetry method. Certain substances such as corrugated rubber, castor oil, and carbon tetrachloride attenuate virtually all the energy of an applied beam into heat. One method of measuring the total acoustic power output of a transducer is to simply direct the ultrasonic beam through a chamber containing castor oil and then to measure the resulting temperature increase with sensitive thermocouples. Alternatively, thermocouple junctions embedded within a small volume of ultrasound-absorbing material can act as point detectors to map out the distribution of ultrasonic energy within a field.

2.1.2.4 Laser Interferometry

When an acoustically transparent membrane is placed in an ultrasonic field, it will undergo cyclic displacements as a result of the propagation of the compression wave. By measuring the phase difference between a fixed, reference laser beam and a laser beam which has been reflected from the surface of the moving membrane, it is possible to calculate the ultrasonic intensity. This method is known as laser interferometry and it is generally considered to offer the highest spatial and temporal resolution of all the available dosimetry techniques. Unfortunately, this system is highly expensive and its use is therefore limited to specialised laboratories.

The NPL employs laser interferometry as its primary standard technique for calibrating the secondary hydrophones which are then used to calibrate the customer hydrophones (Zeqiri, 1991). As a result of the hierarchical nature of the calibration chain, most hydrophones are only initially accurate to a margin of ±7%. Other factors such as inaccuracies in the oscilloscope equipment, temperature effects, and bandwidth limitations further increase the systematic uncertainty of the measurements. Other devices such as radiation pressure balances are similarily susceptible to large measurement errors. In fact, most acoustic measurements conducted in medical physics laboratories are associated with broad margins of

error and this is reflected in the specifications laid down by the British Standards Institute (BSI). For example, The BSI guidelines state that the measured intensity values of ultrasonic therapy equipment should not deviate from those indicated by more than ±30% (pamphlet no. 5724: section 2.5 : 1985).

2.2 CALIBRATION OF THE ULTRASOUND SOURCE

2.2.1 The Ultrasound Source in these Studies

An ultrasound generator (Therasonic 1032, model no.50, EMS Greenham Ltd) of the type commonly used for physiotherapy treatment was employed as the ultrasound source for all the phonophoresis studies. The machine can generate ultrasonic waves at a frequency of either 1.1MHz or 3.3MHz. For both frequency drives, ultrasound could be generated throughout an indicated intensity range of 0 to 2.54W cm^{-2}. Both a large and a small transducer applicator were available for use in conjunction with the generator. The front surface of the small transducer exhibited a total area of $2.0cm^2$. However, the manufacturers specified that the effective radiating area was only $0.7cm^2$ at 1.1MHz or $0.6cm^2$ at 3.3MHz. The large transducer exhibited a surface area of $9.6cm^2$ out of which the specified effective radiating area was $4.4cm^2$ at 1.1MHz and $3.9cm^2$ at 3.3MHz. In addition to producing continuous wave ultrasound, the equipment also had the facility of producing 2ms pulses of ultrasound at on:off ratios of 1:2, 1:4 or 1:9.

It is known that the ultrasound generators used for physiotherapy often suffer from poor calibration and the amount of sound energy actually emitted may not be truly reflected by the control dial on the machine (Williams, 1983). Since the phonophoresis studies described in the following 3 chapters involved the application of 5 different acoustic drives, it was necessary to initially verify the emitted intensities of each of these 5 different outputs. The actual intensity developed at a specific indicated intensity was determined by measuring the total power output at that indicated intensity and then dividing this value by the beam area. In sequential work, a BECA2 system was employed to analyse the beam profile of one particular drive of the ultrasound generator.

2.2.2 Power Output Measurements

A non-compensating radiation force technique was used to make the power output measurements. (Zeqiri, 1991). A particular power balance was selected that had been used to conduct some of the original, pioneering work in this field (Newell,

1963). Figure 2.3 presents a schematic illustration of this equipment. The target in this balance was a brass roof, consisting of two thin sheets of brass 0.2mm thick with an air gap between them and soldered together at the edges. This design ensured that virtually all the ultrasound was reflected at the front surface and directed sideways, perpendicular to the axis of the incoming beam. Four horizontal torsion wires stretched over rigid frameworks eliminated friction and imparted the momentum from the brass target to a pointer. Consequently, the pointer underwent magnified deflection and this could be measured along a vertical scale.

Figure 2.3: Schematic Illustration of the Radiation-Force Balance used to make the Power Output Measurents

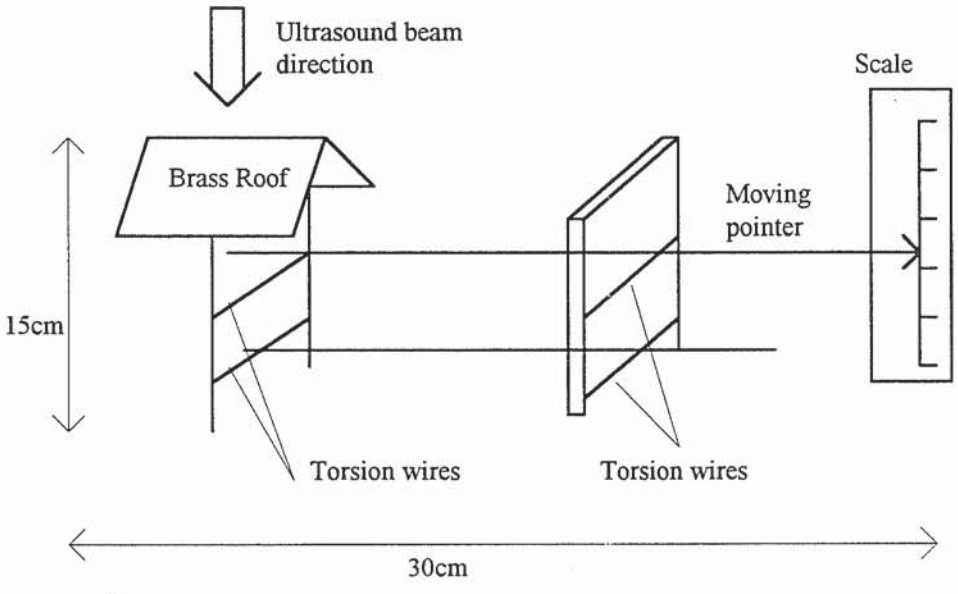

Before use, the whole balance was immersed in a water-filled glass tank. Sections of thick pile carpet were fixed to appropriate areas of the tank walls so as to absorb the reflected sound. Hence, standing waves were avoided within the system. The transducer was clamped in position so that its radiating face was about 1cm below the water surface and approximately 2cm above the brass target. This balance had the disadvantage that at high radiation forces, the pointer was deflected beyond its full scale. When this happened, V-shaped copper weights

were placed on the pointer so as to re-zero it. The magnitude of this shift was noted and taken into account as a tally of total pointer displacement.

The balance was initially calibrated by placing small copper wires of known weight on the brass roof and noting the deflections obtained. Since the water exerts an upthrust on the copper wires, it was necessary to correct for this so as to obtain the actual force values (in N) exerted on the brass target:

$$W_{(water)} = W_{(air)} \times \frac{(SG_{Cu} - SG_{H_2O})}{SG_{Cu}} \qquad (2.12)$$

Where W is the force, measured in Newtons, exerted by the copper weights in the respective medium. SG is the specific gravity of the media where water has a specific gravity of 1 and copper has a specific gravity of 8.93.

Figure 2.4: Calibration Graph for the Radiation-Force Balance

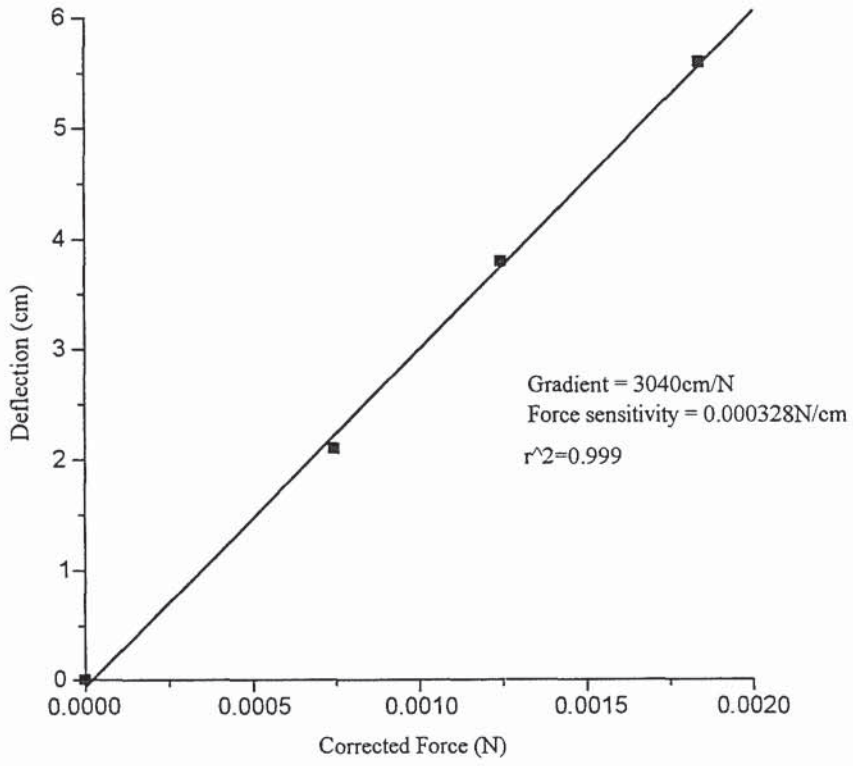

Figure 2.4 displays the calibration plot of the acoustic power balance. A linear relationship between applied weight and deflection was obtained. The gradient of

the curve was 3040cm N^{-1} which is equivalent to a force-sensitivity of 328μN cm^{-1}. The power balance operates because the ultrasonic waves exert a force on the brass roof which is given by eqn (2.11). By substituting c as the velocity of sound in water (1497m s^{-1}) and h=1, it can be calculated that a 1W beam will produce a force of 668μN on the brass target. Since the force-sensitivity of the power balance is 328μN cm^{-1}, it can be determined that the ultrasound-sensitivity is 0.4924W cm^{-1}.

The radiation-force balance was used to measure the power of 5 different drives, each across a range of successively increasing values of indicated intensity. The drives were the 1.1MHz and 3.3MHz outputs of each of the large and the small transducers as well as the 1.1MHz, 1:10 pulsed output of the large transducer. The power developed by the small transducer drives was measured across an indicated intensity range of 0 to 2.25W cm^{-2} whilst the power developed by the cw large transducer drives was measured across an indicated intensity range of 0 to 2W cm^{-2}. The power delivered by the pulsed beam was measured to a maximal SATA intensity of 0.2W cm^{-2}.

After deflection readings had been taken for the whole range of indicated intensities, the intensity dial was turned back down to zero and the measurements were repeated. This was performed in order to check for 'thermal drift' which can cause the 'zero' level to fluctuate. Thermal drift can develop as a consequence of heating of the transducer, target, water or absorbing-carpet (Davidson, 1991). It was found that in this power balance, the 'thermal drift' effects were tiny. Additionally, it was necessary to watch the transducer face for small air bubbles that can arise as a result of cavitation. These were eliminated by tilting the transducer. The mean deflection readings (cm) were converted to values of power (W) by using the ultrasound-sensitivity relationship determined from the calibration.

2.2.3 Validation of the Beam Areas

The beam areas of both the 1.1MHz and 3.3MHz drives, from each of the 2 transducers, were checked by applying a technique of limiting apertures in conjunction with the radiation force balance. This technique is based on the

principle that as long as an aperture area is less than that of the beam area, increasing the aperture allows more energy to reach the brass target. However, once aperture size exceeds the beam area, a further increase in aperture does not affect the energy delivered.

A small aluminium cone, 3cm long and with an aperture of area 0.78cm^2 at its narrow end was interplaced between the transducer face and the brass target. The narrow aperture end was adjacent and very close to the transducer. The ultrasound was switched on at an indicated intensity of 0.5W cm^{-2} for the large transducer or 1W cm^{-2} for the small transducer and the deflection and hence beam power (W) was noted. This procedure was then repeated with other aluminium cones with aperture areas of 3.1cm^2 and 7cm^2. For each output, the power measured by the balance was plotted as a function of aperture area.

Figure 2.5: The Power of the Large Transducer 1.1MHz Beam as a Function of Aperture Area

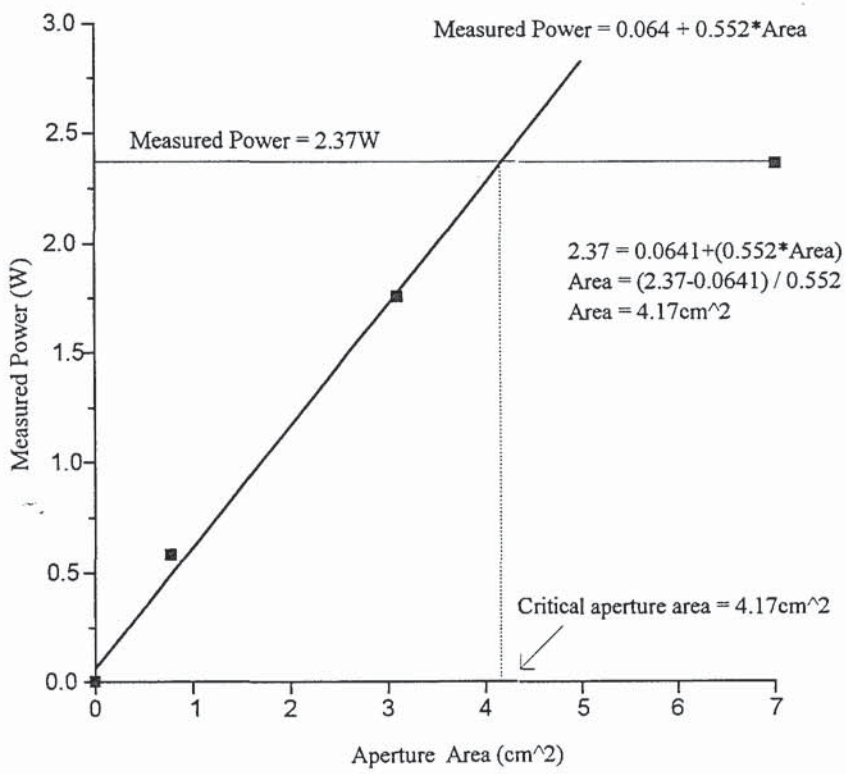

Figure 2.6: The Power of the Large Transducer 3.3MHz Beam as a Function of Aperture Area

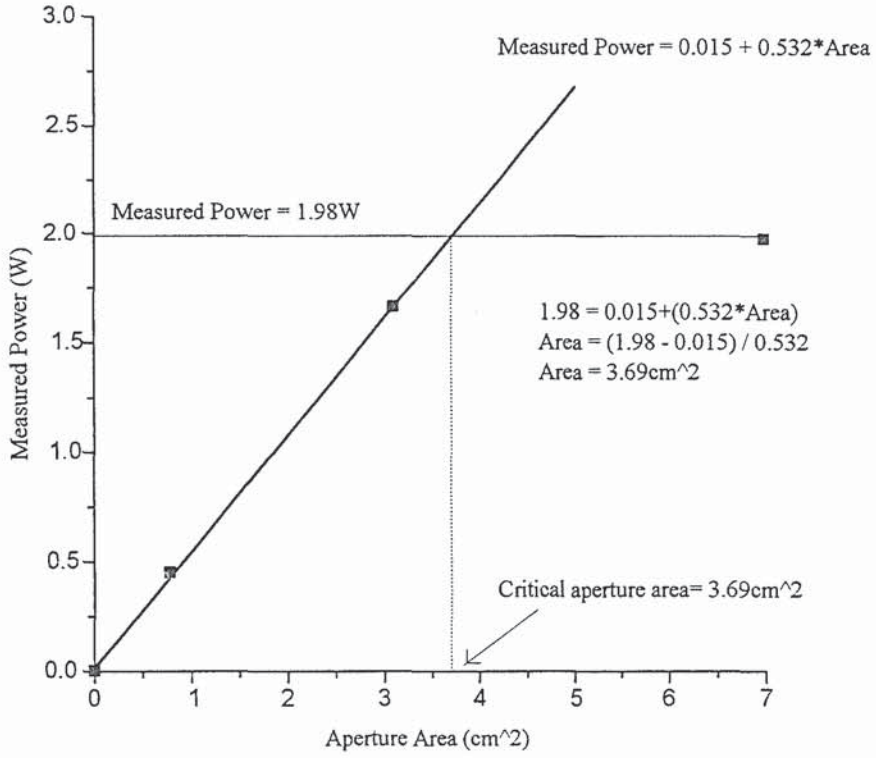

Figure 2.5 displays the large transducer data at 1.1MHz and Figure 2.6 displays the large transducer data at 3.3MHz. In these plots, the first 3 data points constitute an initially increasing linear segment while the power value of the last point constitutes a horizontal segment. The area value at the intersection between the increasing and horizontal lines represents the beam area. It can be seen that a beam area of 4.17cm^2 was calculated for the 1.1MHz output and a beam area of 3.69cm^2 was calculated for the 3.3MHz output. These values compare well with the manufacturers' values of 4.4cm^2 and 3.9cm^2 respectively. It was found that at both frequencies, the small transducer beams did not exceed 0.78cm^2 in area. The manufacturers, specified that the beam areas were 0.7cm^2 at 1.1MHz and 0.6cm^2 at 3.3MHz. Table 2.3 presents all the indicated and calculated beam areas.

The calculated beam area values are approximate because of a number of reasons. Firstly, 2 or 3 points are not sufficient to extrapolate a line and ideally the experiment should have been performed with a greater number of cones (only 3

aluminium cones were available). By repeating each measurement, it was determined that the random error about each point was very small, typically ±2%. However, it has been estimated, from previous long-term use, that the systematic error of the power balance was perhaps ±10% at the 95% confidence limit. This error, caused by effects such as quartz wind streaming, convection currents, heating and minor cavitation will increase the uncertainty of the calculated beam area values. Since the National Physical Laboratory (NPL) has stated that the manufacturers' values for transducer radiating areas are generally reasonably accurate (Preston, 1991), it was decided to use their values to calculate the actual intensities delivered by the generator.

Table 2.3: Comparison of the Calculated and Indicated Beam Areas for each of the 4 Different Outputs

Output	Small Transducer		Large Transducer	
	1.1MHz	3.3MHz	1.1MHz	3.3MHz
Indicated Beam Area (cm^2)	0.70	0.60	4.40	3.90
Calculated Beam Area (cm^2)	<0.78	<0.78	4.17	3.69

2.2.4 Determination of Beam Intensities

Tables 2.4 to 2.8 present the acoustic parameters, measured using the power balance, for each of the 5 beams. Figures 2.7 to 2.11 illustrate the corresponding plots of measured intensity as a function of indicated intensity. It can be seen that there are no error bars in these graphs. This is due to the fact that measurements were only made in duplicate as there was insufficient time to perform triplicate measurements. However, the differences between the first and second measurements were small, typically about ±2%. In each graph, linear regression analysis has been conducted so as to yield a performance ratio which relates measured intensity to indicated intensity. Table 2.9 collates the derived performance ratios for all 5 beams.

Table 2.4: Acoustic Parameters for the 1.1MHz Beam of the Small Transducer

Indicated Int. ($W\ cm^{-2}$)	Deflection (cm)	Measured Power (W)	Measured Int. (Wcm^{-2})
0	0	0	0
0.5	0.9	0.44	0.63
1	1.6	0.79	1.12
1.5	2.4	1.18	1.68
2	3.2	1.57	2.25
2.25	3.6	1.77	2.53

Figure 2.7: The 1.1MHz Output of the Small Transducer

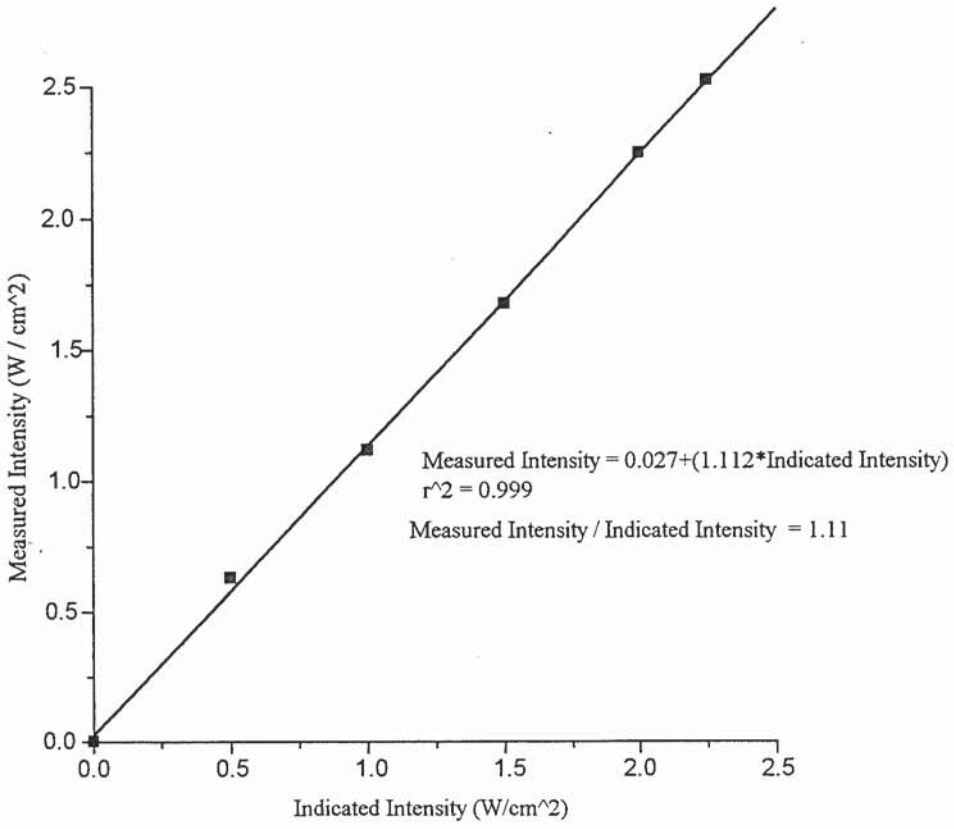

Table 2.5: Acoustic Parameters for the 3.3MHz Beam of the Small Transducer

Indicated Int. ($W\ cm^{-2}$)	Deflection (cm)	Measured Power (W)	Measured Int. ($W\ cm^{-2}$)
0	0	0	0
0.5	0.7	0.33	0.56
1	1.3	0.63	1.05
1.5	1.9	0.93	1.54
2	2.6	1.27	2.12
2.25	2.9	1.44	2.40

Figure 2.8: The 3.3MHz Output of the Small Transducer

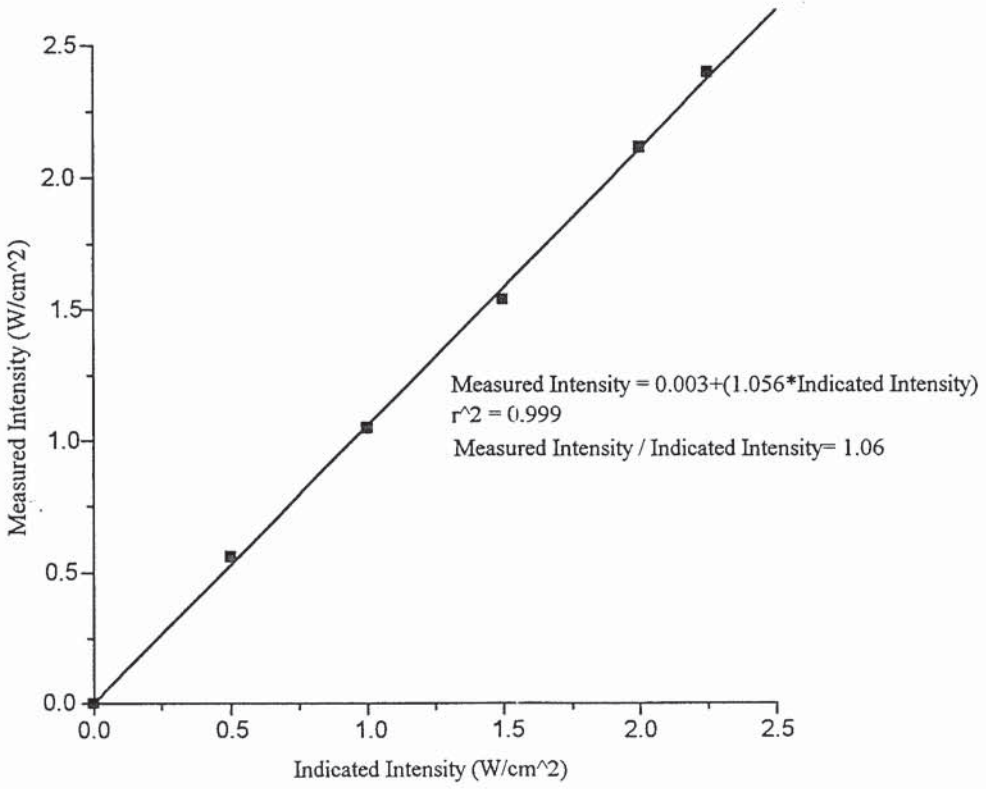

Table 2.6: Acoustic Parameters for the 1.1MHz cw Beam of the Large Transducer

Indicated Int. ($W\ cm^{-2}$)	Deflection (cm)	Measured Power (W)	Measured Int. (Wcm^{-2})
0	0	0	0
0.1	1.1	0.54	0.12
0.3	3.4	1.67	0.38
0.5	5.2	2.56	0.58
1	12	5.9	1.34
1.5	16.8	8.25	1.88
2	22.5	11.08	2.51

Figure 2.9: The 1.1 MHz Output of the Large Transducer

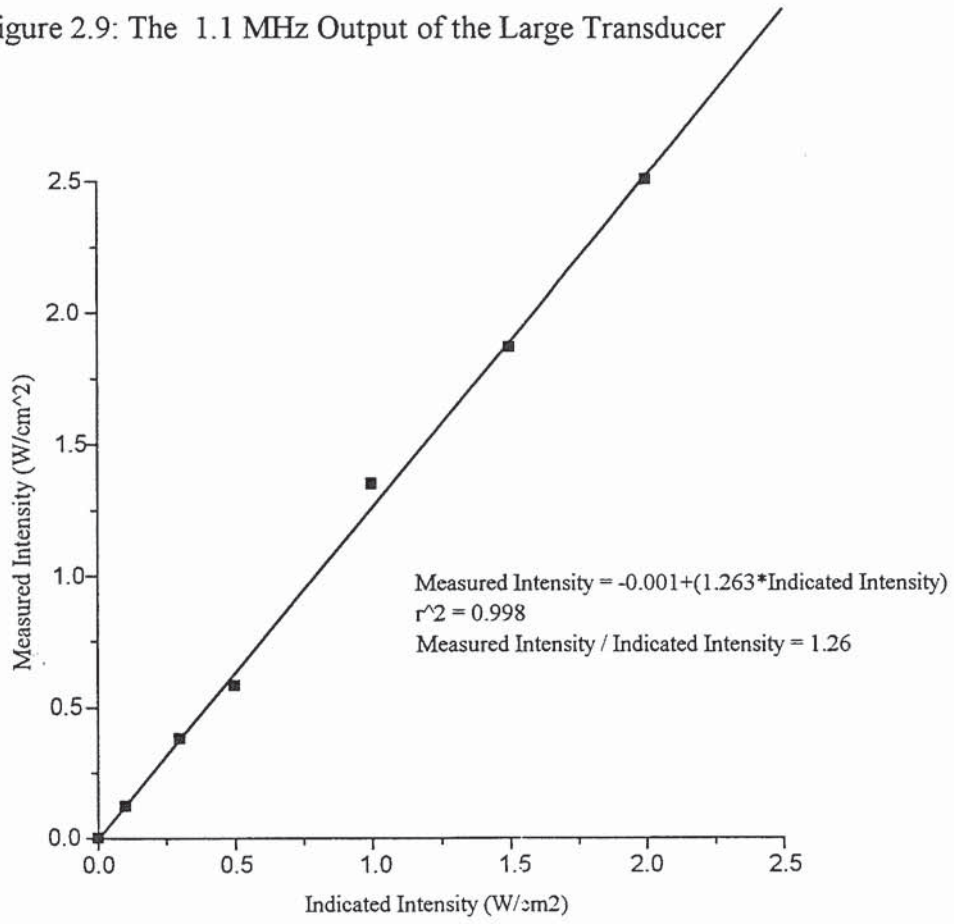

Table 2.7: Acoustic Parameters for the 3.3MHz cw Beam of the Large Transducer

Indicated Int. ($W\ cm^{-2}$)	Deflection (cm)	Measured Power (W)	Measured Int. (Wcm^{-2})
0	0	0	0
0.1	0.7	0.34	0.09
0.5	4.0	1.98	0.51
1	8.1	4.0	1.03
1.5	12.1	5.93	1.52
2	16.3	8.03	2.05

Figure 2.10: The 3.3MHz Output of the Large Transducer

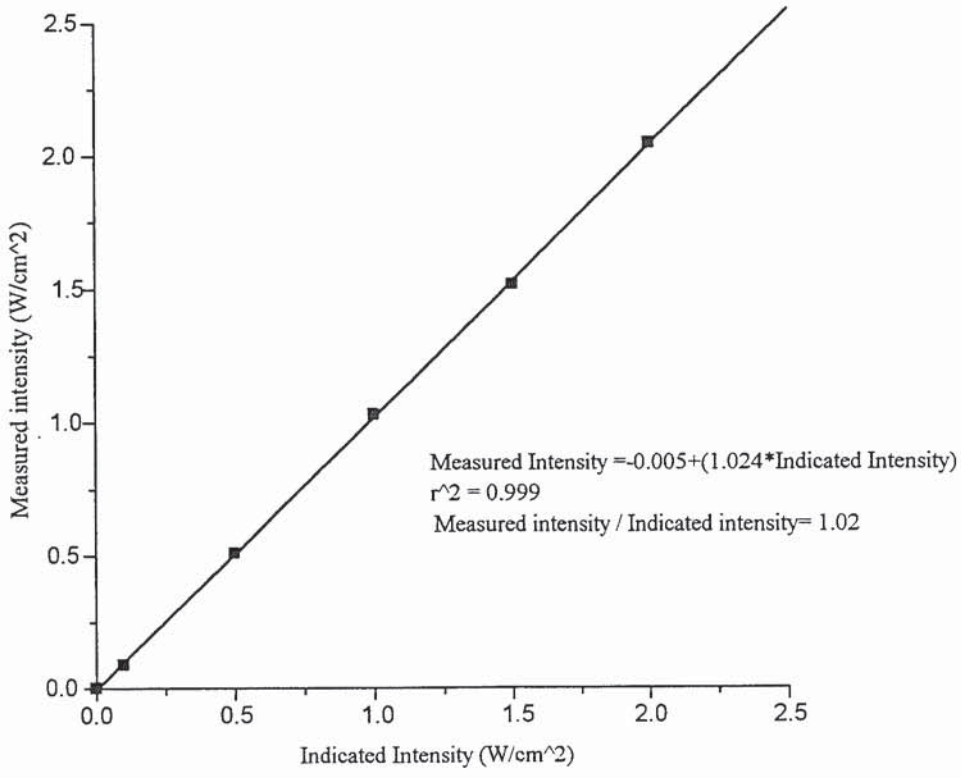

Table 2.8: Acoustic Parameters for the 1.1MHz pulsed (1:9) Beam of the Large Transducer

Indicated Int. ($W\ cm^{-2}$)	Deflection (cm)	Measured Power (W)	Measured Int. (Wcm^{-2})
0	0	0	0
0.05	0.45	0.22	0.05
0.1	0.9	0.44	0.1
0.15	1.35	0.66	0.15
0.2	1.7	0.84	0.19

Figure 2.11: The 1.1MHz Pulsed (1:9) Output of the Large Transducer

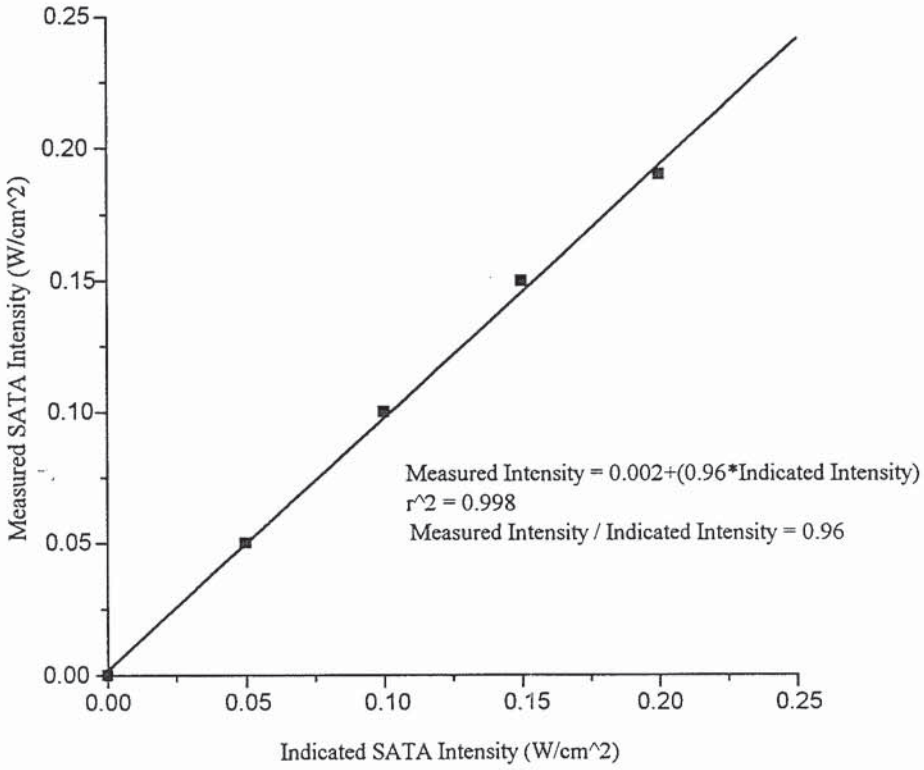

Table 2.9: The Performance Ratios for each of the 5 Outputs used in the Phonophoresis Studies

Output	Small Transducer		Large Transducer		
	1.1MHz	3.3MHz	1.1MHz	3.3MHz	1.1MHz(p)
measured int./indicated int.	1.11	1.06	1.26	1.02	0.96

p denotes that pulsed ultrasound was applied at 1:9 (on:off ratio)

It can be seen that for all 5 ultrasound drives, measured intensity increased linearily with increasing indicated intensity. Furthermore, the performance of all these drives varies between +26% to -0.04%. Since this is within the limits of ±30% set by the BSI, it can be concluded that the machine is adequate for phonophoresis research.

It was decided, for the purposes of this thesis, to quote the indicated values of intensity rather than the measured values. This is because the estimated systematic error associated with the measuring technique (±10% at 95% confidence limits) was the same order of magnitude as the difference between the measured and indicated values. However, for the purposes of comparing the 1.1MHz and 3.3MHz c.w. outputs of the large transducer, the relative difference in performance ratios between different drives was taken into account. It is important to note that the total power delivered by the beam depends upon both the frequency drive and the performance ratio. For instance, at any specific value of indicated intensity, the total power developed by the 1.1MHz large transducer drive is 38% greater than that of the 3.3MHz large transducer drive. This follows from both the difference in intensity performance *i.e.*+26% versus +2%, as well as the difference in beam areas *i.e.* 4.4cm^2 versus 3.9cm^2.

2.2.5 Beam Profile Determinations

It has been demonstrated in section 2.1.1 that the near-zone of the large transducer 3.3MHz beam extends to a distance of 27.58cm from the transducer face. In these

Figure 2.12: Temporal Peak Profiles at Successive Distances from the Large Transducer

(A) 20mm from the transducer face

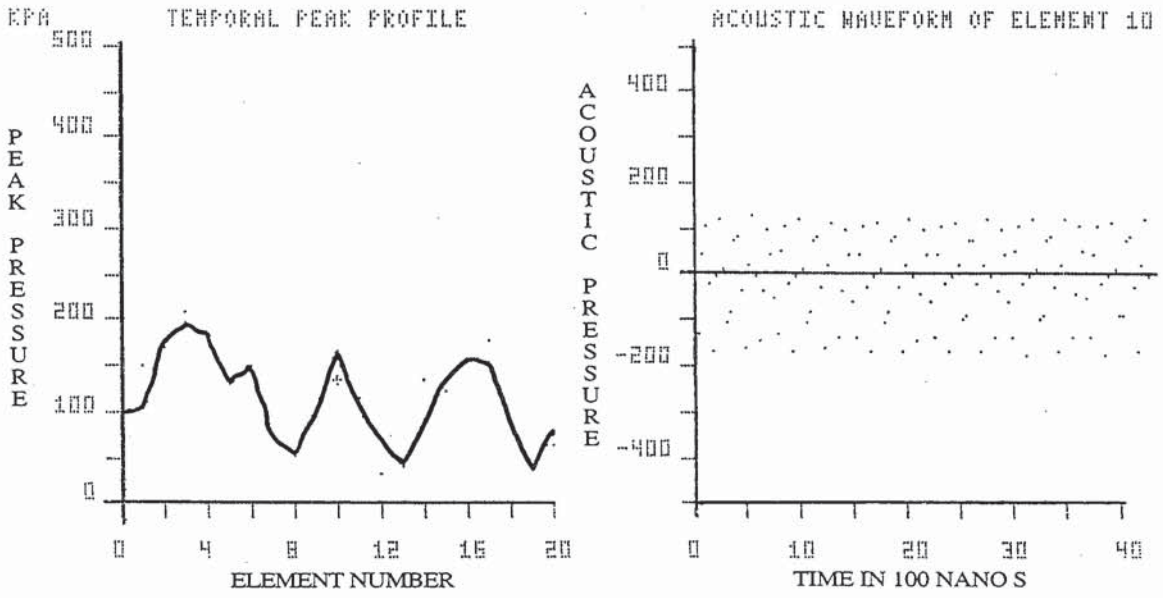

NON-AUTOMATIC SCANNER OPTION CLOCK FRQ = 30 MHZ GAIN = 26 DB PSI = 157
PEAK POS PRES @ CENT (+) = 106 KPA MAX PEAK POS PRES @ CENT (+) = 154 KPA
PRR = 1105 HZ

(B) 40mm from the transducer face

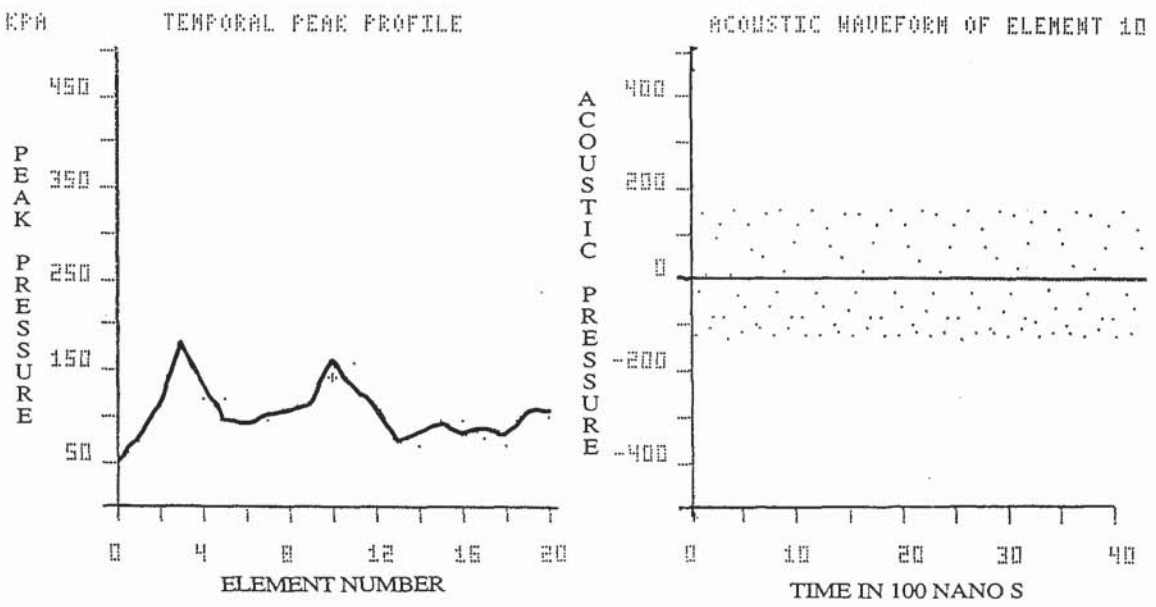

NON-AUTOMATIC SCANNER OPTION CLOCK FRQ = 30 MHZ GAIN = 26 DB PSI = 172
PEAK POS PRES @ CENT (+) = 145 KPA MAX PEAK POS PRES @ CENT (+) = 161 KPA
PRR = 1185 HZ

DEPTH: 40.0 (MM)

(C) 60mm from the transducer face

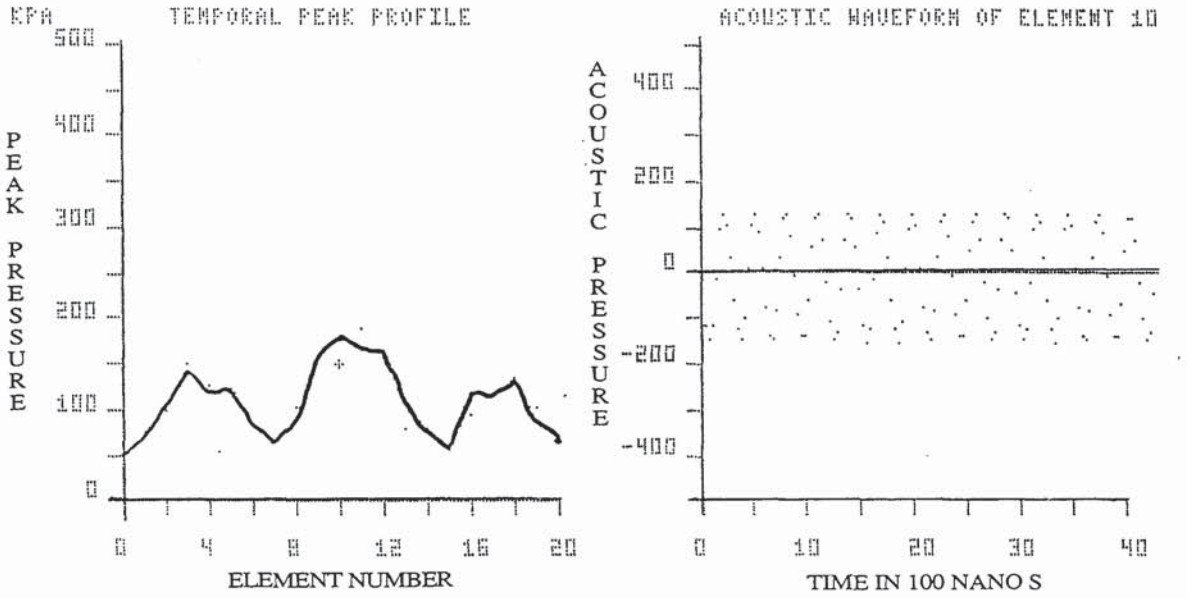

NON-AUTOMATIC SCANNER OPTION CLOCK FRQ = 30 MHZ GAIN = 25 DB PSI = 209
PEAK POS PRES @ CENT (+) = 153 KPA MAX PEAK POS PRES @ CENT (+) = 180 KPA
PRR = 1179 HZ

DEPTH: 60.0 (MM)

(D) 80mm from the transducer face

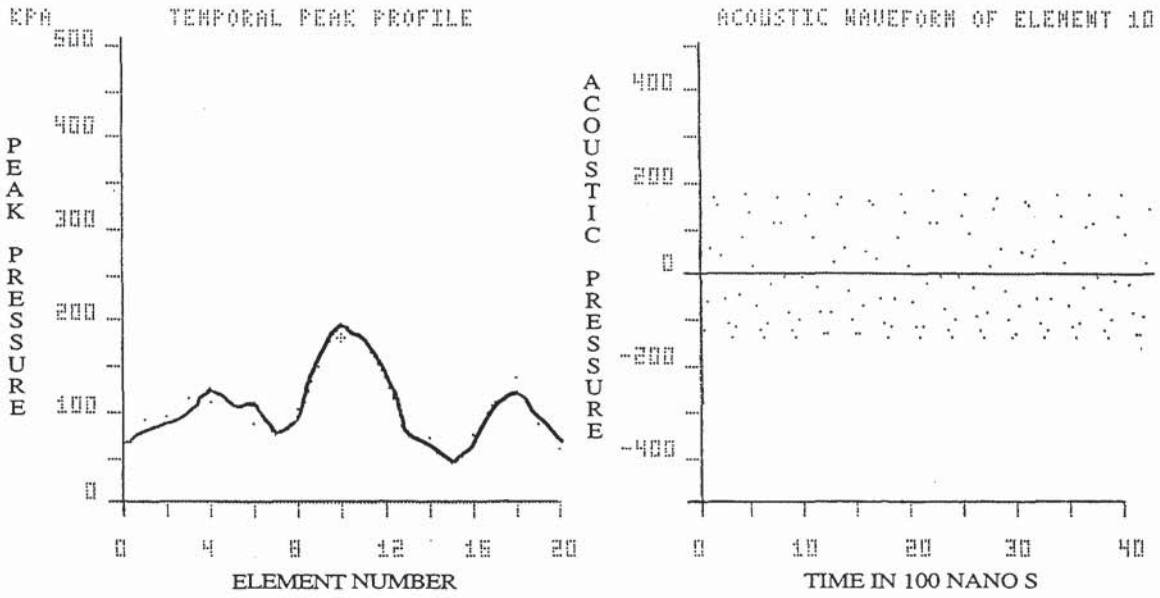

NON-AUTOMATIC SCANNER OPTION CLOCK FRQ = 30 MHZ GAIN = 26 DB PSI = 229
PEAK POS PRES @ CENT (+) = 160 KPA MAX PEAK POS PRES @ CENT (+) = 196 KPA
PRR = 1195 HZ

DEPTH: 80.0 (MM)

experiments, an ultrasound beam calibrator (BECA2) was used to examine the intensity profile of this beam within the first 8cm of the near zone.

Initially, the test tank was filled almost to the top with 20L of distilled water. The large transducer was then positioned approximately 0.5cm below the surface of the water so that its radiating surface was pointing downwards. The 3.3MHz drive was switched on with the indicated intensity set at 0.26W cm^{-2} (which is equivalent to 1W of power). It was found that the hydrophone had to be tilted by approximately 7° from the horizontal in order for the echo component of the beam to be reflected away from the transducer such that no standing waves were created. The position of the reflected beam could be readily discerned from the perturbation it made when it hit the water surface. The gain adjustment of the calibrator rack was fixed at -2.6B and the digitiser set at 30MHz. An Elonex IBM 286M-120 computer was used to co-ordinate the system. Measurements of various parameters of the acoustic field were then undertaken with the multi-hydrophone fixed at successively increasing distances (2cm, 4cm, 6cm and 8cm) from the transducer face.

Figure 2.12 presents the temporal peak profiles measured at different distances from the transducer face. Through each measurement plane, there is a characteristic pattern of peaks and troughs and this follows from the intensity profile depicted in Figure 2.1. It can be seen that the pressure profiles are asymmetric and this is due to the 7° incline of the hydrophone. Figure 2.12 also presents the acoustic waveforms measured at the central hydrophone element.

The software used these data to derive several acoustic parameters which are presented in Table 2.10. It was determined that the difference between the measured frequency values and the nominal frequency was less than the ±5% error limit specified by the manufacturers. It can be seen that at 4, 6 and 8cm, the measurements of total power were close to the indicated power value of 1W. However, at a distance of 2cm from the transducer face, the Beam Calibrator assessed that beam power was 1.75W. The measurement was overestimated as a result of the highly heterogenous acoustic intensities occurring in proximity to the transducer face. These effects are illustrated in Figure 2.1 which shows that the number of acoustic 'hot spots' is greatest near the radiating surface. This effect causes inaccuracies to develop as the hydrophone elements extrapolate point

values of acoustic pressure into total beam intensity values. This feature has been dealt with in greater detail in the literature reports (Preston,1991).

Table 2.10: The Acoustic Parameters of the 3.3MHz Large Transducer Output

Distance (cm)	f (MHz)	Power (W)	SATA Int. ($W\ cm^{-2}$)	SPTA Int. ($W\ cm^{-2}$)	SPTP Int. ($W\ cm^{-2}$)
2	3.375	1.75	0.551	1.070	2.480
4	3.375	1.07	0.332	0.832	2.090
6	3.410	1.04	0.323	0.909	2.180
8	3.390	0.93	0.291	0.942	2.580

Figure 2.13: BECA2 Intensity Determinations at Successive Distances from The Transducer Face

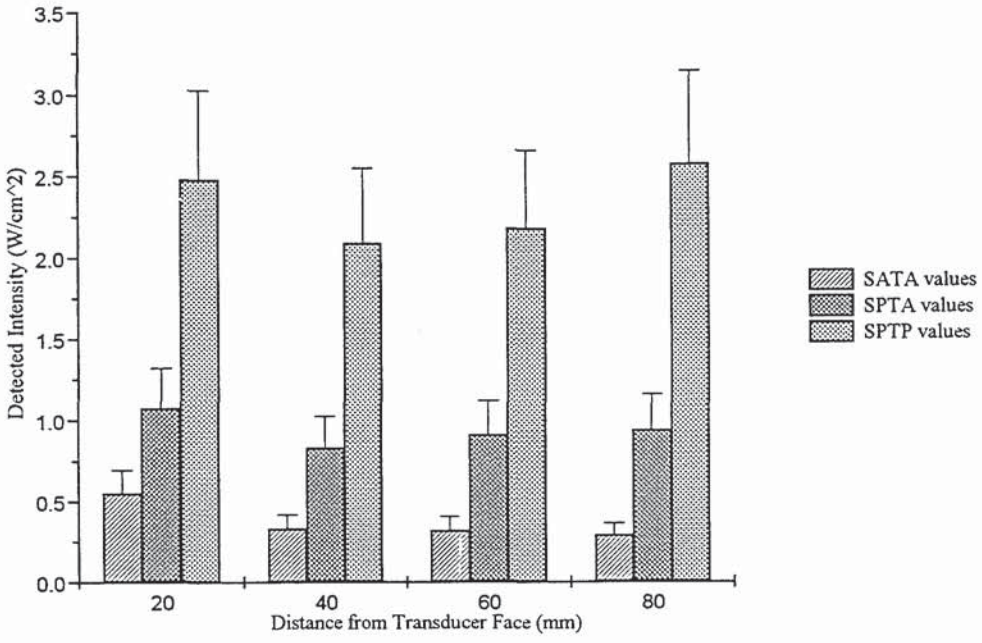

Error bars represent the typical measurement uncertainty (95% confidence limits) for physiotherapeutic equipment operating at cw mode.

The BECA2 also evaluated the SATA, SPTA and SPTP intensities at successive distances from the transducer face. Figure 2.13 displays these parameter values as a function of distance from the transducer face. It can be seen that all three parameters are highest close to the radiating surface and this is due to the measuring inaccuracy already mentioned. Although the measured SATA values were close to the indicated intensity value of 0.26W cm^{-2}, the SPTA intensities were 4 times higher than this and SPTP values were up to 10 times greater.

2.3 ULTRASOUND DOSIMETRY IN EACH OF THE THREE MODELS

Dosimetry determinations were performed on each of the three separate phonophoresis models. These were the agar gel model, the free-field model and the modified Franz cell model.

2.3.1 The Agar Gel Model

The ultrasound effect on drug diffusion through agar gels is dealt with in Chapter 3. In this model, ultrasound was directed through a gel-filled thin-walled cylinder in contact with a gel-filled, thick-walled cylinder. Drug diffusion occured at the interface between the two agar gels. Figure 3.3 depicts the apparatus employed for those diffusion studies. Since the diffusion interface was a distance of 8.4cm from the transducer face and the ultrasonic frequency was 1.1MHz, it can be calculated using Eqn (2.4) that the interface was within the near zone of the beam. In this dosimetry experiment, the BECA2 was employed to measure the attenuation of the gel-filled thin-walled cylinder and hence determine the ultrasonic energy at the interface.

A thin-walled, perspex cylinder was filled with 3% agar gel and then sealed with parafilm at both open ends (see section 3.2 for preparation methods). The cylinder was immersed inside the water-filled test rig and held by hand so that its top surface was pressed against the transducer face. The ultrasound generator was switched on with the frequency set to 1.1MHz and the power fixed at 0.5W. The beam calibrator was used to measure the power at the base of the cylinder. In a control run, the multi-hydrophone measured beam power at the same location, in the absence of the gel and cylinder. Figure 2.14 displays a schematic diagram of the measurement system.

It was found that the interposing gel-column reduced the beam power to 17.9± 4.3% of its value. This indicates that most of the ultrasonic energy is attenuated as the ultrasound propagates through the gel in the thin-walled cylinder. In the actual diffusion experiments, the beam also propagates through a second column of 3% agar gel within a thick-walled cylinder. Since it was impossible to incorporate the thick-walled cylinder into the BECA2 measuring system, the above determination can only be approximate. In the complete model, the beam undergoes further attenuation as it propagates through the gel in the thick-walled cylinder. At the

teflon base, some of the beam reflects back on itself so as to produce a partial standing wave field at the diffusion interface.

Figure 2.14: Schematic Diagram showing the Dosimetry System for the Agar Gel Model

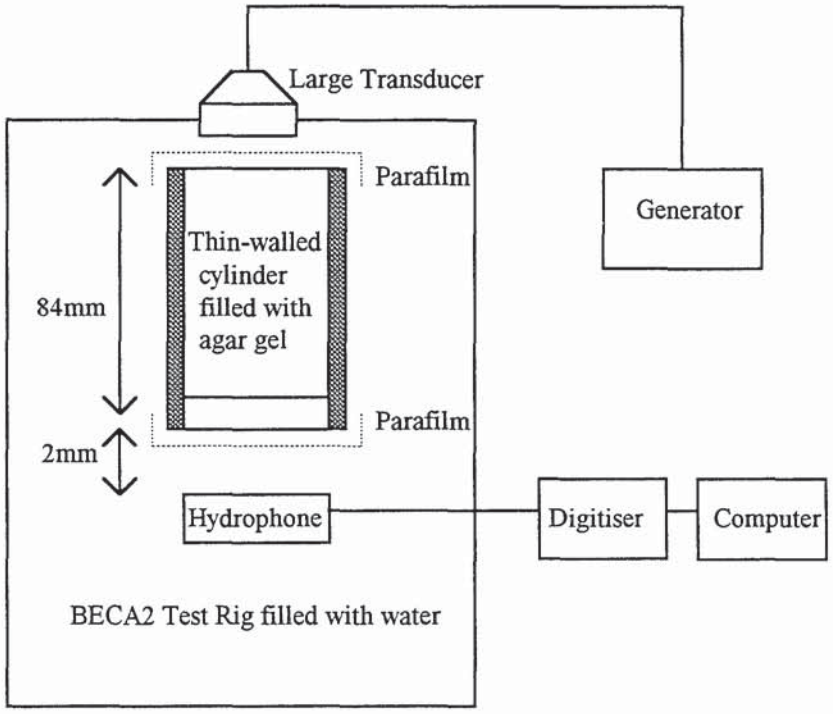

2.3.2 The Free-Field Model

Much of the literature on phonophoresis suffers from the defect of inadequate dosimetry of the ultrasound source (Walmsley and Squier, 1991). This is often due to complex and unpredictable standing wave patterns occurring within the experimental assemblage. For the studies undertaken in chapter 4, it was

necessary to design an acoustic model in which skin samples could be exposed to a well-defined, ultrasonic free-field.

The simplest such system involves placing the skin section flat on a sheet of clingfilm, stretched taught over a water-filled beaker. If the beaker is composed or lined with sound-absorbing material then this would attenuate the incoming energy and prevent standing wave development. Coupling gel, exhibiting a low attenuation coefficient, can be applied to make contact between the transducer, skin and clingfilm. Obviously, the skin is exposed to the near field of the beam. Initially, a plastic beaker 12cm in diameter and 12cm height was investigated for its sound-absorbing properties by comparing its acoustics to that of a stainless steel tub of similar dimensions.

Initially, the steel tub was filled almost to the top with distilled water. A 3.5MHz reversible transducer (Picker, 595522B, 19mm, Long I.F. Series L, A71110Hr) was then used in conjunction with an A-mode scan (Kretz-Technik, Clinical Diagnostic A-scan, Series 4100MG) in order to emit pulses of ultrasound and detect the energy of any echoes. The principles by which this device operates have been outlined in section 2.1.2.2. The transducer of the A-scan was then placed just below the water surface, with its radiating surface pointing downwards toward the metallic base of the container. When the machine was switched on, the outgoing pulse and its corresonding echo were displayed on the screen of the A-scan as two sharp peaks of approximately the same height. The calibrated attenuator of the A-scan equipment was then adjusted so that the peak representing the echo was magnified to reach the full-scale mark on the screen. This happened when the attenuator was set to 2.9 bels. Since the stainless steel-water interface acts as a virtually perfect ultrasound reflector, the attenuator setting can be used as a reference to determine the acoustic reflectivity of other materials.

The A-scan was then used in the same way to measure the reflectivity of the plastic beaker. It was found that the ultrasound echo was now much smaller. The calibrated attenuator was again adjusted such as to enlarge the peak across the full-scale of the screen. This required the attenuated calibrator to be turned up by 1 bel to a value of 3.9 bels. Since a 1 bel increase represents a 10-fold increase in intensity, it follows that the plastic-water interface is reflecting back 10% of the energy.

In order to develop a more sound-absorptive system, the echo tests were repeated with the beaker successively lined on all its inside surfaces with different materials. The linings investigated were foam, thin-pile carpet, thick-pile carpet as well as rubber bands dispersed in the water. Both sections of carpet (Robinson, 1991) and rubber bands (McElnay *et al.*, 1994) have been previously employed to dissipate ultrasound. All these linings were cut into pieces so as to exactly fit on the inside of the circular base and along the inside cylindrical walls of the tub. All the materials had to be left submerged in water for 10 minutes so as to allow all the air bubbles to be released to the surface of the water. In the case of the foam, the lining had to be thoroughly squeezed in order to force out the trapped air in the foam pores.

Table 2.11: Intensity Reflectivity of the Linings

Material (cm)	Adjustment (B)	% Reflection
Steel	2.9	100
Plastic	3.9	10
Foam	3.4	31.6
Thin pile carpet	3.9	10
Thick pile carpet	4.9	1
Rubber bands	4.9	1

Table 2.11 lists the reflectivity of all the tested interfaces. It was determined that the foam lining was less sound-absorbing than the plastic beaker alone since it reflected back over 30% of the energy. The thin pile carpet was as effective as the plastic beaker. The thick pile carpet and the dispersed rubber bands were both found to be the most sound-absorbing. Since the the rubber bands were suspended at varying distances from the transducer, numerous individual acoustic echoes were registered on the A-scan. Since this system also suffers from the potential problem of the bands sinking or amalgamating to one side, it was decided to use the thick pile carpet as the absorptive lining for the free-field model. Further tests with the A-scan demonstrated that tiny variations in the angle the transducer makes with the water did not greatly affect the magnitude of the reflections, thus indicating that holding the transducer by hand is acceptable. Figure 4.2 depicts the apparatus used to apply the ultrasound free-field.

2.3.3 The Modified Franz Cell Model

The permeation studies reported in Chapter 5 involved the attempted phonophoresis of 7 different compounds across rat skin *in vitro*. In the experimental system, ultrasound was directed at the skin surface from a small transducer fixed within the donor compartment of an adapted Franz cell. The distance between the skin and transducer is 2cm. The methods are described in detail in section 5.2.3 and a diagram of the equipment is depicted in Figure 5.3. By using eqn (2.2), it can be calculated that the skin membrane lies just outside the near field at 1.1MHz and well within it at 3.3MHz. The critical distances are 1.6cm and 4.2cm respectively. It has to be noted that in each phonophoresis experiment, a steel mesh, physically supporting an overlying skin sample was present within the receptor cell recess. As can be seen from Table 2.2, steel exhibits a high reflectivity and hence the mesh may play a crucial role in determining the ultrasonic field throughout the skin membrane.

A bilaminar membrane hydrophone (Marconi Y-337611) which had been pre-calibrated at the NPL using laser interferometry, was employed to make the dosimetry determinations. The instrument consists of a central, 1mm-wide, piezoelectric element, embedded within an annular ring, 10cm in diameter. The sensor was connected *via* a single-ended amplifier to an oscilloscope (Hameg 60MHz, HM605). The protruding side arm prevented the large annular ring from being inserted through the Franz cell junction. Consequently, it was decided to omit the Franz cell altogether and measure the ultrasound emitted by the small transducer within a tank of water. Figure 2.15 displays a diagram of the arrangement used to measure the beam energy just beyond the steel mesh. The small transducer was clamped into position at a distance of 2cm directly above the hydrophone. The hydrophone was placed on an inclined stand making a 5° angle with the horizontal. This prevented the partial reflection of any energy back towards the transducer. The transducer output was set to an intensity of 2.25W cm^{-2} on the 1.1MHz drive. These are the baseline values applied in the actual permeation studies described in Chapter 5. Acoustic pressure measurements were then made both with and without the steel mesh lying over the hydrophone sensor.

Figure 2.15: Schematic Diagram showing the Ultrasound Dosimetry Arrangement for the Modified Franz cell Model

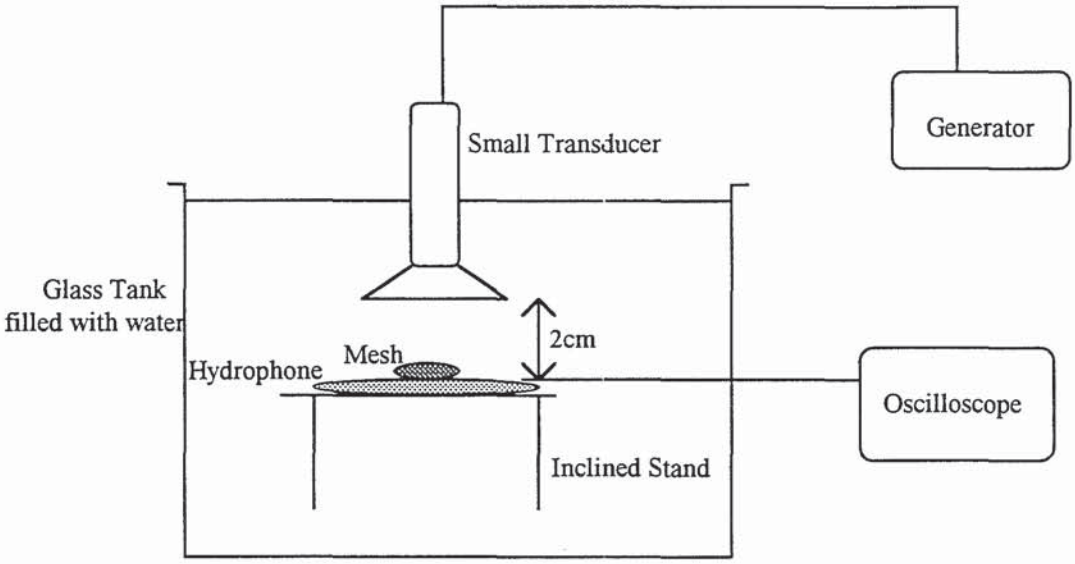

The oscilloscope time base was set to 1μs cm^{-1} and the amplitude was set at 10mV cm^{-1}. It was found that without the mesh, the ultrasonic waves produced a voltage amplitude of 50mV while with the mesh, the ultrasonic waves exhibited an amplitude of only 25mV. This indicates that acoustic pressure is halved as the beam propagates through the steel mesh or in other words, 75% of the energy is reflected back at the steel mesh. However, it was found that if the angle the mesh makes with the horizontal was varied by merely a few degrees, the proportion of energy reflected increased. It has to be remembered that the Franz cell is inverted in the course of the experiment and that the mesh fits loosely within the recess. Consequently, the mesh orientation is likely to vary within and between individual phonophoresis experiments. In conclusion, it can be stated that at least three-quarters and perhaps more of the beam is reflected back on itself so that a complex and unpredictable standing wave profile exists at the skin membrane.

2.4 SUMMARY

Most of the ultrasound generator outputs that were used for the phonophoresis experiments were calibrated using a radiation force-balance technique. It was determined that the performance of the machine was satisfactory and that the generated outputs conformed to BSI standards. An Ultrasound Beam Calibrator validated the frequency, waveshape and beam profile of a specific output of the generator. The dosimetry determinations involved the use of various types of equipment to determine the acoustic field at the diffusion interface in each of the 3 phonophoresis models. Table 2.12 summarises the findings of these experiments.

Table 2.12: The Ultrasonic Field at the Diffusion Interface in each of the Three Models

Model	Transducer	Beam field	Standing wave component
Agar Gel	large	near	small
Free-field	large	near	none
Modified Franz cell	small	far at 1.1MHz near at 3.3MHz	large, (≥75%)

CHAPTER THREE

ULTRASOUND-ENHANCED DIFFUSION IN A NATURAL HYDROGEL

3.1 INTRODUCTION

In order to acquire an understanding of the physics of phonophoresis, it was decided to examine the effects of ultrasound on drug migration in a simple, homogenous matrix. An experimental system was developed in which the diffusion medium consisted of 3%w/v agar gel and this model was based upon, but not identical to, a model employed in previous ultrasound-enhanced diffusion studies (Williams *et al.*, 1990).

Agar gel consists of a network of polysaccharide macromolecules, the two principal components of which are agarose and agaropectin. The macromolecules are held together by relatively weak bonds such as hydrogen bonds and dipole-dipole interactions. The pores within the polymeric mesh contain water and this constitutes a continuous phase through which a solute can readily diffuse. Since 3% w/v agar gel is 97% water, as far as molecular diffusion is concerned, it behaves as a homogenous liquid. However, employing a hydrogel such as agar gel confers the advantage that unlike a real liquid, the macromolecular structure inhibits macroscopic fluid flows developing as a consequence of quartz wind streaming (Williams *et al.*, 1990).

The exposure procedure involved placing two nearly identical agar gels directly in contact with each other and applying a 1.1MHz ultrasonic field. The only difference between the gels was that one contained a uniform distribution of a radiolabelled drug while the other was initially drug-free (refer to Figure 3.3). At the end of the exposure period, serial slices of gel were cut from the previously clear gel and the radioactivity in each slice was measured. Consequently, it was possible to determine the ultrasound-effect on the penetration-depth profile of the test compound. In order to gain an insight into the nature of any phonophoretic mechanism, experiments were also conducted in which the ultrasound beam was substituted by an equivalent heat-alone source.

In order to determine which, if any, physico-chemical parameters are associated with an optimal ultrasound effect, three different test molecules were examined. These were mannitol, a small hydrophilic sugar alcohol; hydrocortisone, a small, fairly hydrophobic steroid; and inulin, a high molecular weight polysaccharide. Furthermore, the ultrasound was applied at several different intensity settings so that any intensity-dependent enhancement effects could be elucidated.

This next part of this chapter starts by discussing the methods used in the agar gel studies. As well as explaining the general experimental techniques, there is an account of the control experiments used to determine whether such factors as gel refrigeration time or exposure at room temperature can influence diffusion. The results of the diffusion studies are reviewed and the overall findings of this work are finally summarised.

3.2 METHODS

3.2.1 The Design of the Perspex Cylinders

For these studies, it was necessary to prepare two different agar gel columns within cylindrical containers. Implicit in this design was the concept that the receptor and donor gels had to exhibit different cross-sectional areas so that the vessel walls would not make contact at the diffusion interface (refer to Figure 3.3). To this end, the technical support staff at Aston University Pharmaceutical Department constructed two types of transparent perspex cylinders. These vessels are illustrated in Figure 3.1.

Figure 3.1: Schematic illustration of the perspex cylinders.

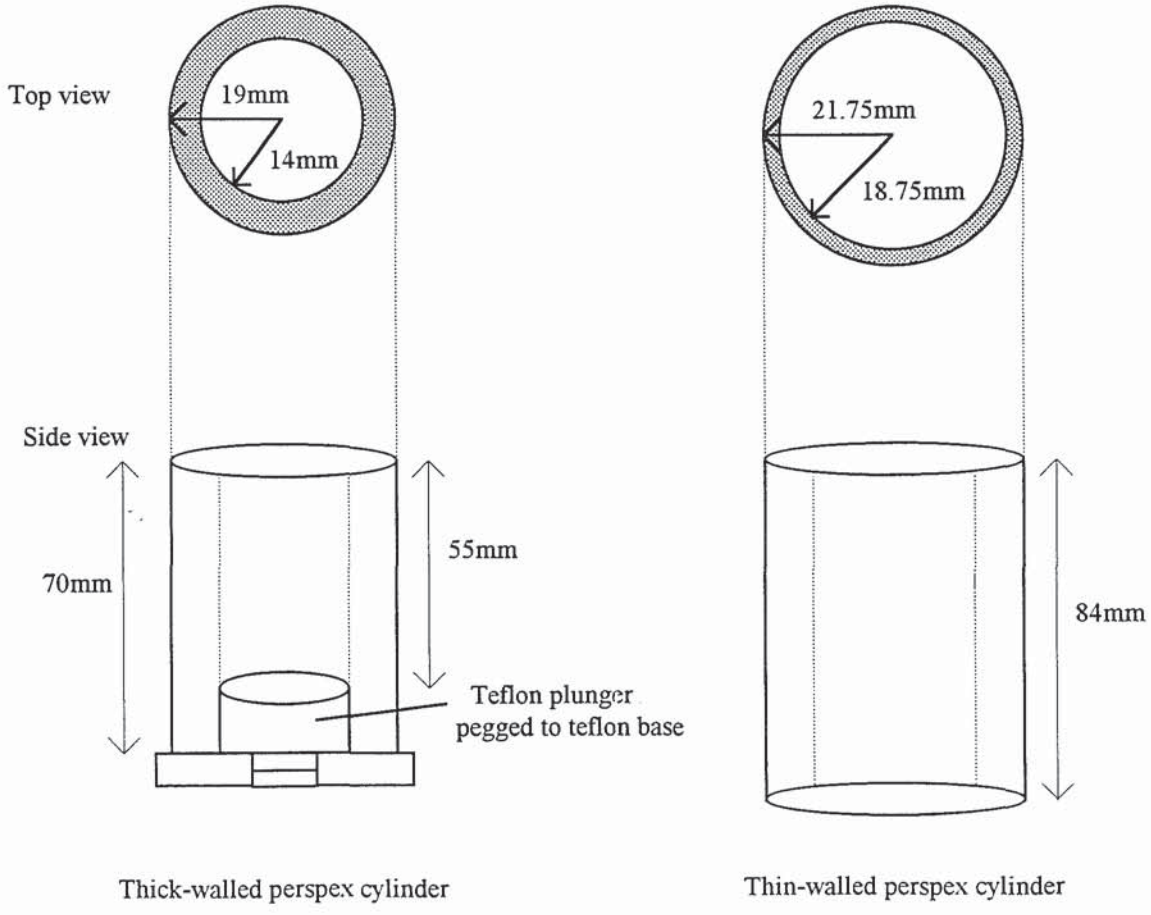

A thick-walled cylinder exhibiting an internal radius of 14mm, an external radius of 19mm and a length of 70mm was designed to be filled with the receptor (initially clear) gel. This cylinder could be pegged to a teflon base with a teflon plunger almost 14mm in radius. A thin-walled cylinder exhibiting an internal radius of 18.75mm, an external radius of 21.75mm and a length of 84mm was designed to contain the radioactive gel disc as well as a drug-free portion termed the contact gel. These cylinder dimensions were very similar, although not identical to those used in previous research involving the agar gel system (Williams *et al.*, 1990).

3.2.2 Preparation of the Receptor Gel

A quantity (1.5g) of agar powder (Grade 1, Oxoid Ltd.) was weighed out into a 100ml beaker into which 50ml of distilled water was then added. This mixture was heated on a hotplate (Rodwell Monotherm) set at full power. During this time, it was necessary to continuously stir the suspension with a glass rod so as to prevent the agar from burning. When the mixture had changed from a cloudy suspension into a clear golden-coloured solution, its temperature was continuously monitored with a mercury thermometer. When the solution attained a temperature of 85°C, the heating was stopped. The solution was poured into a thick-walled perspex cylinder, filling it almost to the top. A teflon plunger, tightly fitted inside the lower end of the cylinder and pegged to a flat teflon base on the bench, prevented the solution from leaking out. The cylinder was left at room temperature for 5 minutes before being refrigerated for between 1.5 to 4 hours.

After refrigeration, the gel had solidified and it was possible to disconnect the teflon plunger from the teflon base. The gel-filled cylinder was fitted into a specially designed micrometer screw gauge, which in turn was clamped to a retort stand. The arrangement is schematically illustrated in Figure 3.2.

The micrometer screw gauge was used to displace the gel vertically in several 0.5mm increments. After each incremental rise, the gel was cut flush to the top surface of the cylinder with a hand-held, flat-surfaced microtome blade. This was repeated until the top of the gel column was completely smooth and flat.

Figure 3.2: A Schematic diagram of the thick-walled cylinder fitted on the micrometer screw gauge.

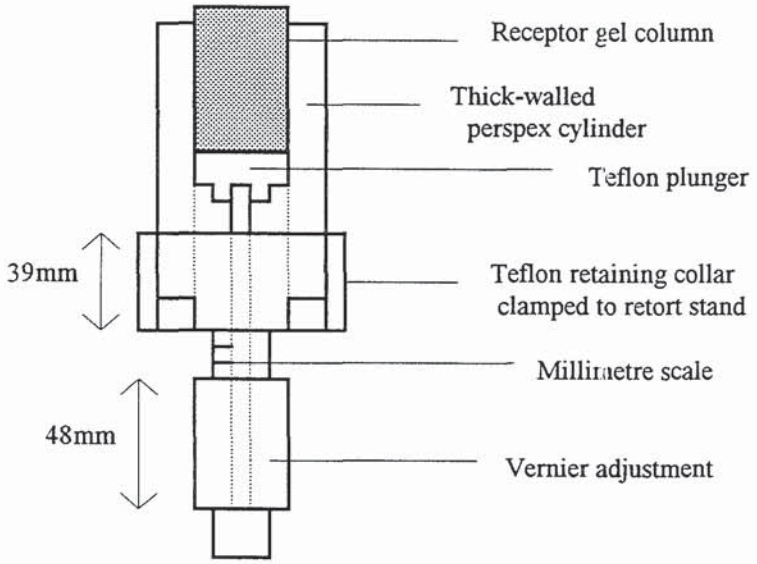

The agar gel was then extruded upwards by 0.5mm and a 0.5mm thick circular section was cut using the same technique. This slice, representing the backround radiation levels, was transferred by tweezers to a scintillation bottle, ready for counting at the end of the experiment. The gel column was then again pushed upwards, by just one more 0.5mm increment so that the top surface of the gel column just protruded above the top surface of the perspex cylinder. The receptor gel was then ready for the diffusion experiment.

3.2.3 Preparation of the Contact Gel

The contact gel was prepared by heating 3g of agar powder (Grade 1, Oxoid Ltd.) and 100ml of distilled water in an identical manner as to that described above for the receptor gel (In practice, it was quite convenient to combine the preparation of the two gel solutions). A thin-walled perspex cylinder, sealed at the base with a double layer of parafilm was then filled almost to the top with this solution. The cylinder was left at room temperature for 5 minutes and then refrigerated for

between 1.5 to 4 hours. After this time period, the cylinder was removed from the fridge and the radiolabelled disc was added as described in section 3.2.4.

3.2.4 Preparation of the Radiolabelled Disc

A small amount of agar powder (0.39g) was weighed out and placed in a 50ml conical flask containing a small magnetic stirring bar. A volume (13ml) of distilled water was then dispensed into the flask so as to produce a 3%w/v agar-water mixture. The flask was then placed on a magnetic hotplate (Rodwell Monotherm) with the heat control set at maximum and the magnetic motor scale set at a value of 2. The agar-water mixture was heated and agitated until the cloudy mixture was transformed into a clear solution. The temperature of the solution was then immediately measured with a differential thermocouple (Digitron instruments, 3202 type K). If the temperature of the solution was less than 85°C, the agar solution was reheated until this temperature was attained.

A 10µl aliquot of the required radiolabelled drug, representing 0.0185MBq of [^{14}C]-mannitol (Amersham), 0.37MBq of [^{3}H]-hydrocortisone (Amersham), or 0.037MBq of [^{3}H]-inulin (Amersham), was then pipetted into the 3%w/v agar solution. The radiolabelled compound was thoroughly mixed into the gel solution by applying the magnetic motor for 30 seconds. The magnetic stirring bar was then removed with a pair of tweezers. All of the solution was then poured into the thin-walled cylinder which had been sealed at the base with two layers of parafilm. This cylinder was then refrigerated for 45 minutes.

After the refrigeration period, the parafilm was removed. The radiolabelled disc was then carefully eased out of its perspex cylinder with tweezers and positioned inside one end of the other thin-walled cylinder containing the contact gel. It was made certain that the flat (originally bottom) surface of the disc was pushed up against the flat (originally bottom) surface of the contact gel. This manoeuvre may cause the other end (originally meniscus surface) of the contact gel to become extruded. Any extruded portion was cut flush to the cylinder surface with a large, sharp cut-throat razor. Finally, the razor was used to trim the meniscus surface of the disc so that a smooth, flat surface was obtained. The radiolabelled disc and contact gel were then ready for the diffusion experiment.

It should be noted that the agar gels prepared in 3.2.2, 3.2.3 and 3.2.4 exhibited a concentration of slightly less than 3%w/v. This is because the gel composition ratio was 3g of agar powder to 100ml of solvent rather than 3g of agar powder to 100ml of solution. Importantly, nearly all the experiments documented in this chapter, including the control experiments, were performed with agar powder derived from the same batch. There were only 2 experiments that were conducted using a different batch of agar powder. The consequences of this are discussed in section 3.3.6. It was observed during the preparation of the agar gels that only a few, tiny air bubbles developed in solution. This is advantageous as the presence of large air bubbles would interfere with drug diffusion as well as the propagation of ultrasound (see section 2.1.1).

3.2.5 Ultrasound-Exposure Protocol

At time zero, the two clamped cylinders were brought together horizontally such that the flat protruding surface of the receptor gel made direct contact with the flat surface of the radioactive disc. 20µl of distilled water was pipetted in between the two gels to act as a coupling medium and to exclude air bubbles. The two gels were left in intimate contact with each other for 50 minutes. A diagram of this arrangement is shown in Figure 3.3

In the ultrasound-exposure experiments, the large transducer of the ultrasound generator (Therasonic 1032 model no.50, E.M.S. Greenham Ltd.) was switched on (1.1MHz drive) at the selected intensity (1W cm^{-2} c.w., 2W cm^{-2} c.w. or 2W cm^{-2} pulsed 1:9). The radiating surface of the transducer was then coated with a layer of coupling medium (Therasonic, E.M.S.Greenham Ltd.). The transducer was then clamped into position so that the whole of its front surface was pressed against the contact agar gel in the thin-walled cylinder. Occasionally, during the experiments, the coupling medium would drip down on to the bench causing a loss of ultrasound transmission between the transducer and the agar gel column. In these situations, the ultrasound generator would automatically beep and more coupling medium was deposited between the transducer and contact gel.

Figure 3.3: A diagrammatic representation of the apparatus arrangement used in the diffusion experiment

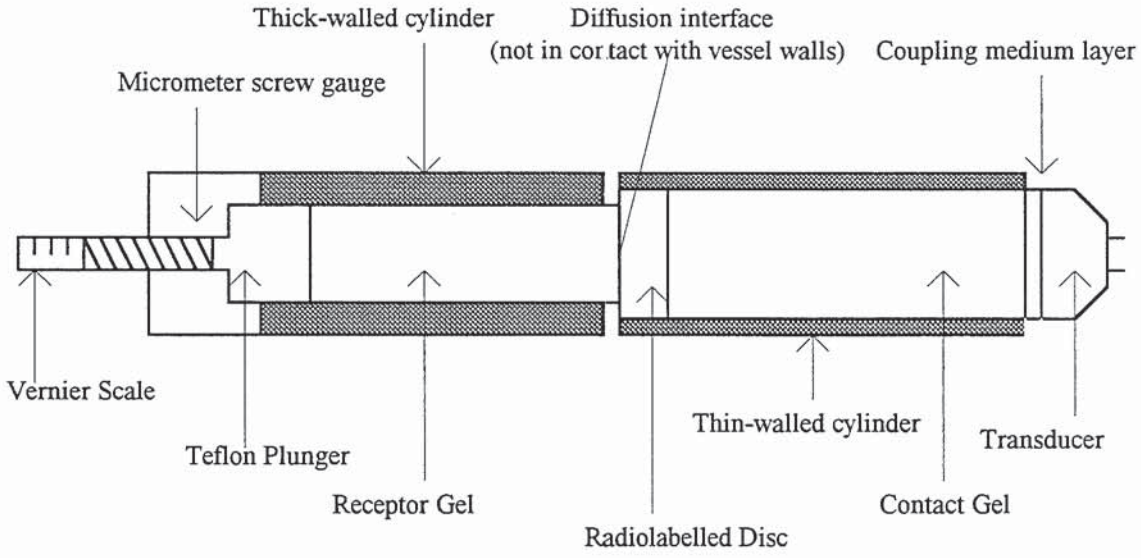

In the control experiments, the transducer was positioned in an identical manner except the machine was switched off and no coupling material was required. All the control and sonication experiments were conducted so that the pressure exerted on the system by each of the equipment components was as subjectively reproducible as possible. Each experiment was performed in triplicate.

After the 50 minute diffusion period was over, the thick-walled cylinder, still fitted to the micrometer screw gauge was re-orientated to a vertical position. The protruding top 0.5mm section of the receptor gel was then cut flush to the top surface of the perspex cylinder, with a hand-held, flat-surfaced microtome blade. The gel was then extruded upwards in a further eleven 0.5mm increments. After each incremental rise, the gel was cut in the same manner with the microtome blade. All the resulting circular sections of agar gel were transferred by tweezers into scintillation bottles. The scintillation bottles were serially numbered, thus facilitating the identification of each serial section in relation to its distance from the face previously exposed to the radioactive disc. After each individual slicing operation, the tweezers were immersed in a beaker containing an aqueous solution of 1%v/v Decon-90. They were then washed thoroughly by first immersing them

in a beaker of distilled water, followed by rinsing with a spray of distilled water ejected from a wash bottle. The microtome blade was only washed by spraying with distilled water. Both tweezers and blade were then thoroughly dried with paper towels. These procedures minimised any transfer of drug between serial slices by the blade or by the tweezers. To this end, fresh solutions of Decon-90 solution and distilled water were used every 4 or 5 slicing operations.

When all 12 serial gel sections and the backround gel section were in the scintillation bottles, 10ml of scintillation liquid (Optiphase Hisafe 3, LKB Scintillation Products) was dispensed into each of the bottles. Each scintillation bottle was then agitated for 20 seconds on a whirlimixer (FSA laboratory supplies) set at maximum power. The scintillation vials were transferred to a liquid scintillation counter (Packard 1900T.R) and the radioactivity emitted by each gel-slice was measured. The machine was pre-calibrated so that it could analyse beta emissions from both ^{3}H and ^{14}C radioisotopes. Furthermore, the activity value of the initial vial containing the background slice was automatically subtracted from subsequent samples, thus yielding the net activity emitted by each serial slice.

3.2.6 Gel Temperature Measurements

The aim of this experiment was to measure the temperature increase produced within the core of the gel disc and receptor gel during sonication with the 1.1MHz, 2W cm^{-2} beam.

All three agar gel components were prepared by heating as described before in sections 3.2.2, 3.2.3 and 3.2.4. The only difference was that the gel disc did not require radiolabelling. The contact gel and receptor gel were refrigerated for 1.5 hours while the disc gel was refrigerated for 45 minutes. After refrigeration, all the gel components in their cylinders were placed in beakers that had been sealed with two layers of parafilm. and left at room temperature. This arrangement allowed the gels to warm to room temperature while minimising the evaporation of water from the gels which would cause gel shrinkage. After 2 hours, the temperature of the gels was monitored with a digitron thermocouple in order to confirm that the gels had reached to at least 2°C of room temperature. This arrangement ensured

that all the gel components were at virtually the same, fixed temperature before sonication.

The contact gel and disc were transferred from the regular thin-walled cylinder to a modified thin-walled cylinder of identical dimensions which had had holes drilled every 0.5cm down one side. These holes had been purposefully designed to allow the thermocouple probe to be inserted inside, thus permitting temperature measurements to be taken. The two cylinders were then placed together as described in section 3.2.5 and 1.1MHz ultrasound was applied at 2W cm^{-2} for 50 minutes. Every 10 minutes, the core temperatures of the gel disc and contact gel were measured at 1cm intervals throughout the length of the thin-walled cylinder. Since the external diameter of the cylinder was 5cm, by inserting the probe inside the cylinder to a distance of 2.5cm, it was ensured that the temperature at the core was being measured. Using this technique, it was possible to determine the thermal profile at the gel core associated with exposure to a 2W cm^{-2}, 1.1MHz ultrasonic field.

3.2.7 Heat-Alone Exposure Protocol

The aim of this experiment was to initially devise a heat-alone exposure system that simulated the heating effect of the 2W cm^{-2}, 1.1MHz beam. In sequential work, this exposure system was applied to the agar gel model and this permitted the effect of heat-alone on drug diffusion to be measured.

All three gel components were prepared and subsequently left for 2 hours at room temperature. The contact gel and the radioactive disc were inserted inside the perforated thin-walled cylinder as described in section 3.2.6. The two cylinders were then brought in contact together as described in section 3.2.5, except ultrasound was not applied. Instead, a hollow copper wire, 3mm in diameter was coiled around the thin-walled cylinder. The copper tube carried a current of circulating water, maintained at 85°C by a thermostatically-controlled water bath (Gallenkamp Thermistor 85). A pump (H.R. Flow Inducer type MHRE, Watson-Marlow Ltd.) set at maximum power drove the water through the coil system. The wire was coiled from the free face end of the contact gel to a distance of 1cm from the receptor gel - disc gel interface. Refer to Figure 3.4.

Figure 3.4: The apparatus arrangement used to investigate the effect of heat-alone on drug diffusion.

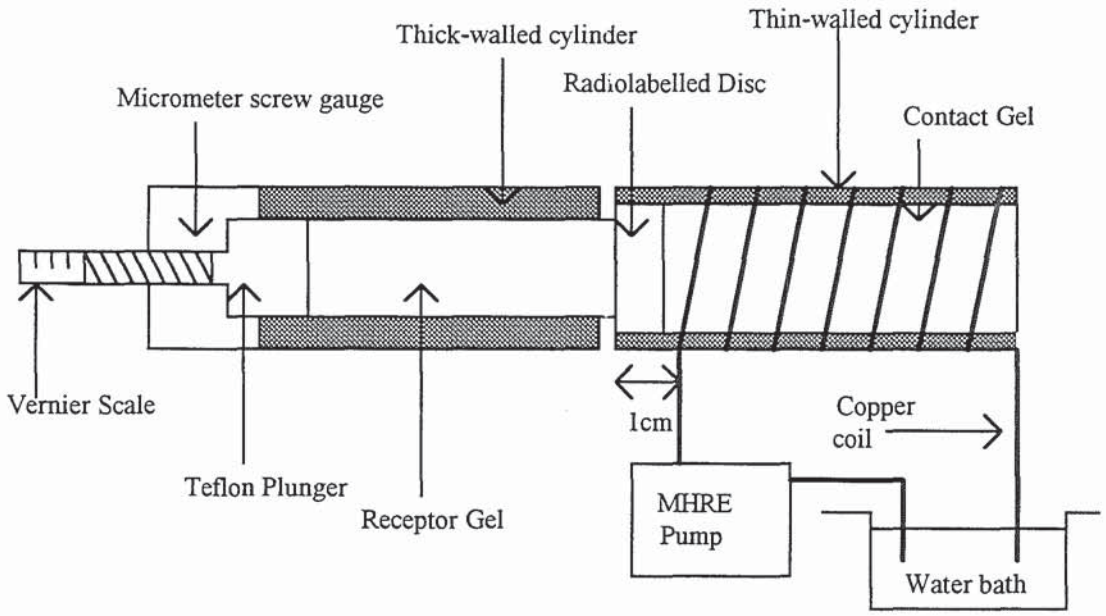

Using this arrangement, the gels were heated for 50 minutes. During this time, the gel core temperatures were measured with a thermocouple every 10 minutes as described in section 3.2.6. Sometimes, when the wire covered a hole, the coil had to be adjusted without causing too much disturbance to the arrangement.

The diffusion of mannitol, hydrocortisone and inulin, under the influence of applied heat-alone was then investigated. To this end, all 3 gel components were prepared as described in sections 3.2.2, 3.2.3 and 3.2.4 However, the gels were then refrigerated and subsequently left to warm to room temperature. The contact gel and the disc were left in the regular thin-walled cylinder for the diffusion experiment which was performed with the coil system illustrated in Figure 3.4. The analytical technique has been described in section 3.2.5.

3.2.8 Data Manipulation

The net activity value of each gel section was transformed by taking its natural logarithm. When these natural log values were plotted as a function of their

associated mean gel depth, a linear relationship was exhibited. Linear regression was employed to find the intercept of this line. The intercept value of the line was subtracted from each logged activity value. This results in the normalisation of the line. This manipulation was conducted separately on the results of each of the three replicates before they were pooled together to yield one line with error bars representing standard deviations. When a mean section depth was reached in which one or more of the runs emitted less than 100 disintegrations per minute (dpm), the line was discontinued. The calculations were conducted using the application 'Cricket-graph' on an IBM-compatible computer. They can be illustrated algebraically:

$$C = Ae^{-Bd} \tag{3.1}$$

$$LnC = LnA - Bd \tag{3.2}$$

$$LnC - LnA = -Bd \tag{3.3}$$

Where C is the concentration (effectively measured in terms of activity in dpm), A is the intercept value and d is the average gel depth in mm (so for example, the first 0.5mm section is assigned d = 0.25mm). Thus a line is obtained with a negative gradient B. The units of B are mm^{-1}. This slope parameter is important because its magnitude is related to the diffusibility of the test species. For example, under control conditions, mannitol permeation was characterised by a mean B value of $-0.90mm^{-1}$ whilst inulin permeation was characterised by a mean B value of $-1.65mm^{-1}$. This indicates that mannitol diffuses much more rapidly through the hydrogel than inulin.

By examining changes in the value of B under different exposure conditions, it was possible to quantitatively analyse the effect of ultrasound or heat-alone on drug diffusion. Individual slope parameters were compared by conducting unpaired t-tests. The first stage of this test involved calculating a t-statistic which is a measure of the relative difference between the two sets of data points. In this case, t is given by:

$$t = \frac{(\overline{B}_1 - \overline{B}_2)}{s\sqrt{\frac{1}{n_1} + \frac{1}{n_2}}} \qquad (3.4)$$

Where $\overline{B}_1$ and $\overline{B}_2$ are the mean values of the two slope parameters being compared, s is the standard deviation of the combined data and n_1 and n_2 are the number of data points associated with each respective slope parameter. The number of degrees of freedom (ν) exhibited by t is given by:

$$\nu = n_1 + n_2 - 2 \qquad (3.5)$$

In the second stage, each calculated t value with its associated ν value was entered into an 'Epistat' application on an IBM-compatible computer. The programme calculated a P value which represents the probability that the difference between the slope parameters developed purely by chance. When $P<0.05$ (the 95% confidence level), it was assumed that the slope parameters differed significantly from each other.

3.2.9 Measurements of the Experimental Variables

A series of studies were conducted in order to determine whether certain experimental variables can significantly affect measured activity. The variables were gel-section vortexing time, refrigeration time and room temperature exposure time.

3.2.9.1 Agitation Time Studies

The aim of this experiment was to determine if the emitted activity measurements of the scintillation counter vary as a function of gel-section vortexing time in scintillation liquid. To this end, an agar gel column, homogeneously distributed with one of the 3 drugs (mannitol, hydrocortisone or inulin) was prepared in the thick-walled cylinder. The gel column was prepared so that each 0.5mm section would contain approximately the same amount of drug as the uppermost section of the receptor gel in the diffusion experiments. Preliminary studies were performed

in order to determine the typical activity values of the uppermost section. The representative activity values were 5000dpm for mannitol, 100,000dpm for hydrocortisone and 10,000dpm for inulin. Circular sections of the gel column were subjected to different agitation times and the effect of this variable on emitted activity was measured. Initially, the volumes of radiolabelled stock solution required were calculated.

For [^{14}C]-mannitol: Require a gel exhibiting 5000dpm *i.e.* 83.3Bq per 0.5mm thick section

No. of such sections in cylinder (length of 55mm) = 55/0.5 = 110

$\therefore$ Required activity per cylinder = 110 * 83.3 = 9167Bq

i.e. Require 9167Bq of activity in cylinder of volume of 33.9cm^3

In practice, 50cm^3 of gel was prepared.

$\therefore$ Require (50/33.9) $\times$ 9167 = 13533Bq

= 0.013533MBq

Converting to volumes $\equiv$ 0.013533/1.85 = 0.007315ml

For [^{3}H]-hydrocortisone: Require a gel exhibiting 100,000dpm per 0.5mm section. The stock solution exhibits 20 times more activity per ml than the mannitol so 0.007315ml is the correct quantity.

For [^{3}H]-inulin: Similarly, require a gel exhibiting 10,000dpm per 0.5mm section. The inulin solution exhibits twice the activity per ml of mannitol so 0.007315ml is the correct quantity.

The preparative procedure involved heating 1.5g of agar powder and 50ml of distilled water as described in section 3.2.2. A solution of the radiolabelled compound (0.0073ml) was then pipetted into the hot agar gel solution. The mixture was agitated for 30 seconds on the magnetic plate. The gel solution was then poured into the thick-walled cylinder so as to completely fill it. The cylinder was refrigerated for between 1.5 to 4 hours. After refrigeration, the cylinder was attached to the micrometer screw gauge. The extrusion-slicing technique described in section 3.2.5 was then used to cut 15 serial gel sections. Each section was transferred to a labelled scintillation vial into which 10ml of Hisafe-3 scintillation fluid (Optiphase Hisafe 3, LKB Scintillation Products) was dispensed. The vials were divided into 5 groups of 3 representing 5 different agitation times, each run in triplicate. The agitation times were 10 seconds, 30 seconds, 1 minute,

2 minutes and 5minutes. The vials were then vortexed for these specific time periods on a whirlimixer (FSA laboratory supplies) before being quantitatively analysed for emitted activity as described in section 3.2.5.

3.2.9.2 Refrigeration Time Studies

The general preparation technique involved refrigerating the agar gels for between 1.5 to 4 hours. The objective of this experiment was to determine if the exact time period that the receptor and contact gels were refrigerated was in itself a factor that can influence subsequent drug diffusion. The experiment was conducted only with mannitol.

Six control runs of the mannitol diffusion experiment were performed in the manner described in sections 3.2.2, 3.2.3, 3.2.4 and 3.2.5 except that in three of the runs, the receptor and contact gels were refrigerated for exactly 1.5 hours whilst in the other three runs, the receptor and contact gels were refrigerated for exactly 4 hours. In both cases, the radioactive disc was refrigerated for 45 minutes. The analytical method and data analysis have been described in section 3.2.5.

3.2.9.3 Room Temperature Exposure Studies

In the diffusion experiments involving sonication, the gels had been tested for drug diffusion immediately after they had been removed from the fridge. In the experiments investigating the effect of applied heat alone, the gels had been left to warm to room temperature before being tested for drug diffusion. Clearly, the two protocols could not be directly compared as the experimental conditions had been altered. In order to determine whether leaving the gel to warm affects the outcome, the passive diffusion of mannitol was investigated in both gel directly removed from the fridge and gel at virtually room temperature.

This method involved preparing the gels as before (sections 2.2.2, 2.2.3, and 2.2.4), including the gel disc containing [^{14}C]-mannitol. The receptor and contact gels were refrigerated for between 90 minutes to 4 hours while the disc was refrigerated for 45 minutes. In three of the six experimental runs, all the gel components were placed in sealed beakers at room temperature. After 2 hours, it was confirmed by thermocouple measurements that all these gels were to within 2°

C of room temperature. A non-sonicated diffusion experiment (section 3.2.5) was then undertaken with both the warmed gels and the gels immediately removed from the fridge.

3.3 RESULTS AND DISCUSSION

3.3.1 General Interpretation of the Data

In this experimental model, diffusion occurs between a gel compartment containing a uniform concentration of radioisotope *i.e.* the radiolabelled disc and a receptor gel compartment which is initially drug-free. No barrier to diffusion is present at the interface between the two gels. By applying Fick's laws of diffusion, it is possible to derive an equation which describes diffusion in such a system (Kneschke, 1961):

$$C = C_0\sqrt{\frac{Dte^{-d^2/4Dt}}{\pi d}} \qquad (3.6)$$

Where C is the drug concentration at a certain depth, C_0 is the initial drug concentration in the drug-containing disc, D is the diffusion coefficient of the permeating molecule and d is the receptor gel depth. It is possible to calculate the D values by analysing the data using nonlinear regression analysis. However, this is not really necessary if the aim is to merely determine whether or not D is increased in the presence of ultrasound. Since the distance d is small compared to the total molecular diffusion path, it is possible to replace eqn (3.5) by a much simpler equation (Williams *et al.*,1990). This simpler relationship has already been presented as eqn (3.1):

$$C = Ae^{-Bd} \qquad (3.1)$$

Where C is the drug concentration at any point within the receptor gel (in dpm), d is the receptor gel depth (in mm), A is the drug concentration within the receptor gel at d = 0 and B is a variable whose value would be expected to change with among other factors, ultrasound exposure (Williams *et al.*, 1990). It is interesting to note that the term B includes the diffusion coefficient D.

However, eqn (3.1) will only hold true as long as the drug-containing disc contains a virtually infinite amount of drug relative to the receptor gel *i.e.* sink conditions are maintained. For the experiments reported in this chapter, it was calculated that over the 50 minute period, not more than about 2% of the total activity had

diffused from the disc to the receptor gel. It can also be assumed that the radiolabelled disc had also suffered a similar diffusion loss to the contact gel. Thus, the gel disc contains, at the end of the diffusion experiment, at least 95% of its original quantity of drug. Therefore, sink conditions are maintained in this model.

Eqn (3.1) can be transformed to yield eqn (3.2):

$$LnC = LnA - Bd \qquad (3.2)$$

Therefore, by plotting the natural log value of each data point as a function of its associated mean gel depth, and performing linear regression, a line was derived for each replicate run with intercept LnA and gradient B. It was necessary to normalise the data by subtracting the LnA value from each experimental run. This is because the magnitude of LnA depended upon the unreproducible contact pressure between the drug-containing disc and the receptor gel. When the data were plotted in terms of LnC - Ln A as a function of d, the value of B was represented by the gradient with the line always passing through the origin. This relationship has been presented as eqn (3.3):

$$LnC - LnA = -Bd \qquad (3.3)$$

It can be seen by looking at the graphs in Figures 3.6 to 3.17 that the logged, normalised plots are linear ($0.989 < r^2 < 0.996$) indicating that drug diffusion in the model correlated well with the theoretical predictions derived from Fick's laws. It was found that, generally, sonication resulted in a decrease in the value of B. This indicates that at any fixed depth in the receptor gel there is a relatively greater drug concentration *i.e.* drug diffusion is enhanced.

Some of the diffusion data were characterised by differences between replicate runs of the same experiment. These have been illustrated graphically as standard deviation error bars in Figures 3.6 to 3.17. One or more of several factors could be potentially responsible for this feature. One reason may be associated with differences in beam geometry produced by tiny variations in the transducer position or the angle that the transducer makes with the contact gel. Such variations would affect the proportion of ultrasound that is reflected off the

perspex walls of the cylindrical vessel. This would increase the standing wave component of the ultrasonic field at the diffusion interface. The production of standing waves and degree of ultrasonic heating would also depend upon the distance of the teflon plunger from the transducer and this factor was not controlled for in this system. The acoustics of this model have been discussed in greater detail in section 2.3.1.

The experimental scatter may also be derived from difficulties in reproducibly cutting sections to precisely the same thickness. In preliminary trials involving the cutting of 47 sections from a clear column of receptor gel, it was determined that the mean slice weight was 0.3114g and the sample standard deviation was 0.0412g. This represents an error of ±3.90% at the 95% confidence level. Furthermore, the receptor gel would sometimes be compressed during the diffusion experiment. As a consequence, the top mm or so, of the gel would end up being sliced into sections that were considerably more or considerably less than 0.5mm in thickness. This phenomenon explains the scatter particularily associated with the first one or two points in the data.

3.3.2 The Significance of the Experimental Variables

3.3.2.1 Agitation Time

The aim of this experiment was to determine if the duration of gel-section agitation in scintillation fluid influenced measured activity. Table 3.1 presents the emitted activities of sections originating from homogenously radiolabelled receptor gels. It can be seen that for all the compounds, agitation time did not influence the mean of the measured activity in any progressive way. The variations in measured activity between different agitation times as well as within each agitation time are probably due to variations in the thickness of the excised gel sections. Refer to section 3.3.1.

Table 3.1: The Effect of Agitation Time on the Activity Measurements of mannitol, hydrocortisone and inulin

Agitation Time (mins)	Measured Activity [^{14}C]-mannitol (dpm)	Measured Activity [^{3}H]-hydrocortisone (dpm)	Measured Activity [^{3}H]-inulin (dpm)
0.167	5891 ± 749	106200 ± 2243	6796 ± 712
0.5	5001 ± 242	99050 ± 9141	5521 ± 1331
1	5256 ± 957	108800 ± 3288	7346 ± 173
2	5067 ± 307	100600 ± 2352	5630 ± 1717
5	5074 ± 584	104900 ± 3664	6845 ± 1966
Grand mean	5258 ± 629	103901 ± 5541	6428 ± 1438

Values represent the mean ± sd of three replicates except for the grand mean where there are fifteen replicates

The gel containing mannitol had been prepared so that each average-sized slice would emit 5000dpm of activity. The gel containing hydrocortisone had been prepared so that each average-sized slice would emit 100,000dpm of activity. The gel containing inulin had been prepared so that each average sized-slice would emit 10,000dpm of activity. The overall mean measured activities per section were 5258dpm for mannitol 103,901dpm for hydrocortisone and 6428dpm for inulin. This indicates that the analytical technique detected all the activity emitted by the gel sections containing [^{14}C]-mannitol and [^{3}H]-hydrocortisone. However, the measured activity value for inulin was much lower than expected. The discrepancy for inulin is probably caused by significant residues of the drug remaining in the agar gel section at equilibrium. The emitted β radiation is attenuated during its passage through the gel and consequently does not interact with the scintillation liquid. However, this feature should not be a problem if it is assumed that there is a linear relationship between inulin concentration in the gel and measured activity. As explained in section 3.3.1, it is the amount of inulin relative to the amount in the first serial section that is of interest in these studies. It can be concluded that a 20 second vortexing time was adequate in order to quantitatively analyse the radiolabelled drug content in the gel sections.

3.3.2.2 Gel Refrigeration Time

The purpose of this experiment was to determine if the period of refrigeration of the receptor gel and contact gel affects subsequent mannitol permeation through the system. It was determined that following 1.5 hours of refrigeration, a slope of logged, normalised mannitol diffusion was characterised by B = -0.8901 ± 0.1736mm^{-1}(mean ± s.d). Following 4 hours of refrigeration, the slope was characterised by B = -0.8523 ± 0.2273mm^{-1} (mean ± s.d.). These two time periods represent the extremes of refrigeration time period used in the general method. It was calculated by applying an unpaired t-test that the slopes were not significantly different (P=0.617). It can be concluded that the exact period of refrigeration does not significantly affect mannitol diffusion.

3.3.2.3 Room Temperature Exposure Time

The objective of this experiment was to ascertain if pre-exposing the gel at room temperature affects the subsequent mannitol diffusion profile. It was found that in a gel just removed from the fridge, logged, normalised mannitol diffusion exhibited a B value of -0.9034 ± 0.2231mm^{-1} (mean ± s.d.). In a gel, equilibrated to room temperature, the logged, normalised slope of mannitol diffusion was -0.80895 ± 0.3895mm^{-1} (mean ± s.d.). By applying an unpaired t-test, it was determined that these slopes were not significantly different (P=0.834).

3.3.3 The Thermal Profile of the Heat-Alone Application

Figure 3.5 presents the temperature profile through the length of the gel core following both sonication at 2W cm^{-2} and the application of the heating-coil. Temperature measurements at both 20 and 50 minutes are shown. It can be seen that the ultrasonic heating profiles were characterised by elevated temperatures in the vicinity of the transducer face and this is due to heat conduction from the hot radiating surface. Thereafter, the temperature droppped with increasing distance from the transducer face and this is due to the progressive absorption of the ultrasound by the agar gel. Irregularities in the thermal profile are due to acoustic maxima and minima developing as a consequence of interference. In contrast, the heating coil produced a simpler thermal profile with the highest temperatures

recorded over the middle of the donor gel column where the heating coil was centred.

Figure 3.5: The Effect of 2W cm^{-2} Ultrasound and an Equivalent Heat-Alone Source on Gel Core Temperatures (n=3)

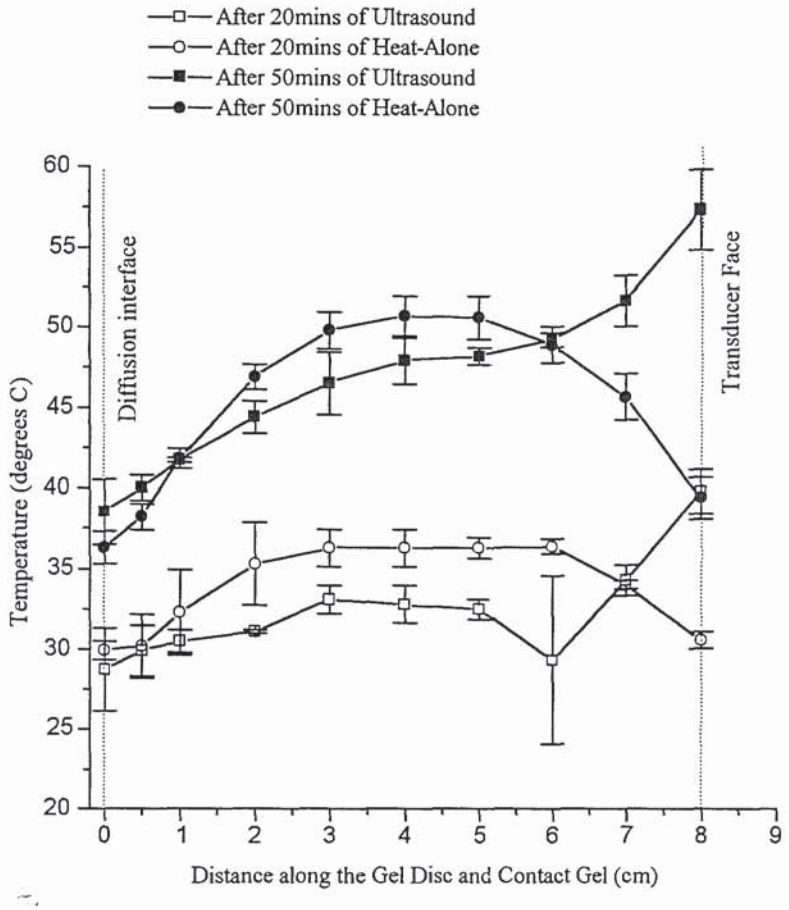

The temperature at the diffusion interface is of particular interest since this value is important for the diffusion of the test compound. It can be seen that both the 2W cm^{-2} beam and the heat-alone application produced interface temperatures of around 30°C at 20 minutes and 37°C at 50 minutes. It can be concluded that the heating coil arranged simulated the ultrasonic heating profile of the ultrasound fairly closely.

3.3.4 Mannitol Diffusion through Agar Gel

Table 3.2 presents the slope parameters derived from linear regression analyses of the different test and control data points. It can be seen that under control conditions, mannitol permeation was characterised by a mean B value of $0.90mm^{-1}$.

Table 3.2: Linear Regression Analysis Data for Mannitol Diffusion through Agar Gel

SATA intensity ($W\ cm^{-2}$)	$-B \pm$ s.d. (mm^{-1})	Enhancement $B_{int.=0} / B_{test\ int.}$	t-test $B_{int.=0}$ v $B_{test\ int.}$
0	0.9034 ± 0.4741	1	-
0.2 (pulsed 1:9)	0.7587 ± 0.2459	1.19	P = 0.156
1	0.7168 ± 0.2396	1.26	P = 0.091 *
2	0.6784 ± 0.2046	1.33	P = 0.037 **
Heat-Alone (≡2)	0.7550 ± 0.3601	1.20	P = 0.228

** represents a significant difference at the 95% confidence level

* represents a significant difference at the 90% confidence level

Sonication increased mannitol penetration through agar gel in a dose-responsive manner. The application of pulsed ultrasound (SATA intensity $0.2W\ cm^{-2}$) and c.w. $1W\ cm^{-2}$ ultrasound resulted in a statistically insignificant increase in mannitol permeation. Only the application of a $2W\ cm^{-2}$ beam produced a significant increase in the drug migration rate. Figure 3.6 presents a graph of logged normalised activity as a function of gel depth for both the control and sonication ($2W\ cm^{-2}$) data.

Figure 3.6: The Effect of 1.1MHz Ultrasound on Mannitol Diffusion through Agar Gel

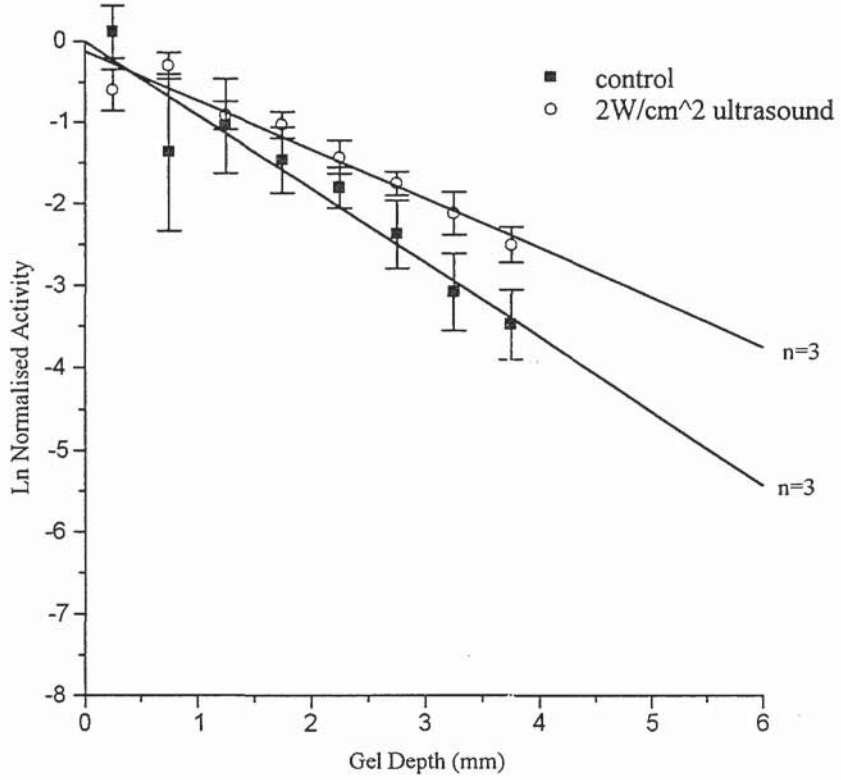

The application of heat-alone also produced an insignificant increase in drug migration as can be seen from Figure 3.7 and Table 3.2. This suggests that the thermal component of the ultrasound is responsible for the diffusion enhancement effect. For a spherical particle or molecule in a homogenous medium, molecular diffusivity and temperature are related according to the following relationship:

$$D = \frac{kT}{6\pi\eta r} \qquad (3.7)$$

Where D is the diffusion coefficient (measured in $cm^2\ s^{-1}$), k is the Boltzman constant ($1.38\times10^{-23} J\ K^{-1}$), T is the absolute temperature (in K), η is the viscosity of the solvent (in $g\ cm^{-1}\ s^{-1}$) and r is the particle radius (in cm). It can be seen that the heat produced in the experiments will directly increase the diffusion coefficient of mannitol. It should be noted that in the hydrogel environment, the mannitol molecules are solvated by the water present within the gel. Each mannitol

molecule is associated with a hydration shell such that the sugar and bound water molecules move as a unit in solution. Therefore, the particle radius value for eqn (3.7) is not the radius of each mannitol molecule but the radius of each hydration shell.

Figure 3.7: The Effect of Heat-Alone on Mannitol Diffusion through Agar Gel

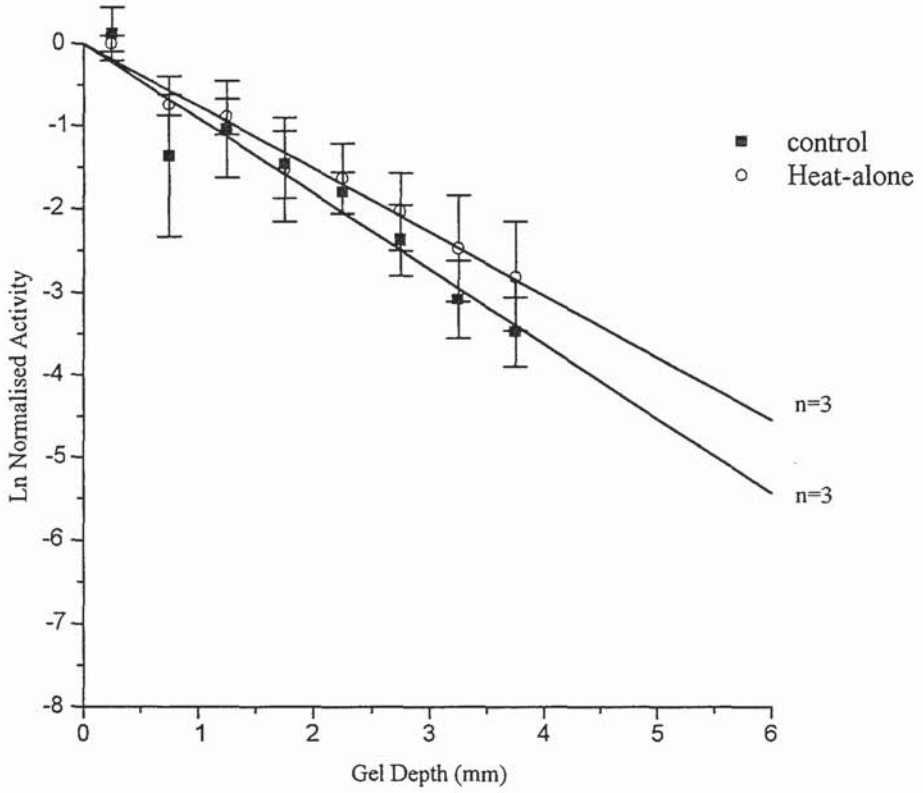

3.3.5 Hydrocortisone Diffusion through Agar Gel

Table 3.3 summarises the slope (B) values obtained from linear regression analyses of the various exposure and control data points for hydrocortisone. Under non-sonicated conditions, the mean B value was 1.27mm^{-1}. This means hydrocortisone permeates more slowly through agar gel than mannitol. In order to determine why this occurs, it is necessary to consider that hydrocortisone is relatively lipophilic (Log P octanol/water = 1.55). Lipophilic molecules will aggregate together upon their introduction into an aqueous environment This process is associated with an increase in entropy and a decrease in free energy which makes it energetically

favourable (Florence and Attwood, 1981). For the purposes of diffusion within agar gel, each of these aggregates of hydrocortisone molecules acts as a single hydrodynamic unit. Consequently, the effective radius of hydrocortisone particles is greater than the radius of solvated mannitol molecules. It can be deduced from eqn (3.7) that hydrocortisone migration will be slower than mannitol migration.

At all intensities, sonication significantly increased the rate of hydrocortisone transport through the gel. Furthermore, the more intense beams produced a greater ultrasound-enhancement effect, thus demonstrating a dose-response relationship. Interestingly, the application of heat-alone also significantly increased hydrocortisone migration. Again, this suggests that the thermal effects of the acoustic field are primarily responsible for enhanced diffusion although other mechanical effects cannot be ruled out.

Table 3.3: Linear Regression Analysis Data for Hydrocortisone Diffusion through Agar Gel

SATA intensity ($W\ cm^{-2}$)	$-B \pm$ s.d. (mm^{-1})	Enhancement $B_{int.=0} / B_{test\ int.}$	t-test $B_{int.=0}$ v $B_{test\ int.}$
0	1.2749 ± 0.2157	1	-
0.2 (pulsed 1:9)	1.0820 ± 0.1528	1.18	$P < 0.001$ **
1	0.9278 ± 0.3967	1.37	$P < 0.001$ **
2	0.8718 ± 0.2260	1.46	$P < 0.001$ **
Heat-Alone (≡2)	0.7397 ± 0.1548	1.72	$P < 0.001$ **

** represents a significant difference at the 95% confidence level

Figure 3.8: The Effect of 1.1MHz Ultrasound on Hydrocortisone Diffusion through Agar Gel

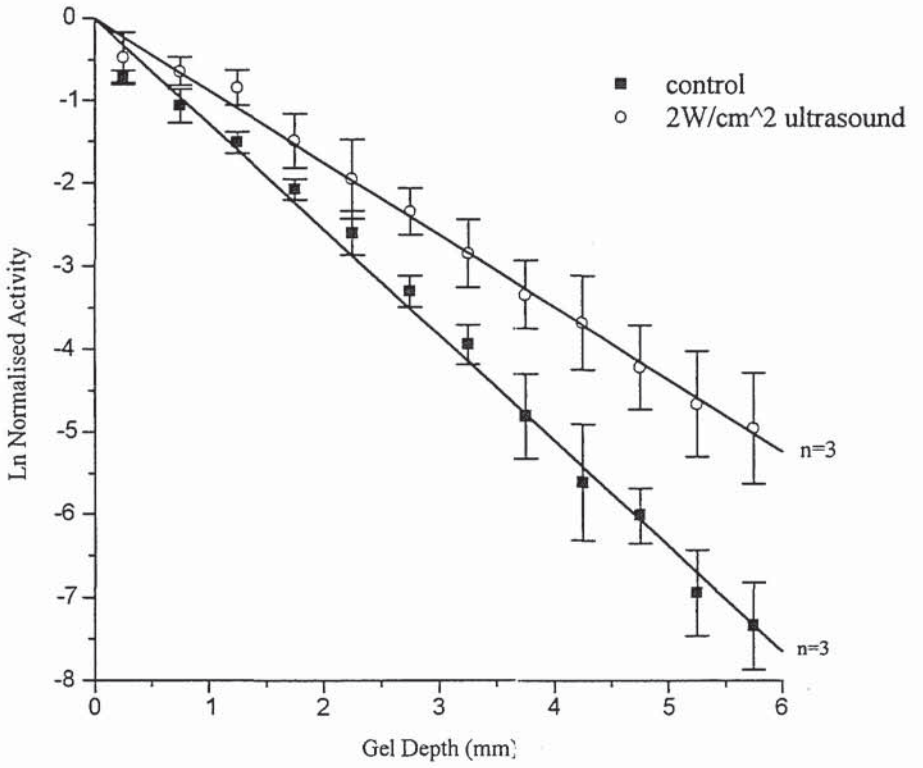

The heat-alone and 2W cm^{-2} ultrasound exposure data are presented in full, in graph format in Figures 3.8 and 3.9 respectively. It can be seen that heating increases hydrocortisone migration much more dramatically than mannitol migration. This is because heat will increase hydrocortisone diffusion by 2 separate mechanisms. Firstly, higher temperatures are associated with a direct increase in molecular diffusivity, *i.e.* the T term in eqn (3.7) is increased. This is the same mechanism that occurs for mannitol. Secondly, heating weakens the cohesive forces acting within each aggregate of hydrocortisone molecules. Consequently, there is a reduction in the hydrocortisone particle radius and a concomitant increase in diffusion.

Figure 3.9: The Effect of Heat-Alone on Hydrocortisone Diffusion through Agar Gel

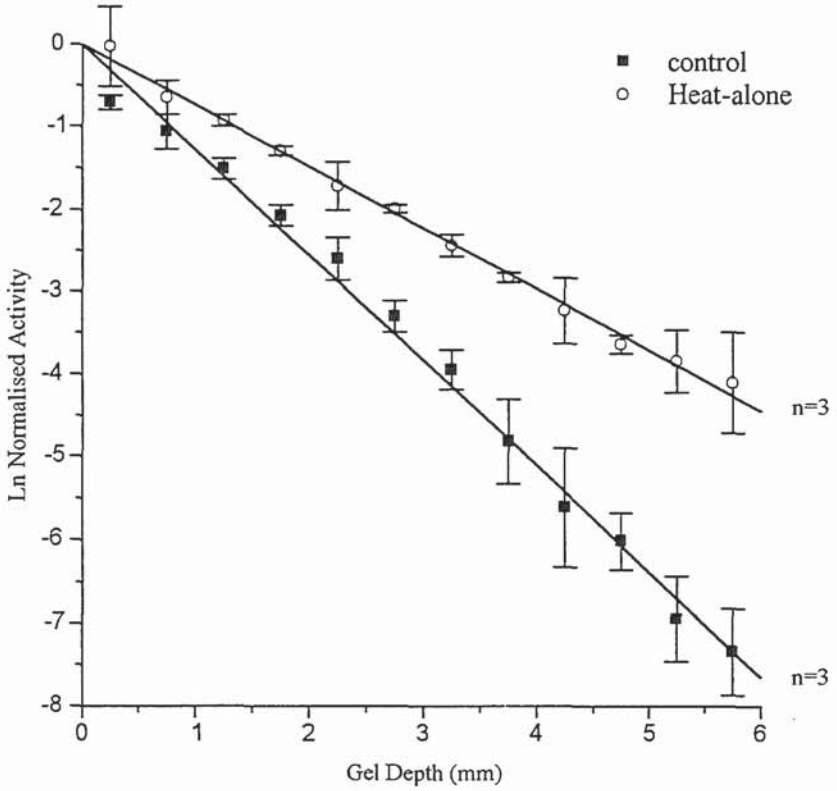

3.3.6 Inulin Diffusion through Agar Gel

Table 3.4 lists the logged, normalised slope parameters (B values) for the inulin migration experiments. Under control conditions, the mean value of B was 1.65mm^{-1}. This means inulin is the slowest penetrant through agar gel out of the 3 compounds investigated. Since inulin exhibits a molecular weight of 5200Da it is sufficiently large to interact with the matrix of the gel and this acts as a physical barrier to diffusion.

Figure 3.10 graphically displays the control as well the 2W cm^{-2} exposure data. It can be discerned that sonication at intensities of both 1W cm^{-2} and 2W cm^{-2} had virtually no effect on inulin migration. Although ultrasonic heating generally increases molecular diffusivity, in this case, the permeation of the large inulin molecules is impeded by the macromolecular mesh of the agar gel.

Table 3.4: Linear Regression Analysis Data for Inulin Diffusion through Agar Gel

SATA intensity ($W\ cm^{-2}$)	$-B \pm$ s.d. (mm^{-1})	Enhancement $B_{int.=0} / B_{test\ int.}$	t-test $B_{int.=0}$ v $B_{test\ int.}$
0	1.6547 ± 0.4681	1	-
0.2 (pulsed 1:9)#	1.2054 ± 0.6219	1.37	$P = 0.016$ **
1	1.5396 ± 0.3310	1.07	$P = 0.376$
2	1.6607 ± 0.3033	1.00	$P = 0.932$
Heat-Alone (≡2)#	1.1063 ± 0.2474	1.50	$P < 0.001$ **

** represents a significant difference at the 95% confidence level

# indicates that in these experiments, the gel was formulated from a new batch of agar powder

Figure 3.10: The Effect of 1.1MHz Ultrasound on Inulin Diffusion through Agar Gel

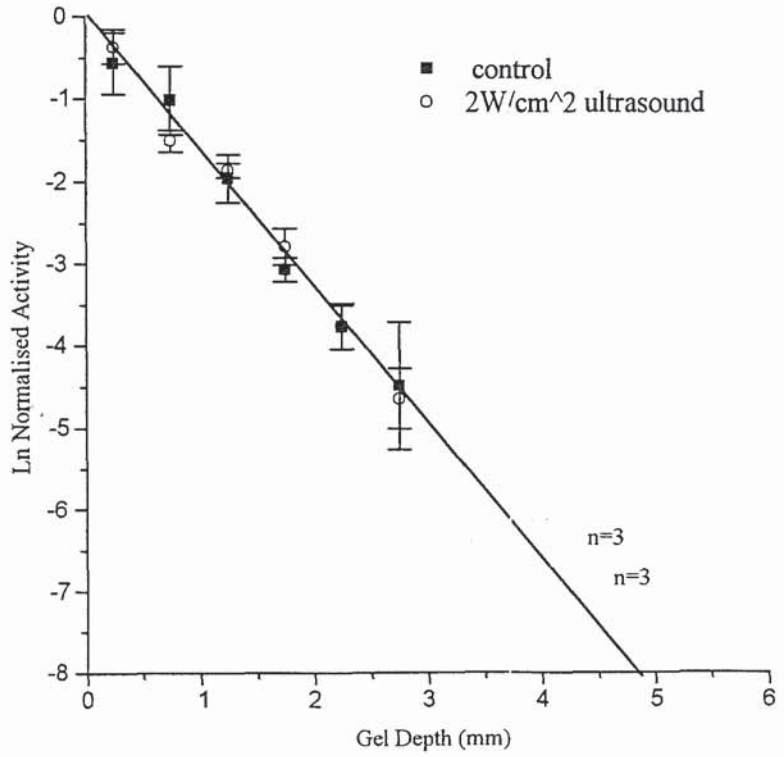

Large decreases in B were observed in inulin experiments involving the application of pulsed ultrasound and heat-alone. However, as mentioned in section 3.2.4, in these experiments, the agar gel had been prepared from a new batch of agar powder. Since agar is a natural product derived from concentrates of red algae, there are batch to batch differences in composition and these are likely to affect the gel properties. This factor poses a significant limitation for work with agar. Further research with this type of model should be conducted with a suitable synthetic hydrogel in which batch to batch variations would be very much reduced. Ideally, the selected synthetic gel should exhibit greater mechanical strength yet less elasticity than agar gel. This should reduce the variability between thicknesses of sequential sections and therefore decrease the contribution to systemic error discussed in section 3.3.1.

3.4 SUMMARY

It was determined that under control conditions, each of the three drugs exhibited a different diffusion rate through agar gel. The most rapidly permeating compound was mannitol, followed by hydrocortisone while inulin exhibited the slowest gel migration rate. Hydrocortisone migrated more slowly than mannitol as a consequence of its more lipophilic nature and therefore greater particle size in the hydrogel. The much larger inulin molecule interacted with the polymeric network of the agar and this suppressed its diffusion through the gel.

Sonication accelerated both the migration of hydrocortisone and to a lesser extent, the migration of mannitol. Since the application of heat-alone increased drug diffusion by a similar magnitude as the ultrasound, it is reasonable to conclude that the thermal effects of the ultrasound are producing these enhanced migration effects. The generated heat is probably directly increasing the themodynamic potential for diffusion. Hydrocortisone transport was more markedly affected by ultrasound than mannitol migration. This indicates that slowly migrating hydrophobic molecules are more susceptible to a greater relative increase in diffusion than rapidly migrating hydrophilic molecules. Sonication did not affect inulin migration as the molecule was too large to readily pass through the aqueous pores of the agar gel.

Just as agar gel consists of polysaccharide macromolecules containing aqueous pores, the stratum corneum is composed of keratinised cells separated by intercellular lipid channels. From the results of the hydrogel experiments, it might be expected that small, hydrophilic molecules would be the ideal candidates for phonophoresis across the skin.

CHAPTER FOUR

IN VITRO PHONOPHORESIS THROUGH RAT SKIN: THE EFFECTS OF PRESONICATION

4.1 INTRODUCTION

Most of the research into phonophoresis has involved models in which percutaneous absorption occurs concurrently with ultrasound exposure. In this chapter, skin samples were subjected to ultrasound and then examined for changes in skin morphology and barrier properties. This chapter starts by discussing the contribution of transfollicular routes in percutaneous absorption and the related issue of the structure of the pilosebaceous follicles. The experimental techniques involved in these studies include lipid staining, ATR-FTIR spectroscopy and *in vitro* permeation studies. The principles and background of each of these methods is also outlined.

In the experimental section, samples of whole rat skin were exposed to ultrasound (1.1MHz or 3.3MHz) across a range of intensities (0 to 2W cm^{-2}). The ultrasound was arranged to be in the form of a non-reflecting beam so as to eliminate unpredictable standing wave effects. The acoustics of this system have been discussed in more detail in section 2.3.2 The sonicated skin sections were then histologically analysed in order to evaluate the nature of any ultrasound-induced perturbations. It was convenient to classify effects into those produced by low intensity ultrasound (<1W cm^{-2}) and high intensity ultrasound (1 to 2W cm^{-2}) respectively. The effects of high intensity ultrasound on the stratum corneum were then investigated using ATR-FTIR spectroscopy. Control and ultrasound-exposed rat skin samples were also used as barriers for percutaneous absorption experiments with several different compounds. Some key permeation experiments were also performed with other skin species.

After discussing the results obtained from each series of studies, the overall conclusions of this work are summarised in the final section.

4.1.1 The Importance of Transfollicular Permeation Routes

Although the cornified layer is acknowledged as the principal barrier to percutaneous absorption, it has also traditionally been viewed as the main pathway for permeation (see section 1.1). This is based upon the fact that, in humans, the

follicles, comprising the sweat glands and pilosebaceous channels, occupy only about 0.1% of the total skin surface area. It was considered that the shunt routes play an insignificant role, at least during the steady-state phase of drug diffusion (Scheuplein, 1967).

Some doubt was cast on this hypothesis following *in vivo* pesticide absorption studies in humans. It was noted that drug penetration was greater from the scalp, which contains a high density of hair follicles, than from the forearm, which is less hairy (Maibach *et al.*, 1971). In studies involving newborn rats, it was observed that transdermal absorption was low on the first day after birth, when follicles are absent and then increased in the following few days as follicles are formed in the animals (Behl *et al.*, 1985; Illel *et al.*, 1991). One team developed a technique in which an area of follicle-free skin was regrown on the back of hairless rats (Illel and Schaefer, 1988; Illel *et al.*, 1991). This model was employed to study the absorption of several different compounds *in vitro*. The compounds were hydrocortisone, niflumic acid, caffeine and p-aminobenzoic acid. For all the agents tested, a much slower penetration rate was observed with follicle-free skin compared with normal skin. In the absence of hair follicles, the linear flux and the amounts permeating in the subsequent 48 hours were 25% to 50% of the values in intact skin. Another group used a skin culture penetration chamber system to assess the *in vitro* permeation of both testosterone and benzo[a]pyrene through whole mouse skin (Kao *et al.*, 1988). In a key step, an in-house derived mouse strain was selected that exhibited 3 different phenotypic variants due to hair density. Significantly, the permeability of both compounds was highest in the skin of the hairy phenotype, lowest in the hairless phenotytpe and intermediate in the fuzzy-haired animal.

A criticism of these studies is that the observed penetration differences between the two skin barriers may have been caused by other features such as stratum corneum thickness. In order to avoid this problem, some workers have investigated only one skin membrane and used histoautoradiography to demonstrate that many drugs selectively deposit in the follicles or sweat glands (Bidmon *et al.*, 1990, Fabin and Touito, 1991). However, these techniques are merely demonstrating tight drug-tissue binding which is not the same as quantitatively important penetration.

Current thinking is that the follicular pathways play a much more important role in transdermal delivery than previously thought (Lauer *et al.*, 1995). Since the hair follicle shafts account for an approximate fractional area of 0.1% of the human skin surface compared to only about 0.01% for the sweat glands, research has tended to focus on the pilosebaceous channels. However, the absence of a model that is truly follicle-free, yet retaining all the other properties of normal skin means that the contribution of the follicular route cannot be truly ascertained.

4.1.2 The Structure and Function of the Pilosebaceous Units

The pilosebaceous unit comprises the hair shaft, hair follicle, and sebaceous glands. The primary role of this structure is the secretion of sebum which exhibits lubricant, bacteriostat and fungicidal actions. Human hair follicles exhibit a mean diameter ranging from 10 to 70μm. The outer root sheath is the most important layer of the follicle with regard to drug delivery. This layer is continuous with the epidermis and constitutes a large surface area for drug absorption below the skin surface. The entire pilosebaceous unit is supplied with an extensive capillary network and this can facilitate drug transport from the hair follicle to the systemic circulation.

In humans, the sebaceous glands are largest and more numerous on the face and upperbody. Here the glands are often composed of several lobes emptying into a common duct, which then joins the pilosebaceous duct. Sebum is secreted by the holocrine mechanism. Cell division occurs at the periphery of the glands in an outer layer of cells. Some of these cells continually migrate into the interior of the gland where they progressively accumulate lipid. During this differentiation phase, the cells can increase in volume by up to 100 times. Finally, the sebaceous cell autodestructs and the lipids are released into the pilosebaceous channel. The lipid secreted by sebaceous glands are synthetised almost entirely within the glands. Human volunteer studies have shown that it takes an average of 8 days for radioactivity from intradermally injected acetate to reach the skin surface in the form of radioactive lipid.

Measuring sebum secretion rates is notoriously difficult and this is due to both theoretical and practical considerations. Initially, to provide a baseline, previously

secreted lipids must be removed from the skin by some form of washing process. It has proved extremely difficult to remove residues of secreted sebum which have accumulated within the pilosebaceous channels. Futhermore, surface lipids can flow away from the collection site or be removed by adhesion. Also, the size and number of sebaceous glands per unit area of skin varies greatly from site to site as well as between corresponding sites on different individuals. Consequently, absolute activity sebaceous gland activity cannot be assessed in terms of values of sebum secretion per unit area.

It is also very difficult to determine the lipid composition of sebum. Although most of the lipid film on the mammalian skin surface is secreted by the sebaceous glands, a small fraction is derived from the stratum corneum. Skin lipids have been collected and measured by applying various devised techniques. However, there is no known method available that will selectively collect pure sebum or pure stratum corneum lipids. Consequently, most of the literature reports deal with the composition of total skin surface lipids, regardless of their source (Downing and Stewart, 1985).

Table 4.1 presents comparative data on the composition of surface lipids derived from humans, rats and guinea pigs (Wheatley, 1965). Human surface lipid contains a higher proportion of free fatty acids than the surface lipid of the other two species. It is known that the contents of dissected human sebaceous glands include only trace amounts of free acids. From this and other observations, it has been deduced that, in humans, bacteria convert sebaceous triacylglycerides into free acids after the sebum leaves the gland. This process is much reduced in rats and guinea pigs. Since it contains a higher proportion of free acids, human surface lipid contains smaller fractions of esterified acids and non-saponifiable lipids, compared to the other two species. In the non-saponifiable lipid fraction, there are several subtle differences between each of the three species. One noticeable feature of human sebum is the presence of squalene. In the other animals, squalene is rapidly converted to sterols, but this biochemical pathway is blocked within human sebaceous glands.

Table 4.1 Composition of the Skin Surface Lipids in Three Different Species (Wheatley, 1965)

4.1.3 The Principles of Lipid Staining

The Sudan-type dyes have been established for many years as the most effective dyes for staining unsaturated, hydrophobic lipids (Bayliss High, 1990). These agents are diazo compounds in which the azo bond acts as a chomophore that imparts the distinctive stain colour to the compound. These dyes undergoe adsorption into cellular fats, thus staining them. In order for this to occur, the sudans must be initially dissolved within a suitable organic solvent which is itself sufficiently aqueous so as not to extract cellular lipids. Thus, the staining process is optimised by dissolving each particular Sudan dye within a specific solvent *e.g.* Oil Red O in 60% aqueous isopropanol. These agents will dye all hydrophobic lipids that are liquid or semi-liquid at staining temperature. Since the melting point depends upon the number of double bonds in the molecule, the Sudan dyes will stain all unsaturated fatty acids, esters and non-saponifiable lipids.

Sudan Black is generally considered the most sensitive and versatile of the Sudan dyes. However, for the precise localisation of fats, Oil Red O (Sudan Red) has been assessed as more effective. This red dye is often employed in conjunction with a haemulum dye which stains nucleated cells, blue.

Tissue specimens are generally prepared for sectioning by pre-embedding within a solid supporting matrix. Embedding in paraffin wax is a simple and routinely used method. However, this technique requires the pre-application of dehydrating and clearing agents to the tissue and these leach out endogenous skin lipids. Consequently, frozen sections are obligatory for lipid histochemistry.

4.1.4 Principles of ATR-FTIR Spectroscopy

Attenuated Total Reflectance Fourier Transform Infrared Spectroscopy is a technique which can used to elucidate the molecular structure of biological membranes such as the stratum corneum.

The infrared region of the electromagnetic spectrum lies at wavelengths between 2.5 and 15μm (4000 to 650cm^{-1}). This corresponds to the natural bending and stretching energies of most molecular vibrations. As molecules absorb infrared radiation, only specific frequencies of the spectrum which are equivalent to the natural vibrational energies of the interacting molecule are absorbed. Hence, each vibrational frequency is characteristic of a specific functional group. Consequently, the process of infrared spectroscopy presents a simple and rapid technique of identifying chemical structures. In recent years, the technique has been radically improved by the development of Fourier transform methods. This modification means that analysis can now be performed with relatively less noise, increased sensitivity, more accurate frequency determination and improved resolution.

In Attenuated Total Reflectance, an infrared beam is emitted through a infrared-transparent crystal. The configuration of the crystal results in the multiple internal reflection of the beam until it exits from the opposite face. The beam is then directed back to the spectrophotometer. During passage through the crystal, the

radiation actually penetrates slightly beyond the reflecting surface of the crystal, before returning. This phenomenon is based on the principle that at the interface between two media exhibiting different refractive indices, radiation will penetrate into the second medium as it is undergoing total reflection. As a result of this effect, any membrane in contact with the crystal (*e.g.* stratum corneum) absorbs infrared energy at frequencies corresponding to its normal absorption spectrum. Multiple reflections amplify the signal. This technique has been extensively used to investigate the effect of chemical enhancers on the stratum corneum. However, only very limited ATR-FTIR work has been conducted in order to research ultrasound-skin interactions (Machluf and Kost, 1993; Nanavaty *et al.*, 1989).

4.1.5 Permeation Studies

The main justification for employing *in vitro* models centres on the concept that the barrier properties of the stratum corneum, which is a non-viable tissue, do not significantly differ in the *in vivo* and *in vitro* environments. Much of the current understanding about the nature of percutaneous absorption has evolved from *in vitro* studies conducted in a controlled environment. These *in vitro* experiments have been employed as a tool to identify and optimise the various parameters which control drug delivery. This has been a great aid in the development of topical pharmaceutical products. However, the model does exhibit several disadvantages. The absence of a functioning blood supply can influence the clearance and therefore permeant transport. Reduced enzymatic activity in the epidermis and the non-renewal of the stratum corneum are other factors. Despite these differences, good correlations have been reported between *in vitro* and *in vivo* models, suggesting that well-designed *in vitro* techniques can deliver beneficial data, predictive of the *in vivo* situation (Franz, 1978).

A diversity of diffusion cells, of various types and designs, may be used for performing *in vitro* penetration studies (Franz, 1975). Many have evolved from the design of Franz, where an intervening skin membrane acts as a barrier between the donor and receptor compartments. Since the skin lies horizontally, its surface is exposed to room temperature and relative humidity while the undersurface can be maintained at body temperature. Hence, the Franz cell system is designed to

simulate the *in vivo* environment. Drug permeation is assessed by a suitable analytical method such as radiochemical scintillation counting.

Ideally, human skin should be used for *in vitro* work as it is most representative of the *in vivo* barrier. The problem with human skin is that parameters such as skin age, site, hairiness and condition confer large inter-specimen and intra-specimen variabilities in terms of barrier properties. Supplies of human skin are frequently limited and this further compounds this problem. In contrast, animal skin is easier to obtain and confers much more control over most of these parameters, thus decreasing variability. However, care must be exercised in using animal skin as a substitute for human skin. The results may differ and this depends both upon the animal species and the nature of the penetrating molecule. Whole skin from Wistar rats was employed for most of the permeation studies and this choice was dictated by the ready availability of this tissue. Since rodent skin is generally more permeable than human skin, some key experiments were repeated with human skin.

Algebraic relationships describing the transport behaviour of permeants through the skin are crucial in order to elucidate the basic principles which control this process. A typical permeation profile of a drug through the skin is presented in Figure 4.1. There is an initial lag phase corresponding to the time period in which penetrant flux through the barrier is attaining equilibrium. This is followed by a linear or steady-state phase which occurs when there is a balance between the ingress and egress rates of drug in and out of the skin membrane. Fick's first law of diffusion can be appied to model the linear phase. The law states that the permeation rate, at any one instance, is proportional to the concentration gradient across the barrier:

$$J = -D\frac{dc}{dx} \qquad (4.1)$$

where J is the amount of drug penetrated through a unit area of skin per unit time (measured in $\mu mol\ cm^{-2}\ h^{-1}$), D is the diffusion coefficient of the drug in the skin (measured in $cm^2\ h^{-1}$), and dc/dx is the drug concentration gradient across the skin (in $\mu mol\ cm^{-4}$).

However, it must be taken into account that the stratum corneum exhibits an affinity for the permeant. Consequently, the drug concentration at the skin surface

Figure 4.1: Typical Profile for Percutaneous Drug Absorption

(from Barry, 1983)

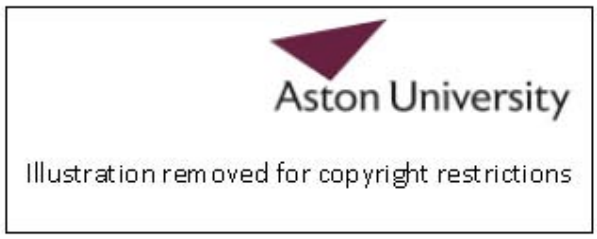

is not identical to that in the donor solution but is related to it according to the membrane-vehicle partition coefficient, P. This presents a measure of the relative affinity of the drug for the stratum corneum and donor solution. Equation 4.1 can therefore be transformed to:

$$J = DP\frac{\Delta C_v}{\delta} \qquad (4.2)$$

Where J is the steady-state flux of the drug, D is the drug diffusion coefficient, ΔC_v is the concentration difference across the membrane (in μmol cm^{-3}), and δ is the membrane thickness (in cm). P, D and δ can be combined into a single constant:

$$K_p = \frac{PD}{\delta} \qquad (4.3)$$

Where K_p is termed the permeability constant (measured in cm h^{-1}). Incorporating this relationship into equation 4.2 yields:

$$J = K_p \Delta C_v \qquad (4.4)$$

If the drug dose in the donor compartment is infinitely large in comparison to the amounts present in the skin and receptor chamber *i.e.* sink conditions apply, then ΔC_v can be replaced with C_v which is the drug concentration in the donor compartment.

The attainment of the linear phase, described by the equations above, is preceded by a non-linear phase where drug permeation progressively increases as it equilibrates with the skin barrier. By extrapolating the linear segment of the profile backwards to the time axis, a lag time (measured in hours) can be determined. The lag time (τ) is given by:

$$\tau = \frac{\delta^2}{6D} \qquad (4.5)$$

The equations listed in 4.1 to 4.5 are frequently not applicable as percutaneous absorption can be influenced by other factors. Depletion of the drug in the donor compartment will reduce the penetration rate and significant drug-skin binding will exert the same effect. If the donor compartment contains a small volume of drug solution, then vehicle evaporation will increase drug concentration during the course of the permeation experiment. This can increase the driving force for diffusion or alternatively the solute can precipitate out, thus reducing drug activity. Certain vehicles such as water or ethanol can also enhance drug delivery. Permeation can also be mediated *via* transfollicular pathways and this feature further complicates the model.

Although, Fick's first law of diffusion is a valid approximation for *in vitro* permeation, it does not readily apply to the *in vivo* situation. This is because in most therapeutic applications, it is unusual for skin to be in contact with a permeant of a constant concentration or 'infinite' dose. Another reason is that the period of application is frequently too short for steady-state conditions to be established. *In vivo* penetration profiles are derived from Fick's second law of diffusion which is:

$$\frac{dc}{dt} = D\frac{d^2c}{dx^2} \qquad (4.6)$$

The resulting equations which model the entire absorption profile rather than merely the steady-state segment are complex and they can be further complicated by including terms to address additional processes such as metabolism or epidermal binding. The penetration profile shown in Figure 4.1 can be mathematically described by the following equation, provided that penetration is from an infinite dose (Scheuplein, 1978a):

$$M = CK\left\{\frac{Dt}{h} - \frac{h}{6} - \frac{2h}{\pi^2}\sum_{n=1}^{\infty}\frac{(-1)^n}{n^2}\exp\left[\frac{-dn^2\pi^2 t}{h^2}\right]\right\} \qquad (4.7)$$

Where M is the cumulative amount of drug in the receptor solution (in μmol), C is the drug concentration in the donor cell (in μmol cm^{-3}), D is the diffusion coefficient of the drug through through the skin (in $cm^2\ h^{-1}$), K is the skin-vehicle partition coefficient, h is the skin thickness (in cm) and t is the time elapsed (in hours).

4.2 METHODS

4.2.1 Preparation of skin barriers

Whole skin was obtained from male Wistar rats, 4 to 5 months old and weighing 250 to 300g. The animals were sacrificed by cervical dislocation and the back of each rat was shaved with electric clippers (Oster model no.50). A pencil line was drawn along the approximate position of the spine. The whole-thickness intact skin was excised using a sharp pair of scissors. Adhering fat and any other visceral debris were removed from the undersurface. The skin was cut in two along the pencil line. The skin was further cut so that 3 rectangular sections of tissue (side length, 2 to 3cm) were obtained from each half of the skin. These sections were either used immediately, or stored in the frozen state at -20°C between sheets of aluminium foil for a period of up to 1 month

Whole skin was similarly excised and prepared from guinea pigs (Duncan-Hartley, 250-300g).

Further studies involved the use of whole human skin. Supplies were obtained from amputated male legs (South East Staffordshire Health Authority). The strips of intact whole skin were cut into rectangular sections, side length 2 to 3cm, and the underlying subcutaneous fat was excised from each of these sections.

Other experiments required the use of separated human epidermis. This was prepared by immersing sections of whole human skin in a beaker of water maintained at a temperature of 60 ± 1°C for 1 minute. The sections were removed and allowed to dry for 1 minute. By using fine tweezers to press down the dermis and regular tweezers to gently pull up the epidermis, the epidermal layer was teased out of each whole skin sample. These specimens of epidermis were stored overnight at 4°C. The following day, the samples were rehydrated with several drops of distilled water before use.

4.2.2 Ultrasound-Exposure Protocol

In order to prevent ultrasonic reflections, an ultrasound-absorbing system was designed and comprised a water-filled, carpet-lined plastic beaker. The acoustics are described in detail in section 2.3.2.

The beaker was filled with distilled water and then left to stand for about 10 minutes to allow the escape of air bubbles. A sheet of clingfilm was stretched taught over the surface of the water and secured with rubber bands. This provided a physical base to support the skin samples to be sonicated. Each skin section was coated with 0.5g of ultrasound coupling gel (Henley's Medical) on the inner surface and 1g of gel on the outer surface. The skin sample was placed flat upon the sheet of clingfilm comprising the exposure system described above. The large transducer of the ultrasound generator (Therasonic 1032, model no.50, EMS Greenham Ltd) was placed on top of the sample so that the skin was compressed flat between the transducer and the clingfilm. A frequency was selected (1.1MHz or 3.3MHz) and the generator was switched on at a set intensity (0, 0.1, 0.2, 0.5, 1.75 or 2W cm^{-2}). The transducer was hand-held perpendicular to the skin surface for 5 minutes whilst the skin was irradiated (See Figure 4.2).

Following exposure to either ultrasound or heat alone, the skin sections were blotted with a paper towel and then washed with distilled water. This procedure was then repeated so as to remove the coupling gel from the skin samples. The tissue was then blotted a final time and then left to completely dry at room temperature for approximately 20 minutes. Particular care had to be exercised with the human epidermis samples as these membranes were particularily susceptible to tearing. Furthermore, as both sides of the epidermis exhibit the same appearance, an awareness of membrane orientation had to be maintained during the whole process. Following washing and drying, the skin samples were transferred to the diffusion cells.

Figure 4.2 Beaker Assembly Employed as an Ultrasound Free-Field

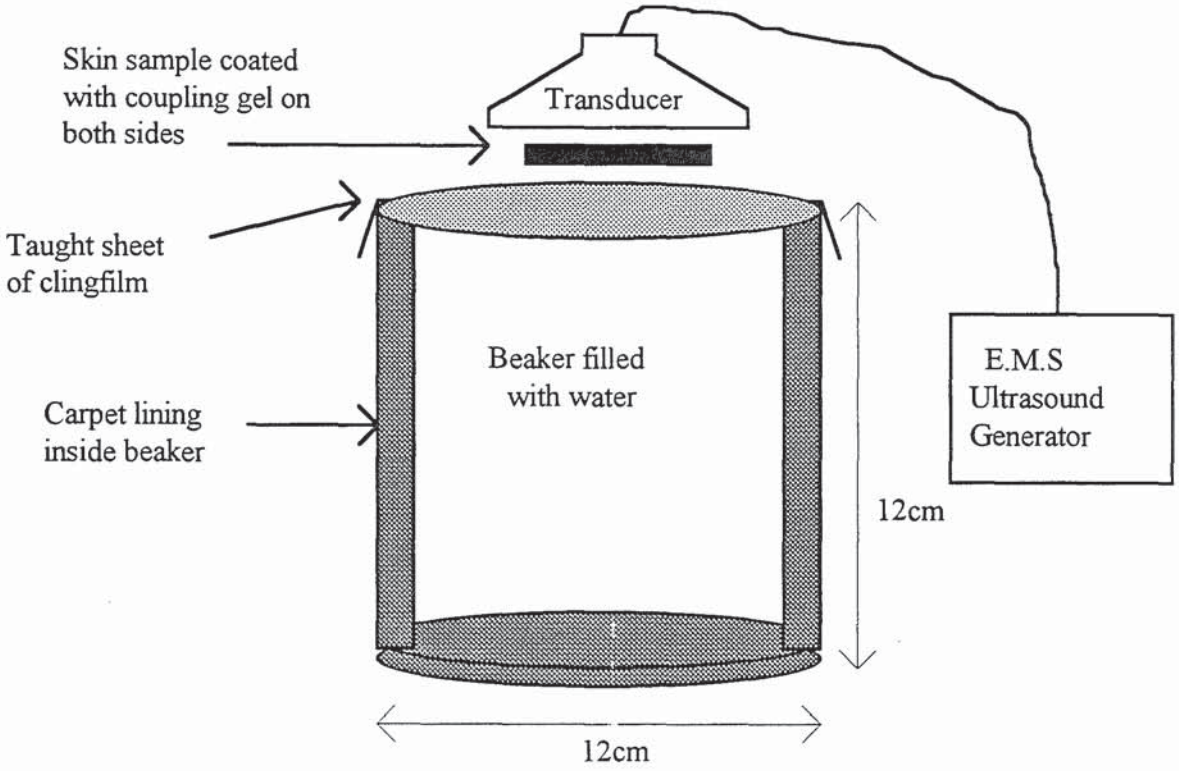

4.2.3 Heat-Alone Exposure Protocol

An aluminium and perspex cylinder, 3.7cm in diameter and 6cm in length (approximately the same surface area as the large transducer) was employed to simulate the heating effect of the ultrasound free-field. The hollow interior of the probe, was connected by rubber tubing to a thermostatically controlled water pump (Churchill-Matrix). When the pump was switched on, the circulating hot water heated the aluminium probe towards an equilibrium temperature. When the thermostat indicated that the desired temperature had been attained, the cylinder was empoyed to heat skin samples on the carpet-lined beaker using exactly the same technique as described for the ultrasound transducer (refer to section 4.2.2).

Due to inefficiencies in heat conduction within the system, the actual temperature at the skin surface, in the centre of the probe-exposed area, was slightly lower than that indicated by the thermostat dial. Therefore, the heating probe was pre-calibrated with a differential thermocouple (Digitron instruments, 3202 type K). This was used to record the temperature at the central point of the heated skin surface, following 5 minutes of contact. The skin temperature was determined to be approximately 10% less than that indicated by the thermostat. *i.e.* a dial setting of 67°C resulted in a final skin surface temperature of only 60°C. Therefore, the thermostat dial was fixed to a value which was 10% greater than the desired skin temperature.

4.2.4 Surface Temperature Measurements

In the first series of experiments, the ultrasound free-field was applied across samples of whole rat skin by using the beaker assembly described in section 4.2.2. After an application time of 5 minutes, a thermocouple was used to measure the skin surface temperature at the centre of the sonicated region. The study was conducted at two separate acoustic frequencies (1.1MHz and 3.3MHz), each across a range of intensities (0, 0.2, 0.5, 1, 1.5, 1.75 and 2W cm^{-2}). Each experiment was composed of three replicate exposure runs. A fresh sample of whole skin was employed for each run. A plot of final measured skin surface temperature as a function of indicated intensity was obtained.

In further studies, the skin surface temperature-time profile of a specific ultrasonic beam (1.1MHz, 2W cm^{-2}) was compared with the profile generated by a heat-alone probe (thermostatted to 67°C). Both applications had previously been shown to heat whole rat skin samples to surface temperatures of 60°C. Each modality was applied to the skin over a successive range of time periods (1, 2, 3, 4, and 5 minutes) after which central surface temperatures were recorded. Plots of surface temperature as a function of application time were derived.

4.2.5 Diffusion cell design

An array of Franz-type diffusion cells were employed for the permeation studies. These cells consist of an upper donor chamber and a lower receptor chamber, exhibiting between 2.2 to 3.3cm^2 of surface area for diffusion to take place. The top rim of each receptor compartment was recessed so that a stainless steel mesh could be inserted to physically support the overlying skin sample. The rims of both chambers were coated with white soft paraffin and the skin sections were then mounted centrally, epidermis uppermost. The two halves of the Franz cell were secured with a strip of parafilm and held together by a spring clamp. The receptor chamber, which exhibited a capacity varying from 24 to 33 ml, could be sampled *via* a side-arm. This was sealed with parafilm in between sampling to prevent evaporation of the receptor phase. Continuous and thorough agitation of the receptor solution was attained by a magnetic mixing bar driven by an external motor (I.K.A. minimart magnetic plate). The fluid in the receptor compartment was maintained at 37°C by a thermostatic water pump (Churchill-Matrix) which circulated water through a jacket surrounding the main chamber body. A schematic illustration of a Franz cell is presented in Figure 4.3.

4.2.6 Preparation of the Donor and Receptor Solutions

The small volume of donor solution was prepared by pipetting 5µl of the appropriate radiolabelled drug into a small sample tube and then adding 95µl of ethanol. The drugs were [^{14}C]-sucrose (20.42GBq/mmol, Amersham); [^{14}C]-mannitol (2.07GBq/mmol, Amersham); [^{3}H]-hydrocortisone (2.37-2.92TBq/mmol, Amersham); [^{3}H]-5-fluorouracil (555GBq/mmol, NEN); and [^{3}H]-aminopyrine (4GBq/mmol, Amersham). The tube was sealed with parafilm and thoroughly shaken by hand for 1 minute. The composition of the receptor phase depended upon the nature of the penetrating molecule. For sucrose, mannitol, 5-fluororacil and aminopyrine, the receptor solution was distilled water but for hydrocortisone, 5% v/v aqueous ethanol was employed. In either case, the solutions were partially degassed by heating to 38°C and then sonicated in an ultrasound bath (Kerry, Pulsatron 125) for 3 minutes.

Figure 4.3 Schematic Illustration of a Franz diffusion cell

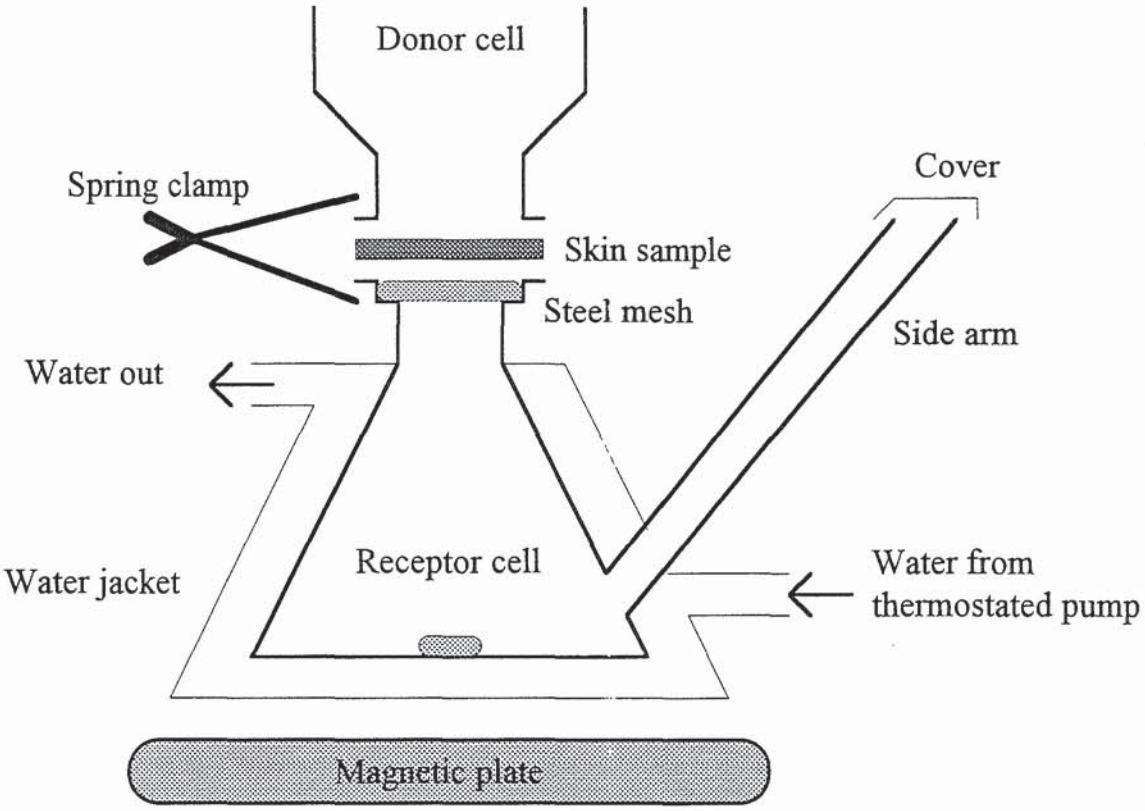

4.2.7 Permeation Procedure

Initially, the thermostat was set to 37°C and the array of cells was allowed to reach this temperature. The prepared receptor-phase solution was then poured into the cell. The skin sections were mounted and the Franz cell secured in the manner described in section 4.2.5. The receiver solution was stirred for 2 minutes to allow most of any undissolved air to accumulate on the underside of the skin. The cell was then carefully inverted and rocked in order to allow any such air bubbles to escape through the side arm. A 100µl aliquot of the donor solution under study was then deposited on the skin surface. The Franz cell was then repeatedly tilted in order to ensure even spreading of the solution over the skin surface. Magnetic agitation was then restarted and the experiment run for 5 hours. After the first

hour, the small volume of ethanol had evaporated from the skin surface and the cell was re-inverted at regular intervals to remove any air bubbles.

After deposition of the donor solution, 1.1ml aliquots of receiver solution were withdrawn at 30 minute intervals. Each 1.1ml sample was transferred to a labelled scintillation vial into which 10ml of scintillation fluid was dispensed (Optiphase Hisafe 3). The vials were then thoroughly shaken for 15seconds on a whirlimixer (FSA laboratory supplies). The vials were then placed in a Packard 1900T.R. liquid scintillation counter. The machine was pre-calibrated to quantitatively analyse the beta emissions from both ^{3}H and ^{14}C radioisotopes. The counter measured the activity of each 1.1ml aliquot. These activity values were converted to drug concentration values according to the activity / mole ratio of the radiolabelled drug. After the removal of each 1.1ml aliquot, the receiver compartment was refilled with an identical volume of drug-free solution. This process caused the receptor solution to be progressively diluted during the course of the experiment. Consequently, it was necessary to mathematically correct each successive sample concentration for the cumulative dilution and loss resulting from previous samplings. This was determined by applying the following equation:

$$C_t = C_{mt} + \left[V_s \cdot \frac{\sum_{t=1}^{t=n-1} C_m}{V_r} \right] \qquad (4.8)$$

where C_t is the actual current concentration of drug in the receptor phase at time t, C_{mt} is the apparent (*i.e.* measured) current concentration of drug in the receptor phase, V_s is the sample volume withdrawn for analysis, V_r is the volume of the receptor solution, and ΣC_m is the summed total of the previous measured concentrations.

The drug concentrations in the receptor phase at each 30 minute time point were determined from the radioactivity readings and these were corrected for dilution in the manner described. The amount of drug penetrating the skin per unit area was calculated by dividing the obtained concentrations by the surface area available for diffusion and this value was different for each individual Franz cell. Each permeation experiment was conducted in replicate ($n \geq 3$). All these algebraic manipulations were carried out using a Microsoft Excel application on an IBM-

compatible computer. A graph of the cumulative amount penetrated per unit area generally demonstrated a linear profile region which was described by linear regression. The slope of the linear phase was divided by the initial concentration of the donor solution to yield the permeability coefficient (refer to Eqn. 4.4). The lag time values were obtained by extrapolating the linear regression line back to the time axis.

4.2.8 Histological Techniques

A wax-embedding method was used to prepare sections of whole rat skin that were subsequently stained with haematoxylin and eosin dyes. This technique was satisfactory for preparing slides to examine the gross structural morphology of rat skin. However, this method was not suitable for detecting any ultrasound-induced changes in lipid distribution. Consequently, a second set of studies was conducted in which the specimens were sectioned in the frozen state and subsequently stained with sudan-type dyes

4.2.8.1 Haematoxylin and Eosin Staining

An ultrasonic free-field (1.1MHz) was applied to whole rat skin sections at a range of intensities (0, 1, 1.5, 1.75 and 2W cm^{-2}). Two samples of rat skin were exposed to heat alone (surface temperatures of 42°C and 60°C). Following heating or ultrasound exposure, the coupling gel was removed by blotting and washing as described earlier. 1mm wide strips of tissue were cut out through the diameter of each skin sample with a sharp razor blade. The skin strips were placed in sample tubes containing 4% neutrally buffered formalin and left to fix overnight. The strips were then inserted in plastic cassette holders and transfered to an enclosed automatic tissue processor (Shandon Hypercenter 2). The machine dehydrated the skin samples by treatments with 95% aqueous ethanol for 1 hour, followed by pure ethanol for 3 hours. Xylene was then applied as a clearing agent for 4 hours. The skin strips were then wax-impregnated with paramat wax (BDH) under vacuum. The wax-impregnated strips were blocked out inside the cassette holders by immersion in fresh molten parraffin wax delivered by an automated wax dispensing machine (Boova 39 Professional Embedding Centre). The wax was allowed to cool down to form a solid block encasing the tissue strip. The blocks were placed

on ice prior to cutting with a base sledge microtome (IS300 Anglia scientific). 5μm wide transverse strips were cut out from the block in the cassette and 'floated out' on a beaker of water at room temperature and then a beaker of water at 48°C. The folds and wrinkles in the wax were carefully removed by gentle stretching with tweezers. The sections were placed on glass slides and dried for 10 minutes at 60°C in a slide dryer (Luckham Model SD350).

The slides containing the sections were then placed in an enclosed automatic stainer (Shandon Linistain GLX). The apparatus removed the wax with sequential washes of xylene, IMS and water and then stained the tissue using the Gills haematoxylin and eosin technique. Cover slips were then placed on the slides using xam (adherent in 60% acetone, BDH) as the mountant.

The sections were photographed with a camera (Olympus PM6) attached to a microscope (Olympus BH) set at ×100 magnification. The film (Fujicolor 35mm Super G) was exposed for 5 seconds under dark room conditions with the microscope condenser set at low power. The film was developed in the standard manner. A 1mm long scale on a graticule was fitted into the eyepiece and this was calibrated with reference to a 1cm long micrometer slide scale. Distinct features in the photos, such as hair follicles, were measured with the graticule and hence by proportion, the scale of the photos was calculated.

4.2.8.2 Sudan-type staining

Four rectangular sections of whole-skin were obtained from each of three different rats. A skin section from each animal was subjected to a specific acoustic/thermal regimen and hence each regimen was conducted in triplicate. The regimens were the application of an ultrasonic free-field (1.1MHz) at 0, 0.1, and 1W cm^{-2} and simple heating to a central skin surface temperature of 42°C (See section 4.2.8.1 for details). After removal of the coupling gel, three strips of tissue, approximately 4mm wide and 8mm long, were dissected out from the central area of each skin section. The strips of tissue were placed on their sides on small pieces of cardboard and frozen in that position by immersion in liquid nitrogen. The frozen strips of tissue were then sprayed with a cooling aerosol ("Freeze -it" E-series, Shandon Scientific Ltd.) in order to prolong freezing before being transferred to an automated freezing microtome (Anglia Scientific 600 Cyrotome). This instrument was pre-programmed to equilibrate at a temperature of -28°C. An adhesive gel (Cyro-M-Embedding Compound, Bright Instruments Ltd.) was

used to embed the strips of skin into the requisite position within the microtome chamber. Approximately a dozen 9μm-thick sections were cut through different angles from each tissue strip. A large number of sections were required in order to ensure that at least a few sections would be lying through the same plane of the skin as whole pilosebaceous structures.

The 9μm-thick sections were transferred to labelled glass slides and left to dry in an oven at 37°C for 1 hour. The slides were fixed by immersing the slides for 1 hour in Joplin bottles containing neutrally buffered formalin (0.4%w/v sodium dihydrogen orthophosphate, 0.65%w/v di-sodium hydrogen orthophosphate and 4%v/v formaldehyde). Two different lipid staining techniques were attempted, the Sudan Black method and the Oil red O method.

A working solution of Sudan Black was prepared by mixing Sudan Black powder (BDH) in 70% aqueous ethanol to produce a saturated solution. The slides containing the sections were rinsed in 70% aqueous ethanol and then immersed for 15 minutes in a Joplin bottle containing sudan black solution. Just enough 70% aqueous ethanol was sprayed onto the slide so that it replaced virtually all the Sudan Black that was unbound to the specimen. The slide was left to stand for 5 seconds in order for the differentiating process to develop. The specimen was then gently washed with distilled water.

A working solution of Oil Red O was prepared by mixing 60ml of a stock solution of Oil Red O with 40ml distilled water and filtering just before use through Whatman no.1 filter paper. The slides containing the sections were then rinsed in a solution of 60% aqueous isopropanol (BDH). The slides were then immersed for 15 minutes in Oil Red O. The slides were differentiated in 60% isopropanol for 20 seconds which was then washed off with distilled water. Several drops of Mayer's haemalum were deposited over the tissue sections and left for 3 minutes. This agent counterstains nuclei purple and hence aids structure identification. The slides were rinsed in distilled water.

Following staining, the specimens were mounted in warm glycerine jelly (BDH). The slides were viewed through a Fluorescence microscope (Jenamed) at a magnification of ×125. Many of the 9μm-thick sections did not lie within the same plane as the hair follicles under study. These specimens were discarded. Suitably orientated sections were photographed, under dark room conditions, with

a camera (Olympus OM-4) attached to the microscope. A microscope filter ensured the specimens were subjected to white light and the film (Fujicolor 35mm Super G) was exposed by the automated shutter release mechanism. The film was developed in the standard manner. The resultant photos were scaled with a graticule and a 1cm long micrometer slide scale.

4.2.9 ATR-FTIR Studies

Sections of whole rat skin were subjected to an ultrasound free-field (1.1MHz drive) at 1W cm^{-2} or 0W cm^{-2} (control) using the exposure system previously described. Infrared spectra of the skin specimens were then recorded using a Mattson 3020 FTIR spectrophotometer (Galaxy System) eqipped with a zinc selenide internal reflection element (Graseby Specac Inc.). The skin specimens were placed over the analyser element of the spectrophotometer. Care was taken to ensure that the central area of each exposed membrane was positioned over the analyser element. A perspex block was placed over the skin, thus ensuring fairly reproducible contact between the stratum corneum and analyser. A spectrum was taken, representing an average of 16 scans. Each treatment (*i.e.* control and ultrasound exposure) were conducted in triplicate. Between scans, the analyser surface was wiped clean with acetone in order to remove residues of material from previous skin samples. An infrared spectrum was obtained of absorbance as a function of wavelength.

4.3 RESULTS AND DISCUSSION

4.3.1 The Effects of High Intensity Ultrasound on Rat Skin

4.3.1.1 Histological Studies

Figure 4.4 shows a section through a control sample of rat skin. The stratum corneum can be discerned as feint, wavy lines (S); the viable epidermis is stained orange-red (E); while the dermal protein appears orange-brown (D). The nucleated cells of the sebaceous glands and epidermis can also be distinguished. The apparently empty spaces within the dermis are an artefact of the sectioning process.

The only detectable change in the skin following exposure to 1W cm^{-2} ultrasound was perhaps a slight thinning of the statum corneum (See Figure 4.5). Following sonication at 1.5W cm^{-2}, macroscopic examination revealed that although most of the sample appeared unaltered, in the central zone of each skin sample, where the energy deposition had been greatest, the skin surface was slightly raised and discoloured. Consequently, photomicrographs were taken from both a site derived from the centre of the section as well as from the periphery. These are presented in Figures 4.6 and 4.7 respectively. The appearance of the outer site (Figure 4.6) was similar to control skin except that the stratum corneum was significantly thinner. At the central site (Figure 4.7), sonication had detached the cornified layer from the epidermis and furthermore produced congealing of the dermal tissue. The dermis consists of fibres of collagen, elastin and pectin embedded in a semigel matrix of micropolysaccharides. Upon heating, these protein fibres are denatured, thus congealing the dermis. On a macroscopic scale, this causes the affected skin to contract and thicken. Presonication at 1.75W cm^{-2} and 2W cm^{-2} produced complete stratum corneum removal and dermal degeneration throughout virtually the whole area of the exposed skin (see Figures 4.8 and 4.9).

Figure 4.4: Transverse section through Non-sonicated Skin (Scale 1:167)

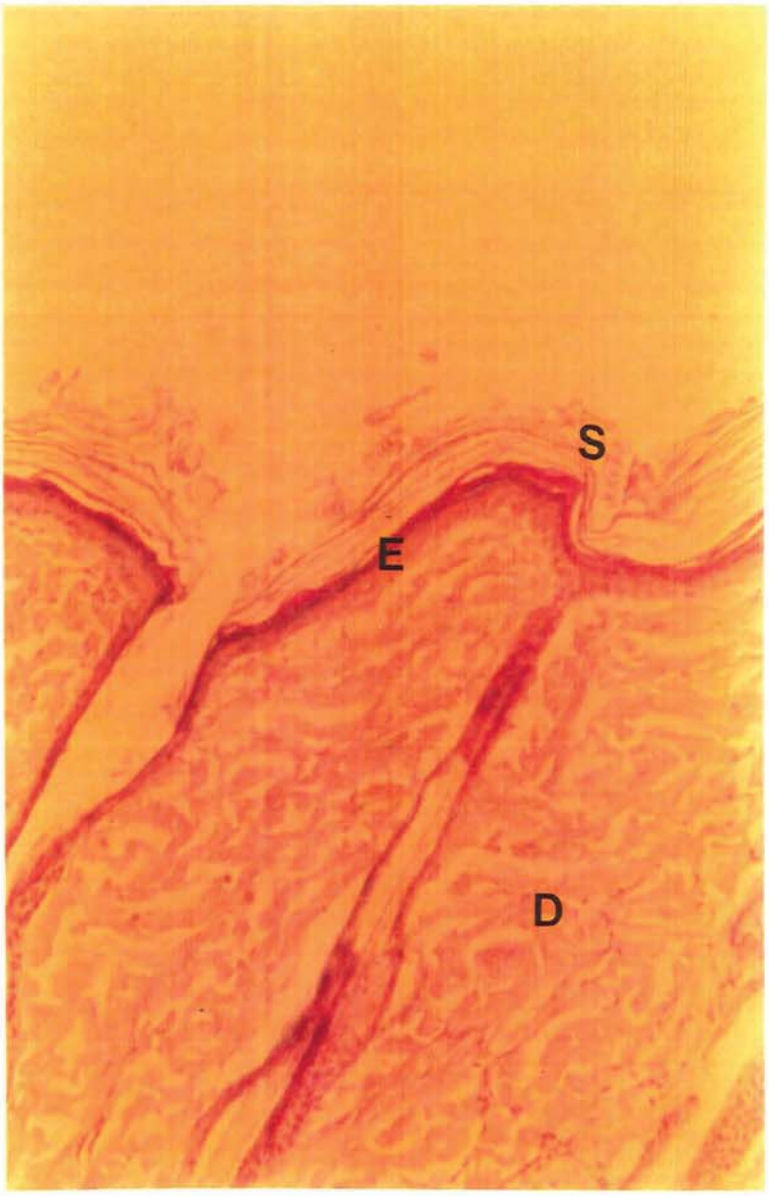

Figure 4.5: Transverse section through skin sonicated at 1W cm^{-2} showing slight disturbance of the stratum corneum (Scale 1:167)

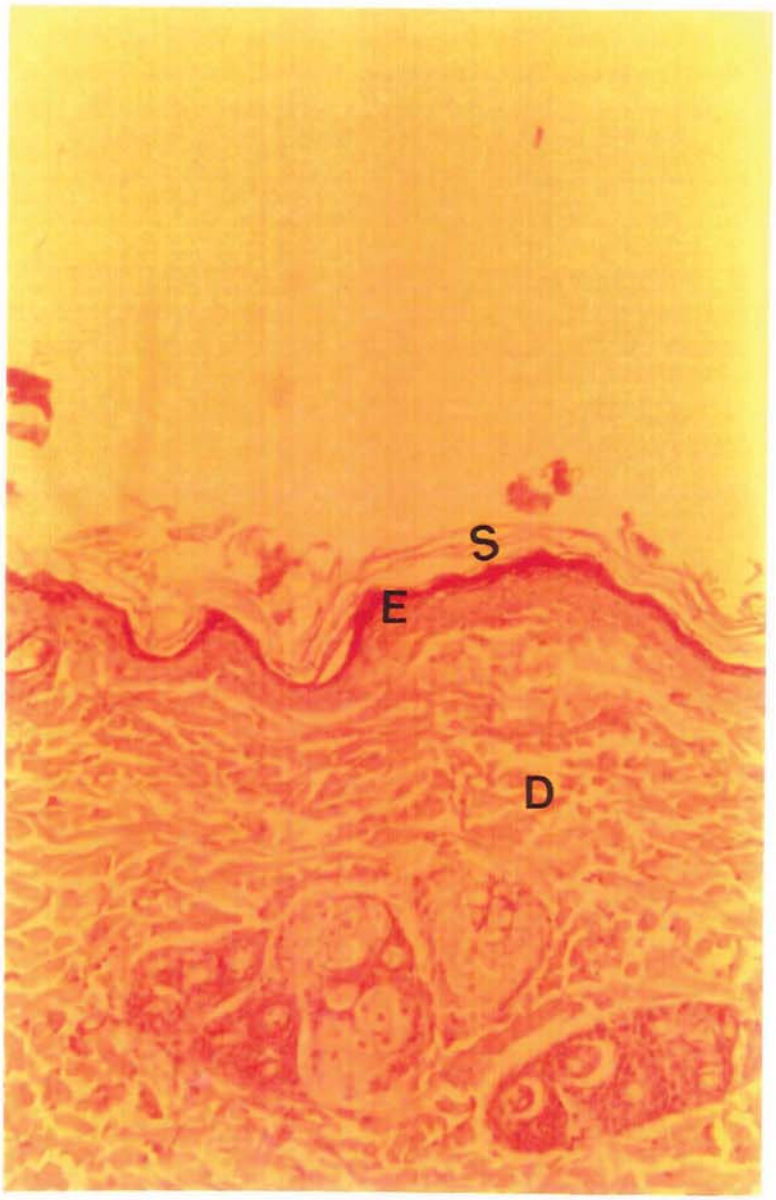

Figure 4.6: Transverse section through periphery of skin sonicated at 1.5W cm^{-2} showing significant disturbance of the stratum corneum (Scale 1:167)

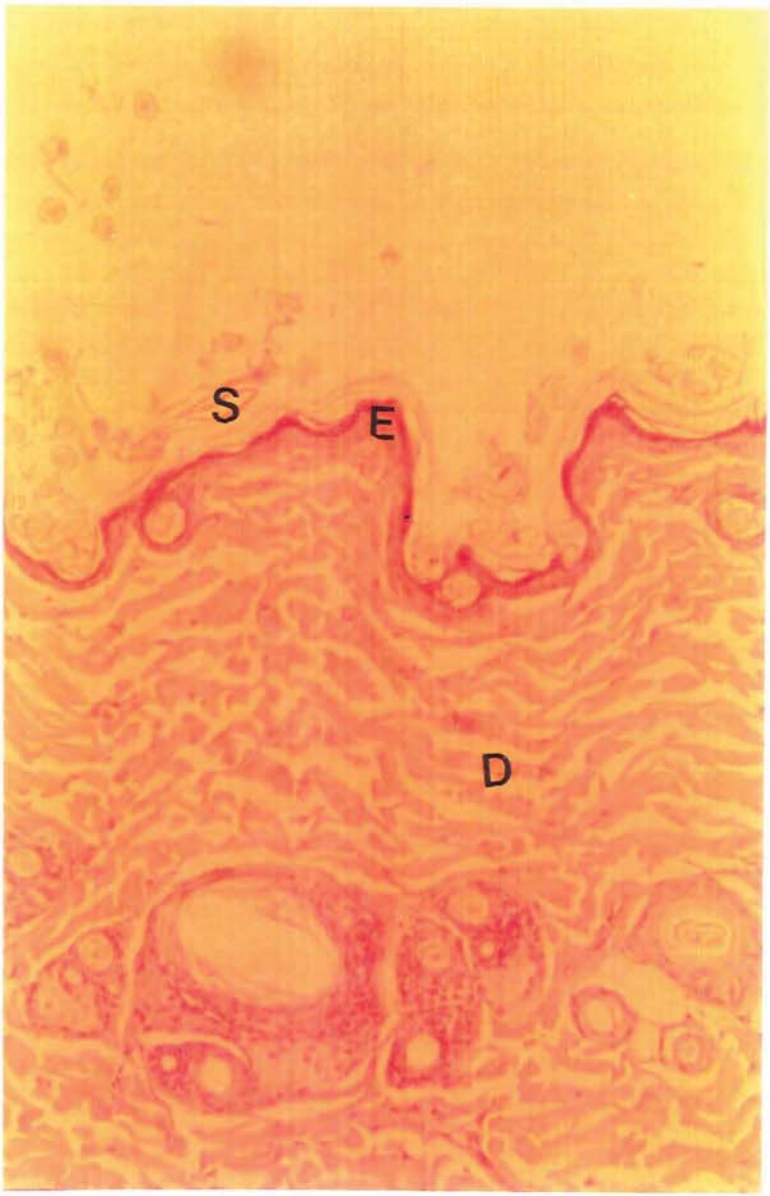

Figure 4.7: Transverse section through centre of skin sonicated at 1.5W cm^{-2} showing detachment of the stratum corneum and dermal degeneration (Scale 1:167)

Figure 4.8: Transverse section through skin sonicated at 1.75W cm^{-2} showing detachment of the stratum corneum and dermal degeneration (Scale 1:167)

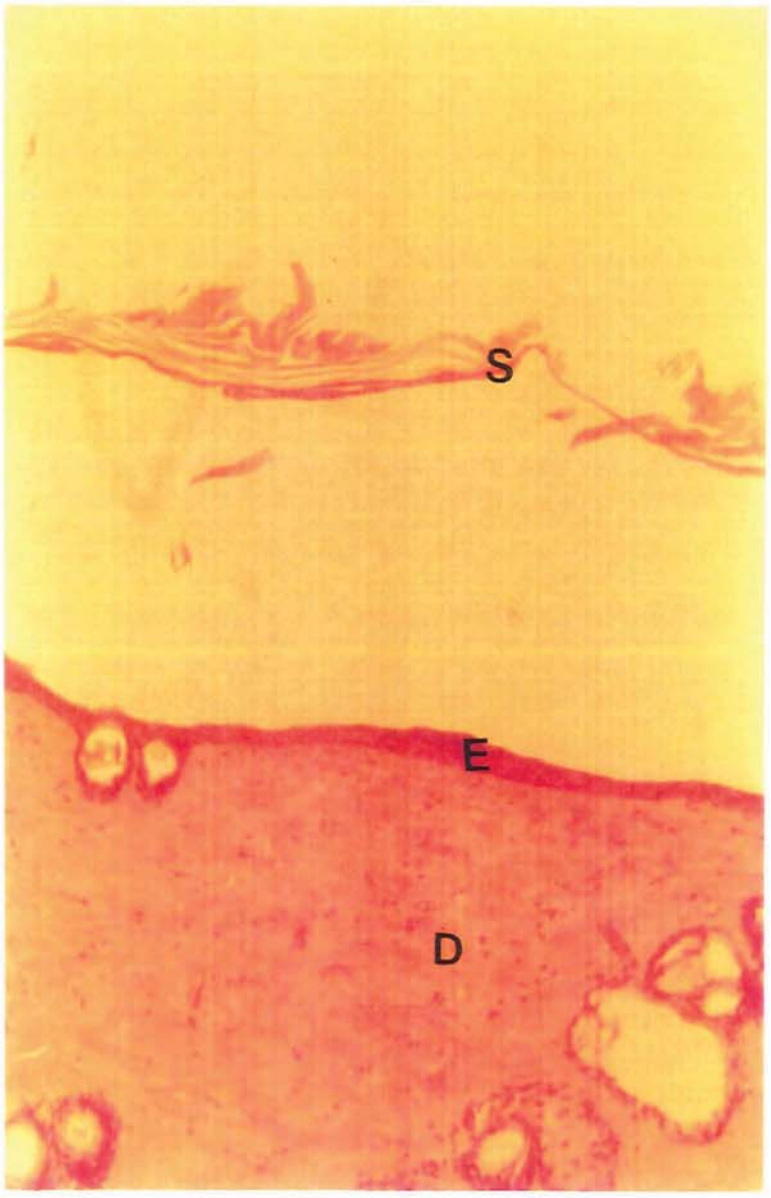

Figure 4.9: Transverse section through skin sonicated at 2W cm^{-2} showing detachment of the stratum corneum and dermal degeneration (Scale 1:167)

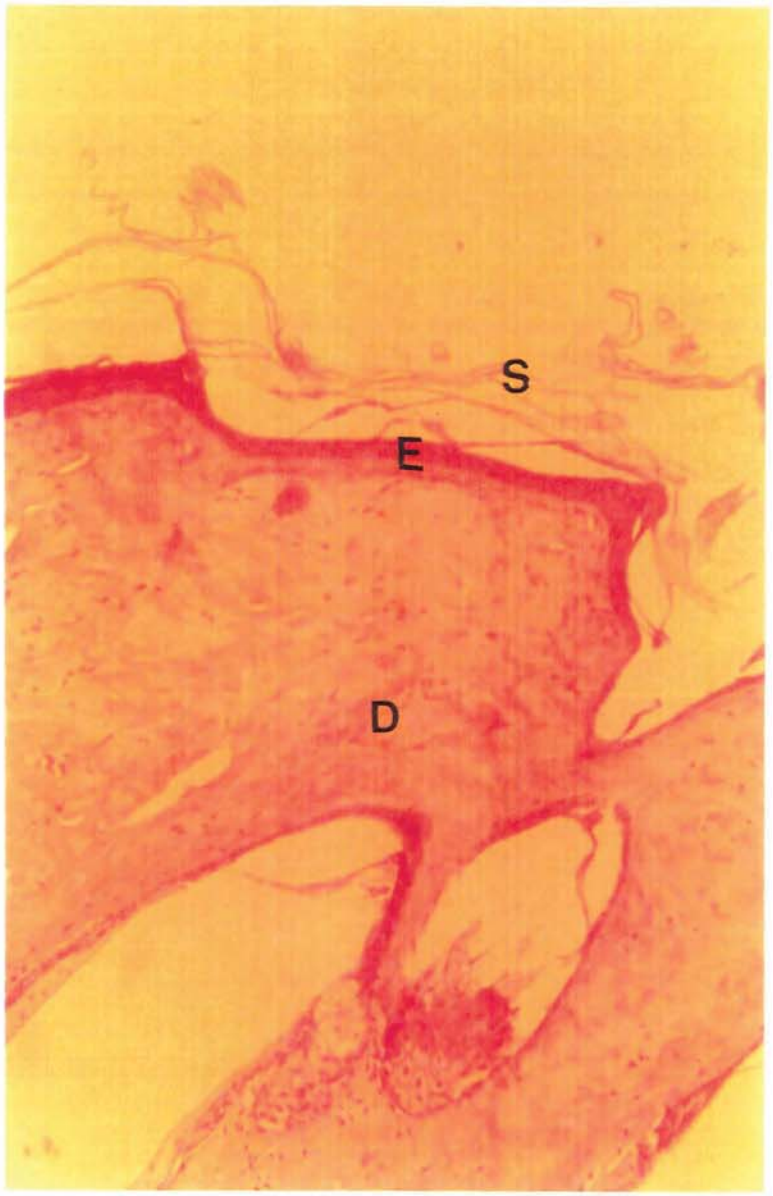

Very similar patterns of progressing injury have been reported in other ultrasound-application studies involving live male Wistar rats (Miyazaki *et al.*, 1992b). These workers applied 1MHz ultrasound, through a layer of coupling gel to the abdominal skin of anaesthetised animals *in vivo*. Following 10 minutes of sonication, whole skin samples were removed and subjected to haematoxylin and eosin staining. At intensities of up to 0.5W cm^{-2}, the skin was histologically unaltered. Minor epidermal atrophy and collagen fibre degeneration were first observed at 0.75W cm^{-2} and these detrimental changes progressed to large scale necrosis as the beam intensity was amplified. Interestingly, in these *in vivo* studies, subcutaneous oedema also developed on an intensity-dependent basis. This feature was obviously absent in the *in vitro* model.

In order to determine to what extent the morphological perturbations observed were an artefact of the thermal effects of ultrasound, a cylinder heated the skin specimens by simple conduction. Initially, the samples were heated to a central surface temperature of 42°C. Such a final surface temperature is also produced by 1.5W cm^{-2} ultrasound as can be seen by referring to Figure 4.10. This heat-alone treatment did not affect the microscopic appearance of the skin. More intense conductive heating to 60°C mimicked the surface temperature increase resulting from 2W cm^{-2} ultrasound (see Figure 4.10). Heating to 60°C induced dermal coagulation throughout the exposed skin areas. The stratum corneum separated at the centre of the section (Figure 4.12) but not at the periphery (Figure 4.11).

Figure 4.10: Central Skin Surface Temperatures Following 5 minutes of Ultrasound Exposure

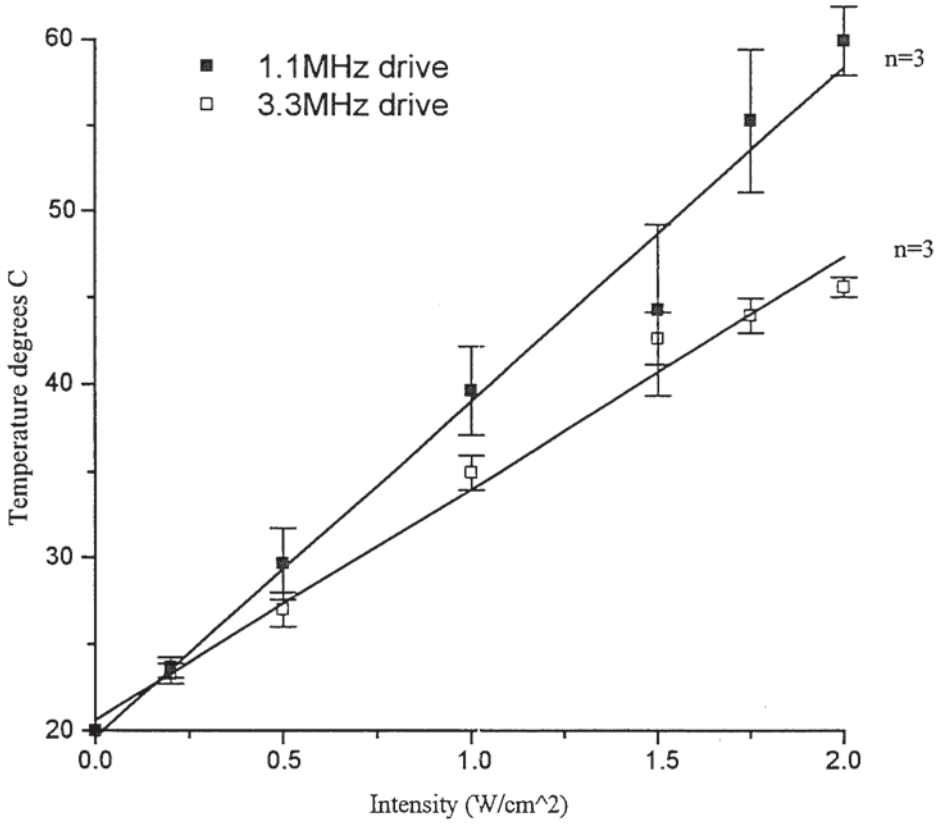

Figure 4.11: Transverse section through periphery of skin directly heated to 60°C showing dermal degeneration (Scale 1:167)

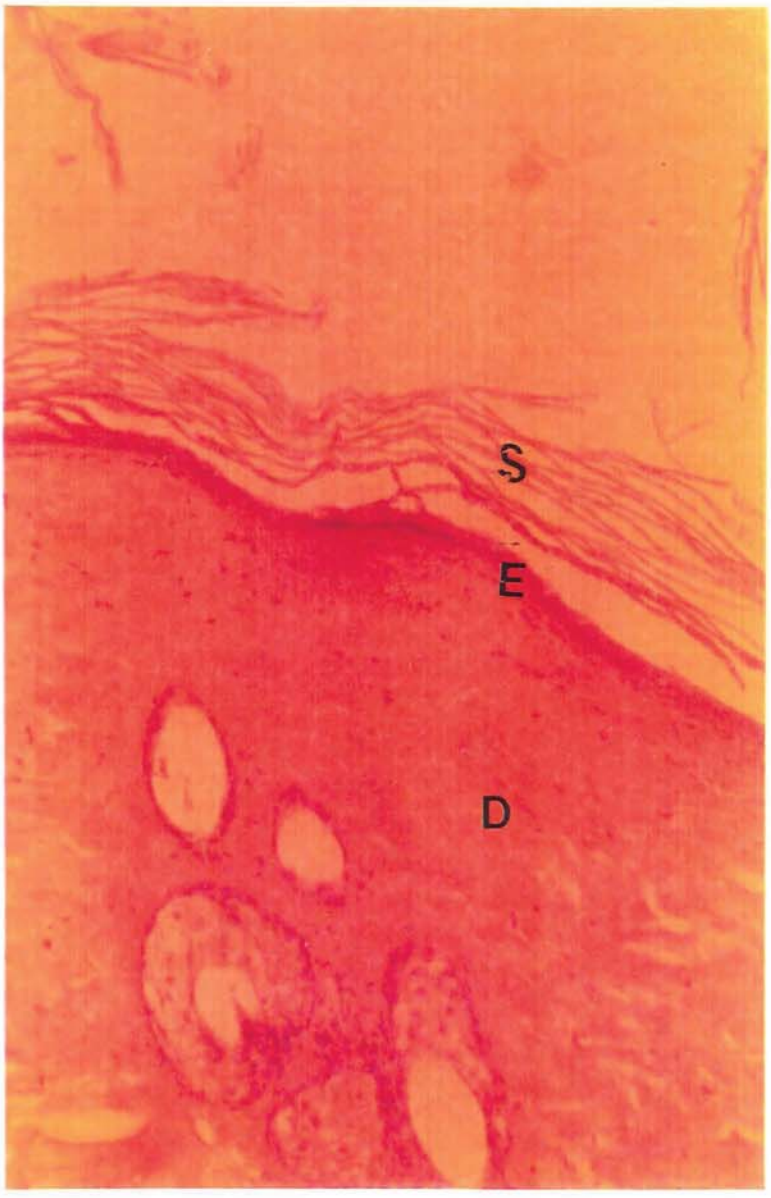

Figure 4.12: Transverse section through centre of skin directly heated to 60°C showing detachment of the stratum corneum and dermal degeneration (Scale 1:167)

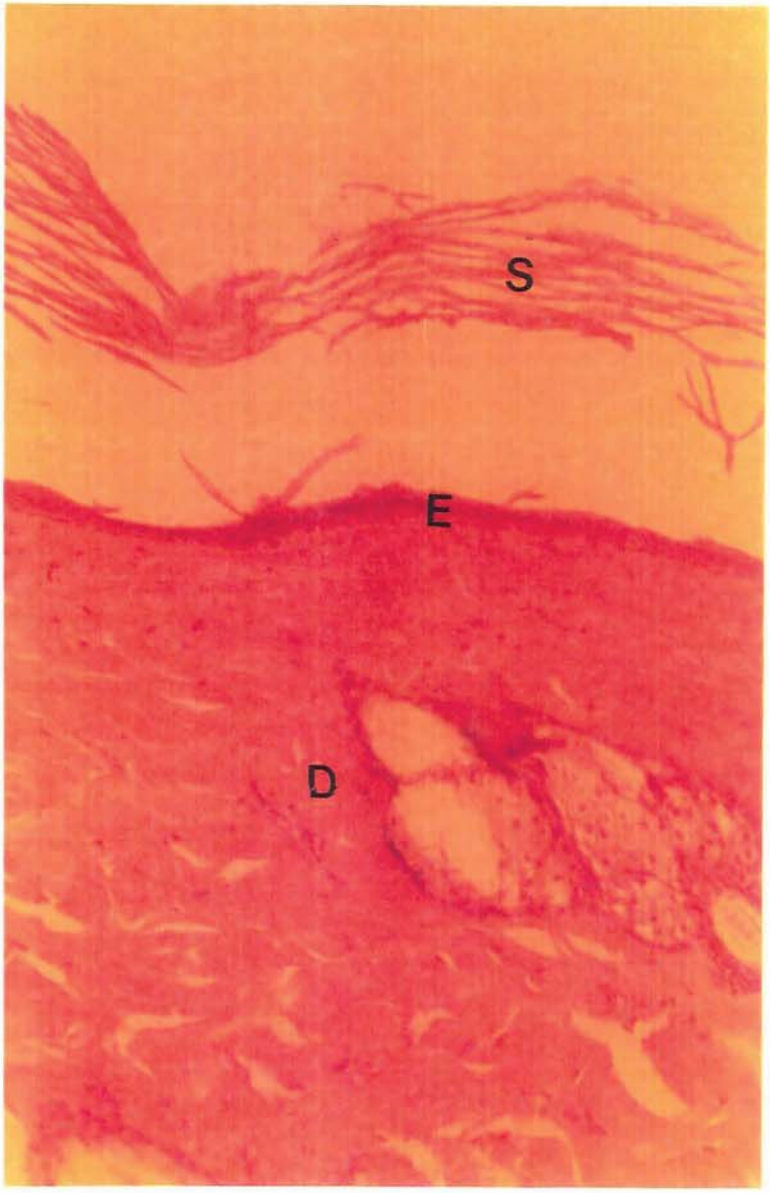

Figure 4.13: The Effect of 5 minutes of Heat Alone and 1.1MHz Ultrasound on Skin Surface Temperatures

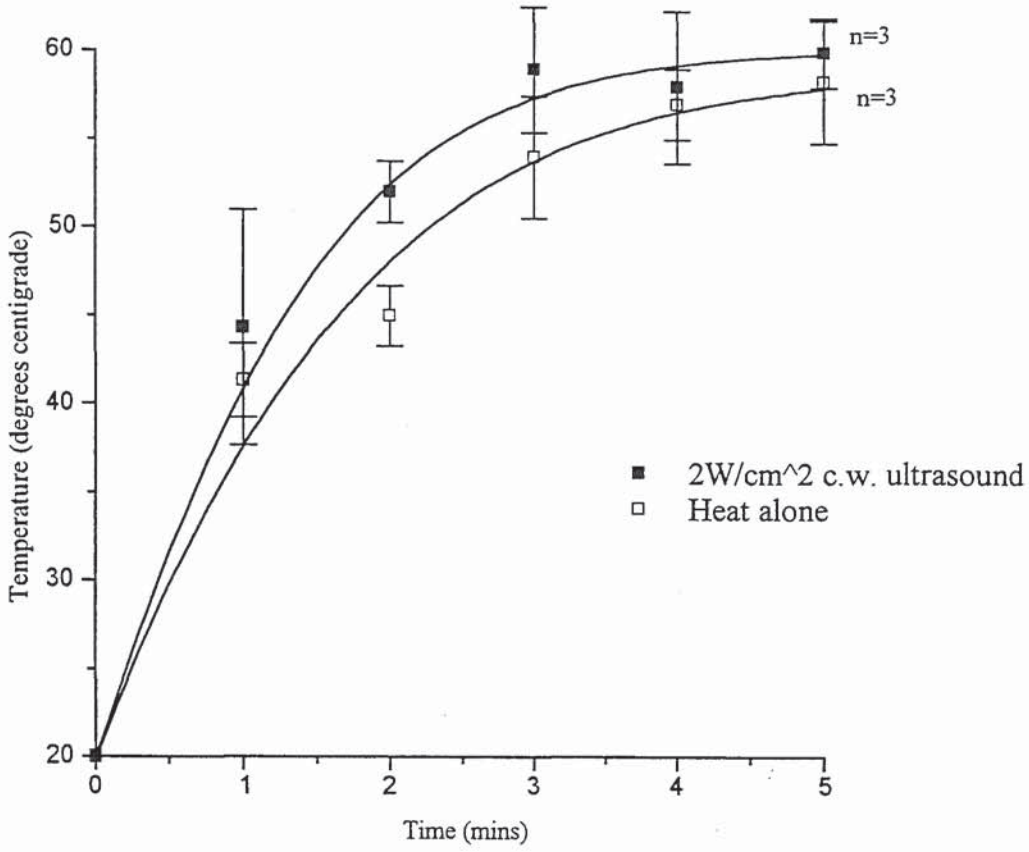

It can be concluded that ultrasound and conductive heating produced dermal congealing and stratum corneum separation and these were qualitatively similar. However, acoustic heating caused more structural damage than conductive heating to a similar final surface temperature as evidenced by comparing Figure 4.9 with Figure 4.11. This could be because the ultrasound actually generated more heat than the heating probe. From Figure 4.13, it can be seen that sonication resulted in higher measured surface temperatures over most of the 5 minute application period even though final measurements were similar for both modalities. Furthermore, all these temperature readings are taken only at the central point of exposure and do not represent the entire, exposed surface areas. One crucial factor is that ultrasound generates heating throughout the entire depth of the tissue as a result of ongoing beam attenuation. This contrasts with the conductive heating model where a temperature gradient exists between the upper layers of the skin that are in contact with the hot surface, and the lower layers that are not. Consequently,

there is good evidence to suggest that the applied heat controls underestimate the total heat energy delivered to the skin samples by the ultrasonic field. It is also likely that the mechanical effects of the ultrasound are contributing to stratum corneum separation and dermal degeneration as discussed in section 1.3.

4.3.1.2 ATR-FTIR Spectroscopy

Figure 4.14 presents the ATR-FTIR spectra of both control and sonicated (1W cm^{-2}) rat stratum corneum obtained over the frequency range 600 to 4000cm^{-1}. Figure 4.15 presents the the difference spectrum generated by subtracting the control spectrum from the sonicated spectrum. From the membrane biophysics literature, the resulting major absorption bands can be assigned to corresponding molecular vibrations (Potts, 1989).

It can be seen from the difference spectrum that although the profiles are generally fairly similar, there are also some distinct differences between them. A major difference between the profiles occurs at 2920cm^{-1} and 2850cm^{-1}. Absorption at 2920cm^{-1} is caused by the asymmetric stretching of C-H bonds within lipids while absorption at 2850cm^{-1} is produced by the symmetric stretching of C-H bonds within lipids. The two peaks exhibited by sonicated stratum corneum are much smaller than the two corresponding peaks exhibited by control stratum corneum.

Sonication resulted in the peaks at 2360cm^{-1} and 2340cm^{-1} exhibiting more variation in size. Infrared absorption at these frequencies is due to carbon dioxide trapped within the stratum corneum. There are natural variations in the quantity of trapped air and this result is therefore of no biophysical significance.

Sonication resulted in a loss of the fine structure of the peaks over the frequency range 1740cm^{-1} to 1400cm^{-1}. The peaks at these frequencies are caused by C=O stretching, N-H bending (within amide linkages) and C-H bending and stretching. Ultrasonic heating may have caused a more random arrangement of hydrogen bonding between these functional groups. This would explain the observed decrease in these molecular vibrations.

It should be stated that the skin samples used in all these spectroscopic studies were derived from different animals and different anatomical sites. Consequently, it is possible that the observed absorption differences were caused by these changes.

Figure 4.14A: ATR-FTIR Spectrum of Control Skin

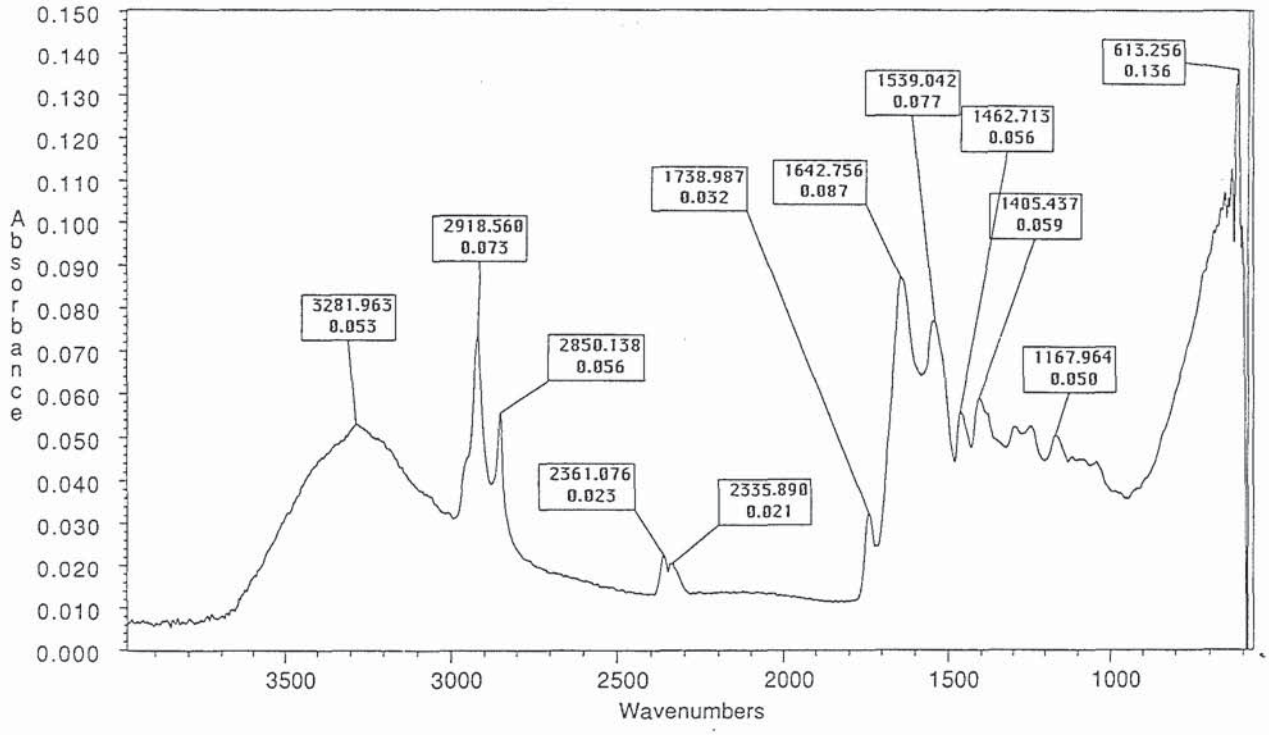

Figure 4.14B: ATR-FTIR Spectrum of Skin Exposed to 1.1MHz Ultrasound

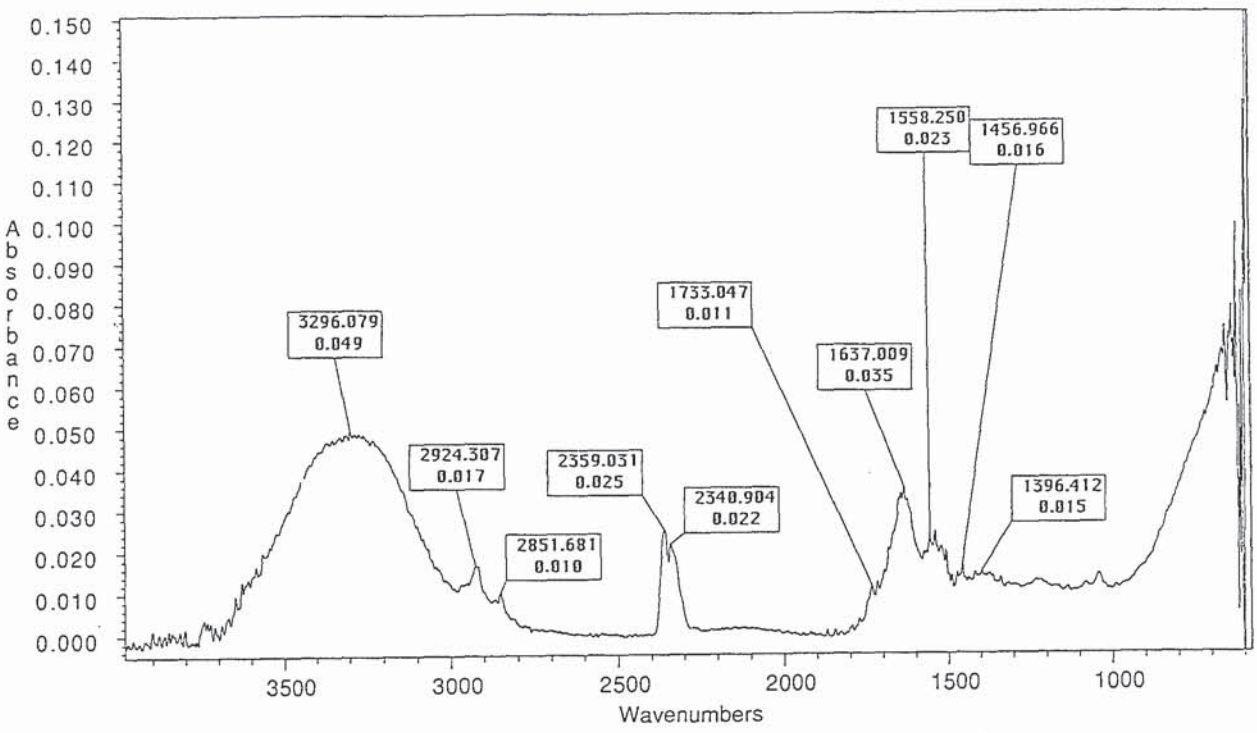

Figure 4.15: The ATR-FTIR Difference Spectrum

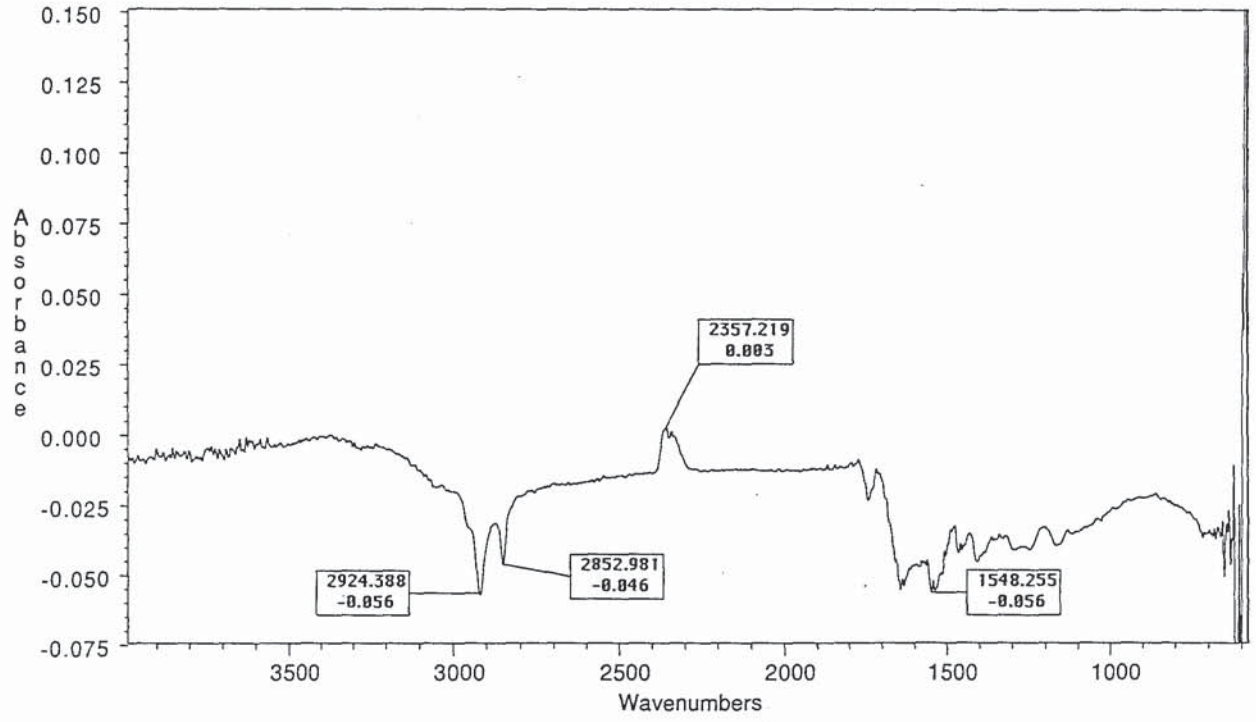

4.3.2 The Effects of Low Intensity Ultrasound on Rat Skin

In pilot studies with Sudan Black, it was determined that the extent of staining was extremely variable. Consequently this stain was not employed further.

Figure 4.16 shows a photomicrograph of a control section of whole rat skin stained with Oil Red O. Unsaturated hydrophobic lipids, including fatty acids, esters and non-saponifiable lipids have been stained red (L). The nucleated cells of the epidermis (N) and sebaceous glands have been stained blue and hence these structures can be readily distinguished. It can be seen that in the absence of ultrasound, the unsaturated, hydrophobic lipids were predominantly concentrated within the cells of the sebaceous glands so as to almost entirely fill these structures. The hair follicle shaft was relatively free of dyed lipids. It can be seen that pre-sonication at 0.1W cm^{-2} resulted in the transport of these lipids out of much of the sebaceous gland so that they filled all of the hair follicle shaft, right up to the skin surface. See Figure 4.17. The same process was observed following exposure to 1W cm^{-2} ultrasound. This phenomenon has not been previously described in any of the literature reports.

Figure 4.16: Oil-Red-O stained section through non-sonicated skin showing sebum concentrated within the sebaceous gland (Scale 1:200)

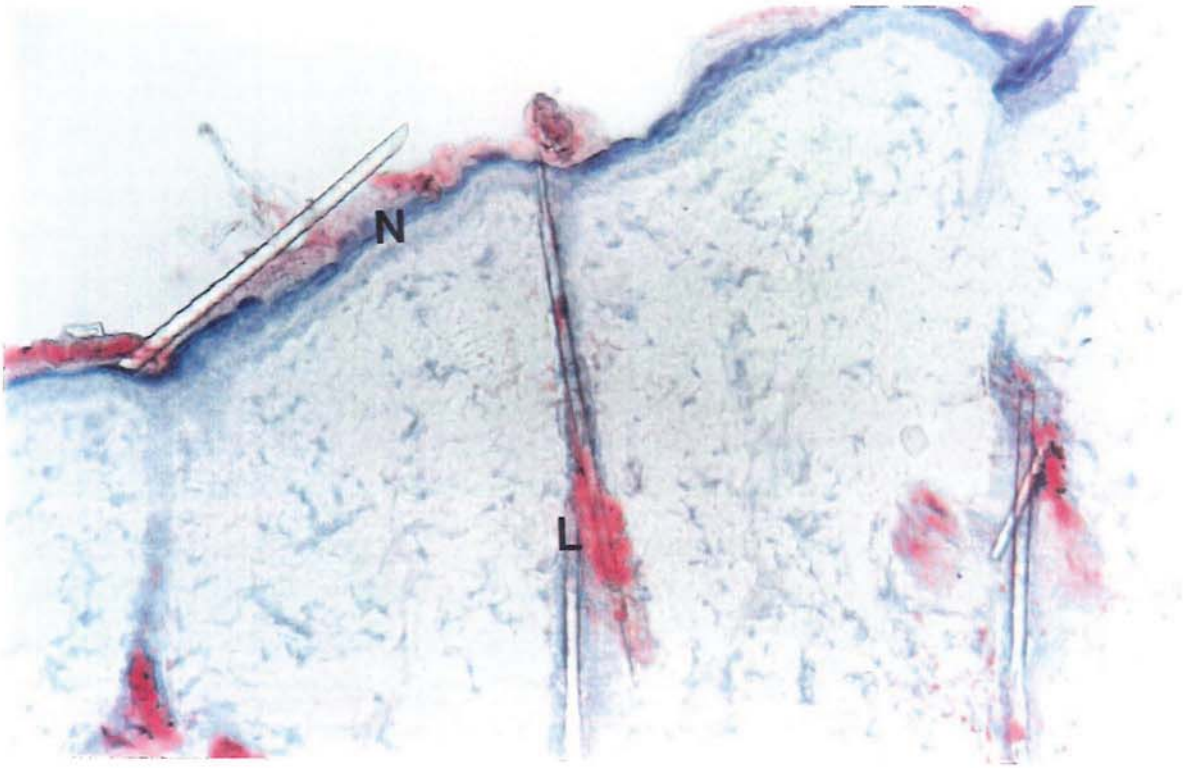

Figure 4.17: Oil-Red-O stained section through skin sonicated at 0.1W cm^{-2} showing sebum deposition within the hair follicle shafts (Scale 1:200)

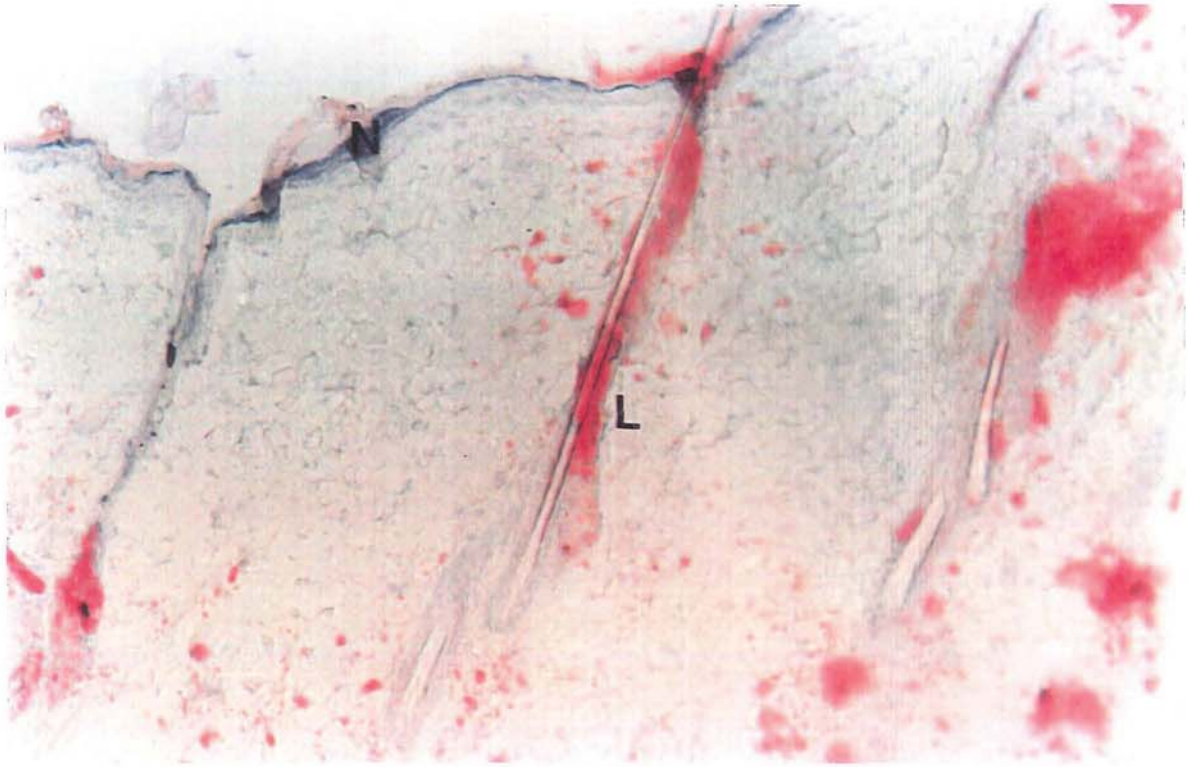

Figure 4.18: Oil-Red-O stained section through skin directly heated to 42°C showing sebum deposition within the hair follicle shafts (Scale 1:200)

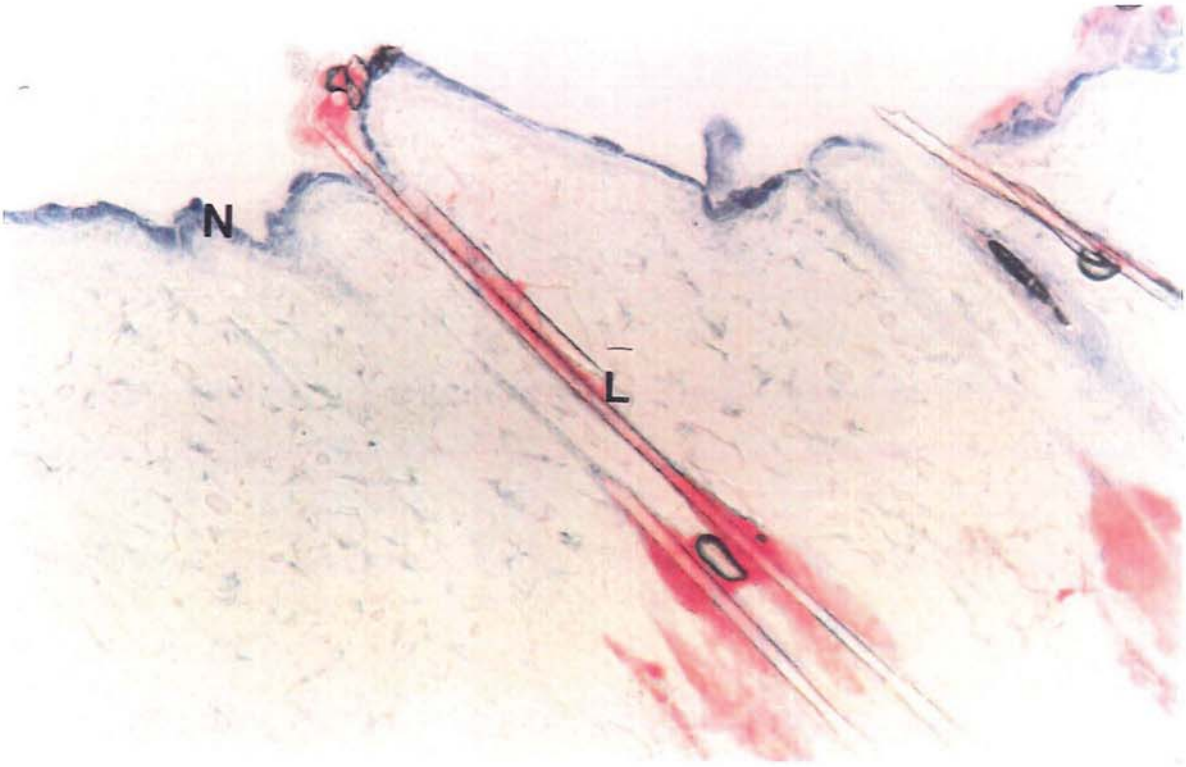

Heat, by virtue of the application of ultrasound is unlikely to be causing the sebum transfer effect as the application of 0.1W cm^{-2} ultrasound, in control experiments, resulted in a negligible surface temperature increase as shown in Figure 4.10. Consequently, it is more probable that mechanical forces are responsible. The sebaceous glands may be being compressed during the positive pressure phases of the acoustic wave, thus promoting the discharge of lipid. However, since the sebaceous glands are much smaller than the ultrasonic wavelength, a difference in acoustic pressure, at any one instance, across the gland cannot be causing the effect. Alternatively, second-order effects such as microcurrents and stable cavities developing within or in the vicinity of the sebaceous gland could cause sebum release *via* a yet unknown mechanism.

Although the heating component of low intensity ultrasound (0.1W cm^{-2}) was probably not responsible for lipid release, simple heating to a surface temperature of 42°C did cause lipid release, as shown in Figure 4.18. Heating of the sebaceous gland produces a consequent thermodynamic increase in its internal pressure, thus promoting the release of its contents. The lipid release patterns produced by ultrasound and heat alone were visually indistinguishable. This suggests that both the thermal and mechanical effects of ultrasound can discharge lipids from the sebaceous glands. The mechanical forces dominate at lower intensities but both attributes operate at higher intensities (1 to 2W cm^{-2}).

4.3.3 Percutaneous Absorption Studies through Whole Rat Skin

Sections of whole rat skin were sonicated (1.1MHz or 3.3MHz) at a series of intensities (0 to 2W cm^{-2}) under free-field conditions. The subsequent percutaneous absorption of [^{14}C]-sucrose, [^{14}C]-mannitol, [^{3}H]-hydrocortisone, [^{3}H]-5-fluorouracil and [^{14}C]-aminopyrine was then investigated using the Franz diffusion model. These compounds were selected because taken together, they exhibit a fairly wide range of n-octanol / water partition coefficient (P) values, *i.e.* $-2.6 < \text{LogP} < 1.55$. The structures and physico-chemical properties of sucrose, hydrocortisone, 5-fluorouracil and aminopyrine are documented in section 5.1. Mannitol is a highly hydrophilic ($\text{Log } P_{\text{octanol/water}} = -2.6$), hexahydric alcohol of molecular weight 182.2 (Leo *et al.*, 1971).

4.3.3.1 Sucrose

A series of experiments were conducted in order to assess the effect of presonication intensity (1.1MHz drive) on the percutaneous absorption of sucrose. Flux, permeability coefficients and lag times derived from the initial linear portions of the resulting rate curves are summarised in Table 4.2. A sample of permeation profiles, representing control (0W cm^{-2}), low intensity (0.1W cm^{-2}) and high intensity (2W cm^{-2}) ultrasound are presented in Figure 4.19. The data showed that at this frequency, ultrasound can both enhance and reduce sucrose absorption depending upon the applied intensity. However, lag times remained relatively unaffected by ultrasound.

Table 4.2 Permeation data for Sucrose across Whole Rat Skin following sonication at 1.1MHz

Intensity (W cm^{-2})	Flux (pmol cm^{-2} h^{-1})	K_p (μm h^{-1})	Lag Time (hours)
0	11.4874 ± 3.0134	6.3135 ± 1.6562	0.82 ± 0.86
0.1	≈0	≈0	-
0.2	≈0	≈0	-
0.5	≈0	≈0	-
1	4.3123 ± 1.8484	4.3123 ± 1.0159	0.70 ± 0.93
1.5	9.6849 ± 1.9030	5.3229 ± 1.0459	0.49 ± 0.39
1.75	55.0512 ± 6.5052	30.2564 ± 3.5753	0.78 ± 0.25
2	51.3645 ± 2.6170	28.2302 ± 1.4383	1.25 ± 0.10
2 p (1:9)	≈0	≈0	-

Values represent the mean ± sem of at least three replicates. p denotes pulsed ultrasound was applied at the on:off ratio indicated in brackets

The absorption of sucrose through non-sonicated skin can be described in terms of 3 distinct stages. There is an initial mean lag time of just over 1 hour. This is followed by a mean linear flux of 11.49 pmol cm^{-2} h^{-1}. This represents a mean permeability coefficient of 6.31μm h^{-1}. Since sucrose is generally considered too

hydrophilic to diffuse through the bulk stratum corneum (measurements in section 5.2.2 indicated that Log $P_{octanol/water}$ = -2.4), this transport is most likely to be mediated *via* a transfollicular route. From 4 hours onwards, there is a plateau indicating that penetration has stopped. This occurs because the ethanol evaporates from the skin surface causing a fall in the hydrodynamic force necessary to drive sucrose through this transfollicular pathway.

Figure 4.19: The Effect of Presonication on Sucrose Penetration through Rat Skin

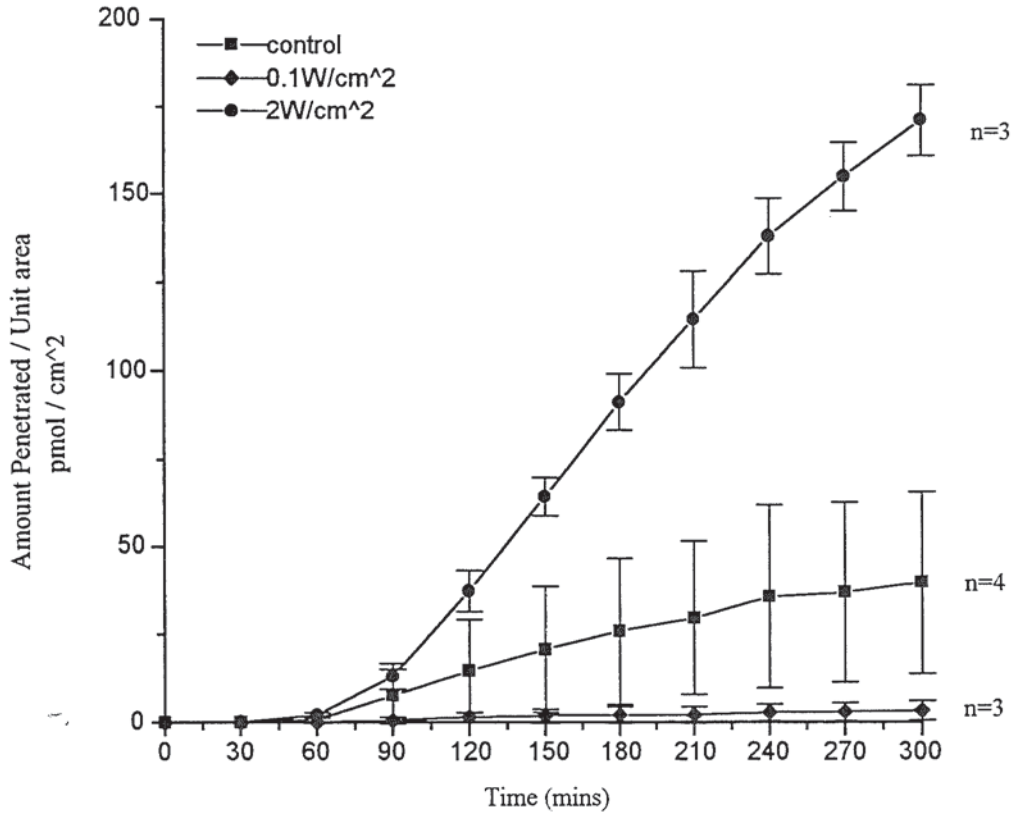

The application of high intensity ultrasound (2W cm^{-2}) increased sucrose flux to 51.36 pmol cm^{-2} h^{-1} representing a mean permeability coefficient of 28.23μm h^{-1}. At this intensity, ultrasound totally detached the stratum corneum from the epidermis (see section 4.3.1.1). The removal of the lipoidal barrier allows sucrose

to directly diffuse into the underlying hydrophilic layers of the epidermis and dermis. The resulting high penetration rate rapidly depleted the donor compartment (1819pmol) of sucrose. Therefore, from 2.5 hours onwards, the penetration rate progressively decreased.

Presonication at a low intensity (0.1W cm^{-2}) resulted in a virtually complete inhibition of sucrose permeation. It has already been established that low intensity ultrasound discharges sebaceous lipids into the hair follicle shaft and that furthermore, sucrose penetration is mediated *via* a transfollicular pathway. Consequently, it follows that the hair follicle shafts constitute that transfollicular route. The horny layer is absent over much of the inner surface of the hair follicle shaft and the outer root sheath provides continuation with the epidermis (Lauer *et al.*, 1995). In non-sonicated skin, sucrose can utilise this route to directly diffuse into the dermis. The application of low intensity ultrasound fills the hair follicle shaft with hydrophobic lipids, thus blocking this pathway.

A plot of permeability coefficient as a function of intensity reveals a complex profile (Figure 4.20). At low intensities (0.1 to 0.5W cm^{-2}), presonication resulted in a virtual complete suppression of sucrose transport. This is due to the deposition of sebaceous lipids within the hair follicle shafts. Following the application of 1W cm^{-2} and 1.5W cm^{-2} ultrasound, sucrose flux recovered to approximately its control value. Although the follicular route was still blocked, areas of the stratum corneum exposed to high local intensities had detached from the underlying tissue and penetration was occuring through these barrier gaps. Presonication at 1.75W cm^{-2} resulted in the permeability coefficient increasing dramatically to a value approximately 5 times that of the control value. This is mediated by the complete removal of the bulk stratum corneum. However, augmenting the intensity to 2W cm^{-2} produced an insignificant reduction in sucrose flux (t-test: P=0.605). At this intensity, ultrasound congeals dermal proteins and this is associated with a concomitant increase in the thickness of the layer. When the stratum corneum is absent, an increase in the thickness of the dermis results in reduced permeability.

Figure 4.20: Sucrose Penetration as a Function of Presonication Intensity

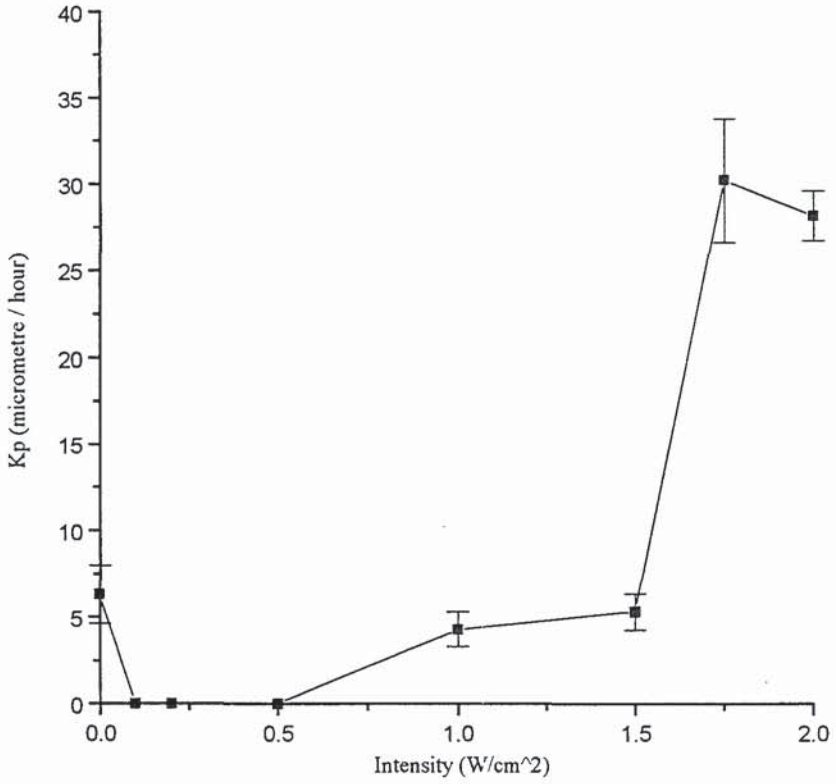

It was determined that pulsing the 2W cm^{-2} beam at a 1:9 on: off ratio resulted in a virtual complete suppression of sucrose flux. The SATA intensity of this output is equal to that of the 0.2W cm^{-2} cw beam. This result suggests that changes in the ultrasound mode do not affect the sebum discharge effect.

A series of experiments were carried out in order to evaluate the effect of presonication intensity at 3.3MHz on the percutaneous absorption of sucrose. Relevant absorption parameters calculated from the initial linear portions of the resulting rate curves are summarised in Table 4.3.The data show that, at this frequency, ultrasound suppresses sucrose penetration throughout the intensity range 0.1 to 2W cm^{-2}. This indicates that 3.3 MHz ultrasound releases lipids from the sebaceous glands. It must be noted that at identical values of indicated intensity, the total power output of the 3.3 MHz drive is approximately 40% lower than that of the 1.1MHz drive.

Table 4.3 Permeation data for Sucrose across Whole Rat Skin following sonication at 3.3 MHz

Intensity ($W\ cm^{-2}$)	Flux ($pmol\ cm^{-2}\ h^{-1}$)	K_p ($\mu m\ h^{-1}$)	Lag Time (hours)
0	11.4874 ± 3.0134	6.313 ± 1.6562	0.82 ± 0.86
0.1	≈0	≈0	-
1	≈0	≈0	-
2	≈0	≈0	-

Values represent the mean ± sem of at least three replicates

This is due to the differences in beam area and transducer efficiency discussed in section 2.2.4. Consequently, the 3.3MHz beam set at an indicated intensity of 2W cm^{-2} produced the same skin surface heating as the 1.1MHz beam set to 1.25W cm^{-2} (See Figure 4.10). Considering that there are probably subtle differences in energy distribution patterns between the two outputs, it can be concluded that the 3.3MHz beam at 2W cm^{-2} could promote the lipid release effect but exhibited insufficient energy to measurably perturb the stratum corneum.

Experiments were conducted in order to evaluate the effect of heat-alone on the subsequent penetration of sucrose. An aluminium cylinder was employed as a heat source (refer to section 4.2.3). The calculated parameters of this experiment are summarised in Table 4.4.

Table 4.4 Permeation data for Sucrose across Whole Rat Skin following direct heating

Final Surface Temp (°C)	Flux ($pmol\ cm^{-2}\ h^{-1}$)	K_p ($\mu m\ h^{-1}$)	Lag Time (hours)
20	11.4874 ± 3.0134	6.3135 ± 1.6562	0.82 ± 0.86
42	≈0	≈0	-
60	≈0	≈0	-

Values represent the mean ± sem of at least three replicates

The data show that simple heating to both 42°C and 60°C suppresses sucrose penetration through whole rat skin. This is due to the thermal discharge of sebum into the pilosebaceous channels. Although heating to 60°C is associated with some degradation of the cornified layer, compromised stratum corneum can still prevent the ingress of sucrose. A permeation profile representing control, heat alone (to 60°C) and 1.1MHz, 2W cm^{-2} ultrasound is presented in Figure 4.21. Interestingly, although the ultrasound and heat-alone regimen induce similar temperature increases at the skin surface (see Figure 4.13), the two regimens produce opposite effects in terms of sucrose permeation. This is due to the different histological effects produced by the two modalities (see section 4.3.1).

Figure 4.21: The Effect of Presonication and Heat Alone on Sucrose Penetration through Rat Skin

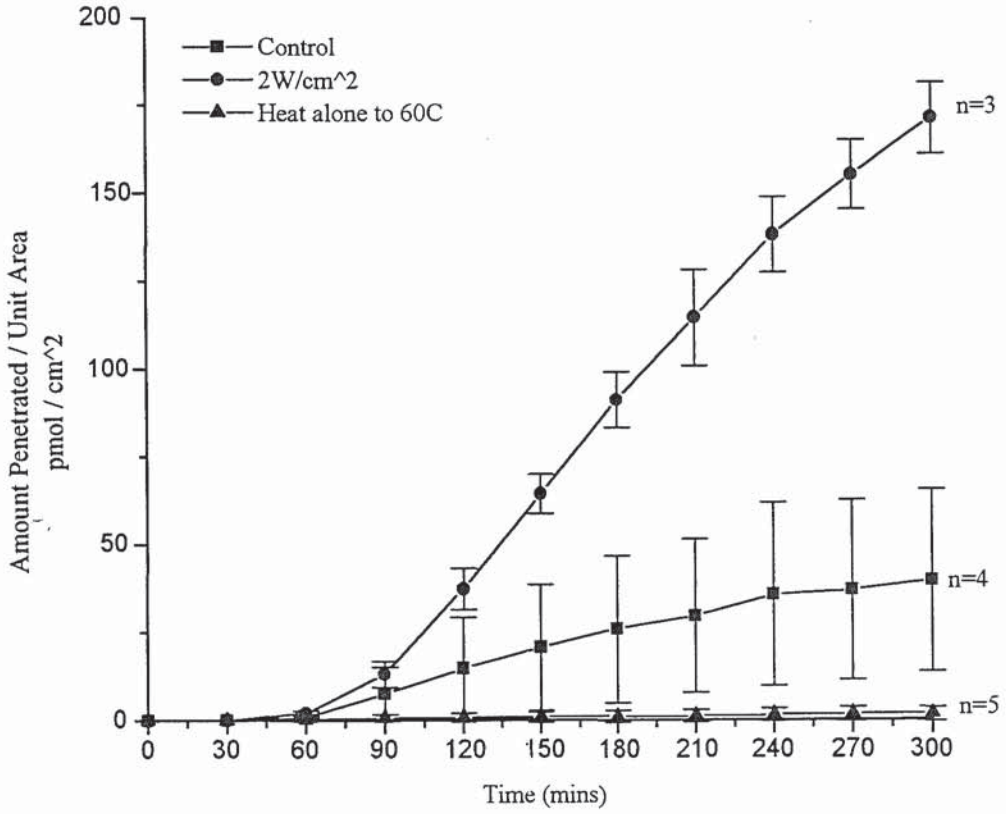

4.3.3.2 Mannitol

A series of experiments was conducted in order to determine the effect of presonication intensity (1.1MHz drive) on the percutaneous absorption of mannitol. Mannitol was investigated because, like sucrose, it is a small, highly hydrophilic, sugar molecule. The objective was to determine if the permeation behaviour of mannitol was comparable to that of sucrose. Flux, permeability coefficients and lag times derived from the linear portions of the resulting rate curves are summarised in Table 4.5. A sample of permeation profiles, representing control (0W cm^{-2}), low intensity (0.1W cm^{-2}) and high intensity (2W cm^{-2}) ultrasound are presented in Figure 4.22. As observed with sucrose, presonication can both enhance and reduce mannitol absorption depending upon the applied intensity while lag times remain relatively unchanged.

Table 4.5 Permeation data for Mannitol across Whole Rat Skin following sonication at 1.1MHz

Intensity ($W\ cm^{-2}$)	Flux ($pmol\ cm^{-2}\ h^{-1}$)	K_p ($\mu m\ h^{-1}$)	Lag Time (hours)
0	90.5084 ± 19.5106	5.0637 ± 1.0916	0.17 ± 0.47
0.1	≈0	≈0	-
0.2	≈0	≈0	-
0.5	≈0	≈0	-
1	169.3882 ± 51.6298	9.4768 ± 2.8885	0.31 ± 0.48
1.5	490.0357 ± 152.6622	27.4161 ± 8.5410	0.71± 0.51
1.75	484.7306 ± 102.9341	27.1193 ± 5.7589	0.80 ± 0.45
2	375.6595 ± 21.0171	21.0171 ± 2.9770	1.34 ± 0.56
2 p (1:9)	≈0	≈0	-

Values represent the mean ± sem of at least three replicates. p denotes pulsed ultrasound was applied at the on:off ratio indicated in brackets

Again, it can be seen that the permeation of mannitol through non-sonicated skin can be described in terms of 3 distinct stages. There is a short lag time of less

Figure 4.22: The Effect of Presonication on Mannitol Penetration through Rat Skin

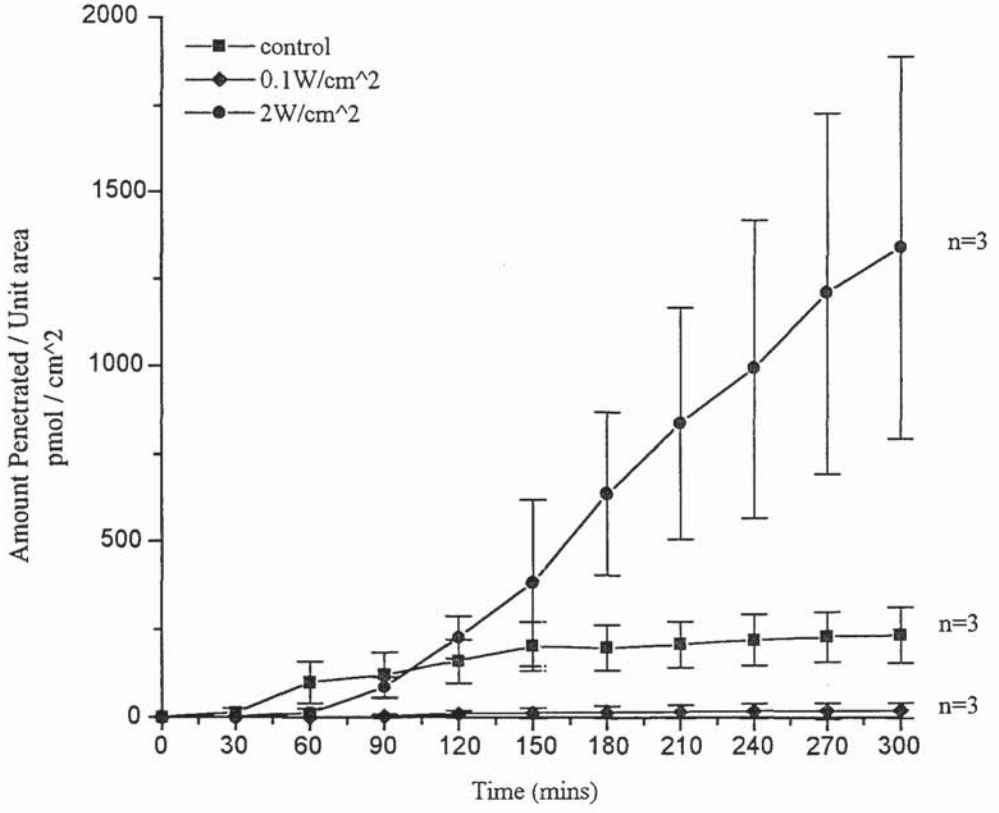

than 0.5 hours. This is followed by a steady-state flux of 90.51 pmol cm^{-2} h^{-1}. This represents a mean permeability coefficient of 5.06μm h^{-1}. From 2.5 hours onwards, there is a plateau indicating that drug absorption has ceased and this is due to the evaporation of ethanol and a consequent reduction in the available hydrodynamic force. By comparing Table 4.2 with Table 4.5, it can be seen that steady-state mannitol flux was approximately 9 times greater than steady-state sucrose flux. However, because the amount of mannitol in the donor compartment (17874pmol) was about one order of magnitude greater than the amount of sucrose in the donor compartment (1819pmol), the permeability coefficients were comparable. Interestingly, the mean lag time for mannitol absorption was shorter than the mean lag time for sucrose absorption. This may be because mannitol exhibits a smaller molecular weight than sucrose (182.2 Da versus 342.3 Da).

High intensity (2W cm^{-2}) ultrasound degraded the stratum corneum and the flux increased to 375.67 pmol cm^{-2} h^{-1}. From this value, a permeability coefficient of 21.02μm h^{-1} was derived. At this permeation rate, the mannitol in the donor

compartment (17874pmol) was progressively depleted and this was manifested in a decreasing penetration rate from 4.5 hours onwards.

Presonication at a low intensity (0.1W cm^{-2}) resulted in the virtual total suppression of mannitol absorption. This indicates that this compound primarily penetrates via the hair follicle shafts.

Figure 4.23 presents a graph of permeability coefficient as a function of presonication intensity. At low intensities (0.1 to 0.5W cm^{-2}), ultrasound completely suppressed the subsequent flux of mannitol. This is due to sebaceous lipids blocking the transfollicular route.

Figure 4.23: Mannitol Penetration as a Function of Presonication Intensity

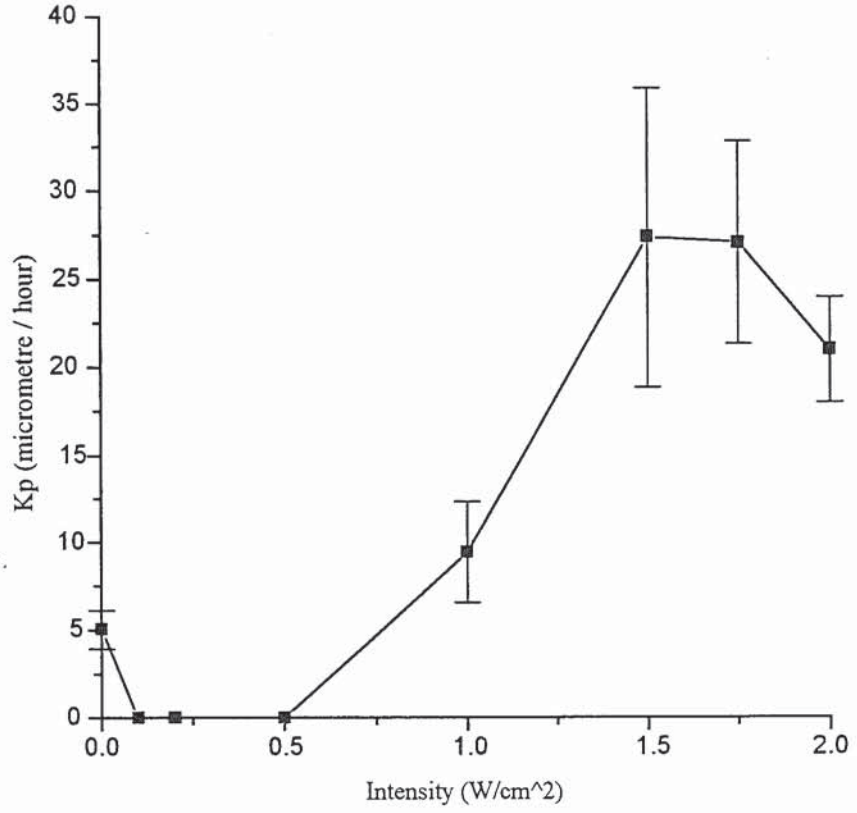

Following the application of 1W cm^{-2} ultrasound, mannitol flux recovered to approximately its control value. Although the shunt pathway was still blocked, regions of the stratum corneum exposed to high local intensities had detached from the underlying tissue and permeation was occuring through these barrier gaps. Presonication at 1.5W and 1.75W cm^{-2} resulted in the permeability coefficient increasing to over 5 times its control value. This was mediated by the degradation of the bulk stratum corneum. Following the application of 2W cm^{-2} ultrasound, there was a slight reduction in permeabilty which was probably caused by an increase in the thickness of the dermis.

By comparing Figure 4.20 and Figure 4.23, it can be seen that the profile of mannitol penetration as a function of presonication intensity exhibits the same general trend as that for sucrose. This is not surprising considering that both molecules are small and highly hydrophilic. The two drugs only exhibit vastly different permeability coefficients following exposure to 1.5 W cm^{-2} ultrasound. This is due to the unpredictable morphological effects developing at this mid-range intensity.

Presonication with a 1:9 pulsed output at SATA intensity 0.2W cm^{-2} inhibited mannitol permeation again indicating that the sebum discharge phenomenon is not affected by variations in ultrasound mode.

A series of investigations were conducted in order to evaluate the effect of 3.3MHz ultrasound on subsequent mannitol absorption. The derived permeation parameters are summarised in Table 4.6.

Table 4.6 Permeation data for Mannitol across Whole Rat Skin following sonication at 3.3 MHz

Intensity ($W\ cm^{-2}$)	Flux ($pmol\ cm^{-2}\ h^{-1}$)	K_p ($\mu m\ h^{-1}$)	Lag Time (hours)
0	90.5084 ± 19.5106	5.0637 ± 1.0916	0.17 ± 0.47
0.1	≈0	≈0	-
2	≈0	≈0	-

Values represent the mean ± sem of at least three replicates

The data show that penetration ceased following sonication at both 0.1 W cm^{-2} and 2W cm^{-2}. This is due to the blockage of the transfollicular route with released lipids. Presonication at 2W cm^{-2} did not degenerate the stratum corneum due to the same interplay of factors discussed in the previous section.

Table 4.7 shows the mannitol permeation parameters following exposure of the skin barriers to heat alone. The data show that simple heating to both 42°C and 60°C suppressed mannitol penetration and this is due to sebum deposition within the hair follicle shafts. Heating to 60°C was associated with some adverse effects on the stratum corneum but there was sufficient lipoidal barrier remaining to prevent drug diffusion.

Table 4.7 Permeation data for Mannitol across Whole Rat Skin following direct heating

Final Surface Temp (°C)	Flux (pmol cm^{-2} h^{-1})	K_p (μm h^{-1})	Lag Time (hours)
20	90.5084 ± 19.5106	5.0637 ± 1.0916	0.17 ± 0.47
42	≈0	≈0	-
60	≈0	≈0	-

Values represent the mean ± sem of at least three replicates

4.3.3.3 Hydrocortisone

A series of studies were carried out in order to assess the effect of presonication intensity (1.1MHz drive) on the percutaneous absorption of hydrocortisone. Flux values, permeability coefficients and lag times derived from the steady state segments of the resulting rate profiles are summarised in Table 4.8. Figure 4.24 depicts 3 absorption profiles, representing sham ultrasound (0W cm^{-2}), low intensity ultrasound (0.1W cm^{-2}) and high intensity ultrasound (2W cm^{-2}). The results demonstrate that ultrasound can both enhance and reduce hydrocortisone

penetration depending upon the applied intensity. However, sonication did not significantly affect the length of the lag phase.

The absorption of hydrocortisone through control skin can be described in terms of two stages. There was an initial mean lag time of just under 90 minutes. This was followed by a mean linear flux of 0.1049 pmol cm^{-2} h^{-1}. This represents a mean permeability coefficient of 1.34μm h^{-1}. The mechanism of steady-state hydrocortisone absorption is currently uncertain. Traditionally, absorption was thought to be mainly mediated by diffusion through the bulk stratum corneum (Scheuplein, 1967). However, more recent reports have proposed that follicular pathways play an important role (Illel *et al.*, 1991, Lauer *et al.*, 1995).

The application of high intensity ultrasound (2W cm^{-2}) increased hydrocortisone flux to 0.81pmol cm^{-2} h^{-1}. This represented a mean permeability coefficient of 10.19μm h^{-1}. Presonication at this intensity resulted in the degradation of the horny layer and consequently rapid hydrocortisone diffusion through the underlying strata of the skin. A constant penetration rate was sustainable over 5 hours since 78pmol of hydrocortisone were initially deposited on the skin surface. However, the application of this ultrasound regimen was not associated with a shortened mean lag time. Although the degradation of the stratum corneum increased bulk diffusion, diffusion *via* the shunt pathway was retarded by sebum deposition in the pilosebaceous channels.

Table 4.8 Permeation data for Hydrocortisone across Whole Rat Skin following sonication at 1.1MHz

Intensity (W cm^{-2})	Flux (pmol cm^{-2} h^{-1})	K_p (μm h^{-1})	Lag Time (hours)
0	0.1049 ± 0.0234	1.3438 ± 0.2995	1.43 ± 0.78
0.1	0.0478 ± 0.0064	0.5732 ± 0.0774	1.20 ± 0.49
1	0.2067 ± 0.0611	2.6030 ± 0.7697	1.32 ± 1.06
1.5	0.4485 ± 0.2049	5.7451 ± 2.6244	1.74 ± 1.52
1.75	0.5815 ± 0.1522	7.3237 ± 1.9170	1.18 ± 0.96
2	0.8084 ± 0.1397	10.1857 ± 1.7595	1.88 ± 0.56

Values represent the mean ± sem of at least three replicates

Figure 4.24: The Effect of Presonication on Hydrocortisone Penetration through Rat Skin

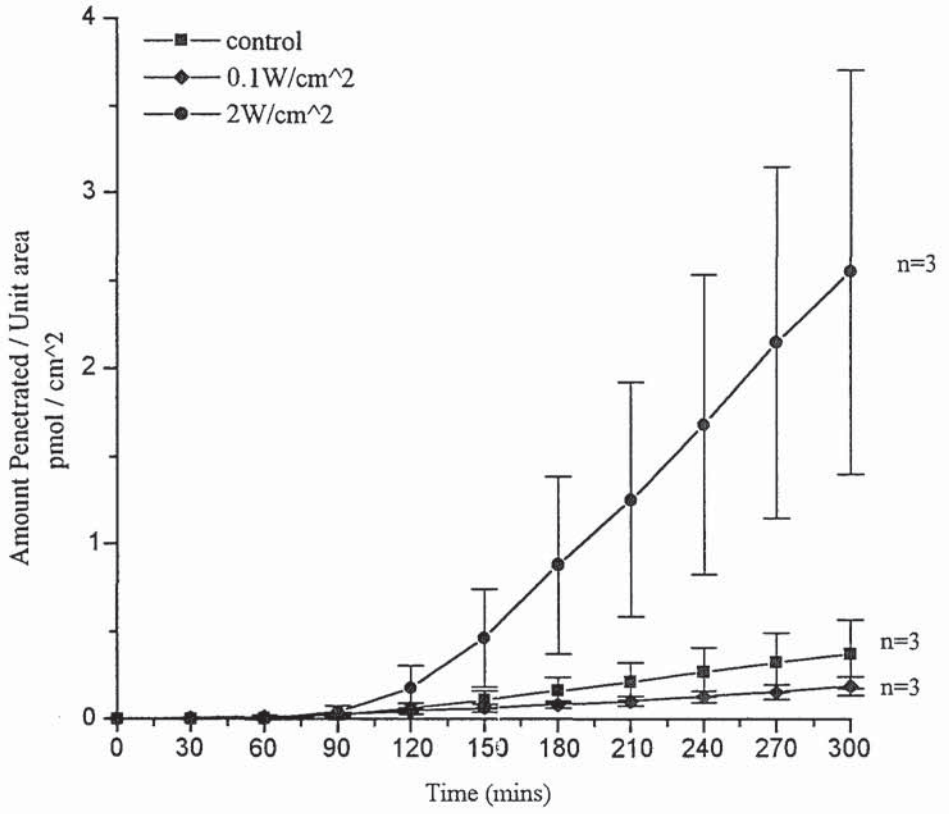

Presonication at a low intensity (0.1W cm^{-2}) reduced mean hydrocortisone flux to 0.1 pmol cm^{-2} h^{-1} which is equivalent to a permeability coefficient of 0.57μm h^{-1}. This is significantly less than the permeability coefficient of control skin (P = 0.0208, alternate t-test). This result suggests that the pilosebaceous route constitutes a major absorptive pathway for hydrocortisone in Wistar rat skin, contributing to about half of total penetration. This compares well with the results derived from published studies involving hairless-rat skin (Illel *et al.*, 1991). In those experiments, follicle-free skin was grown on the back of the animals and its permeability to hydrocortisone was compared with regular skin. It was determined that the *in vitro* flux through follicle-free skin was approximately 40% of the flux through normal skin.

Figure 4.25 presents a plot of permeability coefficient as a function of intensity. Following presonication at 0.1W cm^{-2}, hydrocortisone transport was reduced due to the suppression of the follicular route by lipids. Although relatively lipophilic compounds such as hydrocortisone can permeate through the sebum-filled channels, the process occurs at a slower rate. Following sonication at 1W cm^{-2}, hydrocortisone penetration recovered to a level that was statistically unchanged from the control value. Although the hair follicle shafts were still blocked, partial thinning of the stratum corneum permitted enhanced flux through this layer. This compensated for the reduction in the importance of the follicular route.

Figure 4.25: Hydrocortisone Penetration as a Function of Presonication Intensity

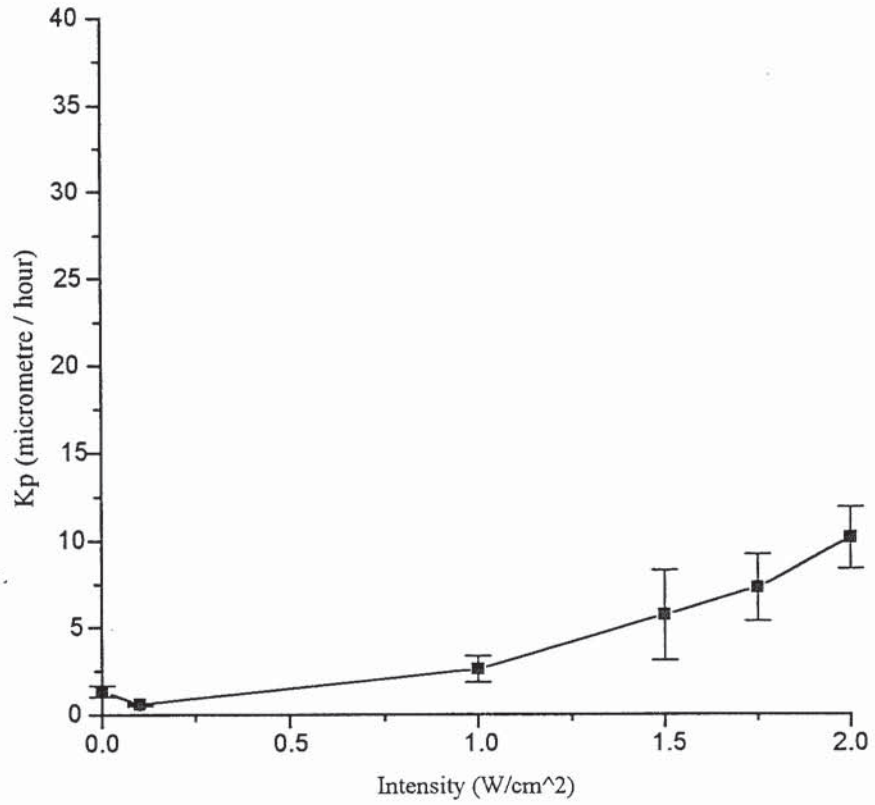

In the intensity range 1 to 2W cm^{-2}, the permeability coefficient increased with rising intensity in an approximately linear fashion. Successive increases in beam intensity resulted in progressively greater thinning of the cornified layer and hence gradually increasing hydrocortisone flux. This behaviour contrasts with the rapid permeability increases observed for sucrose and mannitol over the same intensity range. The difference in patterns is due to the fact that hydrocortisone can diffuse through stratum corneum lipids whilst the hydrophilic drugs cannot.

Table 4.9 presents the hydrocortisone permeation parameters following exposure of the skin sections to heat alone. The data show that pre-heating to 42°C reduced the mean permeability coefficient of hydrocortisone to less than half of its mean control value. This effect was statistically significant ($P = 0.039$). The reduction in permeability is due to the blockage of the transfollicular pathway with thermally discharged sebaceous lipids. Pre-heating to 60°C significantly increased the mean permeability of the system. This is because the stratum corneum had been partially degraded by the heat, thus permeabilising it to hydrocortisone. This change compensated for the loss of the transfollicular pathway.

Table 4.9 Permeation data for Hydrocortisone across Whole Rat Skin following direct heating

Final Surface Temp (°C)	Flux (pmol cm^{-2} h^{-1})	K_p (μm h^{-1})	Lag Time (hours)
20	0.1049 ± 0.0234	1.3438 ± 1.0916	1.43 ± 0.78
42	0.0387 ± 0.0101	0.6113 ± 0.1595	1.31 ± 0.93
60	0.1295 ± 0.0131	2.0435 ± 0.2075	1.55 ± 0.35

Values represent the mean ± sem of at least three replicates

Hydrocortisone permeation *in vitro* through ultrasound-exposed skin has also been investigated by other workers. One team (Machluf and Kost, 1993) applied a 1MHz 1:4 pulsed beam at 3W cm^{-2} for 2 hours to hairless mouse skin within a temperature-controlled Franz-cell system. It was reported that subsequent

hydrocortisone transport was unaffected by sonication. This suggests that there may be significant species differences in these ultrasound effects.

4.3.2.4 5-Fluorouracil

A group of experiments were conducted in order to determine the influence of 0.1W cm^{-2} ultrasound (1.1MHz drive) on the subsequent absorption of 5-fluorouracil. The relevant absorption parameters derived from the initial linear segment of the permeation profile are summarised in Table 4.10.

Table 4.10 Permeation data for 5-fluorouracil across Whole Rat Skin following sonication at 1.1 MHz

Intensity ($W\ cm^{-2}$)	Flux ($pmol\ cm^{-2}\ h^{-1}$)	Kp ($\mu m\ h^{-1}$)	Lag Time (hours)
0	0.1545 ± 0.0296	1.1310 ± 0.2166	0.20 ± 0.31
0.1	0.1996 ± 0.03995	1.4611 ± 0.2924	0.33 ± 0.31

Values represent the mean ± sem of at least three replicates

The absorption of 5-fluorouracil through control skin can be described in terms of three stages. There was a short mean lag time of 0.2 hours. This was followed by a mean linear flux of 0.15 pmol $cm^{-2}\ h^{-1}$. This represents a mean permeability coefficient of 1.13$\mu m\ h^{-1}$. From 2 hours onwards, the penetration rate decreased. This may due to the evaporation of ethanol and a loss in the requisite hydrodynamic force.

The absorption of 5-flurouracil through skin pre-exposed to 0.1W cm^{-2} can be outlined in terms of three similar stages. There was a mean lag time of 0.33 hours. This was followed by a steady state phase characterised by an average penetration rate of 0.20 pmol $cm^{-2}\ h^{-1}$. This represents a mean permeability coefficient of 1.46 $\mu m\ h^{-1}$. From 2 hours onwards, the permeation rate decreased due to the loss of ethanol from the skin surface.

The data show that presonication at 0.1W cm^{-2} did not significantly affect the penetration profile of 5-fluorouracil. Since ultrasound exposure blocked the hair follicle shafts with hydrophobic lipids, significant 5-fluorouracil penetration cannot be mediated in rat skin *via* this pathway.

4.3.2.5 Aminopyrine

Studies were carried out in order to determine the effect of 0.1W cm^{-2} ultrasound (1.1MHz drive) on the subsequent penetration of aminopyrine. The relevant absorption parameters, derived from the steady-state segment of the permeation plot, are summarised in Table 4.11.

Table 4.11 Permeation data for aminopyrine across Whole Rat Skin following sonication at 1.1 MHz

Intensity (W cm^{-2})	Flux (pmol cm^{-2} h^{-1})	K_p (μm h^{-1})	Lag Time (hours)
0	18.0302 ± 1.7864	7.7962 ± 0.7724	0.85 ± 0.46
0.1	20.2908 ± 0.8012	8.7737 ± 0.3464	0.93 ± 0.18

Values represent the mean ± sem of at least three replicates

The penetration of aminopyrine through control skin can be described in terms of two phases. There was a mean lag time of 0.85 hours. This was followed by a steady state flux of 18.03 pmol cm^{-2} h^{-1}. This represents a mean permeability coefficient of 7.79μm h^{-1}. Aminopyrine penetration through skin pre-exposed to 0.1W cm^{-2} can be described in terms of two similar stages. There was a mean lag time of 0.94 hours followed by a linear phase characterised by an average penetration rate of 20.29pmol cm^{-2} h^{-1}. This represents a mean permeability coefficient of 8.77μm h^{-1}.

It can be seen that presonication at 0.1W cm^{-2} did not significantly change the penetration profile of aminopyrine. Since ultrasound discharges sebaceous lipids into the pilosebaceous shafts, significant aminopyrine penetration is not mediated *via* this route.

4.3.4 Permeation Studies across other Skin Barriers

In the first series of transport studies, samples of whole guinea pig skin and whole human skin were examined for evidence of the sebum-release effect. In a second set of studies, human epidermis samples were exposed to ultrasound and the subsequent permeation of sucrose, mannitol and hydrocortisone was investigated.

4.3.4.1 Sucrose Permeation in Different Species

Sections of whole guinea pig skin and whole human skin were subjected to 0.1W cm^{-2} ultrasound (1.1MHz drive). The subsequent absorption of sucrose was then investigated using the Franz diffusion model and compared to that across whole rat skin. Hence, an insight into the species specifity of the sebum discharge phenomenon could be attained. Flux values, permeability coefficients and lag times derived from the steady state segments of the profiles are presented in Table 4.12.

Table 4.12 Permeation data for Sucrose Through Different Skin Species following Presonication at 0.1W cm^{-2}

Species (site)	Flux (pmol cm^{-2} h^{-1})	K_p (μm h^{-1})	Lag Time (hours)
Wistar Rat (dorsal)			
control	11.4874 ± 3.0134	6.3135 ± 1.6562	0.82 ± 1.66
ultrasound	≈0	≈0	-
Guinea Pig (dorsal)			
control	1.4447 ± 0.4214	0.7940 ± 0.2316	1.09 ± 0.65
ultrasound	≈0	≈0	-
Human (leg)			
control	≈0	≈0	-
ultrasound	≈0	≈0	-

Values represent the mean ± sem of at least three replicates

The data show that sucrose permeation through control guinea pig skin was only 12% of that through control rat skin. This is probably due to differences, between the two rodents, in the fractional surface area occupied by the pilosebaceous follicles. The application of low intensity ultrasound resulted in the guinea-pig skin becoming totally impermeable to sucrose. This indicates that ultrasound can release sebaceous lipids from the sebaceous glands of this species of guinea pigs, thus reducing the flux of sucrose. The human skin was effectively impermeable to sucrose, both with and without presonication. These skin samples were obtained from regions of the leg in which hair follicles were extremely sparse or absent.

4.3.4.2 Hydrocortisone Permeation through Human Epidermis

Absorption studies were performed with human epidermis samples in order to determine the effect of high intensity ultrasound (2W cm^{-2}, 1.1MHz drive) on the subsequent permeation of mannitol, sucrose and hydrocortisone. It was found, both with and without ultrasound, that the permeation of sucrose and mannitol was generally small but the data also exhibited extreme inter-sample variability. This is probably due to site-to-site differences in the consistency of intercellular stratum corneum lipids. The effect has been observed in other human epidermis transport studies involving highly hydrophilic molecules.

Figure 4.26 shows the permeation profile of hydrocortisone through human epidermis, following both control and high intensity ultrasound. A profile representing the flux of skin pretreated with 2.5% azone is also included to provide an additional reference. Table 4.13 shows the flux, permeability coefficients and lag times derived from the linear portion of each penetration profile.

Table 4.13 Permeation data for Hydrocortisone through Human Epidermis following sonication at 2W cm^{-2}

Treatment	Flux ($pmol\ cm^{-2}\ h^{-1}$)	K_p ($\mu m\ h^{-1}$)	Lag Time (hours)
control	0.0180 ± 0.0024	0.2310 ± 0.0308	0.94 ± 0.55
2W cm^{-2} ultrasound	0.0179 ± 0.0023	0.2295 ± 0.0298	0.58 ± 0.57
2.5% azone	0.1157 ± 0.2414	1.4836 ± 0.3095	0.23 ± 0.95

Values represent the mean ± sem of at least three replicates

Figure 4.26: The Effect of Presonication on Hydrocortisone Penetration through Human Epidermis

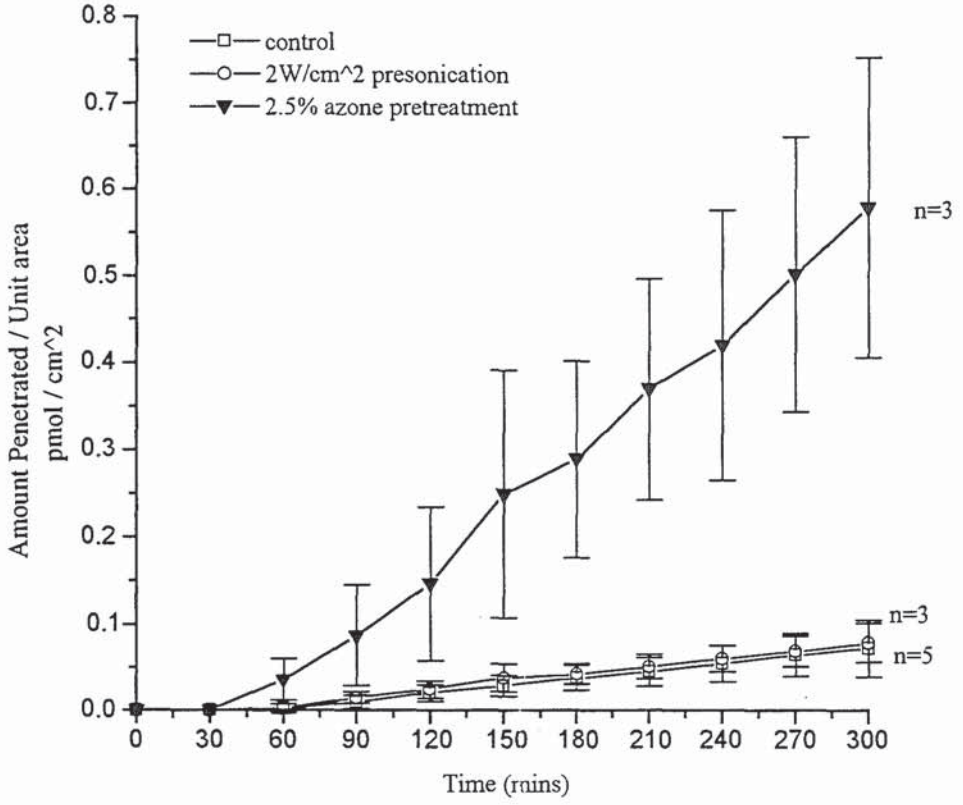

The penetration of hydrocortisone through control skin can be described in terms of two phases. There was a mean lag time of 0.94 hours. This was followed by a steady state flux of 0.018 pmol cm^{-2} h^{-1} which represents a mean permeability coefficient of 0.23μm h^{-1}. Hydrocortisone penetration through skin pre-exposed to 2W cm^{-2} can also be described in terms of a lag time of 0.58 hours followed by a linear phase characterised by an average penetration rate of 0.018pmol cm^{-2} h^{-1}. This represents a mean permeability coefficient of 0.23μm h^{-1}.

It can be seen that presonication at 2W cm^{-2} did not significantly change the penetration profile of hydrocortisone. This contrasts with the observation that the same beam produced an approximately 8-fold increase in subsequent hydrocortisone permeability in the whole rat skin model (refer to section 4.3.3.3). These differences are caused by the fact that ultrasound attenuation depends upon

tissue depth. The application of the 2W cm^{-2} beam heated the epidermis specimens to surface temperatures of 37°C after 5 minutes of irradiation. This temperature is much lower than the 60°C attained by whole skin samples exposed to an identical ultrasound regimen. Many workers have postulated that ultrasound increases the fluidity of the stratum corneum lipids, thus permeabilising the skin barrier. In the epidermis model, any such lipid perturbations would have already been affected during the heat separation required to prepare the epidermis specimens.

It can be seen that azone pretreatment increased hydrocortisone flux through human epidermis by approximately 7-fold. The mechanisms by which azone achieves this effect are discussed in section 5.1.

4.4 SUMMARY

When certain species of rodent skin are subjected to an ultrasound free-field *in vitro*, sebum is discharged from the sebaceous glands so as to fill much of the hair follicle shafts. The phenomenon occurs following exposure to low intensities of ultrasound (0.1 to 1W cm^{-2}) and it is probably mediated by the mechanical effects of the beam. At higher intensities, ultrasonic heating probably acts as an additional mode of action. The sebum discharge effect has been shown to suppress the transfollicular absorption of some non-lipophilic molecules and it would be expected to perhaps enhance the local delivery of lipophilic molecules. Hence, the process is important in phonophoresis.

The deposition of sebaceous lipids within the hair follicle shafts means that the transfollicular absorption pathway is blocked for hydrophilic molecules that partially or totally penetrate *via* this route. Consequently, this phenomenon has important implications for topical drug delivery in that it can be used as a probe to elucidate the relative follicular contribution to total penetration. Care must be taken in applying this probe as it has yet to be established as to whether ultrasound causes sebum to overflow on to the skin surface, thus suppressing flux across the bulk stratum corneum. More sensitive histological techniques need to be performed to assess whether this is the case.

In these rat skin studies, it was found that the highly hydrophilic compounds sucrose (Log $P_{octanol/water}$ = -2.4) and mannitol (Log $P_{octanol/water}$ = -2.6) penetrate virtually entirely *via* the pilosebaceous route. The shunt pathway was responsible for approximately half of all hydrocortisone penetration in this model (Log $P_{octanol/water}$ = 1.55). However, 5-fluorouracil (Log $P_{octanol/water}$ = -0.95) and aminopyrine (Log $P_{octanol/water}$ = 0.8) exhibited negligible shunt permeation. This indicates that other physico-chemical parameters apart from partition coefficient govern the relative affinity of the permeant for the various pathways of absorption.

Although sebaceous gland histology is similar in most mammals, there are species differences in their gross morphology. Furthermore, there are huge site and species differences in the number and surface areas of pilosebaceous units. It has yet to be established whether the sebum discharge effect occurs in regions of human skin that are rich in sebaceous glands. Crucially, it is not known whether the process will develop in the *in vivo* situation when other artefacts of an

ultrasonic beam such as standing waves, blood cell banding and vasodilation may develop. Consequently, further studies must be designed and performed in order to further investigate this phenomenon.

At high intensities, ultrasound irreversibly degraded the stratum corneum and the dermis. This was probably mediated by both the thermal effects as well as the mechanical effects of the ultrasound. This damage was intensity - dependent and followed the general patterns observed in the literature reports. It was found that hydrocortisone flux was increased through pre-sonicated skin that appeared histologically unaltered from control skin. This indicates that traditional histology techniques may be too insensitive to detect irreversible thinning of the stratum corneum. At very high intensities, further increases in intensity, resulted in slightly reduced penetration. This is mediated by thickening of the dermis when the stratum corneum had been completely detached.

CHAPTER FIVE

IN VITRO PHONOPHORESIS THROUGH RAT SKIN: THE EFFECTS OF SIMULTANEOUS ULTRASOUND

5.1 INTRODUCTION

Among the physicochemical factors influencing the percutaneous absorption of drugs, the oil / water partition coefficient of the permeant plays a major role. For hydrophilic drugs, the rate-limiting step in absorption is presented by the initial partitioning and diffusivity through the lipophilic stratum corneum. In this situation, permeation is termed barrier-controlled. For highly lipophilic drugs, the rate-limiting step in absorption is partitioning out of the stratum corneum into the relatively aqueous environment of the viable epidermis. For these compounds, permeation is described as hydrodynamic-layer controlled. As a result of these effects, log-log plots of percutaneous absorption as a function of partition coefficient generally yield a parabolic curve with peak absorption occuring at an intermediate oil / water partition coefficient. In one human volunteer study, it was determined that for a homologous series of salicylates, the log value of the optimal n-octanol / water partition coefficient was 2.44 (Yano *et al.*, 1986).

So far, systematic studies, examining phonophoretic enhancement as a function of permeant partition coefficient have been lacking in the literature reports. In these *in vitro* studies, seven different permeants were selected, each exhibiting a n-octanol / water partition coefficient value in the range -2.4 to 3.86. Figure 5.1 presents the chemical structures of these compounds while Table 5.1 lists some of their physico-chemical properties. It is apparent that apart from the partition coefficient, other differences such as molecular weight, water solubility, dipole moment, pKa *etc* exist between these molecules. Ideally a homologous series should have been examined but expenditure limitations prevented this. In particular, these permeants exhibit significant differences in molecular weight. However, it has been determined that for small molecules, the diffusion coefficient is approximately inversely proportional to the cubed root of molecular weight. As can be seen in Table 5.1, there is less variation in this parameter between the molecules.

The aim, in this chapter is to investigate the role of lipophilicity in drug permeation and the effect of ultrasound. One specific objective was to determine if ultrasonic energy can influence the hydrodynamic-layer so as to increase the absorption rate of highly lipophilic drugs. Whole rat skin was employed as the barrier membrane. A Franz-cell system was modified so that an ultrasound beam could be directed toward the skin surface during most of the permeation period. Since any observed

enhancement could be an artefact of ultrasonic heating, it was necessary to develop heat-alone treatments that would warm the skin surface to a comparable extent as the ultrasound.

Figure 5.1: The Chemical Structures of the Selected Permeants

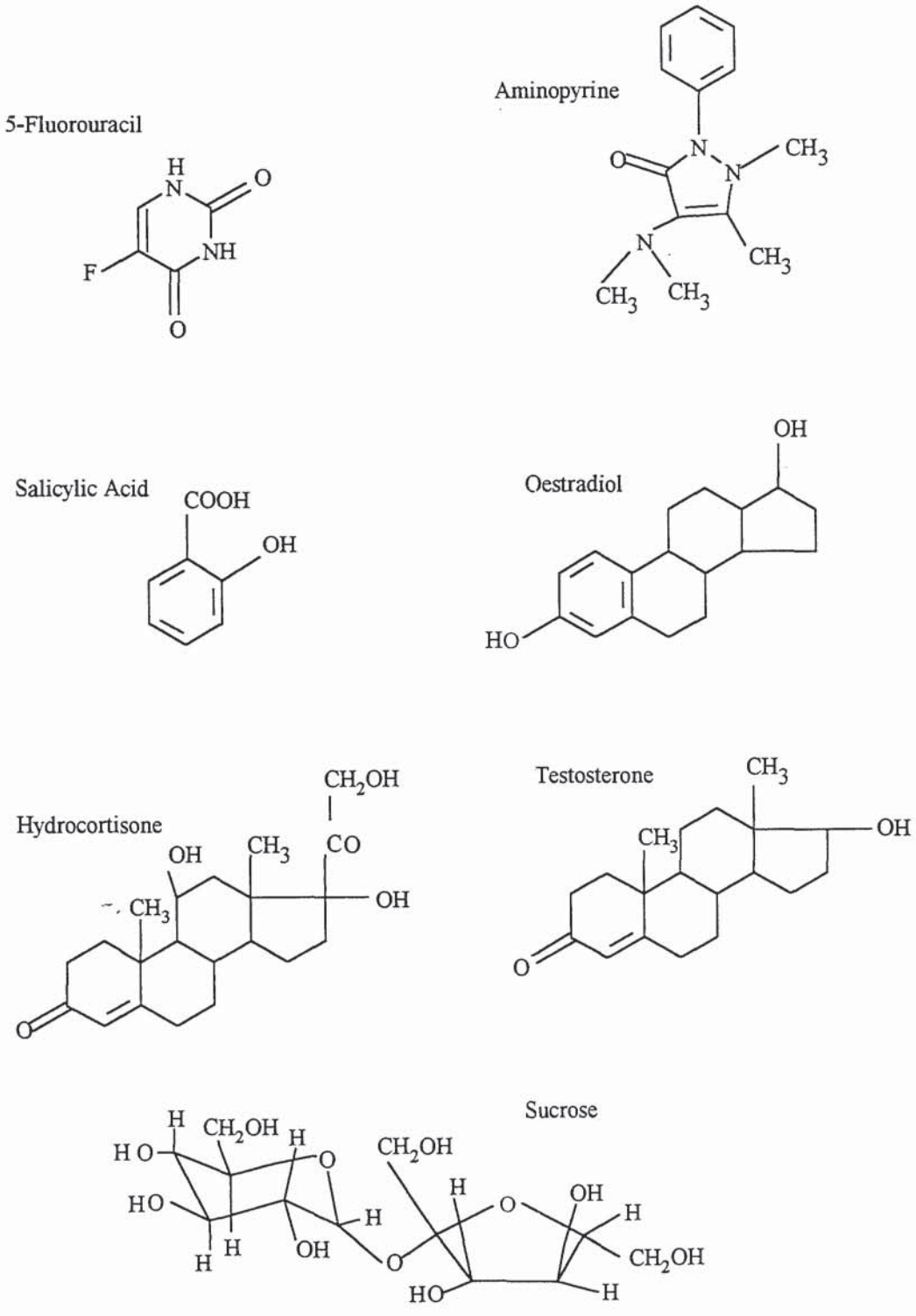

Table 5.1: Some Physico-chemical Properties of the Selected Permeants

Molecule	Log $P_{oct./water}$	Water sol. (μmol/ml)	Mol.Wt. (Da)	$\sqrt[3]{}$Mol.Wt.
sucrose	-2.40*	5843	342.3	7.00
5-fluorouracil	-0.95	93.7	130.1	5.07
aminopyrine	0.80	240	231.3	6.14
hydrocortisone	1.55	0.8	362.5	7.13
salicylic acid	2.25	15.7	138.1	5.17
testosterone	3.32	virtually insol.	288.4	6.61
oestradiol	3.86	virtually insol.	272.4	6.48

*The Log P value for sucrose was experimentally determined. All the other values were derived from the literature (Leo *et al.*, 1971).

As a consequence of the limited permeability of the stratum corneum, numerous chemical enhancers have been developed which, when co-applied with the drug, significantly and reversibly enhance skin flux. Two extensively studied enhancers are azone and oleic acid and their chemical structures are presented in Figure 5.2.

Figure 5.2: Chemical structures of the Penetration Enhancers used in this Study

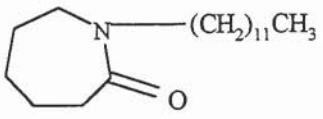

1-Dodecyclazacycloheptan-2-one
(azone)

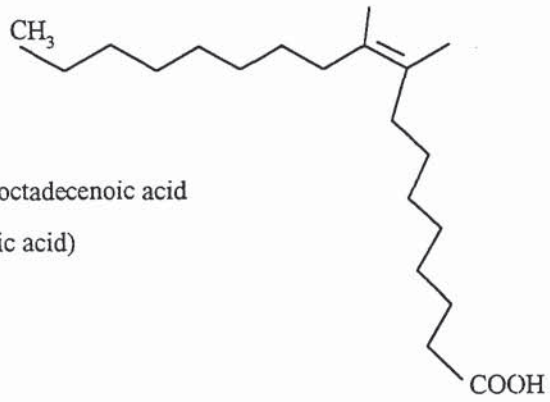

cis-9-octadecenoic acid
(oleic acid)

Azone is a clear, colourless, lipophilic liquid at room temperature, exhibiting a molecular weight of 281.5 Da. Current thinking is that azone partitions into the intercellular lipids of the stratum corneum and interacts with the structured lipids so as to make them more fluid. This decreases the diffusional resistance subsequently experienced by a penetrant molecule (Hadgraft *et al.*, 1995). Although azone can enhance the absorption of a wide range of compounds, it is generally more effective at promoting the absorption of hydrophilic agents. Numerous studies have shown that the extent of enhancement varies parabolically as a function of azone concentration with the optimal concentation depending upon the individual model employed. In general, azone is most effective when employed in the concentration range 1 to 10%.

Oleic acid is a *cis*-unsaturated fatty acid, existing as a liquid at room temperature. Although the compound has been used for many years to enhance the percutaneous absorption of both hydrophilic and hydrophobic compounds, its mode of action was not well understood. However, recent attenuated reflectance infrared spectroscopy studies on humans *in vivo* have helped shed light on this issue (Naik *et al.*, 1995). It now appears that oleic acid permeabilises the stratum corneum *via* 2 separate mechanisms. The main mechanism is associated with the phase separation of oleic acid from the endogenous solid lipids of the stratum corneum. The existence of oleic acid in a liquid state results in high permeability being exhibited at the boundary between the solid and liquid domains. This effect occurs throughout the depth of the cornified layer. A secondary enhancement effect is mediated by oleic acid inducing lipid disordering in the upper layers of the stratum corneum.

Although one group has demonstrated that ultrasound and dimethylsulphoxide can act synergistically in promoting amphotericin absorption (Romanenko and Aravisky, 1991), very little work has been conducted on the combined effects of ultrasound and enhancers. In order to shed more light on this issue, permeation experiments were designed in which ultrasound was applied to skin samples that had been pretreated with either azone or oleic acid.

Apart from the general permeation method, this research involved the application of various supplementary techniques. These included; TLC analysis, partition coefficient measurements, synthetic membrane studies, thermal profile determinations, histological studies, and permeant recovery experiments. All these

methodologies are explained in detail in this chapter. The first part of the discussion deals with the thermal effects developed by each ultrasound and heat-alone regimen. It was convenient to classify the permeants studied into those that were hydrophilic, (sucrose, 5-fluorouracil, and aminopyrine) and those that were hydrophobic, (hydrocortisone, salicylic acid, testosterone and oestradiol). The permeation data for each of these groups are discussed separately. The final section includes a summary of the major findings of these studies as well as some ideas for further research in this field.

5.2 METHODS

5.2.1 TLC Techniques

Thin-layer Chromatography (TLC) is a method of flat-bed chromatography that involves the passage of a solvent (mobile phase) across a uniform layer of a finely divided insoluble adsorbent (stationary phase). When different compounds are applied to the adsorbent layer, they migrate across it at different rates with the transport of the solvent. As an analytical technique, TLC is recognised as a rapid and sensitive system for the identification and separation of compounds. The major experiments in this chapter required the application of solutions containing [^{14}C]-sucrose and [^{3}H]-5-fluorouracil. Since the vials containing these agents had been stored in the laboratory for a long period, TLC was employed to analyse the samples in order to ensure that the original compound had not degraded during storage. Slightly different methodologies were employed to analyse the purity of each of the two radiolabelled compounds.

5.2.1.1 TLC of Sucrose

The mobile phase, consisting of 41ml butanol (BDH), 23ml ethanol and 36ml water was prepared and transferred to the chromatography tank (Panglass Shandon Chromatatank). A strip of filter paper, 15mm wide and 200mm long was employed as the stationary phase. This paper strip was marked into 8mm wide divisions with a soft pencil. The filter paper was attached to the top of the tank while the base was immersed several millimetres below the solution level. A 2μL volume (728pmol, 0.0148MBq) of [^{14}C]-sucrose was then pipetted to a central origin, 1.6mm above the level of the solution. The cover was then placed over the top of the chromatography tank and the system was left for 4 hours until the front of the mobile phase had diffused upwards to a distance of 88mm above the origin. The filter paper was then removed and subsequently thoroughly dried in a current of warm air from a blower. The paper strip was cut into 8mm wide sections and these were transferred to labelled scintillation vials. Scintillation fluid was added and following vortexing, the activity of each vial was measured in a scintillation counter (Packard 1900 TR). The analytical technique has been described in detail in section 4.2.7.

5.2.1.2 TLC of 5-fluorouracil

The development chamber (Panglass Shandon Chromatatank) was filled with a mixture consisting of 60ml n-butanol (BDH), 15ml 1%v/v aqueous acetic acid (BDH) and 15ml distilled water. A pre-coated plastic sheet (Merck, 0.2mm layer thickness) was employed as the stationary phase or chromatoplate. A 30mm wide and 80mm long strip was cut out of this sheet and a soft pencil was used to mark out 8mm wide divisions. The top of the chromatoplate was fixed to the tank top while the base was immersed in the solvent to a depth of 8mm. An origin was created by pipetting out 1μL of [^{3}H]-5-fluorouracil (66.66pmol, 0.0326MBq, NEN) to a central spot, 16mm above the level of the solution. The chromatography tank was then covered and the system left for 3 hours until the solvent front had diffused upwards to a distance of 64mm from the origin. The plastic strip was removed from the tank and dried in a current of warm air generated by a blower. The strip was cut into 8mm wide sections and each of these was transferred to a labelled scintillation vial. The vials were vortexed and their emitted activity was measured in the manner described in section 4.2.7.

TLC was also performed on a sample of pure 5-fluorouracil. A small quantity (5mg) of unlabelled 5-fluorouracil (Sigma) was weighed out and dissolved in 10ml of distilled water. A small volume of this solution (1μl) was then pipetted to the origin, 16mm from the solution level. The TLC procedure was performed in the same manner as described above for the radiolabelled compound. Qualitative analysis was performed by exposing the chromatoplate to a beam of ultra-violet light generated from a lamp (Allen 425 LCF 750Q). A wavelength of 254nm was employed. The region of 5-fluorouracil deposition was indicated by the emission of blue light.

5.2.2 Measurement of the Partition Coefficient of Sucrose

A volume of distilled water (20ml) was added to a beaker containing an excess (200ml) of octan-1-ol (Fisons). The two liquids were vigorously vortexed overnight so as to saturate the water with octanol. Similarily 20ml of octanol was washed with an excess of distilled water (200ml) by vortexing overnight. The following day, a 3μL volume (1092pmol, 0.0222MBq) of [^{14}C]-sucrose was

deposited into a centrifuge tube. Small volumes (2ml) of each of the washed liquids were then dispensed into the centrifuge tube. The tube was covered with parafilm and was then subject to agitation on a shaker for 1 hour. The tube was then transferred to a centrifuge (Starstedt) and spun at 4000 rpm for 10 minutes so as to separate the aqueous and organic layers. Three 0.1ml aliqouts were pipetted out of the octan-1-ol layer and transferred to labelled scintillation vials. Most of the organic layer was then carefully removed by pipette, caution being exercised so as not to agitate the liquid contents. Three 0.1ml aliquots were then removed from the aqueous solution and transferred to labelled scintillation vials. After the addition of scintillation fluid, all the vials were vortexed and counted in the manner described previously. A background count was also performed by measuring the emission from a vial containing pure scintillation fluid.

The activity readings of each of the 6 vials was corrected by subtracting the background count. A mean activity value was calculated for the corrected octan-1-ol readings as well as for the corrected distilled water readings. The octanol / water partition coefficient was determined by dividing the mean activity value of the organic solvent by the mean activity value of the aqueous solvent.

5.2.3 General Technique for Investigating Phonophoresis

Sections of intact whole skin were excised from the backs of male Wistar rats (see 4.2.1). Each skin sample was transferred to a Franz diffusion cell and secured as a barrier between the donor and receptor halves. Details of this procedure are described in 4.2.6. A main difference was that, in these studies, the Franz cells were jacketed at 28°C.

The donor solution consisted of a small volume (100μL) of ethanolic solution containing 5% v/v of the radiolabelled drug. The radiolabelled compounds were: [^{14}C]-sucrose (1819pmol, 0.0370MBq, Amersham); [^{3}H]-5-fluorouracil (333.3pmol, 0.1628MBq, NEN); [^{14}C]-aminopyrine (2313pmol, 0.0093MBq Amersham); [^{3}H]-hydrocortisone (63.36pmol, 0.1850MBq, Amersham); [^{14}C]-salicylic acid (9250pmol, 0.0185MBq, NEN); [^{3}H]-Testosterone (57.81pmol, 0.1850MBq, NEN); and [^{3}H]-oestradiol (63.36pmol, 0.1850MBq, Amersham). The small volumes were prepared and deposited on the skin surface in the manner

described in 4.2.6. In studies involving the application of chemical enhancers, the skin, whilst mounted in the Franz cell, was pretreated with ethanolic solutions of either 1% v/v azone (South Staffordshire Health Authority) or 1% v/v oleic acid (Merck). These chemicals were allowed to soak into the skin over a period of 1 hour and subsequently, the donor solutions were added.

The receptor solution consisted of distilled water for those experiments involving sucrose, 5-fluorouracil, aminopyrine and salicylic acid. For phonophoresis experiments with hydrocortisone, testosterone and oestradiol, the receptor solution consisted of 5% aqueous ethanol. This is to accommodate differences in water-solubility between the two groups of compounds, as can be seen by referring to Table 5.1. In either case, the solutions were degassed by heating to 30°C and then sonicating in an ultrasound bath (Kerry, Pulsatron 125) for 3 minutes.

These diffusion experiments were initiated in the manner described in 4.2.7. After 1 hour, the ethanol had largely evaporated from the skin surface and the Franz cell was inverted to remove any bubbles from the skin underside. The donor compartment was then filled with ultrasonic coupling gel (Henleys Medical). Care was taken to minimise the production of air bubbles within the gel. The skin was subjected to either: control conditions in which the donor compartment was merely sealed with parafilm; ultrasound-exposure; or heat-alone. In all cases, permeation was allowed to proceed for a further 4 hours. Throughout the 5-hour period, 1.1ml aliquots of receptor solution were withdrawn at 30 minute intervals and replaced with an equal volume of receptor medium. Each experiment consisted of at least three replicate runs.

In the ultrasound-exposure experiments, a small transducer of the ultrasound generator (Therasonic 1032, model no.50, EMS Greenham Ltd) was positioned inside the donor cell, facing downwards so that its radiating surface was 2cm distant from the skin surface. A specially designed teflon collar which slotted over the top rim of the donor cell, fixed the transducer in position, perpendicular to the skin surface. Unless otherwise stated, a 1.1MHz beam was employed at an intensity of 2.25W cm^{-2}. However, in some permeation experiments, other ultrasonic fields were also investigated. These included 3.3MHz beams, applied across a successive range of intensities (0, 0.75, 1, 1.5 and 2.25W cm^{-2}) and at 1:2 pulsed mode (SATA intensity 0.75W cm^{-2}). In all cases, ultrasound transmission between the transducer and skin sample was mediated by the coupling gel which

filled most of the donor compartment. A schematic illustration of the equipment is presented in Figure 5.3.

Figure 5.3: Schematic Illustration of the Apparatus used to investigate Phonophoresis

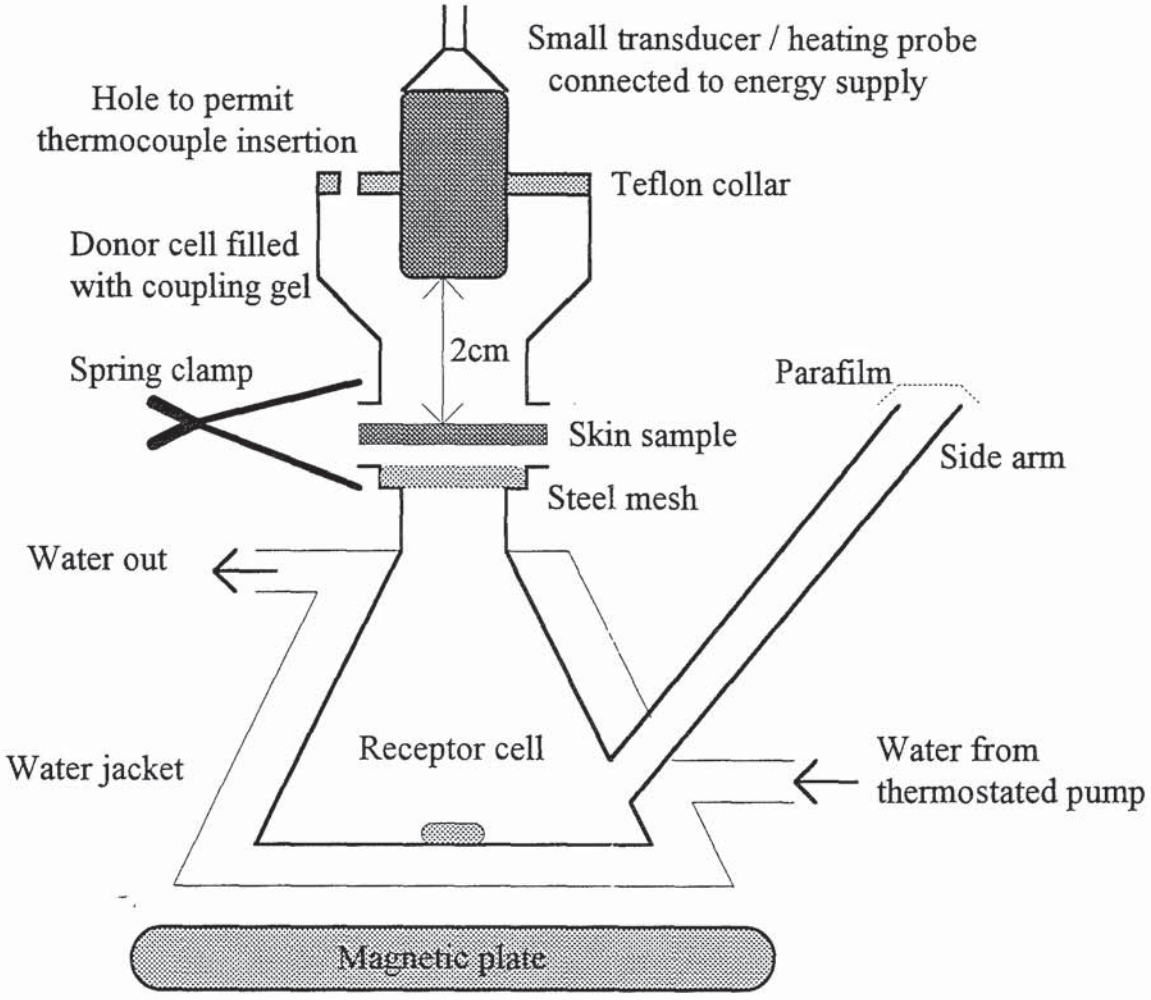

The ultrasound generator was not designed to be continuously operating for 4 hour periods. Therefore, the machine was switched off for 10 minute intervals following each 50 minute period of sonication. An in-built feature of the generator was that the transducer face must be free of coupling gel when the ultrasound is

being switched on. This permits the transducer to re-calibrate itself. Therefore, at the end of each 10 minute rest interlude, the transducer was removed from the Franz cell, wiped clean of residues of coupling gel, recalibrated, re-inserted into the Franz cell, and switched on. The sonication experiments were always performed using the same individual diffusion cell so that the beam acoustics within the apparatus remained as reproducible as possible. This issue has been discussed in greater detail in section 2.3.3. Since only one transducer was available and the sonication period was 4 hours, this meant that a maximum of only two experimental runs could be performed in one day. This was a major limitation of these methods.

The heat-alone application was mediated by a heating probe that was electrically connected to a variable ac supply module (Variac). The probe, which was 1.6cm in diameter, was fixed by a teflon collar, through the central axis of an individual donor cell. The probe was thus aligned normal to the skin sample and its front surface was a distance of 2cm from the skin surface. By adjusting the module control dial to a specific applied voltage, it was possible to warm the skin surface to a certain temperature. In another variant of the heat-alone application, the probe was placed directly on the skin surface with no intervening coupling gel present.

The analytical procedure and algebraic manipulations necessary to obtain the lag time, flux and permeability coefficient values have been described in section 4.2.7. Since sonication was initiated 1 hour into the lag phase period, enhancement was generally assessed by comparing permeability coefficient values. Comparative values of D/h were also derived by dividing the permeability coefficient by the octanol / water partition coefficient of the permeant assuming that this is proportional to its skin/vehicle partition coefficient.

5.2.4 Temperature Measurement Techniques

Experiments were initiated to determine the skin surface temperature profile associated with each specific ultrasound / heat alone regimen. To this end, a hole was drilled through each teflon collar, so as to permit the insertion of a thermocouple probe (Digitron instruments, 3202 type K) right through the donor

cell, so as to make contact with the skin surface. Consequently, it was possible to record the temperature at points on the skin surface, approximately midway between the centre and edge of the skin sample. The repeated insertion of the thermocouple probe through the donor cell could potentially compromise the skin barrier, create air bubbles in the coupling gel or possibly remove drug from the skin surface. Consequently, the temperature profile associated with each ultrasound / heat-alone regimen was determined from separate sets of experiments in which the skin samples were drug-free. In each experiment, successive temperature measurements were made at 30 minute intervals throughout the 5-hour period. In the ultrasound-exposure experiments, the beam was momentarily switched off during the actual measurement as otherwise, the thermocouple wire would itself heat up as it attenuated the energy.

5.2.5 Procedure for Measuring Testosterone Permeation through Silicone Membranes

The donor solution was prepared by weighing out 0.05g of testosterone powder (sigma) into a beaker and then dispensing 25ml of 5% aqueous ethanol. Since testosterone is susceptible to photodegradation, the beaker was covered with aluminium foil. A magnetic stirring bar was placed in the beaker which was placed on a magnetic plate. The suspension was agitated for 5 hours after which, the suspension was poured into centrifuge tubes. All of these were transferred to a centrifuge (Starstedt) and spun at 5000rpm for 15 minutes. The supernatant from each tube was then pippetted out into a beaker. This solution was filtered (Whatman no.1 filter paper) so as to produce a saturated solution, free of precipitate. Aliquots of the saturated testosterone solution were mixed with small volumes of tritiated testosterone (NEN, 3.2TBq/mmol) in volume ratios 2000:1 (unlabelled : tritiated). Since each donor cell was filled with 5ml of solution, in practice, 15ml of unlabelled testosterone solution was mixed with 7.5µl of tritiated testosterone to make sufficient solution for 3 experimental runs. The unlabelled and tritiated testosterone solutions were mixed in a beaker by magnetic agitation for 10 minutes.

The receptor solution was prepared by making up a 5% aqueous ethanol solution within a large conical flask. This solution was degassed by heating to 30°C and then sonicating in an ultrasound bath (Kerry, pulsatron 125) for 3 minutes.

Membrane barriers were prepared by cutting out circular sections of silicone sheeting (40 durometer matt). The surface area of each section was just larger than the cross sectional area at the franz cell junction. The silicone sheeting was available in thicknesses of 0.005' and 0.020' and sections from both of these sheets were used. Barrier membranes of 0.010', 0.025', and 0.040' were also produced by combining two silicone sections together. Several drops of propylene glycol (sigma) were pipetted on to the lower membrane surface while the upper section was pressed down firmly so as to displace away most of any trapped air. The 0.005' section was positioned on top of the 0.020'.

An array of Franz diffusion cells was employed with the receptor cells jacketted at 28°C. Steel meshes were employed to support the silicone sections as otherwise the membranes stretched under the weight of the column of donor solution. Traces of white soft paraffin B.P. (Pearce Laboratories) were used to adhere the membranes into position at the receptor-donor junction. Before the addition of the donor solution, the diffusion cells were repeatedly inverted in order to remove any air bubbles from the underside of the membranes. The donor cell was then filled with testosterone solution and the Franz cells were covered in aluminium foil so as to prevent photodegradation. Diffusion was allowed to proceed for as long as necessary so that steady-state flux could develop. This depended upon the thickness of the membrane under study. Aliquots of 1.1ml were sampled at 30 minute or 60 minute intervals and quantitatively analysed for testosterone by using radiochemical scintillation counting (see section 4.2).

For each of the 5 membrane barriers, testosterone penetration per unit area was plotted as a function of time. Linear regression analysis was then conducted for the steady-state segments of all 5 lines. The data were combined to produce a graph of steady state flux per unit area as a function of the reciprocal of membrane thickness.

5.2.6 Histological Analysis of Skin Samples

Following exposure to either control, azone-only, or azone plus ultrasound treatment, skin samples were histologically analysed. Each of the treatments was performed in triplicate such that 9 sections of skin were utilised all together. For the azone-only and azone plus ultrasound treatments, the whole skin sections were mounted in modified Franz cells and 100μL of 1% v/v azone was pipetted on to each skin surface. After 1 hour, 100μL of ethanol was deposited and after a further hour, each donor cell was filled with coupling gel. Each skin sample was then left for 4 hours either without ultrasound (for the azone-only treatment) or exposed to a 1.1MHz beam at 2.25W cm^{-2} (for the azone plus ultrasound treatment). In both cases, the skin sections were finally removed from the diffusion cells and residues of coupling gel were wiped off with lens tissue. Control samples of whole rat skin were obtained by direct excision from freshly sacrificed animals.

In all cases, three 1mm wide, 20 mm long strips were then cut out, with a sharp scalpel, from the centrally irradiated area of each skin section. These skin strips were fixed by overnight immersion in 4% neutrally buffered formalin. The wax-embedding technique was then used to prepare 5μm-thick skin sections. Following haematoxylin and eosin staining, the sections were photographed. These procedures have been reviewed in greater detail in 4.2.8.1.

5.2.7 Procedures for Recovering 5-Fluorouracil from the Skin and Gel

It was necessary to initially determine whether the contact time between rat skin and the 5-fluorouracil formulation is a factor which affects the radiochemical scintillation measurements. A longer contact time could potentially cause the radiolabelled species to diffuse deeper into the tissue. The resultant greater attenuation of the β radiation would result in a smaller number of counts being recorded. The calibration method involved placing 9 sections of whole rat skin, epidermis uppermost, on plastic supports. A small volume (100μl) of ethanolic solution containing 5%v/v 5-fluorouracil was deposited on to each skin sample. The skin sections were left undisturbed for a specific time period (15, 60 or 240 minutes) with each time-span experiment conducted in triplicate. The skin samples

were then transferred, using a pair of tweezers, to labelled scintillation vials and 10ml of scintillation fluid (Optiphase Hisafe 3) was dispensed into each vial. The vials were shaken and the emitted activities were counted in the manner described in 4.2.7.

In the recovery studies, percutaneous absorption experiments were initiated with 5-fluorouracil as the test permeant. Three experiments were conducted, each representing the three types of exposure *i.e.* heat alone (to 35°C), ultrasound (1.1MHz, 2.25W cm^{-2}) and control. Each experiment was performed in triplicate. There was no need for samples to be taken during the course of diffusion. After 4 hours, the Franz cells were carefully dissassembled and each skin sample was transferred to a labelled scintillation vial. In addition, much of the coupling gel was scraped out of each donor cell and these contents were also transferred to a separate set of scintillation vials. After the addition of scintillation fluid, all the vials were vortexed and their emitted radioactivities were counted (see 4.2.7).

5.3 RESULTS AND DISCUSSION

5.3.1 Temperature Profile Determinations

As discussed in section 2.3.3, the underlying steel mesh partially reflects the ultrasound so the skin sample is subjected to a complex and unpredictable acoustic field. This means that attenuation of the ultrasound within the skin results in a complex and variable heating profile. Temperature measurements at a point on the skin surface only give an indication of the total heat deposition throughout the tissue. Obviously, a more exact method of total heat determination would in itself interfere with drug transport and the apparatus acoustics. Interestingly, other research teams have recorded temperatures at the underside of skin samples in their *in vitro* phonophoresis experiments (Brucks *et al.*, 1989). However, measurements at the skin surface are more likely to be pharmaceutically relevant as diffusion through the stratum corneum is generally the rate determining step during percutaneous absorption.

In this section, the ultrasonic parameters; frequency, intensity, duration, and mode were sequentially examined in terms of their effect on skin surface temperatures. In further work, the thermal effects of each of 3 distinct heat-alone applications were characterised.

5.3.1.1 The Effect of Frequency

Figure 5.4 presents the temperature-time profiles associated with control conditions, 2.25W cm^{-2} ultrasound at 1.1MHz, and 2.25W cm^{-2} ultrasound at 3.3MHz. It can be seen that under control conditions, the skin surface temperature was initially just above room temperature. However, at 60 minutes there was a marked increase in temperature which reached a plateau at 90 minutes. This effect is due to the deposition of coupling gel which insulates the skin from the cooler air above and thus allows heat from the receptor compartment (jacketted at 28°C) to be more efficiently retained within the skin.

Figure 5.4: Skin Surface Temperature Profile during Sonication
- The Effect of Frequency

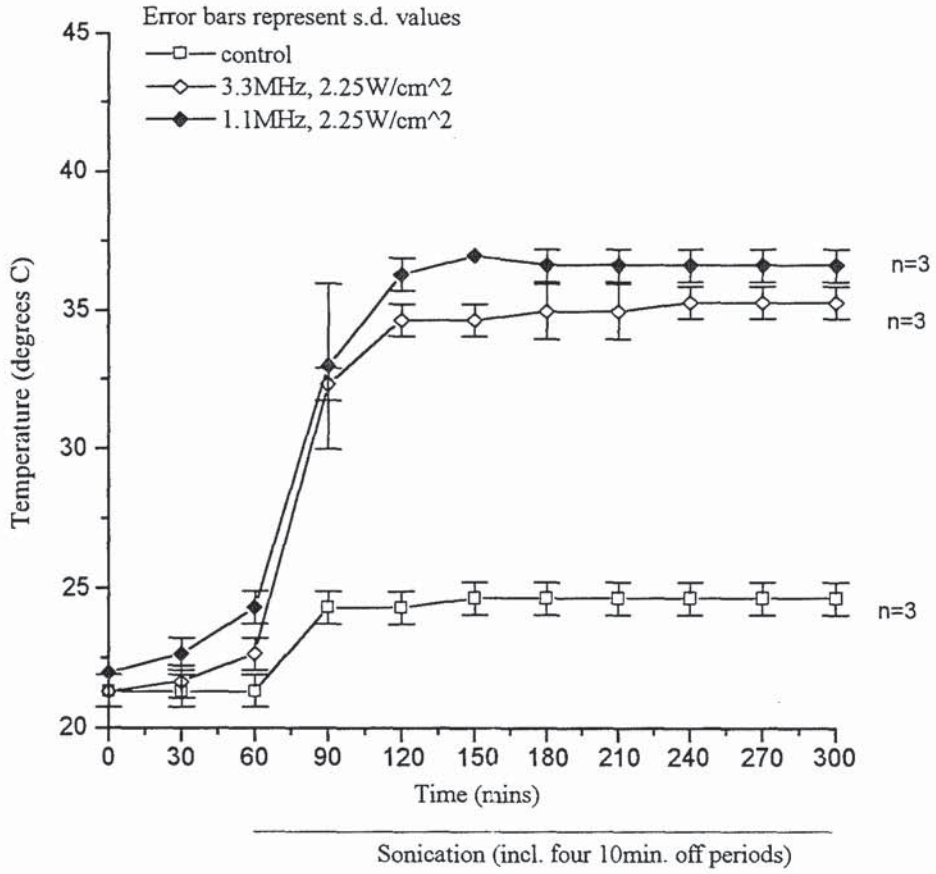

It can be seen that the application of the 1.1MHz beam at 60 minutes caused the skin temperature to rise, rapidly at first and then progressively less so. By 120 minutes, an equilibrium skin surface temperature of 37°C was attained and this temperature was maintained throughout the remaining period of the experiment. During this phase, the energy output of the transducer was equal to the energy lost from the apparatus via conduction.

It can be seen that the temperature-time profile of the 3.3MHz beam was similar to the profile of the 1.1MHz beam. However, a slightly lower equilibrium temperature of approximately 35°C was attained at the higher frequency. The main reason for this is that the 3.3MHz beam exhibits a smaller cross-sectional area and therefore conveys a lower total power output. This issue has been discussed in greater detail in section 2.2.4.

It can be seen from Figure 5.4 that switching off the ultrasound for 10 minute interludes did not produce noticeable deviations in the thermal profiles. This can be explained in terms of the relatively high specific heat capacity exhibited by the coupling gel. Crucially, sonication at both frequencies did not produce temperature increases that should cause irreversible damage to the skin structure. Some workers have suggested 45°C as a cut-off point with temperatures in excess of this value being potentially destructive to skin (Bronaugh *et al.*, 1982). Even taking into account ultrasound-induced deep heating, it is unlikely that such temperatures are being generated within the skin membranes in this model.

5.3.1.2 The Effect of Intensity

Figure 5.5 shows the temperature versus time data for various intensities of 3.3MHz ultrasound.

Figure 5.5: Skin Surface Temperature Profile During Sonication - The Effect of Intensity

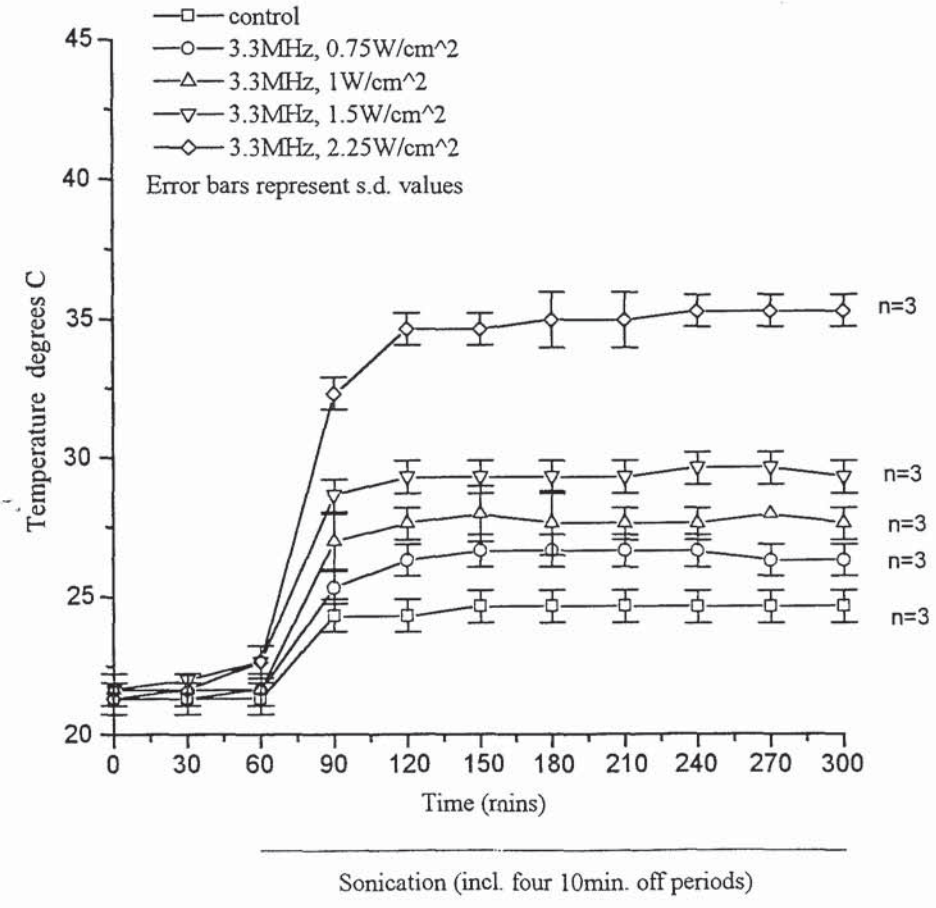

The general profile of these graphs is similar to that described above. When the beam is switched on, surface temperatures begin to increase but the rate progressively decreases until a plateau phase is reached at 120 minutes. From Figure 5.5, it is clear that the equilibrium temperature attained is dependent upon the intensity setting.

5.3.1.3 The Effect of Duration and Mode

The skin samples in the diffusion cells were exposed to three different regimens of 3.3MHz ultrasound, each of which conveyed the same total energy. The three regimens were a 0.75W cm^{-2} beam delivered for 4 hours, a 2.25W cm^{-2} beam delivered in 1:2 (on:off) pulsed mode for 4 hours and a 2.25W cm^{-2} beam delivered for 1.33 hours. The thermal profile of each of these beams is presented in Figure 5.6.

Figure 5.6: Skin Surface Temperature Profile during Sonication - The Effect of Duration and Mode

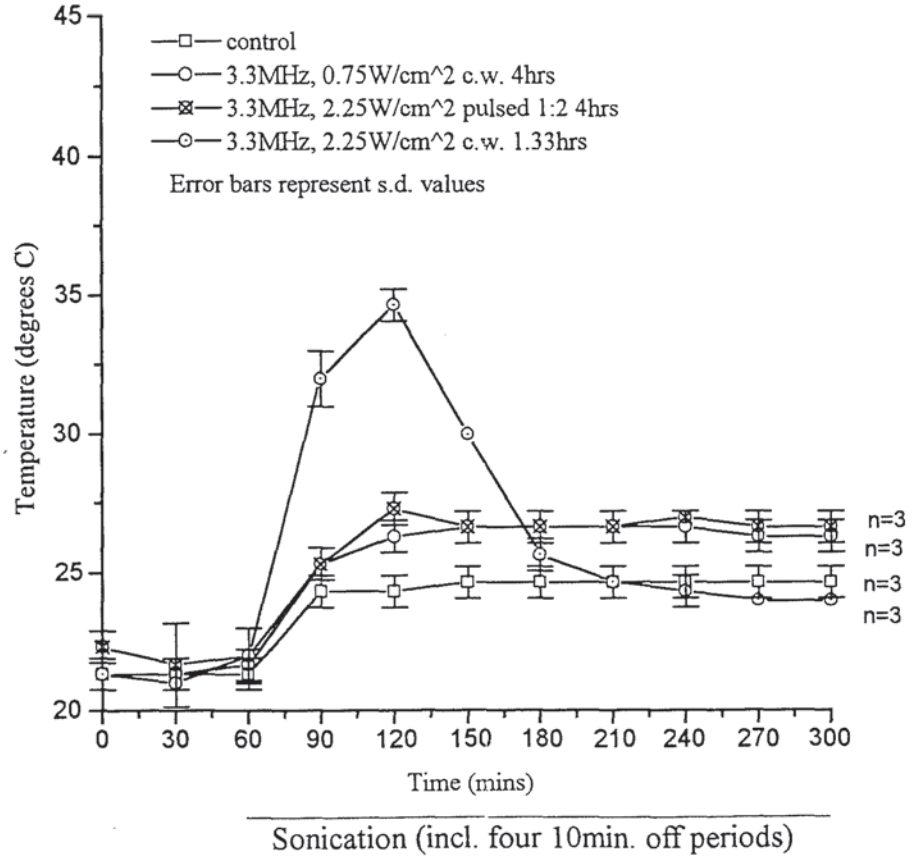

It can be seen that both of the 4-hour applications resulted in similar plateau

temperatures being attained. This is due to the fact that both of these beams conveyed the same power output. The 1.33 hour application induced much greater temperature increase initially but the skin temperature then decreased, reaching control levels from 210 minutes onwards.

5.3.1.4 The Effect of Heat Alone

It was determined from pilot studies that by adjusting the pd at the ac supply module to 12V, it was possible to simulate the surface temperature-profile generated by a 2.25W cm^{-2} beam at 3.3MHz. By employing a 25V supply, it was possible to create a profile that formed a plateau at 45°C.

Figure 5.7: Skin Surface Temperature Profile during the Heat-Alone Treatments

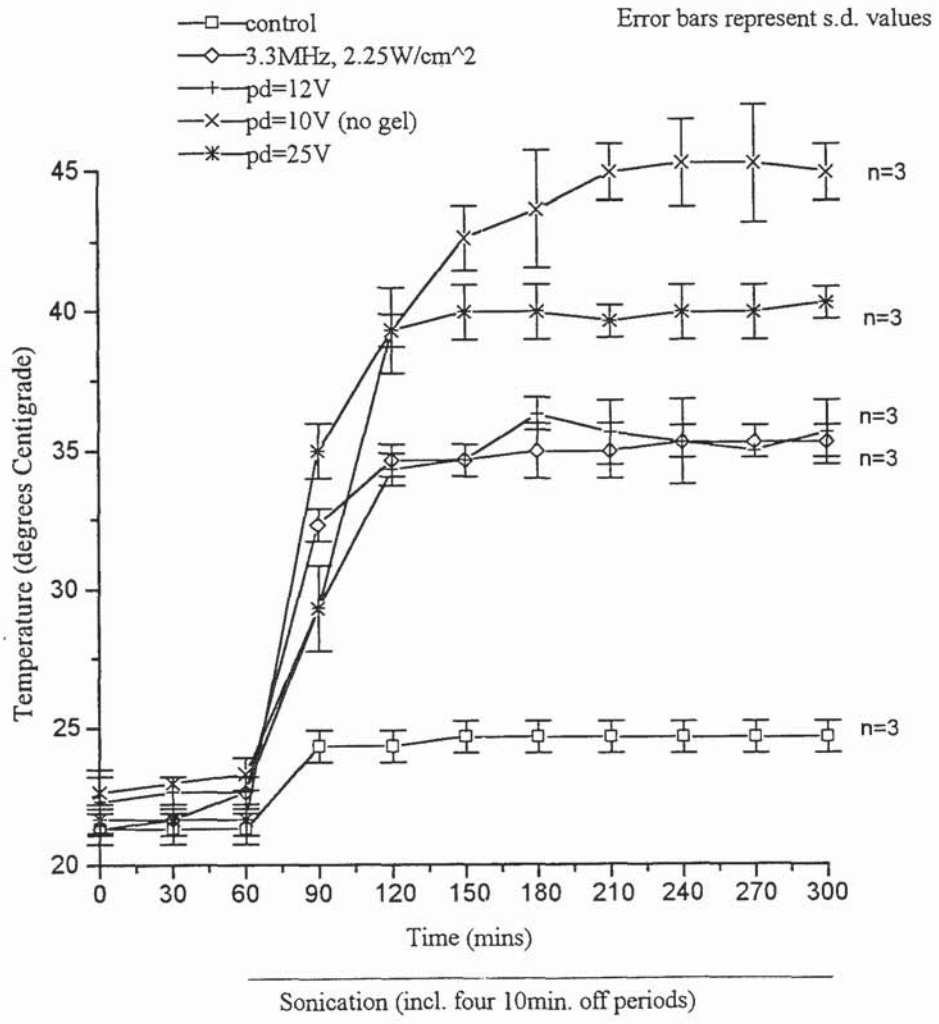

An applied pd of 10V was used to generate heat alone in the absence of coupling

gel. This modality resulted in an equilibrium temperature of 40°C being attained. All these temperature-time profiles are presented in Figure 5.7. It must be noted that while sonication causes heating throughout the depth of tissue, the heat-alone applications are mediating a more surface-confined effect.

5.3.2 Attempted Phonophoresis of Hydrophilic Compounds

5.3.2.1 Permeation of Sucrose

It was found from TLC analysis of the sucrose samples that 89.4% of the emitted activity was localised between 56 to 72mm from the origin. Furthermore, 71.2% of the radioactivity on the chromatoplate was concentrated between 56 to 64mm from the origin. The whole length of the chromatoplate was 88mm. A similar distribution of activity was found in a second run of this experiment. These results indicate that the available sample of [^{14}C]-sucrose was not degraded and could be used for the permeation experiments.

Experiments were performed in order to assess the separate effect of ultrasound and azone on the percutaneous absorption of sucrose. The permeation profiles of sucrose through control, ultrasound-exposed and azone pretreated skin are presented in Figure 5.8. The flux, permeability coefficients and lag times derived from the linear portions of these resulting rate curves are summarised in Table 5.2.

Table 5.2: Data relating to the Attempted Phonophoresis of Sucrose

Treatment	Flux (pmol cm^{-2} h^{-1})	K_p (μm h^{-1})	Lag Time (hours)
control	0.8751 ± 0.5447	0.4810 ± 0.0610	1.15 ± 0.51
us	0.6328 ± 0.2936	0.3478 ± 0.0329	0.99 ± 0.39
azone	0.4715 ± 0.3302	0.2592 ± 0.0370	0.57 ± 0.62

Values represent the mean ± sem derived from linear regression analysis between 90 and 300 minutes.

Figure 5.8: The Effect of 1.1MHz Ultrasound and Azone on Sucrose Penetration

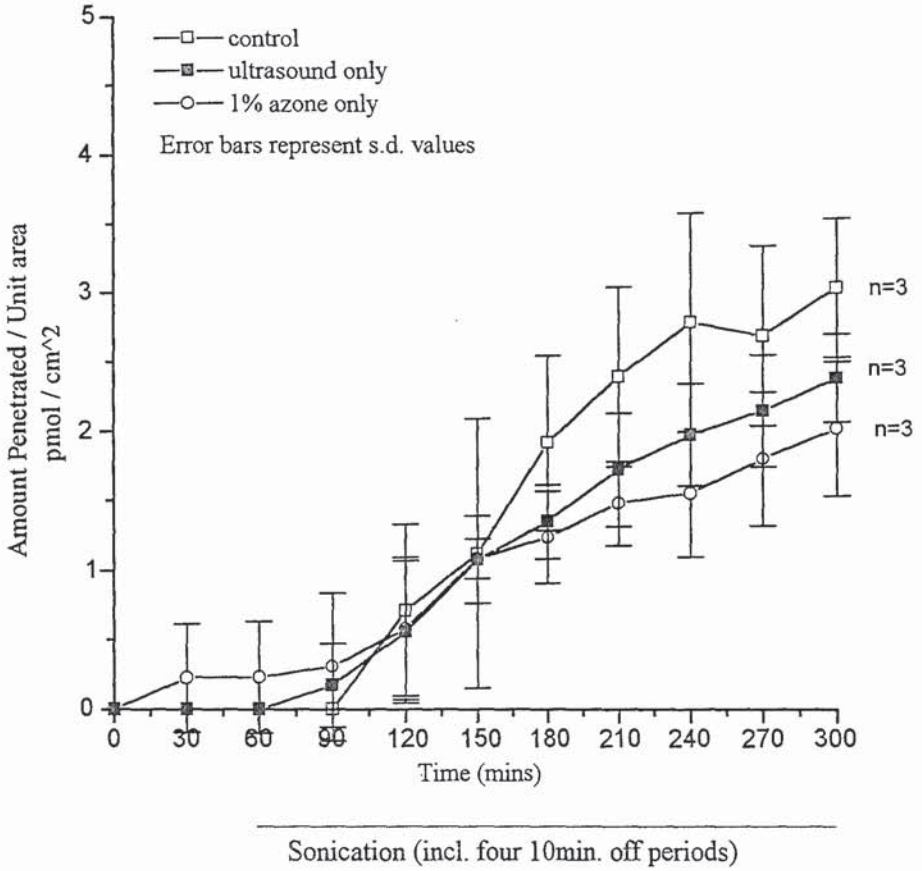

The absorption of sucrose, under control conditions, can be described in terms of 2 distinct stages. There is an initial mean lag time of just over 1 hour. This is followed by a mean linear flux of 0.88 pmol cm^{-2} h^{-1}. This represents a mean permeability coefficient of 0.48μm h^{-1}. As discussed in section 4.3.3.1, this flux is mediated by penetration through the transfollicular route.

Contrary to the general expectation, ultrasound application resulted in sucrose flux decreasing to a mean value of 0.63 pmol cm^{-2} h^{-1} which represents a mean permeability coefficient of 0.35μm h^{-1}. The observed reduction in barrier permeability was probably caused by the ultrasound discharging sebum into the pilosebaceous channels. This suppresses the transport of highly hydrophilic molecules like sucrose through the hair follicle shafts. This phenomenon has been discussed in section 4.3.3.1. However, compared to the control treatment,

sonication did not significantly reduce sucrose permeation (P = 0.1025, student's t-test). It must be noted that the method involved the ultrasound being switched off during the first hour of the experiment. Sucrose permeation could occur through the hair follicle shafts during this initial hour. This explains why penetration was insignificantly reduced when the experimental period was examined as a whole.

Azone pretreatment resulted in sucrose flux decreasing to a mean value of 0.47pmol cm^{-2} h^{-1} which represents a mean permeability coefficient of 0.26μm h^{-1}. This is only 54% of the flux observed under control conditions (P = 0.037, student's t-test). Azone is a viscous liquid and it would be expected to readily deposit within the hair follicle shafts. Since it is an extremely lipophilic agent ($LogP_{octanol/water}$ = 6.21), its accumulation within the pilosebaceous shafts results in the approximate halving of sucrose permeation. Although azone permeabilises the stratum corneum by fluidising the intercellular lipids, sucrose is far too hydrophilic to partition into even such modified stratum corneum. Indeed, the fact that azone treatment reduces sucrose flux is further evidence that sucrose penetration is mediated by the pilosebaceous channels.

5.3.2.2 Permeation of 5-Fluorouracil

Initially, TLC analysis was performed in order to assess the purity of the available samples of [^{3}H]-5-fluorouracil. Radioactivity measurements showed that 98.7% of the emitted activity of the chromatoplate was located between 40 to 56mm from the origin. The total length of the chromatoplate was 64mm. Similar distributions of activity were found in a repeat run of the experiment. A reference sample of pure 5-fluorouracil was determined to be also concentrated in this region of the chromatoplate. These results indicate that the available samples of [^{3}H]-5-fluorouracil had not degraded.

A series of permeation studies were conducted in order to evaluate the effects of ultrasound, heat alone, azone and oleic acid on the percutaneous absorption of 5-fluorouracil. Table 5.3 presents the flux values, permeability coefficients and lag times derived from linear regression analysis of all the resulting rate curves. Table 5.4 presents relevant statistical comparisons between the permeability coefficients of these treatments. Figure 5.9 illustrates the permeation profiles of the treatments; control, ultrasound only, azone only, and azone with ultrasound.

Table 5.3: Data Relating to the Attempted Phonophoresis of 5-Fluorouracil

Treatment	Flux (pmol cm^{-2} h^{-1})	K_p (μm h^{-1})	Lag Time (hours)
control	0.4226 ± 0.1106	1.2679 ± 0.3316	1.42 ± 0.92
us	0.1927 ± 0.0408	0.5780 ± 0.1223	0.26 ± 0.91
azone	1.8382 ± 0.2189	5.5146 ± 0.6564	1.37 ± 0.42
azone + us	0.2452 ± 0.1532	0.7356 ± 0.4596	-2.24 ± 3.08
azone + heat	0.4918 ± 0.1904	1.4770 ± 0.5711	-0.42 ± 1.87
azone + heat[d]	0.2217 ± 0.0768	0.6652 ± 0.2305	0.36 ± 1.47
oleic acid	0.3053 ± 0.7917	0.9160 ± 0.5183	-1.50 ± 0.93
oleic acid + us	0.2404 ± 0.2694	0.7213 ± 0.1728	-0.48 ± 1.19

Values represent the mean ± sem derived from linear regression analysis between 120 and 300 minutes. [d] denotes the absence of coupling gel.

Table 5.4: The Effects of Ultrasound, Azone and Oleic acid on the Permeability Coefficient of 5-Fluorouracil

Comparison Treatment $_1$: Treatment $_2$	Enhancement [K_{p1} / K_{p2}]	t-test K_{p1} v K_{p2}
us : control	0.46	P = 0.058
azone : control	4.35	P < 0.001
oleic acid : control	0.72	P = 0.551
azone + us : azone	0.13	P < 0.001
azone + heat alone : azone	0.27	P < 0.001
azone + heat alone[d] : azone	0.12	P < 0.001
oleic acid + us : oleic acid	0.79	P = 0.725

Figure 5.9: The Effects of 1.1MHz Ultrasound and Azone on 5-Fluorouracil Penetration

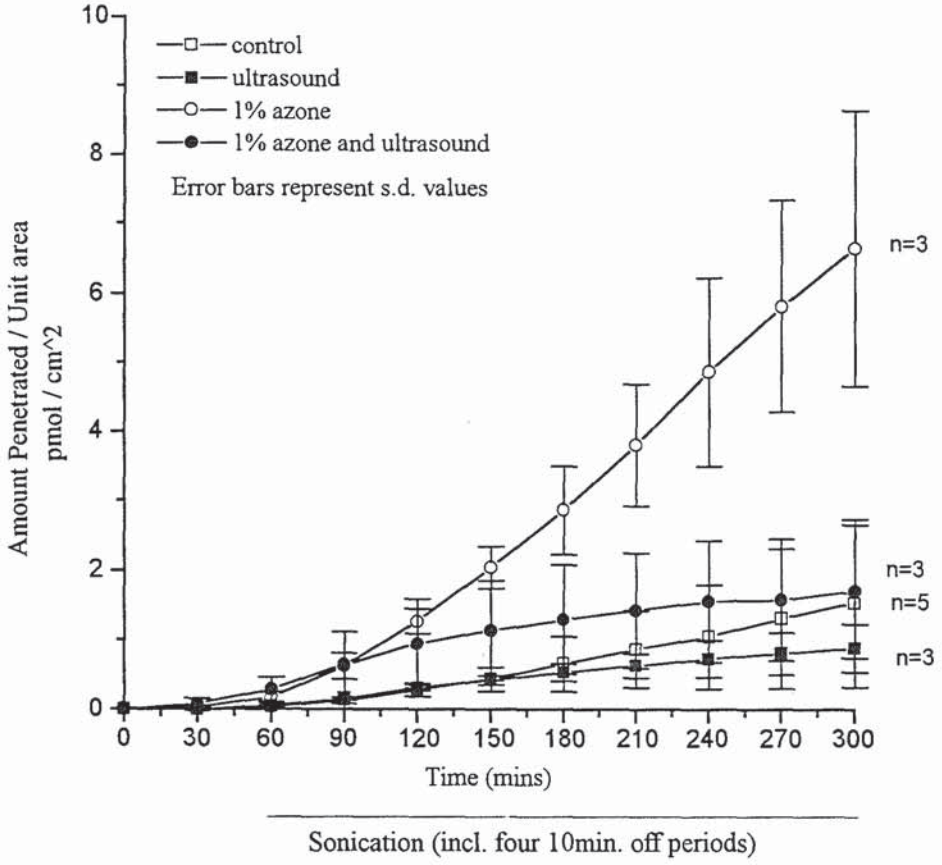

Under control conditions, 5-fluorouracil absorption can be described in terms of 2 distinct phases. There is an initial mean lag time of almost 90 minutes. This is followed by a mean steady state flux of 1.42 pmol cm^{-2} h^{-1} which is equivalent to a mean permeability coefficient of 0.27μm h^{-1}. As was determined in section 4.3.2.4, 5-fluorouracil penetration through rat skin is mediated by diffusion through the bulk stratum corneum.

As can be seen from Figure 5.9, sonication from 60 minutes onwards, produced a change in the permeation profile of 5-fluorouracil. The rate curve now exhibited 3 separate phases. Following the lag time, there followed a linear phase which was of a very similar magnitude to that observed in the control treatment. However, from 120 minutes onwards, the penetration rate slightly decreased with time. Since 333pmol of 5-fluorouracil were initially deposited on the skin surface, this

effect cannot be due to drug depletion on the donor side. Furthermore, since 5-fluorouracil permeation occurs mostly through the bulk stratum corneum (refer to section 4.3.2.4), the release of sebum into the pilosebaceous shafts is unlikely to be producing the phenomenon. One possibility is that ultrasound is accelerating drug diffusion from the skin surface, into the overlying volume of aqueous gel. The relatively large volume of available gel ($\approx 6cm^3$) and hydrophilicity of 5-fluorouracil ($Log\ P_{octanol/water} = -0.95$) would tend to facilitate such a process. Consequently, the concentration of 5-fluorouracil at the skin surface progressively declines during the period of ultrasound exposure. This results in the diminution of the thermodynamic driving force necessary for percutaneous absorption.

Following the application of azone, 5-fluorouracil penetration was characterised by a mean lag time of over 1 hour. This was followed by a linear flux of mean value 1.84pmol cm^{-2} h^{-1} which is equivalent to an average permeability coefficient of 5.51μm h^{-1}. This indicates that azone pretreatment enhances 5-fluorouracil penetration by over 4-fold. This effect is mediated by the azone molecules inserting themselves within the intercellular lipids of the stratum corneum, thus fluidising them. These perturbations are particularily effective at promoting the permeation of hydrophilic agents such as 5-fluorouracil (Sugibayashi *et al.*, 1985).

The combination of azone pretreatment and ultrasound irradiation produced a compex 5-fluorouracil absorption curve. Following the lag phase, there was a short period of steady state flux which was comparable to the flux observed in the azone alone experiments. However, from 90 minutes onwards, the permeation rate began to progressively decrease with time. By 240 minutes, the flux had become negligible. This curve-flattening effect is caused by the loss of permeant from the skin surface. Interestingly, the rate curve of the combination treatment is approximately parallel to the rate curve of the ultrasound-only treatment. This suggests that, in both cases, the same ultrasonic mechanism is accelerating 5-fluorouracil diffusion, from the skin surface into the coupling gel.

In order to determine whether ultrasonic heating was promoting the reverse diffusion effect, the effect of azone with heat-alone (to 35°C) on 5-fluorouracil permeation was investigated. It can be seen from Figure 5.10 that under these conditions, a plateau effect also developed. A decrease in flux was first observed at 150 minutes and by 270 minutes, permeation was negligible. It can be

concluded that the thermal effects of ultrasound are producing the back-diffusion effect.

Figure 5.10: The Effects of Azone and Heat-Alone on 5-Fluorouracil Penetration

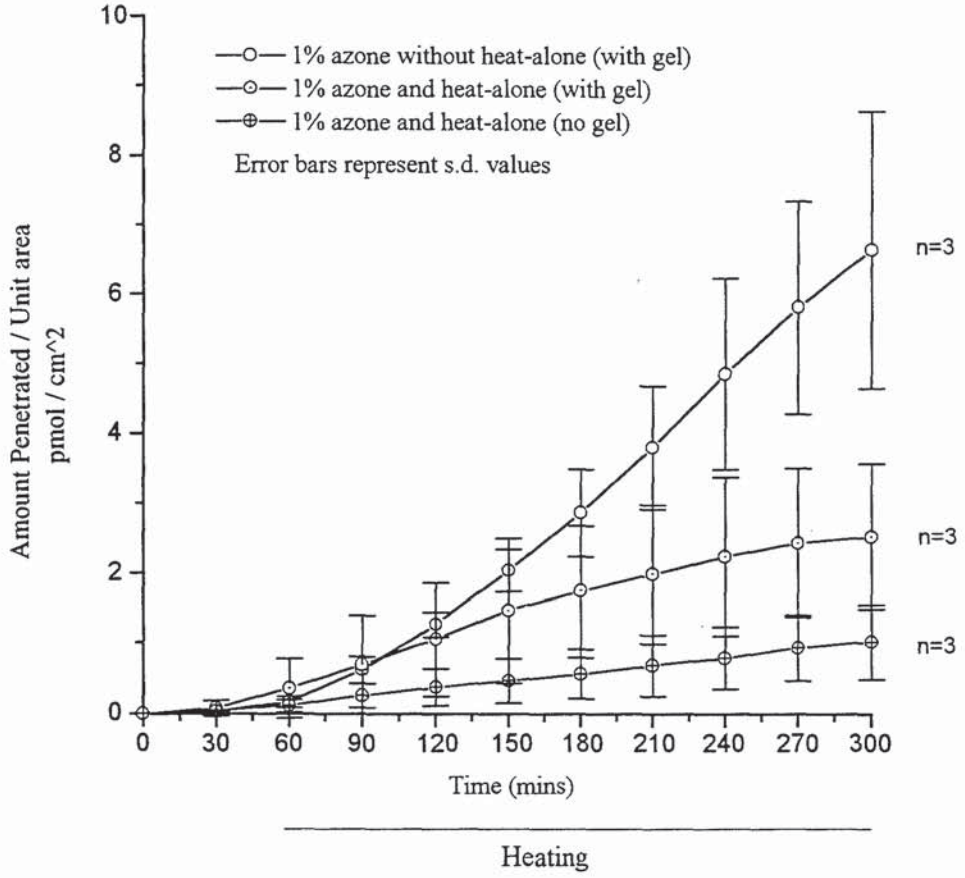

In a sequential experiment, azone-pretreated skin was exposed to heat alone in the absence of coupling gel. From Figure 5.10, it can be seen that following a short lag phase, 5-fluorouracil flux remained at a steady state throughout the experiment. Since the drug could not diffuse into an overlying gel layer, sink conditions were maintained for percutaneous absorption. Interestingly, the permeability coefficient in this experiment was lower than in any of the other azone-exposed experiments. A possible explanation of this effect is that the coupling gel, which is approximately 90% water, is a powerful hydrating agent and will in itself act as an absorption enhancer. No such enhancement occurs in the absence of coupling gel.

Permeant recovery experiments were set up in order to determine the distribution of 5-fluorouracil between the skin and gel layer. Initially, the analytical technique was calibrated in order to ascertain whether the time of contact between rat skin and 5-fluorouracil solution is a factor which affects the number of counts emitted from the sample vials. As can be seen from Table 5.5, the contact time between the drug formulation and skin did not affect the measured activity values.

Table 5.5: 5-Fluorouracil Radioactivity Counts in Skin as a Function of Formulation-Skin Contact Time

Absorption Time (minutes)	DPM ($\times 10^3$)
15	846.074 ± 195.278
60	724.311 ± 44.542
240	721.770 ± 166.338

Values represent the mean ± sd of three replicates.

Following calibration, permeation experiments were conducted in which the skin samples were subjected to either control conditions, ultrasound exposure, or heat-alone exposure. At the end of the 5-hour period, the skin sections and coupling gel volumes were isolated and their radioactivities measured.

Figure 5.11 presents the radioactivities detected from recovered volumes of coupling gel following their exposure to each of the three treatments. It can be seen that the heated gel exhibited the highest activity, the sonicated gel exhibited an intermediate level of radioactivity while the control gel exhibited the least activity. The ultrasound-exposure methodology involves the loss of small quantities of gel at the end of each hour, when the transducer is wiped clean and re-calibrated. No such loss of gel occurs in the heat-alone experiments. This probably explains the slightly lower activity in the sonicated gel in comparison to the heated gel.

Figure 5.12 presents the recovered activities of skin samples, following their exposure to each of the three treatments. It can be seen that the sonicated and heated sections contained significantly less radioactive drug than control skin. Both these experiments show that heating within the donor cell, whether generated

Figure 5.11: Radioactivity of the Recovered Coupling Gel Following Three Different 5-Fluorouracil Exposure Regimens

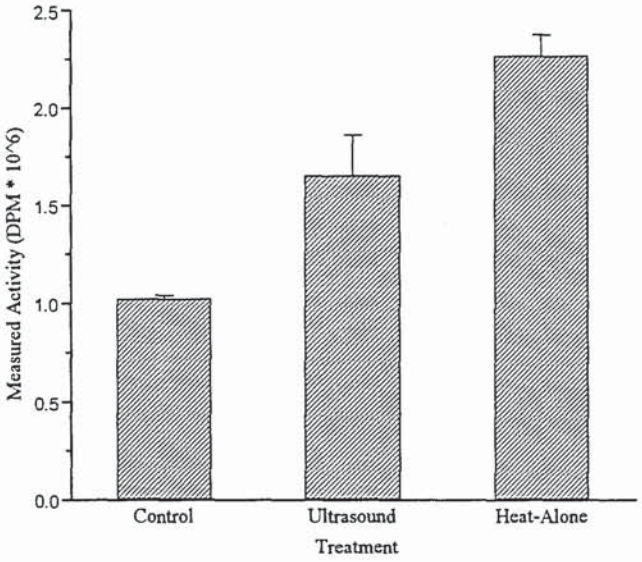

n=3, error bars represent s.d. values

Figure 5.12: Radioactivity of the Recovered Skin Samples Following Three Different 5-Fluorouracil Exposure Regimens

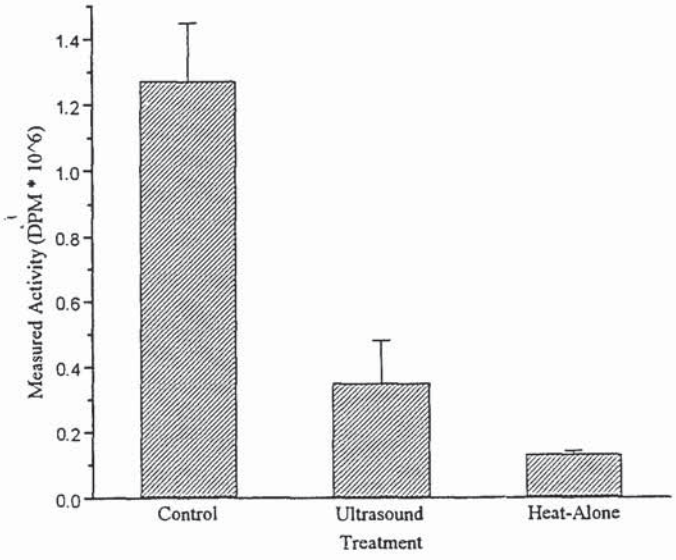

n=3, error bars represent s.d. values

directly or *via* ultrasound attenuation enhances the back-diffusion of 5-fluorouracil into the overlying gel. This back-diffusion process reduces the thermodynamic driving force for permeation and it is manifested in the curve-flattening effects seen in Figure 5.9 and Figure 5.10.

In contrast to azone, the application of oleic acid did not significantly promote 5-flurouracil flux through rat skin (refer back to Table 5.3). This means that the phase separation induced by oleic acid is not as effective as the increased lipid fluidity induced by azone in mediating enhanced 5-fluorouracil permeation.

5.3.2.3 Permeation of Aminopyrine

Several experiments were performed in order to assess the effect of concurrent ultrasound application and / or azone pretreatment on the percutaneous absorption of aminopyrine. The permeation profiles, representing control, ultrasound, azone pretreatment, and azone pretreatment followed by ultrasound are illustrated in Figure 5.13. Table 5.6 presents the flux values, permeability coefficients and lag times derived from linear regression analysis of the resulting profiles. Table 5.7 lists relevant statistical comparisons between the permeability coefficients.

Table 5.6: Data Relating to the Attempted Phonophoresis of Aminopyrine

Treatment	Flux (pmol cm^{-2} h^{-1})	K_p (μm h^{-1})	Lag Time (hours)
control	8.9012± 1.0865	3.8492 ± 0.4698	1.20 ± 0.49
us	7.2937 ± 1.5706	3.1540 ± 0.6792	1.00 ± 0.89
azone	14.6512± 0.7317	6.3357 ± 0.3164	1.39 ± 0.20
azone + us	9.3135± 0.7004	4.0275 ± 0.3029	0.79 ± 0.32

Values represent the mean ± sem deived from linear regression analysis between 90 and 300 minutes.

It appears that without ultrasound or enhancers, aminopyrine exhibits a biphasic permeation profile. The mean lag period lasts for just over 1 hour. Subsequently, there is a linear flux of mean value 8.90 pmol cm^{-2} h^{-1}. This translates to a mean permeability coefficient of 3.85μm h^{-1}. As discussed in section 4.3.2.5, this permeation is mediated by diffusion through the bulk stratum corneum.

Table 5.7: The Effect of Ultrasound and Azone on the Permeability Coefficient of Aminopyrine

Comparison	Enhancement Ratio $[K_{p1}/K_{p2}]$	t-test K_{p1} v K_{p2}
us : control	0.82	P = 0.842
azone : control	1.65	P < 0.001
azone + us : azone	0.64	P < 0.001

Figure 5.13: The Effects of 1.1MHz Ultrasound and Azone on Aminopyrine Penetration

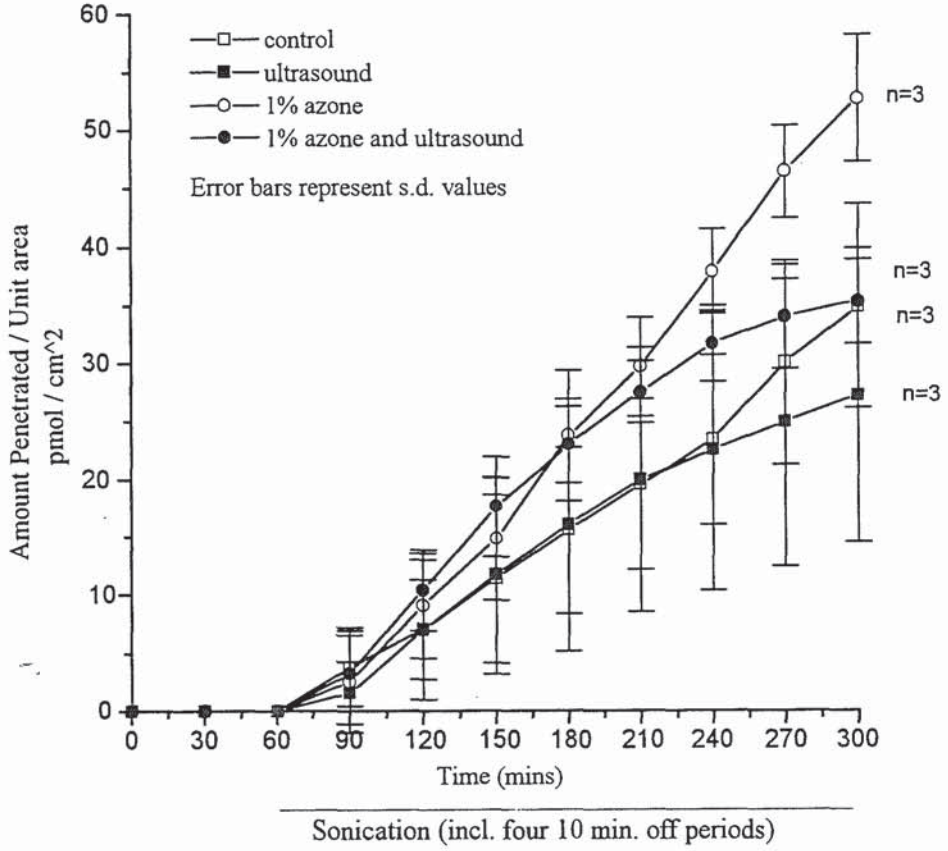

When the skin membranes were sonicated, the resulting aminopyrine absorption curve exhibited 3 distinct segments. The first segment was a lag time of a mean value of 1 hour. The second segment was associated with steady-state behaviour

in which the penetration rate closely matched the rate observed during the control treatment. However, from 210 minutes onwards, the penetration rate began to gradually decrease with time. This effect cannot be due to drug depletion in the donor compartment since approximately 2.24nmol of aminopyrine should still be available at the skin surface at this time-point. Furthermore, since aminopyrine permeation is mostly mediated *via* the bulk stratum corneum (refer to section 4.3.2.5), the release of sebum into the pilosebaceous shafts is unlikely to be causing the plateau effect. Just as ultrasonic heating accelerated the diffusion of 5-fluorouracil from the skin surface into the overlying gel (see section 5.3.2.2), it is likely that the same process occurred with aminopyrine.

The pre-application of azone produced a new penetration curve. It was observed that there was an initial lag period which averaged 1 hour in duration. This was followed by a steady-state flux of mean value 14.65pmol cm^{-2} h^{-1} which is equivalent to a mean permeability coefficient of 6.34μm h^{-1}. It can be seen from Table 5.7 that azone pretreatment significantly enhanced aminopyrine permeation through rat skin. This is due to the factors already described in 5.3.2.2.

The combination of azone application and ultrasound irradiation resulted in a complex pattern of aminopyrine penetration. There was a lag phase which lasted less than 1 hour. The subsequent steady-phase period was associated with a flux which was comparable to the flux observed in the azone-alone treatment. However, from 210 minutes onwards, the permeation rate started to progressively decrease with time. Again, this feature was probably mediated by the progressive loss of permeant from the skin surface into the overlying gel.

5.3.2.4 Ultrasound Effects on the Permeation of Hydrophilic Compounds

Figure 5.14 displays the permeation data for the three hydrophilic compounds. The graph is presented in the form of a log-log plot of diffusivity per barrier thickness as a function of the octanol / water partition coefficient. Log-log plots have been used before to illustrate this type of absorption data (Yano *et al.*, 1986). Each normalised diffusivity value was obtained by dividing the measured permeability coefficient by the octanol / water partition coefficient assuming that this is proportional to skin / vehicle partition coefficient. The units of this parameter are μm h^{-1}.

Figure 5.14: Diffusivity of the Hydrophilic Permeants

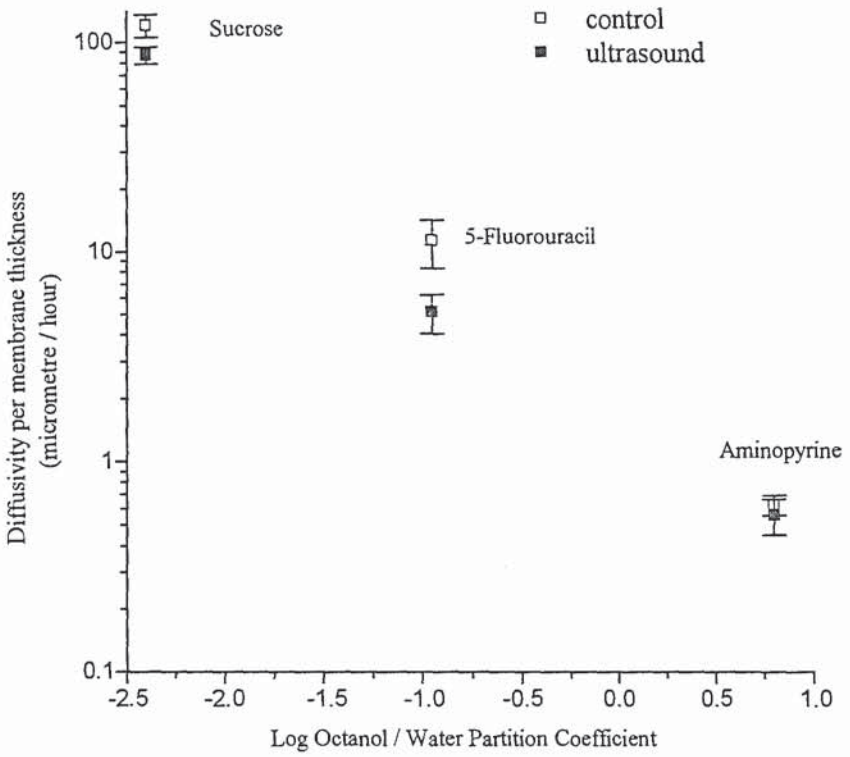

error bars represent s.e.m. values

It can be seen that sucrose exhibited the greatest diffusivity per membrane thickness. This is because sucrose flux is mediated *via* the pilosebaceous shunt route, thus allowing the molecule to bypass the horny layer. In contrast, 5-fluorouracil and aminopyrine exhibited lower values of diffusivity per membrane thickness as these agents penetrate through the bulk stratum corneum (refer to section 4.3.2). 5-Fluorouracil exhibited a higher normalised diffusivity than aminopyrine. This could be due to differences in the mechanisms of penetration through the stratum corneum*i.e.* transcellular versus intercellular.

Sonication reduced the diffusivity per membrane thickness of all three permeants. However, the effects were not statistically significant. For 5-fluorouracil, the phenomenon was due to ultrasonic heating accelerating drug diffusion from the skin surface into the overlying coupling gel. It is very likely that the same process occurred in the aminopyrine experiments and possibly in the sucrose experiments. The coupling gel is composed of a macromolecular network containing aqueous regions through which small hydrophilic agents can readily diffuse through. As discussed in section 3.3.4, heating accelerates solute diffusion through such a system. Sonication of rat skin also discharges sebum into the hair follicle shafts

and this phenomenon suppresses the percutaneous absorption of sucrose. No evidence could be found of any synergistic effects between ultrasound and azone or oleic acid.

Hydrophilic permeants such as aminopyrine and 5-fluorouracil are potentially good candidates for phonophoresis as they normally permeate slowly through the stratum corneum. As can be seen by referring back to Table 1.2, many workers have reported promising ultrasound-enhancement effects for hydrophilic drugs in similar *in vitro* systems. These include mannitol (Kost *et al.*, 1986), digoxin (Pinton *et al.*,1991), and caffeine (Machluf and Kost, 1993), However, in this model, ultrasonic heating caused aminopyrine and 5-fluorouracil to preferentially diffuse into the coupling gel, thus reducing their concentration at the skin surface. This phenomenon has not been documented in the literature reports as in most models, the permeant is homogenously dispersed within the bulk of the donor vehicle. However, the model documented in this chapter is probably closer to phonophoresis in its clinical use. Interestingly, one recent *in vivo* study has employed a protocol in which drug deposition was followed by the application of coupling gel (Hofmann and Moll, 1993).

5.3.3 Attempted Phonophoresis of Hydrophobic Compounds

5.3.3.1 Permeation of Hydrocortisone

A series of permeation studies were conducted in order to evaluate the effects of ultrasound, heat alone, azone and oleic acid on the percutaneous absorption of hydrocortisone. Table 5.8 displays the flux values, permeability coefficients and lag times derived from linear regression analysis of the resulting rate curves. The permeation profiles of the treatments; control, 1.1MHz ultrasound only, oleic acid only, oleic acid with 1.1MHz ultrasound; are shown in Figure 5.15.

Under control conditions, hydrocortisone penetration is characterised by an initial mean lag time of just over 2 hours. At steady-state, there is a mean linear flux of 0.007pmol cm^{-2} h^{-1} which can be converted to a mean permeability coefficient of 0.12μm h^{-1}. As discussed in section 4.3.3.3, hydrocortisone permeates through

both the bulk stratum corneum and the pilosebaceous pathway with the shunt route contributing to nearly half of total drug permeation.

Table 5.8: Data Relating to the Attempted Phonophoresis of Hydrocortisone

Treatment	Flux (pmol cm $^{-2}$ h $^{-1}$)	K_p (μm h $^{-1}$)	Lag Time (hours)
control	0.0073 ± 0.0105	0.1161 ± 0.1661	2.27 ± 0.83
1.1MHz	0.0133 ± 0.0016	0.2116 ± 0.0257	2.37 ± 0.33
3.3MHz	0.0160 ± 0.0052	0.2543 ± 0.0824	2.19 ± 0.89
oleic acid	0.0494 ± 0.0092	0.7859 ± 0.1349	1.79 ± 0.56
oleic acid + 1.1MHz	0.0583 ± 0.0029	0.9283 ± 0.0467	1.60 ± 0.16
azone	0.0407 ± 0.0054	0.6478 ± 0.0858	2.01 ± 0.38
azone + 1.1MHz	0.1021 ± 0.0125	1.6254 ± 0.1981	1.89 ± 0.36
azone + 3.3MHz	0.0953 ± 0.0172	1.5170 ± 0.2737	2.08 ± 0.51
azone + 35°C	0.0710 ± 0.0032	1.1295 ± 0.0513	2.12 ± 0.13
azone + 45°C	0.1237 ± 0.0165	1.9682 ± 0.2622	2.19 ± 0.37

Values represent the mean ± sem derived from linear regression analysis between 150 and 300 minutes.

From Figure 5.15, it can be seen that sonication from 60 minutes onwards resulted in an increase in hydrocortisone flux. Although the increase was significant at the 90% confidence level, it was not significant at the 95% confidence level (P=0.052). Since ultrasound releases sebaceous lipids from rat skin and this process retards hydrocortisone flux (section 4.3.3.3), it is likely that this process counteracted a significant phonophoretic effect.

After the application of oleic acid, hydrocortisone penetration was essentially biphasic. At first there was a lag phase with a mean duration of just under 2 hours. This was followed by a steady-state flux of mean value 0.05pmol cm^{-2} h^{-1} which represents a mean permeability coefficient of 0.79μm h^{-1}. These data indicate that the pre-application of oleic acid enhances hydrocortisone permeation approximately 7-fold.

Figure 5.15: The Effects of 1.1MHz Ultrasound and Oleic acid on Hydrocortisone Penetration

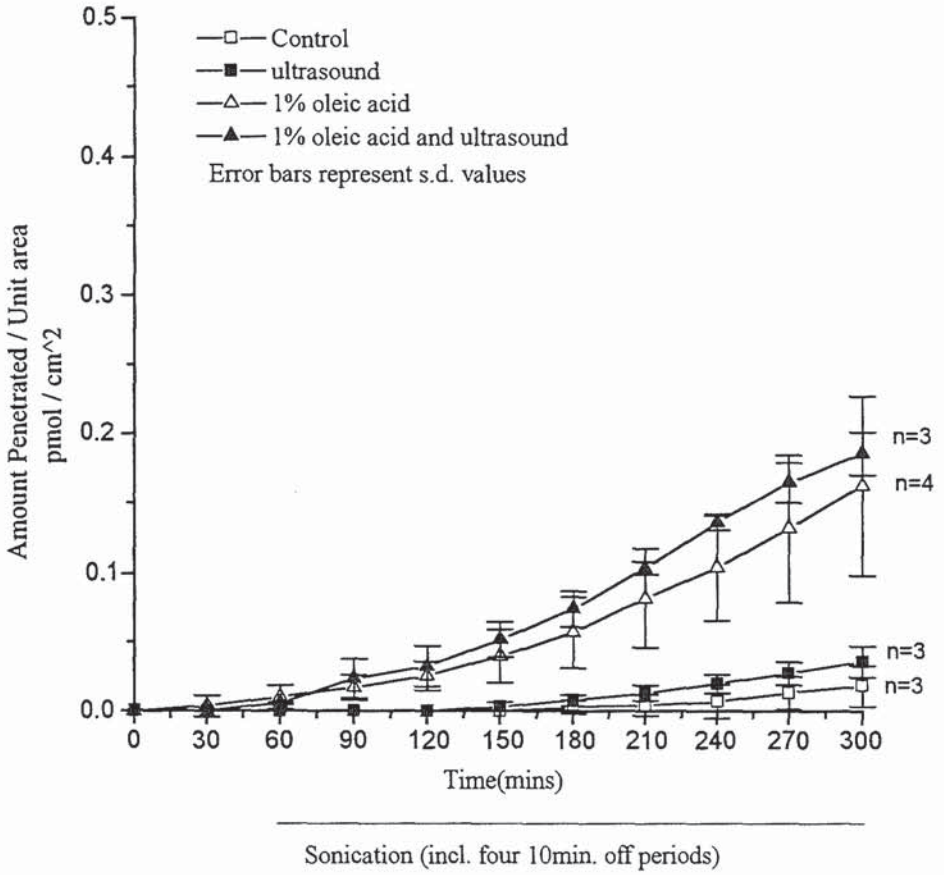

Figure 5.15 illustrates the rate curves representing oleic acid pretreatment as well as sonication following oleic acid pretreatment. In the absence of ultrasound, the mean permeability coefficient was 0.79μm h^{-1} whilst ultrasound exposure was associated with a mean permeability coefficient of 0.93μm h^{-1}. However, these values are not significantly different (P=0.324, t-test). Thus, there is no evidence of synergism between ultrasound and oleic acid.

The permeation profiles of the treatments; control, 1.1MHz ultrasound only, azone only, and azone with 1.1MHz ultrasound; are shown in Figure 5.16. It can be seen that azone pretreatment enhanced hydrocortisone permeability by almost 6 times.

Figure 5.16: The Effects of 1.1MHz Ultrasound and Azone on Hydrocortisone Penetration

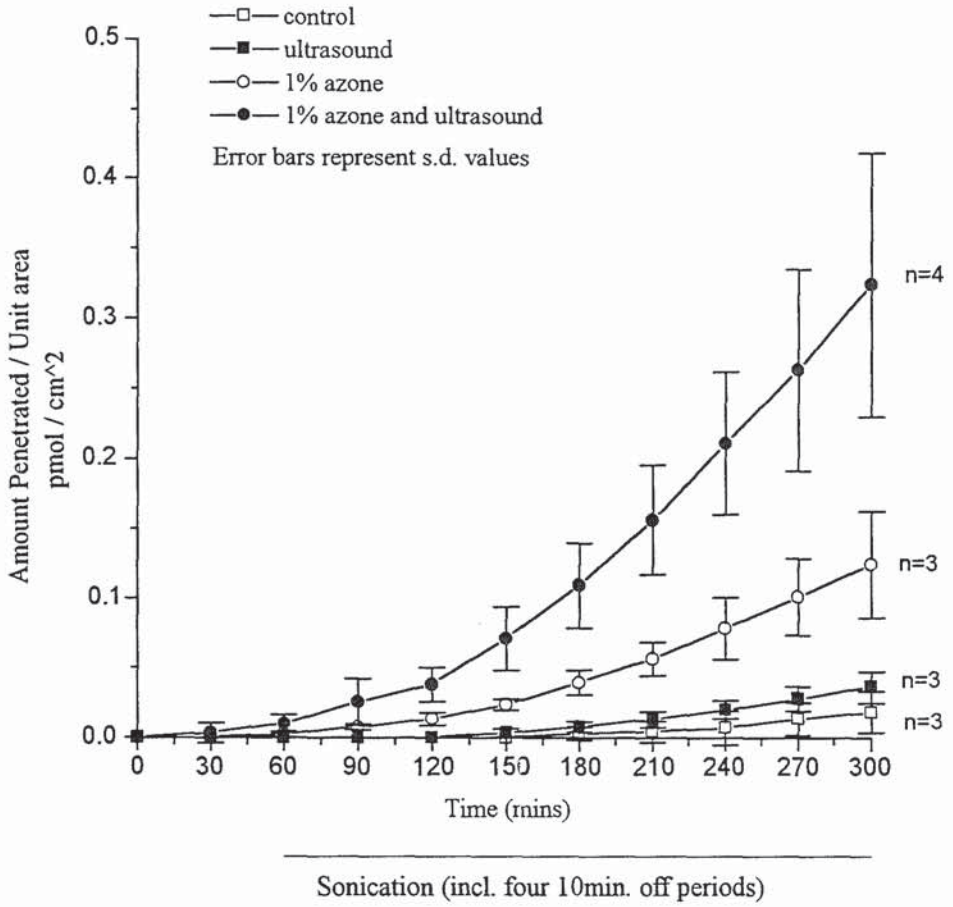

Crucially, sonication of azone-pretreated skin enhanced hydrocortisone permeation by 2.5-fold, compared to azone pretreatment alone. This represents a significant synergistic phenomenon. Figure 5.17 illustrates the effect of azone followed by heat-alone on the hydrocortisone permeation. It can be seen that heating to a surface temperature of 35°C increased the steady-state rate and that more intense heating to 45°C enhanced permeation further. This suggests that ultrasound - azone synergism is mediated mainly by ultrasonic heating, which accelerates azone penetration through the horny layer. Consequently, azone penetrates to a greater depth within the layer, thus permeabilising it to hydrocortisone diffusion.

It was necessary to verify that this synergistic effect was not associated with any detrimental changes to the skin barrier. To this end, a series of histological studies were undertaken in which the skin samples were subjected to control conditions,

azone-only treatment and azone treatment followed by sonication. Examination of the resultant photomicrographs indicated that following all treatments, the stratum corneum and other cutaneous structures remained intact and unaltered. These photomicrographs were similar to those shown in Figure 4.4.

Figure 5.17: The Effects of Heat-Alone and Azone on Hydrocortisone Penetration

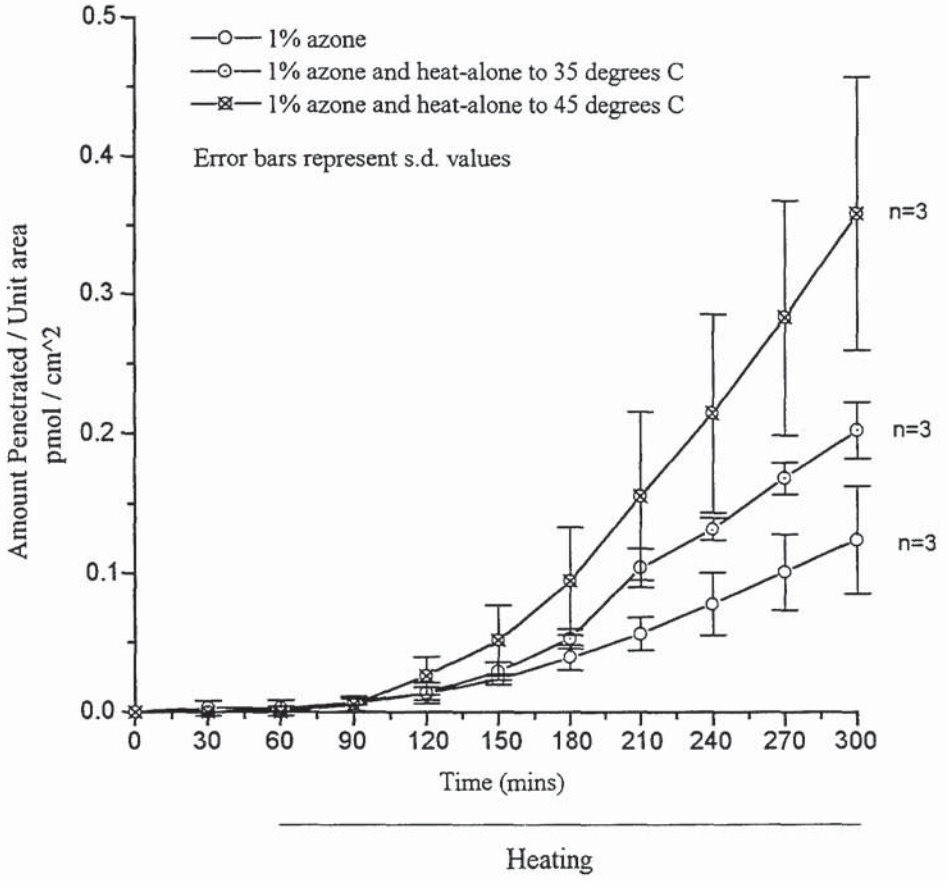

The permeation profiles for the treatments; control, 3.3MHz ultrasound only, azone only, and azone with 3.3MHz ultrasound; are shown in Figure 5.18. Again, ultrasound exposure resulted in an insignificant increase in hydrocortisone flux while the co-administration of azone and ultrasound resulted in a significant synergistic effect. These findings indicate that in this model, small variations in beam frequency do not affect azone or hydrocortisone permeation. This is probably because the two frequency drives generate comparable amounts of heat within the skin samples as can be seen in Figure 5.4. Statistical comparisons

Figure 5.18: The Effects of 3.3MHz Ultrasound and Azone on Hydrocortisone Penetration

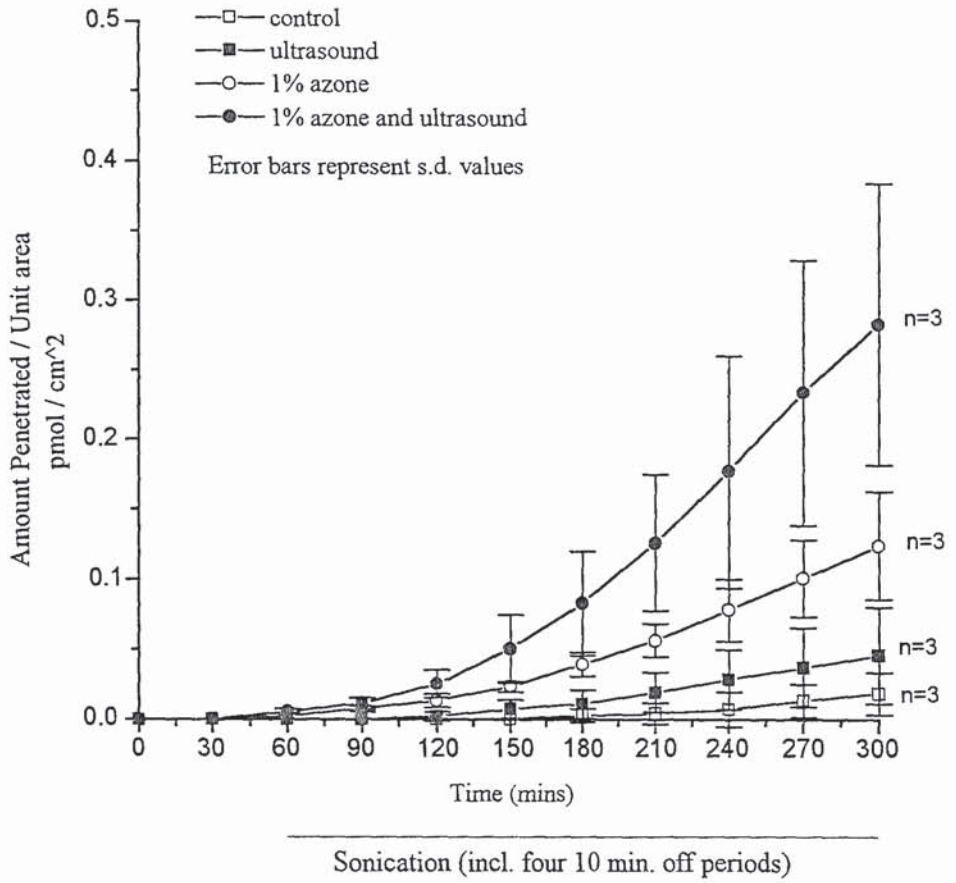

Table 5.9: The Effects of Ultrasound, Heat Alone and Azone on the Permeability Coefficient of Hydrocortisone

Comparison Treatment $_1$: Treatment $_2$	Enhancement $[K_{p1} / K_{p2}]$	t-test K_{p1} v K_{p2}
1.1MHz : control	1.82	P = 0.052
3.3MHz : control	2.19	P = 0.461
azone : control	5.58	P < 0.001
azone + 1.1MHz : azone	2.51	P < 0.001
azone + 3.3MHz : azone	2.34	P = 0.007
azone + 35°C : azone	1.74	P < 0.001
azone + 45°C : azone	3.04	P < 0.001

between the permeability coefficients of each of the azone treatments are presented in Table 5.9.

Several permeation experiments were carried out in order to determine how the intensity parameter (3.3MHz drive) affects hydrocortisone penetration through azone pretreated skin. Figure 5.19 presents a plot of permeability coefficient as a function of intensity.

Figure 5.19: The Effect of Intensity During Hydrocortisone Phonophoresis

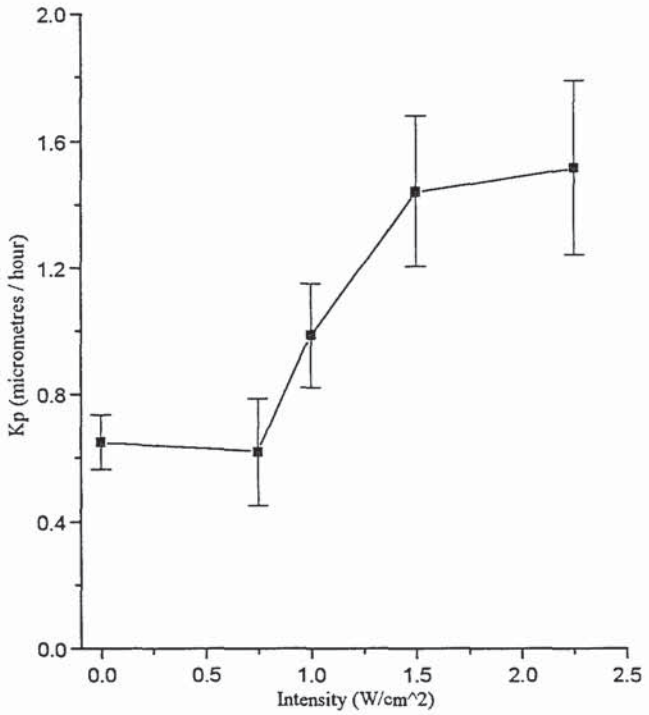

Each point represents the mean ± s.e.m. derived from linear regression analysis of the permeation data between 150 and 300 minutes.

It can be seen that the graph is approximately sigmoidal in profile. Compared to azone alone, sonication at 0.75W cm^{-2} did not increase the permeability coefficient. However, sonication at an intensity of 1W cm^{-2} resulted in the mean permeability coefficient doubling in value. Ultrasound exposure at 1.5W cm^{-2} resulted in the permeability coefficient tripling in value. However, augmenting beam intensity to 2.25W cm^{-2} did not affect a further increase in permeability.

This plateau effect may be due to the fact that at 1.5W cm^{-2}, sufficient heating is generated for azone to diffuse throughout the depth of the horny layer. Since azone does not appreciably permeabilise the other strata of the skin (Sugibayashi *et al.*, 1985), further ultrasonic heating exerts no effect on barrier permeability.

A group of permeation studies were conducted in order to ascertain the effect of duration and mode (at 3.3MHz drive) on hydrocortisone penetration through azone pretreated skin. The relevant parameters are presented in Table 5.10. It can be seen that delivering the same amount of energy in different modes and duration did not markedly affect the resultant flux or permeability coefficient.

Table 5.10: Data Relating to the Effect of Duration and Mode on Hydrocortisone Permeation in Azone Pretreated Skin

Intensity - mode- time	Flux (pmol cm^{-2} h^{-1})	K_p (μm h^{-1})	Lag Time (hours)
0.75W cm^{-2} -cw - 4h	0.0388 ± 0.0105	0.6179 ± 0.1677	2.05 ± 0.77
2.25W cm^{-2} -cw - 4/3h	0.0378 ± 0.0766	0.6010 ± 0.1219	2.04 ± 0.58
2.25W cm^{-2} -p1:2 - 4h	0.0540 ± 0.0124	0.8588 ± 0.1974	2.03 ± 0.65

Values represent the mean ± sem deived from linear regression analysis between 150 and 300 minutes. p denotes pulsed ultrasound in the stated on:off ratio

5.3.3.2 Permeation of Salicylic Acid

A series of permeation studies were performed in order to elucidate the effect of sonication on the percutaneous absorption of salicylic acid. The relevant parameters derived from linear regression analysis of the resulting rate curves are presented in Table 5.11.

Under control conditions, salicylic acid exhibited a mean flux of over 0.005pmol cm^{-2} h^{-1} which is equivalent to a permeability coefficient of over 0.55μm h^{-1}. Salicylic acid exhibits a log octanol-water partition coefficient value of 2.25 which is an optimal value for rapid percutaneous absorption. Ultrasound application did

not significantly affect the permeation rate of salicylic acid (P = 0.390). This suggests that intrinsically rapid permeants are not susceptible to phonophoresis.

Table 5.11: Data Relating to the Attempted Phonophoresis of Salicylic Acid

Treatment	Flux (pmol cm^{-2} h^{-1})	K_p (μm h^{-1})	Lag Time (hours)
control	0.0051 ± 0.0072	0.5555 ± 0.1594	2.25 ± 0.73
us	0.0072 ± 0.0094	0.7759 ± 0.1924	1.36 ± 1.20

Values represent the mean ± sem derived from linear regression analysis between 90 and 300 minutes.

5.3.3.3 Permeation of Testosterone

A group of permeation studies were carried out in order to assess the effects of ultrasound and/or azone on the permeation of testosterone through whole rat skin. The flux values, permeability coefficients and lag times derived from linear regression analysis of the resulting rate curves are presented in Table 5.12. Relevant statistical comparisons between the permeability coefficients of each of the treatments is presented in Table 5.13.

Table 5.12: Data Relating to the Attempted Phonophoresis of Testosterone

Treatment	Flux (pmol cm^{-2} h^{-1})	K_p (μm h^{-1})	Lag Time (hours)
control	0.1227 ± 0.1823	2.1216 ± 0.8141	2.61 ± 0.85
us	0.0714 ± 0.0926	1.2354 ± 0.4137	1.75 ± 0.95
azone	0.1360 ± 0.1727	2.3532 ± 0.7119	2.09 ± 0.84
azone + us	0.0966 ± 0.1140	1.6712 ± 0.5092	2.14 ± 0.78

Values represent the mean ± sem derived from linear regression analysis between 180 and 300 minutes.

It appears that under control conditions, testosterone penetration follows 2 distinct phases. There is an initial mean lag time of just over 2.5 hours. This is followed by a mean linear flux of 0.12 pmol cm^{-2} h^{-1} which is equivalent to a mean permeability coefficient of 2.12μm h^{-1}.

Testosterone exhibits a log octanol / water partition coefficient value of 3.32 and this facilitates the rapid percutaneous absorption of the compound. It can be seen from Table 5.13 that sonication did not significantly affect the percutaneous absorption of testosterone. Again, the data suggest that intrinsically rapid permeants are not susceptible to phonophoretic enhancement.

Azone pre-treatment did not significantly affect testosterone permeation. Azone acts by fluidising the stratum corneum lipids but lipophilic agents, such as testosterone, exhibit rapid diffusivity through the horny layer and are therefore relatively unaffected by such perturbations (Sugibayashi *et al.*, 1985). It can be seen from Table 5.13 that the application of azone with ultrasound did not result in any synergistic effects and this follows from the factors discussed above.

Table 5.13: The Effect of Ultrasound and Azone on the Permeability Coefficient of Testosterone

Comparison	Enhancement Ratio $[K_{p1} / K_{p1}]$	t-test K_{p1} v K_{p2}
us : control	0.58	P = 0.343
azone : control	1.1	P = 0.838
azone + us : azone	0.71	P = 0.442

Testosterone exhibits a log octanol / water partition coefficient of 3.32. Therefore, it is unclear whether the rate limiting step in permeation is mediated by the stratum corneum barrier or by partitioning at the stratum corneum - viable epidermis interface. If testosterone permeation is barrier-limited then a plot of flux per unit area as a function of the reciprocal of stratum corneum thickness should yield a linear relationship *i.e.* $J / A = D. K. C_s / h$ should remain valid across a range of h values. If testosterone absorption is hydrodynamic layer-limited, then such a plot would be non-linear.

Fortunately, the lipoidal properties of the stratum corneum can be mimicked with synthetic silicone membranes. These can be employed individually, or as adhering composites, to produce lipoidal barriers of varying depths. Using this technique, testosterone permeation was studied through silicone membranes, varying in thickness from 0.01285cm to 0.1028cm. In Figure 5.20, steady-state testosterone flux per unit area has been plotted as a function of the reciprocal of membrane thickness. The presence of air bubbles, particularily in the intermembrane spaces of the composite membranes are responsible for the relatively large error bars observed in the data. It can be surmised that there is no evidence that normalised flux is increasing non-linearly with the reciprocal of membrane thickness. Consequently, it can be assumed that testosterone permeation is barrier-limited.

Figure 5.20: Normalised Testosterone Flux through Different Depths of Silicone Membrane

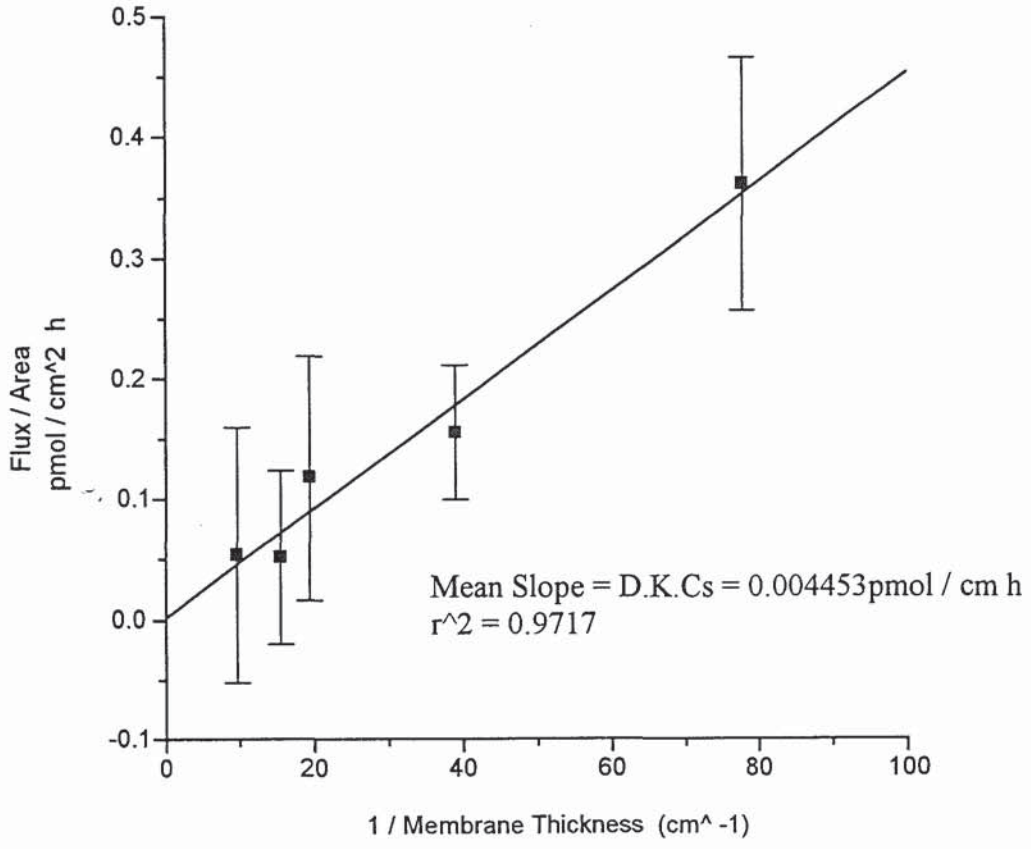

Each point represents the mean ± s.d. derived from linear regression analysis.

5.3.3.4 Permeation of Oestradiol

A series of permeation experiments were undertaken in order to determine the effect of ultrasound on the percutaneous absorption of oestradiol. Table 5.14 lists the flux values, permeability coefficients and lag times derived from linear regression analysis of the resulting rate curves.

Table 5.14: Data Relating to the Attempted Phonophoresis of Oestradiol

Treatment	Flux (pmol cm^{-2} h^{-1})	K_p (μm h^{-1})	Lag Time (hours)
control	0.0066 ± 0.0076	0.1049 ± 0.1208	-2.80 ± 5.85
us	0.0157 ± 0.0066	0.2471 ± 0.1041	-1.13 ± 2.09

Values represent the mean ± sem derived from linear regression analysis between 30 and 180 minutes.

Under control conditions, oestradiol permeation was characterised by a mean flux of over 0.006pmol cm^{-2} h^{-1} which is equivalent to a permeability coefficient of over 0.1μm h^{-1}. Statistical analysis indicated that ultrasound application did not significantly affect absorption (P = 0.273). Oestradiol is highly lipophilic and the rate-limiting step in its permeation must be partitioning from the lipid-rich stratum corneum into the viable epidermis (Yano *et al.*, 1986). Ultrasound does not appear to affect this process. Interestingly, negative lag times were calculated for both the control and sonicated experiments. This feature derived from the fact that oestradiol exhibited a non-classical permeation profile. Initially, there was a short period of very rapid flux before permeation stabilised at the steady-state values documented in Table 5.2. This phenomenon may have been caused by ethanol evaporation in the donor compartment which affects the activity of the permeant.

5.3.3.5 Ultrasound Effects on the Permeation of Hydrophobic Compounds

Figure 5.21 presents a log-log plot of diffusivity per barrier thickness as a function of octanol / water partition coefficient. The centre and right hand side of a parabolic curve can be fitted to this data. Such a pattern is expected because diffusivity through skin is barrier-limited at low partition coefficient values and

hydrodynamic layer-limited at high partition coefficient values. The maximum point of the parabola typically occurs at a $LogP_{(octanol/water)}$ value of 2.5 (Yano *et al.*, 1986). Consequently, it can be seen that hydrocortisone exhibited a normalised diffusivity value that was higher than would be theoretically expected. This occurred because approximately half of hydrocortisone absorption was mediated *via* the transfollicular pathway, as discussed in section 4.3.3.3.

Figure 5.21: Diffusivity of the Hydrophobic Permeants

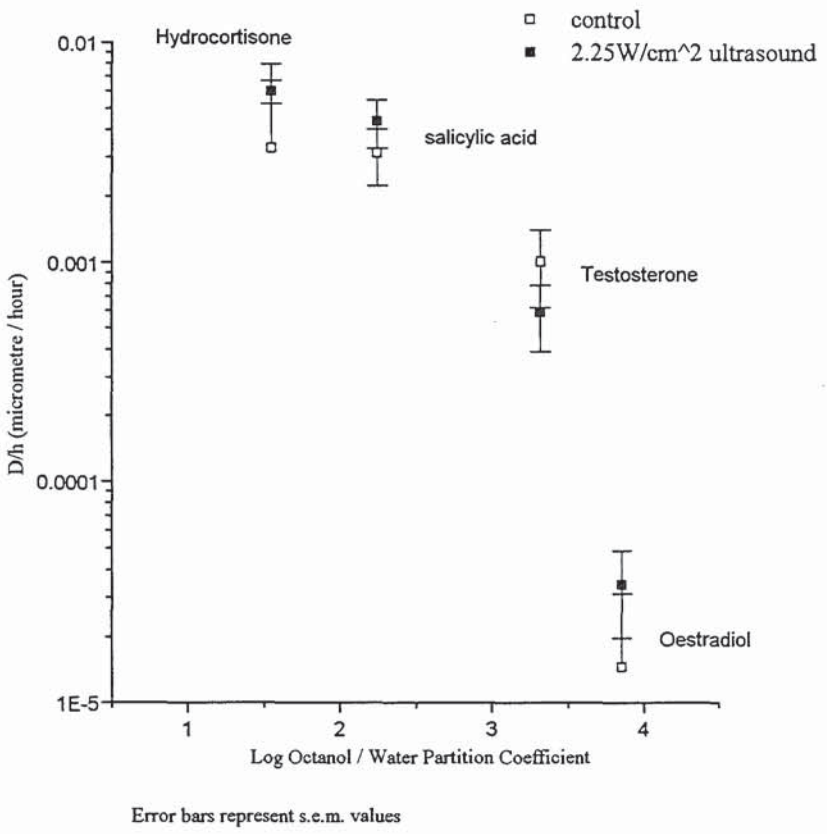

Error bars represent s.e.m. values

Sonication enhanced hydrocortisone permeation although the effect was not statistically significant. The release of sebaceous lipids and / or enhanced back diffusion into the coupling gel may have counteracted any permeabilising effect. Interestingly, significant hydrocortisone phonophoresis has been reported in other *in vitro* models where the drug was homogenously dispersed throughout the donor vehicle (Machluf and Kost, 1993).

A major finding of this chapter was that ultrasound acted synergistically with azone in promoting hydrocortisone permeation. This effect was caused by ultrasonic heating which probably enhanced azone diffusion through the stratum corneum throughout its depth. In contrast, there were no synergistic effects observed between ultrasound and oleic acid.

Ultrasound did not promote the percutaneous absorption of salicylic acid or testosterone. This indicates that rapidly permeating molecules are probably not susceptible to phonophoretic enhancement. Obviously, enhancement is also not desperately sought for such agents.

It has been proposed that acoustic microstreaming at the interface of the horny layer and viable epidermis may perturb the unstirred boundary layer and thus accelerate hydrodynamic layer-controlled diffusion (Murphy and Hadgraft, 1990). In these studies, sonication did not significantly enhance oestradiol absorption. Similar negative effects have been reported in other studies. One group measured the absorption of nicotinate esters in human volunteers (Benson *et al.*, 1991). It was shown that hexyl nicotinate absorption, which is hydrodynamic layer-controlled, was unaffected by ultrasound even though the more hydrophilic, methyl and ethyl esters did undergo phonophoresis under the same conditions. One author has calculated from theory, that at phonophoretic intensities, there is insufficient energy for appreciable microstreaming to develop within the horny layer (Simonin *et al.*, 1995). This explains why ultrasound cannot enhance the permeation of highly lipophilic drugs.

5.4 SUMMARY

Concurrent ultrasound application did not significantly increase the percutaneous absorption of any of the seven permeants studied. Sonication reduced the skin surface concentration of the more hydrophilic molecules by promoting back-diffusion into the coupling gel. Furthermore, the percutaneous absorption of some of these molecules was suppressed by the discharge of sebum. The molecules exhibiting intermediate partition coefficient values did not undergo phonophoresis as they are intrinsically rapid permeants. No evidence could be found to support the hypothesis that ultrasound can enhance the partitioning of lipophilic agents out of the stratum corneum by perturbing the hydrodynamic-layer.

In order to investigate this field further, experiments should be designed in which the reverse-diffusion effect and sebum release phenomenon are removed as artefacts of the permeation system. This can be achieved by dispersing the permeant homogenously throughout the volume of the donor vehicle and utilising skin samples exhibiting a low density of pilosebaceous units. Furthermore, since ethanol and aqueous gel are powerful absorption promoters in their own right, these agents can mask any phonophoresis. This may be overcome by employing a less active vehicle.

The most promising result of these studies was that ultrasound acted synergistically with azone. More research needs to be conducted in order to elucidate which factors are operating in this process so that the effect can be optimised.

CHAPTER SIX

THE EFFECT OF ULTRASOUND ON THE STABILITY OF OLIGODEOXYNUCLEOTIDES *IN VITRO*

6.1 INTRODUCTION

6.1.1 Oligodeoxynucleotides as Inhibitors of Gene Expression

Oligodeoxynucleotides (ODNs) are short chains of nucleotides (typically 6 to 100 units long) which resemble single-stranded DNA. In recent years, these agents have been proposed as an important new class of pharmaceuticals which could be used to directly inhibit gene expression (Weintraub, 1990; Milligan *et al.*, 1993). Such a capability promises beneficial pharmaceutical applications because of the possibility of downregulating the expression of genes which induce disease states. For example, the inhibition of oncogenes in malignant cells could lead to the prevention of cancers. Alternatively, the suppression of viral replicatory genes could be useful in treating numerous infectious disease states.

It has been shown that ODNs can influence gene expression by three separate mechanisms. Firstly, ODNs can bind to sense sequences in chromosomal DNA to create a triple helix. The formation of a triple helix directly inhibits the transcription of the genetic information encoded by the DNA into mRNA. Another possible mechanism involves ODNs hybridising according to Watson-Crick base pairing inside the cell to a corresponding sequence in mRNA molecules and prevent their translation into protein. A third mode of action results from the binding of ODNs to proteins that are crucial for cellular homeostasis. Since ODNs are large, relatively unstable, polar molecules it is relatively difficult to deliver them to their site of action in the cell nucleus. This aspect constitutes the main disadvantage of this therapeutic approach .

Although some studies have been conducted on the stability of DNA on exposure to ultrasound (Hill *et al.*, 1970), there are no data available on the chemical stability of ODNs on exposure to ultrasonic fields. Such information would be important if ODNs were eventually delivered by phonophoresis. The aim of this chapter is to determine the effect of ultrasound on these molecules in aqueous solution *in vitro*. Four different ODNs were evaluated. These were 7-myc phosphodiester, 7-myc phosphothioate, 20mer 5'D-tat and 20mer 5'S-tat. Each molecule was subjected to 30 minutes of ultrasound at 3 different pHs 1, 2 and 7. The stability of one particular nucleotide, 5'D-tat, at both 25°C and 44°C was also examined in the absence of ultrasound. Gel electrophoresis was employed as the analytical technique in conjunction with contact autoradiography.

6.1.2 The Principles of Gel Electrophoresis

The quantitative and qualitative analysis of a charged species can be performed by applying one of a number of electrophoretic methods. In electrophoresis, the test substance is placed within a supporting matrix which is subjected to an electrical potential difference. The electric field causes the rapid acceleration of each component ion until each ion reaches a terminal velocity at which point the frictional forces opposing movement are equal to the applied electric force. After a specified time period, the electric field is switched off. Each charged species will have then migrated a characteristic distance from the origin. The electrophoretic process can be described by the equation:

$$d = \mu \times t \times \left(\frac{V}{L}\right) \qquad (6.1)$$

Where d is the migration distance (in m) of the molecule, μ is the electrophoretic mobility (in $m^2\ s^{-1}\ V^{-1}$), t is the electric field application time (in s), V is the applied voltage (in V) and L is the distance between the electrodes (in m). The electrophoretic mobility (μ) of an ion depends upon several factors including the molecular shape, molecular mass, net charge, overall charge distribution, and the frictional resistance of the supporting matrix.

In gel electrophoresis, the supporting matrix is a semisolid colloid consisting of a macromolecular structure pierced with aqueous pores through which charged species can permeate. Historically, starch gels were employed as the matrix in gel electrophoresis. However, these have been superseded by polyacrylamide gels which can be synthesized with a higher degree of reproduciblity. In particular, the matrix pore size, which is the most important factor affecting frictional resistance, can be finely controlled by adjusting the amount of monomer, polymer and cross-linking agent. These synthetic gels are also better than starch gels since they exhibit greater resolution, versatility, sensitivity, as well ease of handling. However, polyacrylamide gels are synthesized from acrylamide which is a potent carcinogen and adequate protective clothing must be worn. Synthesis involves cross-linking acrylamide with N,N'-methylenebisacrylamide in the presence of a catalyst such as ammmonium persulphate.

ODNs have been frequently separated and analysed by applying gel electrophoresis using polyacrylamide gels as the supporting matrix. Electrophoresis powerpacks are commercially available and these have allowed the process to become even more reproducible. However, the application of high voltages heats the gel which can radically change its properties. Consequently, most commercially available systems are designed with water-jacketted cooling plates to provide temperature control. As well as loading the ODN on to the gel, it is desirable to load an appropriate marker dye into the system. The application of the electric field causes the dye to separate into its two component dyes, each exhibiting a different electrophoretic mobility. This provides a visual reference indicating the progress of electrophoresis.

When ODNs are labelled with radioisotopes such as ^{32}P or ^{35}S, their localisation on a polyacrylamide gel can be determined from contact autoradiography. In this technique, the gel, following electrophoresis is placed in contact with a photographic film for a suitable time period. After development, the film is blackened in the vicinity of the β-particle radiation source and the distribution and extent of blackening indicate the gross distribution of activity in the gel. Although the exposure time can be theoretically calculated from eqn (6.1), in practice, it is determined empirically.

6.2 METHODS

Synthetic ODNs were obtained without a phosphate group at their 5' terminus and were therefore labelled by transfering the γ-^{32}P from [γ-^{32}P]ATP using the enzyme bacteriophage T4 polynucleotide kinase (Sambrook *et al.*, 1989). The radiolabelled ODNs thus produced were then purified by native page electrophoresis using 20% polyacrylamide gel (Sambrook *et al.*, 1989).

6.2.1 Preparation of the Reagents

Table 6.1 lists the formula for each of the buffers that was used for the stability studies. In all cases, after the buffer components had been mixed together in the required proportions, the pH was measured on a pH meter. If necessary, the composition was adjusted by adding the appropriate buffer component until the desired pH was attained. All these prepared buffer solutions were stored in a fridge at 4°C. However, before their use for a stability study, the buffer solutions were removed from the fridge and allowed to warm to room temperature.

Table 6.1: Formulae for the Buffers used in the ODN Stability studies

Buffer	Formula
pH1	25ml of 0.2M potassium chloride + 25ml of 0.2M hydrochloric acid
pH2	25ml of 0.2M potassium chloride + 2.8ml of 0.1M hydrochloric acid
pH7	50ml of 0.1M potassium dihydrogen phosphate + 29.1ml of 0.1M sodium hydroxide

Tris borate buffer (5-fold strength) was prepared from an aqueous solution composed of 5.4w/v tris base (ICN), 2.75% w/v boric acid (Sigma), and 2% v/v EDTA (Biorad) which was adjusted to pH 8 with sodium hydroxide. This 5-fold strength tris borate buffer could be diluted down to single-strength tris borate buffer by the addition of distilled water in the ratio of 4:1. The single-strength solution was modified to 7M urea tris borate buffer by adding 42%w/v urea. This

solution contains the electrolytes which permit current to flow during electrophoresis (Sambrook *et al.*, 1989).

The polyacrylamide gel solution was composed of an aqueous solution containing 20% w/v acrylamide (ICN), 0.66% w/v N,N-methylenebisacrylamide (ICN), 21% w/v urea (ICN) and 20%v/v tris borate buffer (5-fold strength). The solution was prepared by heating a concentrated solution of the acrylamide and N, N-methylenebisacrylamide to 37°C on a hot plate. The urea was incrementally added in small quanties until it all dissolved into the solution. Distilled water was then added in order to make up the volume so that all the compounds were present at the correct concentrations. The solution was filtered through a nitrocellulose 0.45 μm membrane filter and then stored in a tinted bottle at room temperature.

The marker dye was prepared by dissolving 50mg of xylene blue (Sigma) and 50mg of bromophenol blue (sigma) in 7M urea tris borate buffer so as to make a final volume of 10ml. A 10% w/v solution of ammonium persulphate (Sigma) was also prepared for use as a catalyst and this was stored in the fridge.

6.2.2 The Ultrasound Exposure Protocol

A 5μl aliquot of the ODN under study and 95μl of the appropriate buffer (pH 1, 2 or 7) were pipetted into an Eppendorf tube. The tube was spun on a bench centrifuge for 20 seconds so as to mix the component solutions. Immediately after this step, a 5μl aliquot of the ODN-buffer solution was transferred into another Eppendorf tube prefilled with 20μl of 7M urea tris borate buffer. This 'time zero' sample was spun on a bench centrifuge and then stored at -20°C. The bulk of the ODN-buffer solution in the original tube was then sonicated in the exposure system depicted in Figure 6.1.

Ultrasound exposure was mediated by the small transducer of the ultrasound generator (Therasonic no.50, EMS Greenham Ltd.) which was fixed through the central axis of a Franz donor cell by a specially designed teflon collar, as described in section 5.2.3. The donor compartment was clamped in an inverted position so that the transducer was at the base of the assembly, pointing upwards and the

narrow end of the donor compartment was on top. The donor cell was entirely filled with coupling gel (Henleys Medical Supplies Ltd). The Eppendorf tube containing the ODN solution was positioned so that its conical base was totally immersed within the coupling gel but the upper cylindrical part protruded above the gel level.

Figure 6.1: The Sonication System Employed in the Oligodeoxynucleotide Stability Studies

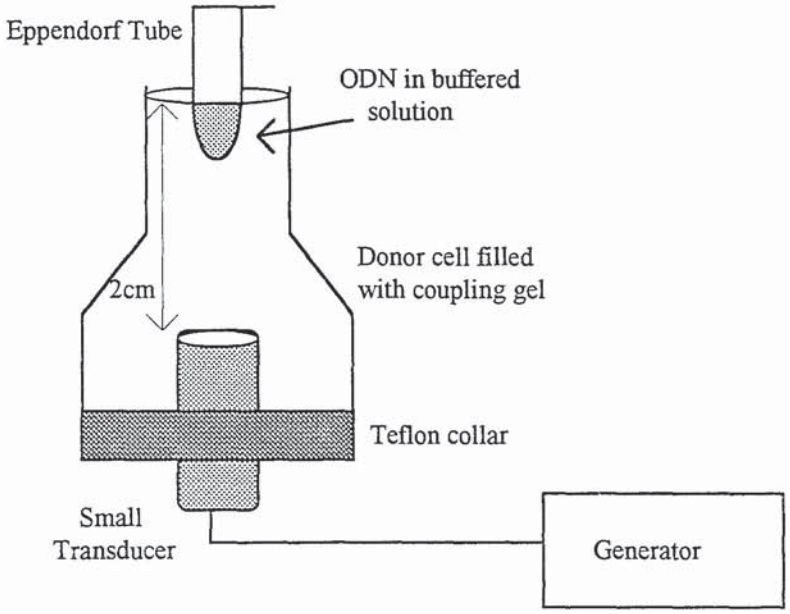

The ODN solution was sonicated for 30 minutes with a 1.1MHz beam, exhibiting an intensity of 1.5W cm^{-2}. At successive time intervals after the beginning of sonication (5, 10, 20 and 30 minutes), the Eppendorf tube was removed from the gel and a 5µl aliquot of ODN solution was pipetted into another labelled Eppendorf tube prefilled with 20µl of 7M urea tris borate buffer. The original Eppendorf tube was then replaced in the sonication system (except at 30 minutes since this marked the end of the experiment). Each Eppendorf tube containing a time-point sample was spun on a bench centrifuge so as to thoroughly mix the ODN solution with the 7M urea tris borate buffer. This results in the ODN solution reverting to a neutral pH. Each time point sample was then refrigerated at -20°C and stored until it was ready for analysis by gel electrophoresis.

6.2.3 Control and Heat-Alone Exposure Protocol

For the control studies, a small volume (5µl) of 20mer 5'D-tat solution and 95µl of the appropriate buffer solution (pH 1, 2 or 7) were pippetted into an Eppendorf tube. The tube was spun on a bench centrifuge for 20 seconds so as to mix the component solutions. The tube was left on the laboratory bench for 30 minutes. The room temperature was measured with a thermocouple (Digitron Instruments, 3202K) and was found to be 25°C.

For the heat-alone studies, the appropriate buffer solution (pH 1, 2 or 7) was preheated in an incubator (Gallenkamp Economy, size 2) set to 44°C. A small volume (95µl) of the heated buffer solution was then pipetted into an Eppendorf tube into which 5µl of 20mer 5'D-tat solution was also added. The tube was spun on a bench centrifuge for 20 seconds and then transferred back into the incubator for 30 minutes.

In both the 25°C and 44°C stability studies, 5µl aliquots of 20mer 5'D-tat solution were removed from the Eppendorf tube at 5 specific time intervals (0,5,10,20 and 30minutes) during the course of the experiment. Again, each aliquot was transferred into another labelled Eppendorf tube prefilled with 20µl of 7M urea tris borate buffer. The contents of each of these labelled tubes were mixed by spinning on a bench centrifuge for 20 seconds. These tubes were stored at -20°C until they were removed for analysis..

6.2.4 Temperature Profile Determinations

A separate set of temperature profile studies were conducted in order to determine the effect of ultrasound on the temperature of the ODN solution in the Eppendorf tube. An Eppendorf tube was filled with 100µl water and then placed in the sonication system in exactly the same manner as described in section 6.2.2. Ultrasound was then applied for 30 minutes, again at 1.5W cm^{-2} at a frequency of 1.1MHz. The tube was temporarily removed at specific time intervals (0, 5, 10

and 20 minutes) and on each occasion, the water temperature was quickly recorded with a thermocouple (Digitron Instruments, 3202K). After each temperature measurement, the tube was immediately replaced in the sonication system. The temperature was also recorded at the end of the experiment *ie.* 30 minutes. This experiment was performed in triplicate.

6.2.5 The Analytical Technique

Denaturing PAGE electrophoresis followed by autoradiography was employed as the analytical technique. Initially, an electrophoresis rig (Biorad Powerpack 3000) was assembled with the glass plates separated with thin spacers. A volume (50ml) of 20% 7M urea polyacrylamide gel solution was mixed with 40µl of Temed (Sigma) and 600µl of 10%w/v ammonium persulphate solution in a beaker. With the rig tipped back, this gel solution was poured into the space between the glass plates so as to fill the rig to the top. Care was taken to ensure that air bubbles did not develop between the plates. A plastic comb (Biorad) was inserted between the glass plates so as to allow wells to form as the gel set. After 20 minutes, the gel had completely set and the comb was removed. The wells were thoroughly washed out with tris borate buffer so as to remove any adhering residues of gel.

The rig was transferred to the complementary electrophoresis powerpack. The inner reservoir of the powerpack was filled to the level of the glass plates with fresh tris borate buffer. The gel was initially 'prerun' by applying a 10W electric field for 30 minutes. This procedure results in the removal of unwanted salts from the polyacrylamide gel. During all this time, cold tap water was ran through the tank to keep the plates cool. After the prerun period, the system was ready for electrophoresis of the ODNs.

The Eppendorf tubes, each containing a sample representing the time point of a specific exposure experiment, were removed from the -20°C freezer. After the samples had thawed out, each 25µl sample was loaded into a specific well of the polyacrylamide gel. In addition, two wells on the left hand side of the gel and one well on the right hand side of the gel were each loaded with 10µl of marker dye. Furthermore, a sample of ATP[γ^{32}P] in tris borate buffer was loaded into yet another well. The sample loading pattern was noted down for later identification. A power setting of 10W was then selected and electrophoresis was allowed to proceed for 2 hours.

After electrophoresis, the rig was detached from the powerpack and carefully disassembled so as to isolate the polyacrylamide gel. The sheet of gel was wrapped in clingfilm whilst care was taken to minimise air bubble entrappment in the process. The wrapped gel was placed inside a dry autoradiography cassette (Hypercasette, Amersham International plc) with the gel uppermost and the wells adjacent to the cassette hinges. The cassette was taken to a dark room and opened under safelight conditions. A photographic film (Hyperfilm-MP, Amersham International plc) was placed on top of the gel so that the top left hand square of the hyperfilm was aligned with the top left hand corner of the gel. A marker pen was used to write a note on the film of its relative orientation. The cassette was then closed and left in a black plastic bag which was refrigerated at -70°C. Following 3 hours of autoradiography, the cassette was transferred to a dark room and allowed to thaw out. The cassette was opened slowly under safelight conditions. The photographic film was developed in the standard manner.

6.3 RESULTS AND DISCUSSION

6.3.1 The Effect of Ultrasound on ODN Stability at pH2 and pH7

Figure 6.2 and Figure 6.3 present the gel activity distributions of the S-myc and S-tat time-point samples respectively. Both ODNs were exposed to ultrasound for 30 minutes at both pH2 and pH7 before analysis. It can be seen that the blackened areas on the film retain their size and location throughout the 30 minutes of ultrasound exposure. This result indicates that 1.5W cm^{-2} ultrasound does not degrade S-myc or S-tat *in vitro* under these pH conditions.

Figure 6.2: Gel activity distribution of S-myc following sonication at pH2 and pH7 (Arrow indicates direction of species migration)

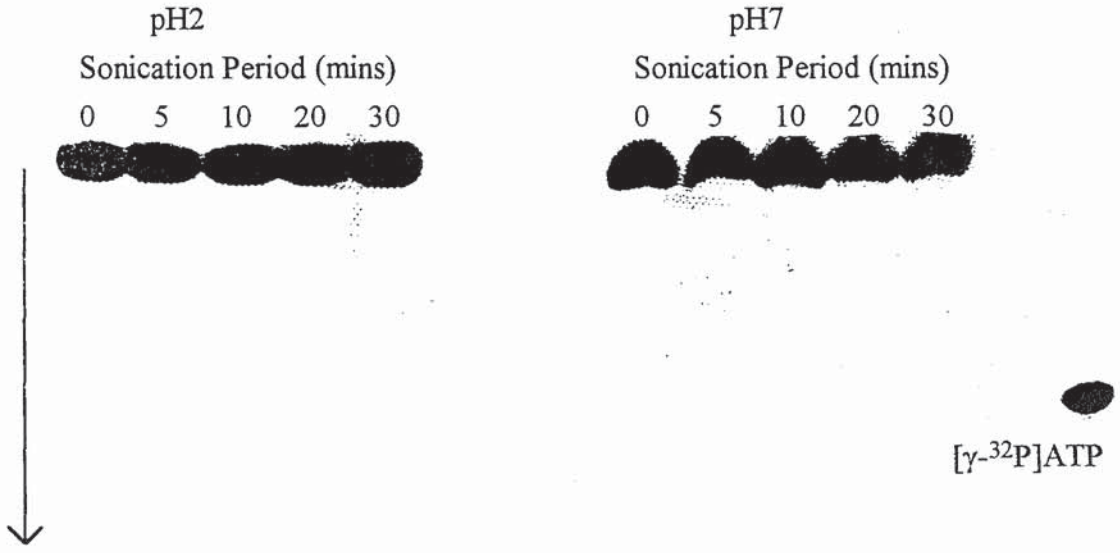

Figure 6.3: Gel activity distribution of S-tat following sonication at pH2 and pH7 (Arrow indicates direction of species migration)

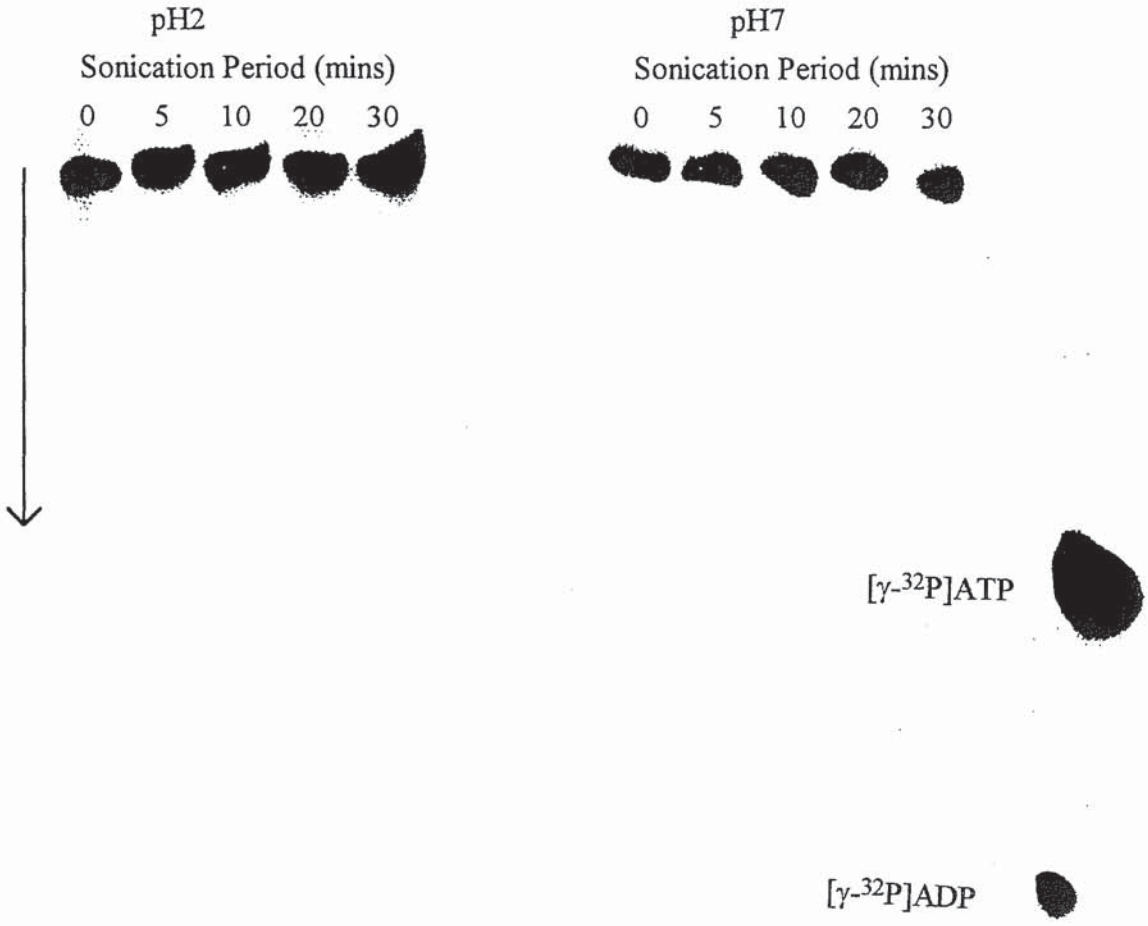

Figures 6.4 and 6.5 show the activity distributions on the polyacrylamide gel of the D-myc and D-tat time-point samples respectively. Both nucleotides were sonicated for 30 minutes at pH2 and pH7 before analysis. Again, it can be seen that the position and size of the blackened areas remain unchanged throughout the sonication period. Although the D-myc samples from the pH7 study can be seen to form a curve, this feature was merely caused by the right hand side wells being incompletely cleaned of gel residues. It can be concluded that D-myc and D-tat are not degraded by 1.5W cm^{-2} ultrasound at pH2 or pH7.

Figure 6.4: Gel activity distribution of D-myc following sonication at pH2 and pH7 (Arrow indicates direction of species migration)

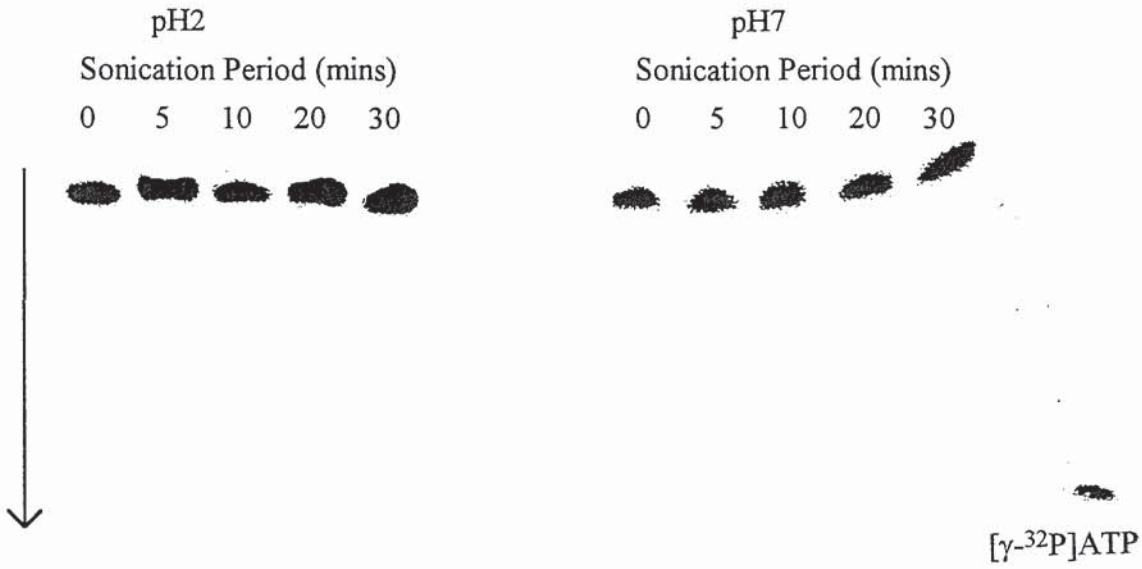

Figure 6.5: Gel activity distribution of D-tat following sonication at pH2 and pH7 (Arrow indicates direction of species migration)

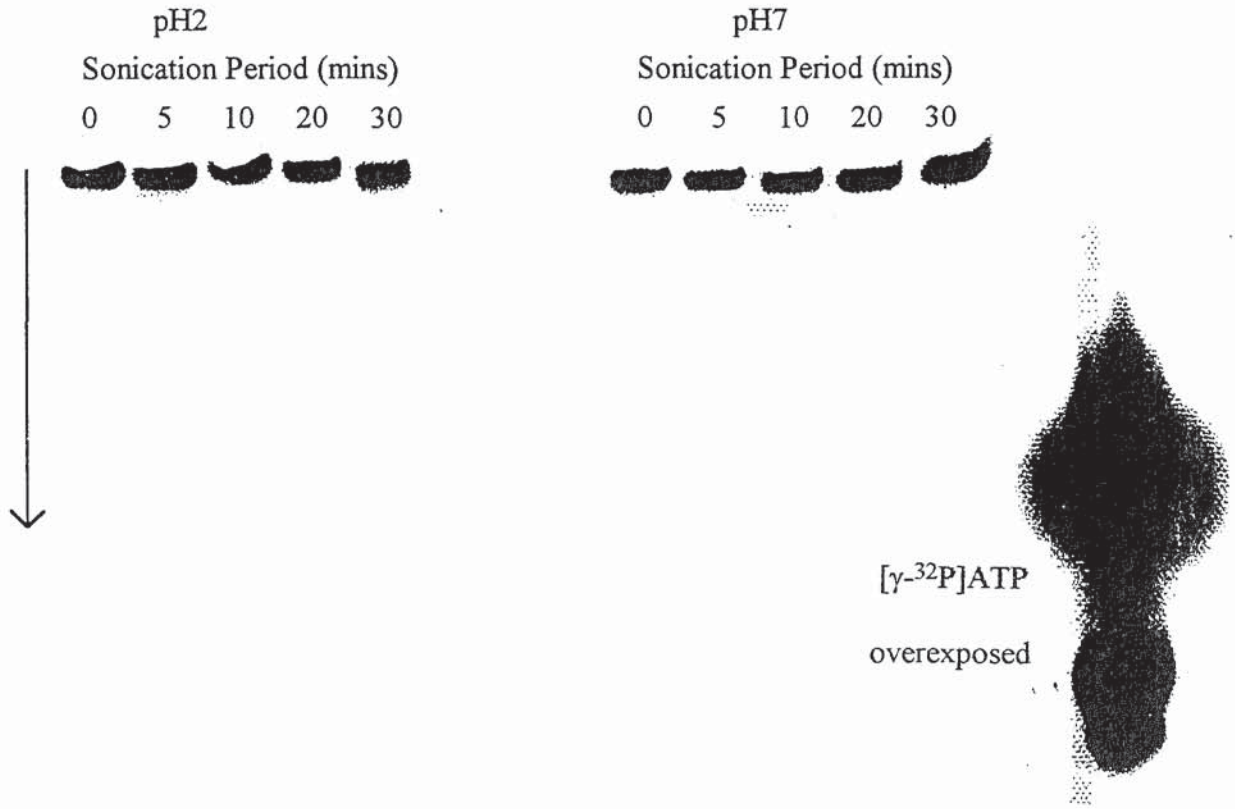

Figure 6.6 shows the effect of ultrasound exposure on the solution temperature within the Eppendorf tube. It can be seen that sonication resulted in the temperature reaching 44°C by 20 minutes. It can be concluded that all 4 ODNs are stable at this temperature at pH2 and pH7. Stability studies conducted in cellular extracts and sera have shown that degradation can potentially proceed to the monomer, dimer or to a range of larger units (Akhtar *et al.*, 1991). Additionally, the removal of the ^{32}P label from the 5' end of the molecule is another possibility.

Figure 6.6: The Solution Temperature within the Eppendorf Tube during Sonication

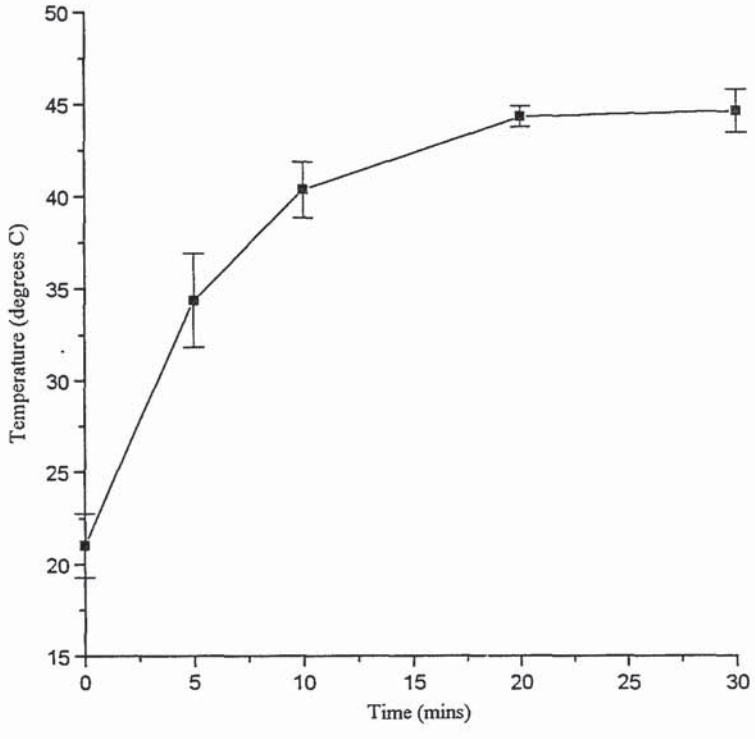

Error bars represent s.d. of three replicate measurements

6.3.2 The Effect of Ultrasound on ODN Stability at pH1

Figure 6.7 illustrates the results of electrophoresis of the S-myc and S-tat samples respectively. Both sets of samples were derived from experiments in which the ODNs were sonicated at pH1. It can be seen that the degradation of S-myc is visible at 20 minutes and that, by 30 minutes, it has completely degraded. In

contrast, S-tat is more stable, exhibiting only partial degradation after 30 minutes of sonication.

Figure 6.7: Gel activity distribution of S-myc and S-tat following sonication at pH1 (Arrow indicates direction of species migration)

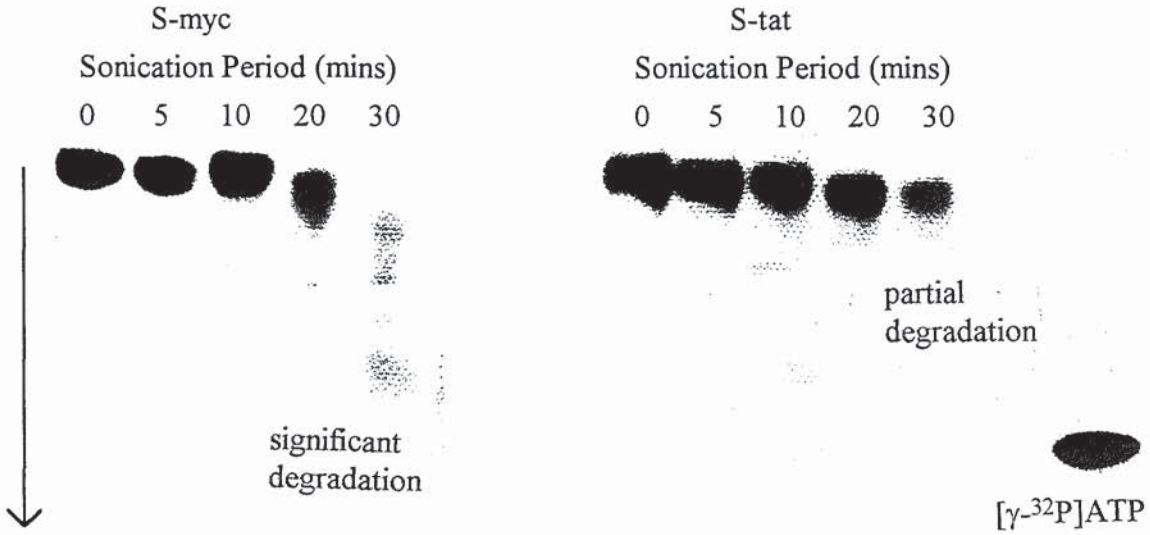

Figure 6.8 includes the results of electrophoresis of the D-myc samples following sonication at pH1. It can be seen that the activity of the D-myc sample at time zero forms a double area of blackening on the photographic film. This indicates that the molecule breaks up even before ultrasound application *ie.* the D-myc hydrolyses in the acidic buffer. From 10 minutes onwards, the film shows progressively weaker and more diffuse β activity. This means that as sonication proceeds, the D-myc undergoes progressively greater degradation into smaller fragments. Figure 6.8 also shows the D-tat time point samples derived from pH1 sonication experiments. The D-tat is unchanged at 0 and 5 minutes but begins to degrade at 10 minutes and from 20 minutes onwards it is completely degraded.

Figure 6.8: Gel activity distribution of D-myc and D-tat following sonication at pH1 (Arrow indicates direction of species migration)

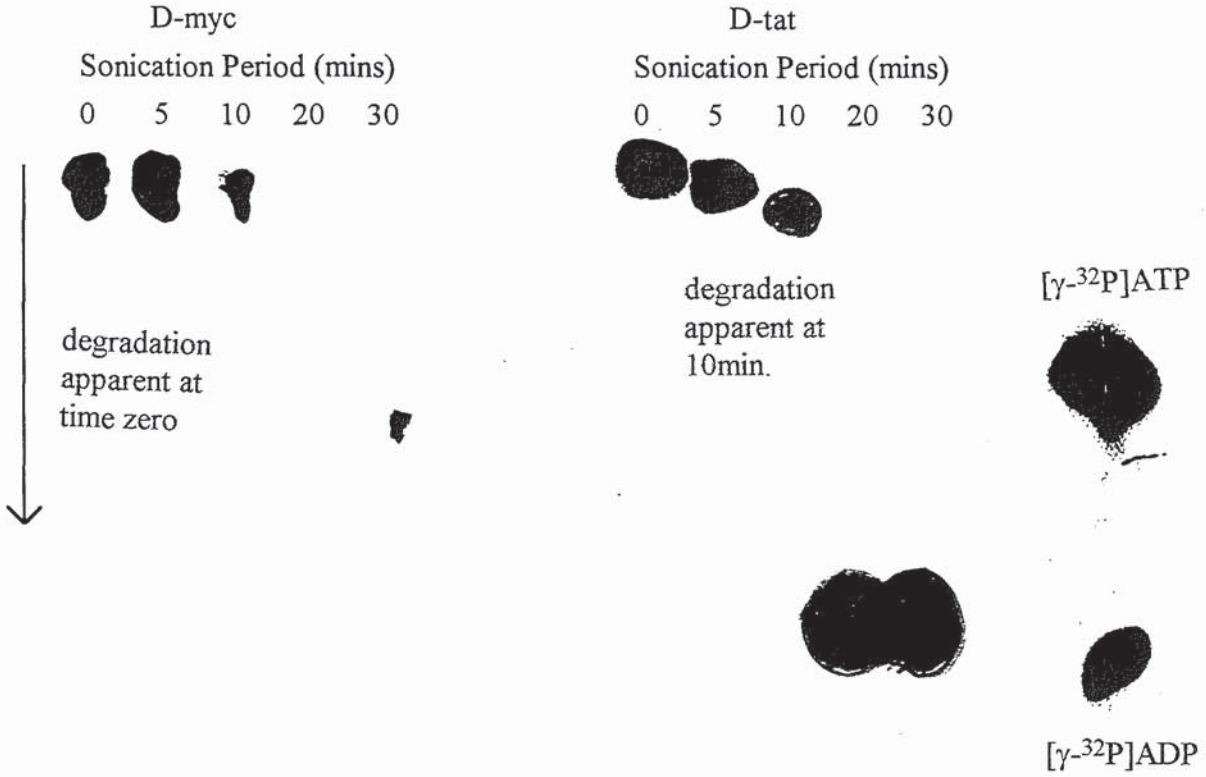

It can be surmised that each S-ODN was more stable than the comparable D-ODN. Significantly, this pattern has been documented in the literature reports. For example, Akhtar and co-workers examined the stability of various ODNs in a range of different cellular extracts and sera (Akhtar *et al.*, 1991). It was shown that, in any given medium, the S-ODNs underwent less degradation than the D-ODNs.

6.3.3 The Effect of Heat-Alone on ODN Stability

Figure 6.9 shows the electrophoresis results relating to the D-tat samples following their exposure to 3 different pHs at 25°C. It can be seen that D-tat is stable under all the conditions investigated.

Figure 6.9 Gel activity distribution of D-tat following exposure at 25°C
(Arrow indicates direction of species migration)

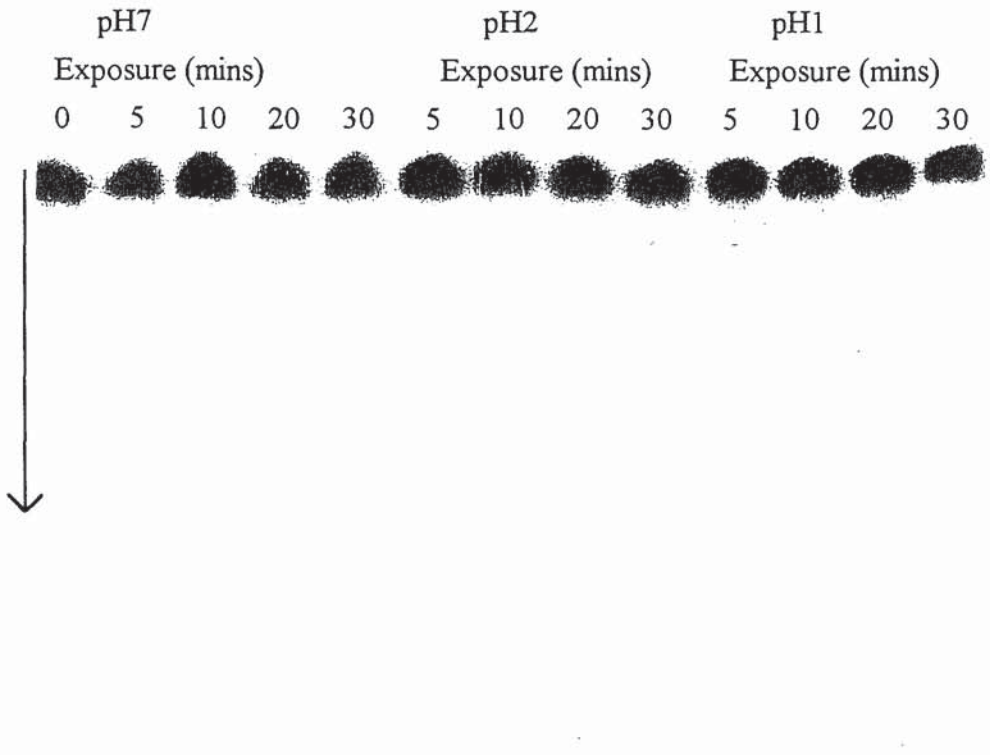

Figure 6.10 Gel activity distribution of D-tat following exposure at 44°C
(Arrow indicates direction of species migration)

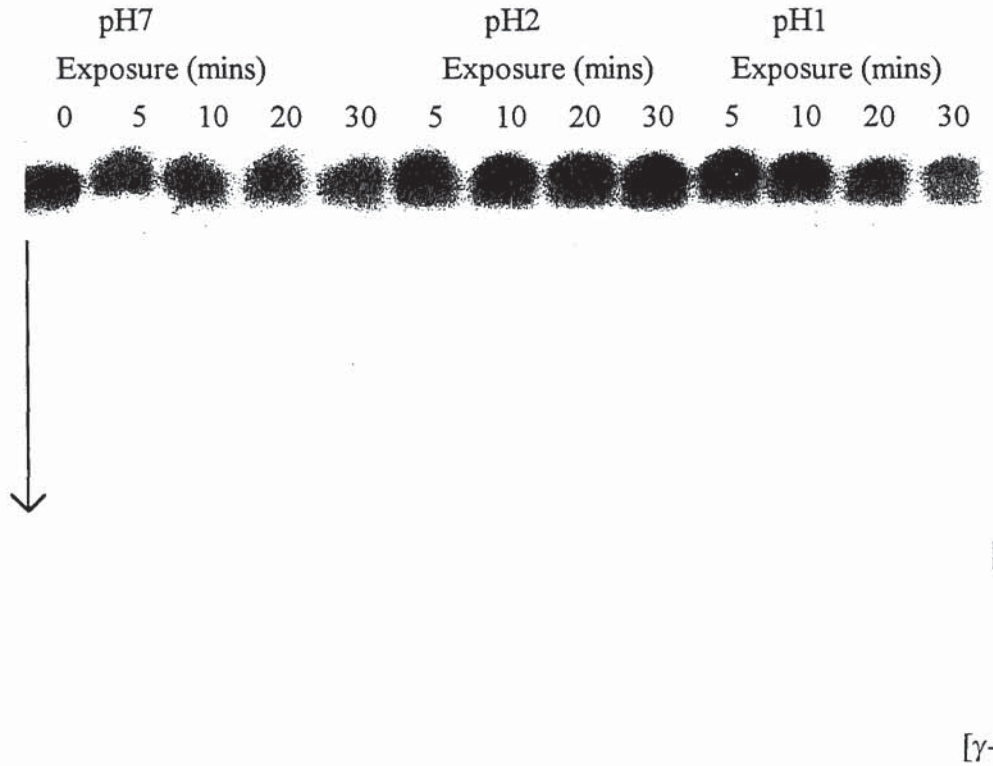

Figure 6.10 shows the gel activities of the D-tat samples following their exposure to 3 different pH solutions at 44°C. Again, the D-tat remained stable under all these conditions. This is an interesting finding since the D-tat did degrade when it was sonicated at pH1 and therefore also subjected to temperatures of 44°C (refer to Figure 6.6). This indicates that ultrasound-induced degradation of D-tat at pH1 must have been induced by the mechanical effects of the beam rather than the thermal effects.

Significantly, it has been demonstrated that 3 minute applications of 1MHz ultrasound can degrade DNA *in vitro* at intensities as low as $0.4Wcm^{-2}$ (Hill *et al.*, 1970). This effect was caused by stable cavitation as was shown by the fact that the process was influenced by the presence and availability of dissolved gas in solution. Specifically, the nucleotide chains were being stretched to breaking point by the hydrodynamic shear fields developing as a result of stable cavitation (Williams, 1983). It is likely that similar forces were exerted on the D-tat structure and at pH1 there was sufficient cumulative disruption to degrade this ODN.

Since the D-tat does not degrade in the control experiments at 25°C and 44°C, no attempt was made to conduct control stability studies on the S-tat and S-myc which exhibited even greater stability, as was shown in section 6.3.2. Attempts were also made to label D-myc with ^{32}P but the D-myc did not label and the stability studies on this particular ODN could not be performed.

6.4 SUMMARY

Ultrasound did not degrade any of the 4 ODNs when they were dispersed in buffer solutions of either pH2 or pH7. However, when the ODNs were sonicated in a pH1 solution, all of the nucleotides degraded but some degraded much more rapidly than others. The order of degradation, starting with the most unstable species first was D-myc > D-tat > S-myc > S-tat. Significantly, previous research has shown that D-ODNs are more susceptible to degradation than S-ODNs and that shorter chain lengths are chemically less stable than longer chain lengths. Thus, it appears that ultrasonic energy does not introduce a new dimension of degradation but that it merely enhances the degradation rate already present.

The D-tat was stable when it was dispersed in pH1 buffer at 25°C and surprisingly also at 44°C. This latter result indicates that a mechanical artefact of the beam such as hydrodynamic shear stress is producing the degradation. Clearly, much more research needs to be conducted in this field.

CHAPTER SEVEN

CONCLUSIONS

CONCLUSIONS

Despite being employed for over 30 years in physiotherapy clinics, no clear consensus exists on the effectiveness of phonophoresis nor on the exact nature of the mechanism(s) involved. In order to shed more light on these issues, ultrasound-enhanced permeation was investigated in three separate *in vitro* models. These were; a model of the diffusion of molecules through agar gel, a model in which sonication of skin was followed by drug permeation, and a model in which skin sonication ran concurrently with drug permeation.

In Chapter 2, a radiation-pressure force balance was deployed to calibrate the outputs of the ultrasound generator. It was determined that the performances of all 5 ultrasound drives were within the limits set by the British Standards Institute and therefore the machine was adequate for phonophoresis research. Various other dosimetry techniques were subsequently applied to characterise the acoustic field at the diffusion interface of each phonophoresis model. In the agar gel model, diffusion occurred within an ultrasound near field associated with a small standing wave component. In the presonication model, the skin samples were subjected to an ultrasound near field in the absence of standing waves. In the modified Franz cell model, the skin samples were either within the near field (at 3.3MHz) or far field (at 1.1MHz) of the beam but in both cases, most of the energy (≥75%) was in the form of a standing wave.

In the first phonophoresis model (Chapter 3), inulin, mannitol and hydrocortisone were chosen to represent a large molecule, a small hydrophilic molecule and a small relatively hydrophobic molecule respectively. These molecules were each assessed for susceptibility to phonophoresis as they diffused, along a concentration gradient, through agar gel. Under control conditions, each compound migrated at a different rate. The order of diffusion, starting with the most rapidly permeating drug first, was mannitol > hydrocortisone > inulin. The mannitol molecule diffused very rapidly as a consequence of its small, hydrophilic nature. These properties are ideal for rapid diffusion within the water-filled pores of the hydrogel. Hydrocortisone migrated more slowly since it is relatively lipophilic. The larger inulin molecule probably interacted with the agar polymer and this suppressed its migration rate. Sonication accelerated the migration of both hydrocortisone and mannitol. However, hydrocortisone transport was more markedly enhanced indicating that slowly migrating hydrophobic molecules are more susceptible to a

greater relative increase in diffusion than rapidly migrating hydrophilic molecules. Sonication did not affect inulin migration as the molecule was too large to readily pass through the aqueous pores of the gel. Since the application of heat alone increased drug diffusion by a similar magnitude as the ultrasound, it is likely that ultrasonic heating directly increases the thermodynamic potential for diffusion.

Just as agar gel consists of polysaccharide macromolecules perforated by aqueous channels, the stratum corneum is composed of protein-rich cells separated by intercellular lipid channels. Current thinking is that the main drug absorption pathway lies through these intercellular lipids (Hadgraft *et al.*, 1995). From the mechanistic data obtained from the hydrogel experiments, it would be predicted that small, relatively hydrophilic molecules would be the ideal candidates for phonophoresis through the stratum corneum lipids.

Chapter 4 focused on the effects of an ultrasound free-field on excised Wistar rat skin. It was determined that morphological changes could be conveniently divided into those that occurred following sonication at low intensities (<1W cm^{-2}) and those that occurred following sonication at high intensities (1 to 2W cm^{-2}).

At low intensities, ultrasound discharged sebum from the sebaceous glands so as to fill much of the hair follicle shafts. This is an entirely novel effect. The phenomenon is probably produced by the mechanical effects of the ultrasound though thermal processes cannot be entirely ruled out. The deposition of sebaceous lipids within the hair follicle shafts means that this absorption pathway is blocked for hydrophilic molecules that penetrate *via* this route. Consequently, this phenomenon has important implications for topical drug delivery in that it can be used as a probe to elucidate the relative follicular contribution to total penetration for these molecules. At this point in time, there is a desperate requirement for such a mechanistic tool for transdermal delivery research (Lauer *et al.*, 1995). From these *in vitro* Wistar rat studies, it was demonstrated that the shunt pathway was responsible for virtually all mannitol and sucrose penetration but negligible aminopyrine and 5-fluorouracil penetration. Low intensity ultrasound approximately halved hydrocortisone permeation. However, for relatively lipophilic compounds such as hydrocortisone, the accumulation of sebum in the hair follicles will merely impede permeation rather than completely suppress it. Therefore, without further information, the relative contribution of each pathway in hydrocortisone absorption cannot be ascertained. Futhermore, care must be

taken in applying this tool as ultrasound may cause sebum to overflow on to the skin surface, thus suppressing flux across the bulk stratum corneum. In addition, it has yet to be established whether sebum release will occur in other species or indeed, *in vivo*. Clearly, more research needs to be conducted in order to address all these issues.

At high intensities (1 to 2W cm^{-2}), ultrasonic waves irreversibly degraded the stratum corneum and the dermis. The extent of injury was intensity - dependent and followed the general patterns described in the literature reports. Both the thermal effects as well as the mechanical effects of the beam probably induced the morphological changes. It was found that ultrasound exposure increased subsequent hydrocortisone flux even though histological analysis of the barrier showed that it appeared histologically identical to control skin. This suggests that traditional histology techniques may be too insensitive to detect localised damage to the stratum corneum.

Chapter 5 evaluated the effect of sonication on the transdermal permeation of seven different candidate molecules. The selected molecules were small (<400Da) and they encompassed a wide range of octanol / water partition coefficients. Again, the barrier was whole Wistar rat skin. Concurrent ultrasound application did not significantly increase the percutaneous absorption of any of the permeants studied. As stated above, the results of the hydrogel studies suggest that hydrophilic molecules would be be more susceptible to ultrasound-enhanced diffusion through the stratum corneum lipids. However, sonication actually reduced the skin surface concentration of these agents by promoting their diffusion into the overlying aqueous gel that was acting as an ultrasonic couplant. The absence of an ultrasound effect for the more hydrophobic molecules was expected from theory as these are intrinsically rapid permeants. For highly lipophilic drugs, absorption is rate-limited by partitioning from the stratum corneum into the viable epidermis. No evidence could be found to support the hypothesis that ultrasound accelerates this step.

A favourable result of this research was that ultrasound acted synergistically with azone in promoting hydrocortsone diffusion. Ultrasonic heating accelerated azone penetration through the horny layer. More research needs to be conducted in order to further characterise the mechanisms involved in this process.

The outcomes of all these permeation studies were complicated by the sebum discharge effect. In further work, permeation models should be designed so that this phenomenon and the reverse diffusion effect are removed as artefacts of the experiment. Such permeation studies should be carried out in conjunction with analytical techniques such as ATR-FTIR spectroscopy and differential scanning calorimetry. Furthermore, research should ideally be conducted with human skin as the barrier membrane. It must also be mentioned that there is a continual need for ongoing collaboration between medical physicists and pharmaceutical scientists. Only thus can the biological interactions of ultrasound be linked to established pharmaceutical methods and principles.

Chapter 6 focused on the effect of ultrasound on the *in vitro* stability of oligodeoxynucleotides (ODNs) in aqueous solution. Four different ODNs were examined, representing two different chemistries and two different chain lengths. Although ultrasound did not measurably degrade any of the ODNs when they were dissolved in solutions at pH2 or pH7, significant degradation was observed in a pH1 solution. However, at this pH, some ODNs were more unstable than others. The order of degradation, starting with the most readily degradable species first was D-myc > D-tat > S-myc > S-tat. Interestingly, D-tat did not exhibit any degradation when it was subjected to an equivalent heat-alone application. This indicates that the mechanical effects of ultrasound produce accelerated nucleotide degradation. Clearly, much more research needs to be conducted in order to elucidate the nature of these sonochemical effects.

REFERENCES

Akhtar S., Kole R., and Juliano R.L., Stability of Antisense DNA Oligodeoxynucleotide Analogs in Cellular Extracts and Sera, *Life Sci.* 49: 1793-1801, 1991

Al-Suwayeh S. and Hikal A.H., Influence of Ultrasound on *in vitro* Diffusion of Indomethacin Through Hairless Mouse Skin, *Pharm. Res.* 8(10) Supplement: S-140, 1991

Antich T.J., Phonophoresis: The Principles of the Ultrasonic Driving Force and Efficacy in Treatment of Common Orthopaedic Diagnoses, *J. Orthop. and Sports Phys. Ther.* 4(2): 99-102, 1982

Antich T.J., Randall C.C., Westbrook R.A., Morrisey M.C., and Brewster C.E., Physical Therapy Treatment of knee Extensor Mechanism Disorders: Comparison of Four Treatment Modalities, *Journal of Orth. and Sports Phys. Ther.* 8(5): 255-259, 1986

Barry, B.W., Dermatological Formulations In: *Percutaneous Absorption* (Ed. Barry B.W.) Marcel Dekker, New York 1983.

Barry B.W., Modern methods of promoting drug absorption through skin, *Mol. Aspects Medicine*, 12: 195-241, 1991

Bayliss High O.B., Lipids. In: *The Theory and Practice of Histological Techniques 3rd Edition* (Eds. Bancroft J.D. and Stevens E.) Churchill-Livingstone, London 1990.

Behl C.R., Bellantone N.H., and Flynn G.L., In: *Percutaneous Absorption* (Eds. Bronaugh R.L. and Maibach H.I.) Marcel Dekker, New York 1985. p183-212

Benson H.A.E. and McElnay J.C., Transmission of Ultrasound Energy Through Topical Pharmaceutical Products, *Physiotherapy* 74(11): 587-589, 1988

Benson H.A.E., McElnay J.C., and Harland R., Phonophoresis of lignocaine and prilocaine from Emla cream, *Int. J. Pharm.* 44: 65-69, 1988

Benson H.A.E., McElnay J.C., and Harland R., Use of Ultrasound to Enhance Percutaneous Absorption of Benzydamine, *Phys. Ther.* 69(2): 113-118, 1989.

Benson H.A.E., McElnay J.C., Harland R., and Hadgraft J., Influence of Ultrasound on the Percutaneous Absorption of Nicotinate Esters, *Pharm. Res.* 8(2): 204-209, 1991

Benson H.A.E., McElnay J.C., Whiteman J., and Harland R., Lack of Effect of Ultrasound on the Percutaneous Absorption of Benzydamine, *J. Pharm. Pharmacol.* 38 supplement 73P, 1986

Bidmon H.J., Pitts J.D., Solomon H.F., Bondi J.V., and Stumpf W.E., Estradiol distribution and penetration in rat skin after topical application, studied by high resolution autoradiography, *Histochemstry.* 95: 43-54, 1990

Bommannan D., Menon G.K., Okuyuma H., Elias P.M., and Guy R.H., Sonophoresis 2. Examination of the Mechanism(s) of Ultrasound Enhanced Transdermal Drug Delivery, *Pharm. Res.* 9(8): 1043-1047, 1992

Bommannan D., Okuyama H., Stauffer P., and Guy R.H., Sonophoresis 1: The Use of High Frequency Ultrasound to Enhance Transdermal Drug Delivery, *Pharm. Res.* 9(4): 559-564, 1992

Bronaugh R., Stewart R., and Congdon E., Methods for in vitro percutaneous absorption studies 2. Animal models for human skin, *Tox. Appl. Pharmacol.* 62: 481-488, 1982

Brucks R., Nanavaty M., Jung D., and Siegel F., The Effect of Ultrasound on the in vitro Penetration of Ibuprofen Through Human Epidermis, *Pharm. Res.* 6(8): 697-701, 1989

Bucks D.W., Maibach H.I., and Guy R.H., Occlusion does not uniformly enhance penetration in vivo, In: *Percutaneous Absorption. Mechanisms-Methodology-Drug Delivery, 2nd Edition.* (Eds. Bronaugh R.L. and Maibach H.I.) Marcel Dekker, New York 1989. 77-89.

Cameron M.H. and Monroe L.G., Relative Transmission of Ultrasound by Media Customarily Used for Phonophoresis, *Phys. Ther.* 72(2): 142-148, 1992

Cameroy B.M., Ultrasound Enhanced Local Anesthesia, *Am. J. of Orthop.* 8(3): 47, 1966

Chan S.Y. and Li Wan Po A., Prodrugs for Dermal Delivery, *Int. J. Pharm.* 55: 1-16, 1989

Chatterjee D.S., A Double -Blind Clinical Study with Benzydamine 3% Cream on Soft Tissue Injuries in an Occupational Health Centre, *J. Int. Med. Res.* 5: 450-458, 1977

Chivers R.C., Fundamentals of Ultrasonic Propagation. In: *Output Measurements for Medical Ultrasound* (Ed. Preston R.C.) Springer-Verlag, London 1991.

Coodley E.L., Bursitis and Post-Traumatic Lesions: Management with Combined Use of Ultrasound and Intra-articular Hydrocortisone. *Am. Pract.* 11(3):181-188, 1960

Cooper, E., Vehicle effects on skin penetration. In: *Percutaneous Absorption. Mechanisms-Methodology-Drug Delivery, 1st Edition* (Eds. Bronaugh, R. L. and Maibach, H. I.) Marcel Dekker, New York 1985. 525-540.

Davick J.P., Martin R.K., and Albright J.P., Distribution and Deposition of Tritiated Cortisol Using Phonophoresis, *Phys. Ther.* 68(4): 1672-1675, 1988

Davidson F., Ultrasonic Power Balances. In: *Output Measurements for Medical Ultrasound* (Ed. Preston R.C.) Springer-Verlag, London 1991.

Dinno M.A., Crum L.A., and Wu J., The Effect of Therapeutic Ultrasound on Electrophysiological Parameters of Frog Skin, *Ultrasound Med. Biol.* 15(5): 461-470, 1989

Downing D.T. and Stewart M.E., Analysis of Sebaceous Lipids. In: *Methods in Skin Research* (Eds. Skerrow D. and Skerrow C.J.) Oxford University Press, Coventry 1985.

Dyson M., Pond J.B., Woodward B. and Broadbent J., The production of red blood cell stasis and endothelial damage in the blood vessels of chick embryo heated with ultrasound as a stationary wave field, *Ultrasound Med. Biol.* 1: 133-148, 1974

Esche R., Untersuchungen der Schwingungskavitation in Flussigkeiten, *Acustica.* 2: 208-218, 1952

Fabin B. and Touitou E., Localization of lipophilic molecules penetration in rat skin in vivo by quantitative autoradiography, *Int. J. Pharm.* 74: 59-65, 1991

Famaey J.P., Medical Phonophoresis with Anti-inflammatories, *J. Belge. Med. Phys. Rehab.* 8(3): 179-183, 1985

Florence A.T. and Attwood D., In: *Physicochemical Principles of Pharmacy* (Eds. Florence A.T. and Attwood D.) Macmillan Education Ltd, Hong Kong, 1981. Chapter 3

Flynn H.G., In: *Physical Acoustics, Vol. IB.* (Ed. Mason W.P.) Academic Press, New York 1964. 57-172.

Franz T.J., Percutaneous absorption. On the relevance of in vitro data, *J. Invest. Dermatol.* 64: 190-195, 1975

Franz T.J., The finite dose technique as a valid in vitro model for the study of percutaneous absotption in man, *Curr. Prob. Dermatol.* 7: 58-68, 1978

Gatev S.P., Ultraphonophoresis and its Effect on the Distribution and Deposition of Hydrocortisone-14C in Experiments, *Voor Kuratol Fizioter Lech Fiz Kult.* 35: 42-45, 1970

Goss S.A., Frizzel :L.A., and Dunn F., Ultrasonic absorption and attenuation in mammalian tissues, *Ultrasound Med. Biol.* 63: 181-186, 1979

Griffin J.E., Enternach J.L., Price R.E., and Touchstone J.C., Patients Treated with Ultrasonic Driven Hydrocortisone and with Ultrasound Alone, *Phys. Ther.* 47(7): 594-601, 1967

Griffin J.E. and Touchstone J.C., Ultrasonic Movement of Cortisol into Pig Tissues. 1. Movement into Skeletal Muscle, *Am. J. Phys.* 42: 77-85, 1963

Griffin J.E. and Touchstone J.C., Low-Intensity Phonophoresis of Cortisol in Swine, *Phys. Ther.* 48(12):1336-1344, 1968

Griffin J.E. and Touchstone J.C., Effects of Ultrasonic Frequency on Phonophoresis of Cortisol into Swine Tissues, *Am. J. Phys. Med.* 51(2): 62-78, 1972

Griffin J.E., Touchstone J.C., and Liu A.C-Y., Ultrasonic Movement of cortisol into pig tissue. 2. Movement into paravertebral nerve, *Am. J. Phys. Med.* 44(1): 20-25, 1965

Hadgraft J., Williams D.G., and Allan G., Azone: Mechanisms of Action and Clinical Effect. In: *Pharmaceutical Skin Penetration Enhancement* (Eds. Hadgraft J. and Walters K.A.) Marcel Dekker, New York-Basel-Hong Kong 1995.

Halle J.S., Franklin R.J., and Karalfa B.L., Comparison of Four Treatment Approaches for Lateral Epicondylitis of the Elbow, *J. of Orth. and Sports Phys. Ther.* 8(2): 62-69, 1986

Hill C.R., Clarke P.R., Crowe M.R., and Hammick J.W., Biophysical effects of cavitation in a 1MHz ultrasonic beam. In: Ultrasonics for Industry Conference Papers (Eds. Hill C.R., Clarke P.R., Crowe M.R., and Hammick J.W.) Iliffe Press, London 1972. 26-30

Hofmann D. and Moll F., The effect of ultrasound and in vivo penetration of benzyl nicotinate, *J. Control. Rel.* 27: 185-192, 1993

Holtzmark J., Johnsen I., Sikeland T. and Skvalem S., Boundary layer flow near an oscillating obstacle in an oscillating incompressible fluid, *J. Acoust. Soc. Am.* 26: 26-39, 1954

Howkins S.D., Diffusion rates and the effect of ultrasound, *Ultrasonics.* 8: 348-351, 1969

Illel B. and Schaefer H., Transfollicular percutaneous absorption: skin model for qualitative studies, *Acta Derm. Venerol.* 68: 427-430, 1988

Illel B., Schaefer H., Wepierre J., and Doucet O., Follicles Play an Important Role in Percutaneous Absorption, *J. Pharm. Sci.* 80(5): 424-427, 1991

Kahn J., Iontophoresis and Ultrasound for Postsurgical Temporomandibular Trismus and Paresthesia, *Phys. Ther.* 60(3): 307-308, 1980

Kao J., Hall J., and Helman G., In vitro Percutaneous Absorption in mouse Skin: Influence of Skin Appendages, *Tox. Appl. Pharmacol.* 94: 93-103, 1988

Kleinkort J. and Wood F., Phonophoresis with 1 Percent Versus 10 Percent Hydrocortisone, *Phys. Ther.* 55(12): 1320-1324, 1975

Kneschke A., Partial Differential Equations. In: *Differential Equations and Boundary Conditions Problems Vol. 2* (Ed. Kneschke A.) Teubner-Verlagsgesellschaft, Leipzig 1961.

Knutson K., Potts R.O., Gizek D.B., Golden G.M., McKie J.E., Lambert W.J., and Higuchi W.I., Macro and molecular physco-chemical considerations in understanding drug transport in the stratum corneum, *J. Control. Rel.* 2: 67-87, 1985

Kost J., Levy D., and Langer R., Ultrasound Effect on Transdermal Drug Delivery, *Proceed. Int. Symp. Control. Rel. Bioact. Mater. 13, Controlled Release Society*: 177-178, 1986

Kost J., Levy D., and Langer R., Ultrasound as a Transdermal Enhancer. In: *Percutaneous Absorption 2nd Edition- Revised and Expanded* (Eds:Bronaugh R.L. and Maibach H.I.) Marcel Dekker Inc. New York. 1989 Chapter 34

Kremkau F.W. and Cowgill R.W., The role of molecular weight and structure in the absorption of ultrasound by proteins, *Proc. IEEE Ultrasonics Symp.*: 696-698, 1984

Lauer A.C., Lieb L.M., Ramachandran C., Flynn G.L. and Weiner N.D., Transfollicular Drug Delivery, *Pharm. Res.* 12(2): 179-186, 1995

Lele P.P., Cavitation and its effects on organised mammalian tissues - a summary. In: *Ultrasound: Its Application in Medicine and Biology* (Ed. F.J. Fry) Elsevier, Holland. 1978

Lenart I. and Auslander D., The Effect of Ultrasound on Diffusion through Membranes, *Ultrasonics* 18: 216-218, 1980

Leo A., Hansch C., and Elkins D., Measurements of Partition Coefficients, *Chem. Rev.* 71: 525-616, 1971

Levy D., Kost J., Meshulam Y., and Langer R., Effect of Ultrasound on Transdermal Drug Delivery to Rats and Guinea Pigs, *J. Clin. Invest.* 83: 2074-2078, 1989

Machluf M. and Kost J., Ultrasonically enhanced transdermal drug delivery. Experimental approaches to elucidate the mechanism, *J. Biomater. Sci. Polymer Edn.* 5: 147-156, 1993

Maibach H.I., Feldman R.J., Miby T.H., and Serat W.F., Regional variation in percutaneous absorption in man, *Arch. Environ. Health.* 23: 208-211, 1971

Mayev R., Development of Ultrasonic Investigations in Medicine and Biology in the USSR, *Ultrasound in Med. and Biol.* 11: 1-11, 1985

McElnay J.C., Benson H.A.E., Hadgraft J., Murphy T.M., The Use of Ultrasound in Skin Penetration Enhancement. In: *Pharmaceutical Skin Penetration Enhancement, Drugs and the Pharmaceutical Sciences Vol. 59* (Eds Walters K. and Hadgraft J.) Marcel Dekker, New York 1994.

McElnay J.C., Benson H.A.E., Harland R., and Hadgraft J., Phonophoresis of Methyl Nicotinate: A Preliminary Study to Elucidate the Mechanism of Action, *Pharm. Res.*, 10 (12): 1726-1731, 1993

McElnay J.C., Kennedy T.A., and Harland R., Enhancement of the percutaneous absorption of fluocinolone using ultrasound, *Br. J. clin. Pharmac.* 21: 609-610P, 1985

McElnay J.C., Kennedy T.A., and Harland R., The influence of ultrasound on the percutaneous absorption of fluocinolone acetonide, *Int. J. Pharm.* 40: 105-110, 1987

McElnay J.C., Matthews M.P., Harland R., and McCafferty D.F., The effect of ultrasound on the percutaneous absorption of lignocaine, *Br. J. clin. Pharmac.* 20: 421-424, 1985

Menon G.K., Bommannan D.B. and Elias P.M., High-Frequency Sonophoresis: Permeation Pathways and Structural Basis for Enhanced Permeability, *Skin Pharmacol.* 7: 130-139, 1994

Menon G.K., Price L.F., Bommannan B., Ellias P.M. and Feingold K.R., Selective Obliteration of the Epidermal Calcium Gradient Leads to Enhanced Lamellar Body Secretion, *J. Invest. Dermatol.* 102: 789-795, 1994

Milligan J.F., Matteucci F.D., and Martin J.C., Current concepts in Antisense Drug Design, *J. Med. Chem.* 36(14): 1923-1936, 1993

Mitragotri S., Blankschtein D., and Langer R., Ultrasound-Mediated Transdermal Protein Delivery, *Science.* 269: 850-853, 1995

Mitragotri S., Edwards D.A., Blankschtein D., and Langer R., A Mechanistic Study of Ultrasonically-Enhanced Transdermal Drug Delivery, *J. Pharm. Sci.* 84(6): 697-705, 1995

Miyazaki S., Kohata Y.,Mizuoka H., Oda M., and Takada M., External Control of Drug Delivery: Enhancement of Transdermal Absorption of Indomethacin by Ultrasound, *Proceed. Intern. Symp. Control. Rel. Bioact. Mater. 18, Controlled Release Society*: 525-526, 1991

Miyazaki S., Kohata Y.,and Takada M., Effect of Ultrasound on the Transdermal Absorption of Indomethacin- Continuous Mode and Pulsed Mode, *Yakuzaigaku* 52(4): 264-271, 1992

Miyazaki S., Mizuoka H., Kohata Y., and Takada M., External Control of Drug Release and Penetration. 6. Enhancing Effect of Ultrasound on the Transdermal Absorption of Indomethecin from an Ointment in Rats, *Chem. Pharm. Bull.* 40(10): 2826-2830, 1992

Miyazaki S., Mizuoka H., Oda M., and Takada M., External control of drug release and penetration: enhancement of the transdermal absorption of indomethacin by ultrasound irradiation, *J. Pharm. Pharmacol.* 43: 115-116 (Communications), 1991

Mohl N.D., Ohrbach R.K., and Crow H.C., and Gross A.J., Devices for the diagnosis and treatment of temperomandibular disorders. Part 3: Thermography, ultrasound, electrical stimulation, and electromyographic feedback, *J. of Prosthet. Dent.* 63(4): 472-476, 1990

Moldover J.R. and Danish D., Phonophoresis with Hydrocortisone: Effect on Serum Cortisol Levels, *Arch. Phys. Med. Rehabil.* 67: 689, 1986

Moll J.M., A New Approach to Pain: Lidocaine and Decadron with Ultrasound, *USAF Med. Serv. Dig.* 30: 8-11, 1977

Mortimer A.J., Trollope B.J., Villeneuve E.J., and Roy O.Z., Ultrasound - enhanced diffusion through isolated frog skin, *Ultrasonics* 26(6): 348-351, 1988

Muir W.S., Magee F.P., Longo J.A., Karpman R.R., and Finley P.R., Comparison of Ultrasonically Applied vs Intra-articular Injected Hydrocortisone Levels in canine knees, *Orthopaed. Rev.* 19: 351-356, 1990

Murphy T.M. and Hadgraft J., A Physico-chemical interpretation of phonophoresis in skin penetration enhancement. In: Prediction of Percutaneous Penetration, Methods, Measurements and Modelling. (Eds: Scott R.C., Guy R.H. and Hadgraft J.) IBC Technical Services Ltd. London 1990. 333-336.

Naik A., Pechtold L.M., Potts R.O., and Guy R.H., Mechanism of oleic acid-induced skin penetration enhancement in vivo in humans, *J. Control Rel.* 37: 299-306

Nanavaty M., Brucks R., Grimes H., and Siegel F.P., An ATR-FTIR Approach to Study the Effect of Ultrasound on Human Skin, *Proceed. Intern. Symp. Control. Rel. Bioact. Mater. 16, Controlled Release Society*: 310-311, 1989

Newell J.A., A Radiation Pressure Balance for the Absolute Measurement of Ultrasonic Power, Phys. Med. Biol. 8(2): 215-221, 1963

Newman J.T., Nellermoe M.D., and Carnett J.L., Hydrocortisone Phonophoresis-A Literature Review, *J. Am. Pod. Med. Assoc.* 82: (8): 432-435, 1992

Nyborg W.L., In: *Physical Mechanisms for Biological Effects of Ultrasound.* (Ed. Nyborg W.L.) HEW Publication, FDA 1971. 78-8062.

Oziomek R.S., Perrin D.H., Herold D.A., and Craig C.R., Effect of phonophoresis on serum salicylate levels, *Med. Sci. Sports Med.* 23(4): 397-401, 1991

Parry J.S., Cleary, B.K., Williams A.R., and Evans D., Ultrasonic dispersal of cervical cell aggregates, *Acta Cytol.* 15: 163-166, 1971

Pelucio-Lopes C., Machet L., Vaillant L., Patat F., Lethieq M., Furet Y., Pourcelot L., and Lorette G., Phonophoresis of azidothymidine (AZT), *Int. J. Pharm.* 96: 249-252, 1993

Pinton J., Valliant L., Machet C., Patat F., Lethiecq M., Pourcellot L., Guilloteau D., and Lorette G., Does Phonophoresis increase the ex-vivo Percutaneous Absorption?, *J. Invest. Dermatol.* 96(4): 650 abstracts, 1991

Pottenger F.J. and Karalfa B.L., Utilisation of Hydrocortisone Phonophoresis in United States Army Physical Therapy Clinics, *Milit. Med.* 154: 355-358, 1989

Potts R.O., Physical characterization of the stratum corneum: The relationship of mechanical and barrier properties to lipid and protein structure. In*: Transdermal Drug Delivery: Developmental Issues and Research Initiatives* (Eds. Hadgraft J. and Guy R.H.) Marcel Dekker, New York 1989, 23-57

Pratzel H., Dittrich P.,and Kukovetz W., Spontaneous and Forced Cutaneous Absorption of Indomethacin in Pigs and Humans, *J. Rheumatol.* 13(6): 1122-1125, 1986

Preston R.C., The NPL Ultrasound Beam Calibrator. *IEEE Trans. Ultrason. Ferroelec. Freq. Contr. 35, UFFC*: 122-139, 1988

Preston R.C., Hydrophone-Based Measurements on a Specific Acoustic Pulse Part 1: Field Characterisation. In: *Output Measurements for Medical Ultrasound* (Ed. Preston R.C.) Springer-Verlag, London 1991.

Quillen W.S., Phonophoresis: A Review of the Literature and Technique, *Athl. Train.* 15: 109-110, 1980

Quillen W.S., Ultrasonic Phonophoresis, *Phys. Sportsmed.* 10: 211, 1982

Robinson C.P., Hydrophones. In: *Output Measurements for Medical Ultrasound* (Ed. Preston R.C.) Springer-Verlag, London 1991.

Romanenko I.M. and Aravisky R.H., Comparable Levels of Amphotericin B in the Skin and Subcutaneous Fatty Tissue After Local Application of Amphotericin Ointment and with Preliminary Treatment by Dimethylsulphoxide, *Antibiotiki I Khimioterapiia* 36(9): 29-31, 1991

Roques C.F., Cotonat J., Marque P., Chatain M.,and Fellez A., NSAID Blood Rates After Transdermal Application Using Manual Massage, Ultrasound Therapy and Iontophoresis, *Br. J. Rheumatol.* 31 S2 (Meeting Abstract): 171, 1992

Sambrook J., Fritsch E.S., and Maniatis P. In: *Molecular cloning - a laboratory manual* (Eds. Sambrook J., Fritsch E.S., and Maniatis P.) Cold Spring Harbour Laboratory Press, New York 1989.

Saxena J., Sharma N., Makoid M.C., and Banakar U.V., Ultrasonically Mediated Drug Delivery, *J. Biomater. Appl.* 7(3): 277-296, 1993

Scheuplein R., Mechanism of Percutaneous Absorption 2, *J. Invest. Dermatol.* 48: 79-88, 1967

Scheuplein R., The skin as a barrier. In: *The Physiology and Pathophysiology of Skin*. (Ed. Jarret A.) Academic Press, London 1978a. 1669-92.

Scheuplein R., Site variations in diffusion and permeability. In: *The Physiology and Pathophysiology of Skin Vol. 5.* (Ed. Jarret A.) Academic Press, London 1978b. 1731-52.

Simonin J.P., On the mechanisms of in vitro and in vivo phonophoresis, *J. Control. Rel.* 33: 125-141, 1995

Singh S. and Singh J., Transdermal Delivery of Drugs by Phonophoresis. A Review, *Drug Des. Del.* 5: 259-265, 1990

Skauen D.M. and Zentner G.M., Phonophoresis, *Int. J. Pharm.* 20: 235-245, 1984

Sloan K.B., Prodrugs, In: *Topical and Ocular drug Delivery, Drugs and the Pharmaceutical Sciences Vol. 53.* (Ed. Sloan K.B.) Marcel Dekker, New York 1992.

Smith W., Winn F., and Parette R., Comparative Study using Four Modalities in Shinsplint Treatments, *J. Orthop. Sports Phys. Ther.* 8(2): 77-80, 1986

Stratford P.W., Levy D.R., Gauldie S., Miseferi D., and Levy K., The evaluation of phonophoresis and friction massage as treatments for extensor carpi radialis tendinitis: a randomized controlled trial, *Physiother. Can.* 41(2): 93-99, 1989

Sugibayashi K., Hosoya K.I., Morimoto Y., and Higuchi W.I., Effect of the absorption enhancer azone on the transport of 5-fluorouracil across hairless rat skin, *J. Pharm. Pharmacol.* 37: 578-580, 1985

Sun Y. and Liu J.C., Transdermal Drug Delivery by Phonophorsis: Basics, Mechanisms and Techniques of Application. In: *Drug Permeation Enhancement: Theory and Application. Drugs and the Pharmaceutical Sciences Vol. 62* (Ed. Hsieh D.S.) Marcel Dekker, New York 1994

Tachibana K., Transdermal Delivery of Insulin to Alloxan-Diabetic Rabbits by Ultrasound Exposure, *Pharm. Res.* 9(7): 952-954, 1992

Tachibana K. and Tachibana S., Usage of Ultrasonic Vibration as a New Transdermal Insulin Delivery System, *Diab. Res. Clin. Pract.* 1-5: supplement S166, 1988

Tachibana K. and Tachibana S., Transdermal delivery of insulin by ultrasonic vibration, *J. Pharm. Pharmacol.* 43 Communications: 270-271, 1991

Tachibana K. and Tachibana S., Use of Ultrasound to Enhance the Local Anesthetic Effect of Topically Applied Aqueous Lidocaine, *Anesthesiology*. 78: 1091-1096, 1993

ter Haar G.R. and Daniels S., Evidence for ultrasonically induced cavitation in vivo, *Phys. Med. Biol.* 26: 1145-1149, 1981

ter Haar G.R., Daniels S., Easthaugh K.C., and Hill C.R., Ultrasonically induced cavitation in vivo. *Br. J. Cancer*. 45: 151-155, 1982

Tyle P. and Agrawala P., Drug Delivery by Phonophoresis, *Pharm. Res.* 6(5): 355-361, 1989

Tyle P. and Kari B., Iontophoretic devices In: *Drug Delivery Devices. Fundamentals and Applications.* (Ed. Tyle P.) Marcel Dekker, New York 1988. 421-454.

Ueda H., Sugibayashi K., Morimoto Y., Skin Penetration-enhancing effects of drugs by phonophoresis, *J. Control. Rel.* 37: 291-297, 1995

Walmsley A.D. and Squier C.A., Role of Ultrasonics in Facilitating Cutaneous Drug Penetration, *J. Dent. Res.* 70: 720 onwards, 1991

Walmsley A.D., Squier C.A., and Kremer M., The thermal effect of ultrasound during phonophoresis in vivo, *IADR Meeting*, Glasgow, July 1992

Weintraub H.M., Antisense RNA and DNA, *Sci. Am.* 262: 40-46, 1990

Wentz P.W. and Downing D.T., Stratum corneum: Biological and biochemical considerations, In: *Transdermal Drug Delivery. Developmental Issues and Research Initiatives*. (Eds. Hadgraft J. and Guy R.H.) Marcel Dekker, New York 1989. 1-22.

Wheatley V.R., Composition of Skin Surface Lipids, *Scand. J. clin. lab. Invest.* 17 suppl.85: 11-19, 1965

Wiechers J.W., The barrier function of the skin in relation to percutaneous absorption of drugs, *Pharm. Weekbl. Sci.* 11: 185-198, 1989

Williams A.R., Release of serotonin from human platelets by acoustic microstreaming, *J. Acoust. Soc. Amer.* 56: 1640-1643, 1974

Williams A.R., *Ultrasound: Biological Effects and Potential Hazards* (Ed. Williams A.R.) Academic Press, London 1983

Williams A.R., phonophoresis: an in vivo evaluation using three topical anaesthetic preparations, *Ultrasonics* 28: 137-140, 1990

Williams A.R., McHale J., Bowditch M., MIller D.L., and Reed B., Effects of MHz ultrasound on Electrical Pain Threshold Perception in Humans, *Ultrasound in Med. and Biol.* 13(5): 249-258, 1987

Williams A.R., Rosenfield E.H., and Williams K.A., Gel-sectioning technique to evaluate phonophoresis in vitro, *Ultrasonics* 28: 132-136, 1990

Wing M., Phonophoresis with Hydrocortisone in the Treatment of Temporomandibular Joint Dysfunction, *Phys. Ther.* 62(1): 32-33, 1982

Yano T., Nakagawa A., Tsuji M., and Noda K., Skin Permeability of Various Non-Steroidal Anti-inflammatory Drugs in Man, *Life Sci.* 39: 1043-1050, 1986

Zeqiri B., Overview of Measurement Techniques In: *Output Measurements for Medical Ultrasound* (Ed. Preston R.C.) Springer-Verlag, London 1991.

Ziskin M.C. and Michlovitch S.L. Therapeutic Ultrasound. In: *Contemporary Perspectives in Rehabilitation, Vol.1. Thermal Agents in Rehabilitation.* (Ed. Michlovitch S.L.) F.A. Davis Company, Philadelphia 1986. Chapter 7